Sustainable Masonry

*Series Editor*
*Noël Challamel*

# Sustainable Masonry

## *Stability and Behavior of Structures*

Thierry Ciblac
Jean-Claude Morel

ISTE
WILEY

First published 2014 in Great Britain and the United States by ISTE Ltd and John Wiley & Sons, Inc.



ISTE Ltd
27-37 St George's Road
London SW19 4EU
UK

www.iste.co.uk

John Wiley & Sons, Inc.
111 River Street
Hoboken, NJ 07030
USA

www.wiley.com



Library of Congress Control Number: 2014941563

British Library Cataloguing-in-Publication Data
A CIP record for this book is available from the British Library
ISBN 978-1-84821-495-8

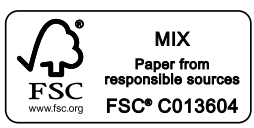


Printed and bound in Great Britain by CPI Group (UK) Ltd., Croydon, Surrey CR0 4YY

# Contents

# Preface

This book is the result of the meeting of two complementary approaches to the same subject: masonry. The first is the approach developed by Thierry Ciblac at the *Ecole Nationale Supérieure d'Architecture de Paris la Villette* (National School of Architecture of Paris La Villette), which revisits historical design methods using digital tools. The second consists of studies led by Jean-Claude Morel at the *Ecole Nationale des Travaux Publics de l'Etat* (National Civil Engineering School), which are based on experiments with masonry structures of earth materials. The convergence of these two approaches occurs through the common use of the theory of yield design.

This book was written to promote understanding of the mechanical stability of masonry structures in a contemporary context and to introduce it to the readers. This approach will allow contractors to carry out diagnostics on existing heritage and to design new structures.

The challenges presented by sustainability criteria have provided – or restored – respectability to masonry constructions using earth materials. The latest research in this area has been formalized by putting it into perspective with historical approaches. This is done with the dual purpose of making design methods used for old structures (mostly from the eighteenth century) more accessible and providing "simple" tools for understanding their behavior. In particular, developments relative to graphic statics, take on new educational and demonstrative values with the use of digital tools.

We wish to thank Noël Challamel for proposing the idea for this book, for his detailed proof-reading of the manuscript and for his valuable advice.

Such a book is the fruit of a collective effort. Experimental work, in particular, is the result of a team effort where students, contractors, technicians, engineers and researchers cooperate.

Work on dry stone began in 1998 at ENTPE, instigated by Patrick Cohen in the Luberon Regional Natural Park.

Work on earth began in 1981 at ENTPE, instigated by Myriam Olivier and later, Ali Mesbah. These two researchers were eager to share their knowledge, and J.C. Morel benefitted from their expertise upon arrival at ENTPE. Note that Claude Boutin encouraged J.C. Morel to study the theory of yield design in order to apply it to earth materials.

The authors are particularly thankful to a number of PhD students, whose work has enriched this book. Laboratories and funding involved in these PhDs are specified as following:

– Abalo P'kla (DGCB, *Ecole Nationale des Travaux Publics de l'Etat* – National Civil Engineering School);

– Boris Villemus (DGCB, *Ministère de l'Ecologie, du Développement Durable et de l'Energie-MEDDE* – Ministry of Ecology, Sustainable Development and Energy);

– Givanildo Azeredo (DGCB, *Conselho Nacional de Desenvolvimento Científico e Tecnológico CNPQ-Brésil* – National Council for Scientific and Technological Development CNPQ-Brazil);

– Anne-Sophie Colas (DGCB, *Ministère de l'Ecologie, du Développement Durable et de l'Energie-MEDDE* – Ministry of Ecology, Sustainable Development and Energy);

– Quoc Bao Bui (*Centre National de la Recherche Scientifique-CNRS* - National Centre for Scientific Research);

– Apostolia Th. Oikonomopoulou, (*ARIAM-LAREA, Ministère de la Culture et de la Communication* – Ministry of Culture and Communication);

– Hong Hanh Le (LGCB, *Ecole Nationale des Travaux Publics de l'Etat* – National Civil Engineering School).

These PhDs were carried out with the assistance of technical staff:

– Odile Roque (MEDDE technician);

– Jean-François Halouze (MEDDE technician);

– Sébastien Courrier (MEDDE technician);

– Erwan Hamard (MEDDE technician);

– Stéphane Cointet (MEDDE technician);

– Joachim Blanc-Gonnet (CNRS research engineer).

The experimental work which forms the basis of the first part of this book was carried out in close cooperation with builders, notably via the *Ecobâtir* network, which includes Nicolas Meunier, Vincent Rigassi and Alain Marcom, experts in earthen construction. In the field of dry stone, the series of experiments were conducted by Paul Arnaud (OPUS) and Philippe Alexandre (Lithos-APARE) at Le Beaucet. The second series was conducted in Saint-Germain-de-Calberte by the *Artisans Bâtisseurs en Pierres sèches* (Dry Stone Builders' Association) led by Marc Dombre and Christian Emery. The third series was conducted at Pont de Montvert by the *Artisans Bâtisseurs en Pierres sèches*, led by Bruno Durand and Thomas Brasseur.

Denis Garnier co-supervised Anne-Sophie Colas' thesis, the second thesis on dry stone retaining walls, bringing her valuable skills to the optimum implementation of yield design.

Rabia Charef-Morel carried out careful proof-reading of the manuscript and created Figures 4.1, 4.2, 4.3, 11.1 and 11.3.

Paul McCombie, Nicolas Meunier, Bruno Durand provided the photographs in Figures 1.1 and 1.3.

Research was also done in the context of two national projects: PEDRA and RESTOR:

– RGCU PEDRA project No. 10 MGC S 017, studies on dry stone or weak mortar masonry of the Civil and Urban Engineering Network, coordinated by Eric Vincens of the *Ecole Centrale de Lyon* (Lyon Central School).

– RESTOR project, restoration of dry stone retaining structures, of the PNRCC program of the Ministry of Culture and Communication, coordinated by Eric Vincens of the *Ecole Centrale de Lyon* (Lyon Central School).

Studies on rockfill dams and dry stone masonry revetment were initiated at the instigation of EDF.

Finally, J.C. Morel was supported by the Rhône-Alpes region in furthering his studies in England, with a 5 month placement at the University of Bath.

The sections on graphic statics, principles of yield design and stability of curvilinear masonry, written by Thierry Ciblac, are directly related to his teaching and research activities at the MAP Maacc/CNRS-MCC UMR 3495 (ex. ARIAM-LAREA) laboratory at the *Ecole Nationale Supérieure d'Architecture de Paris La Villette*. The author wishes to thank Louis-Paul Untersteller and François Guéna, founders and successive directors of the laboratory, and the initiators of the research focus on digital tools to help preserve heritage masonry. The quality of their welcome, their support and their experiences as educators and researchers has been an invaluable aid. The development of graphic statics in dynamic geometry has been the subject of collaboration with the Department of Architecture of the Massachusetts Institute of Technology, under the MIT-France program, with Professor John Ochsendorf and Philippe Block, then a student, whom we also wish to thank.

Thierry CIBLAC and Jean-Claude MOREL

June 2014

PART 1

# Technologies and Construction Process

# 1

# Introduction to Sustainable Masonry

## 1.1. Definitions of sustainable masonry

This book is particularly focused on masonry structures made of local materials, stone and earth. They are among the first materials to have been used by humans to build shelters thousands years ago and they are called, in this book, Earth Materials. In this context, earth masonry deals with adobe or compressed earth block, or rammed earth if the material is manufactured in successive layers.

This book does not particularly apply to baked clay brick and cement sand blocks, which are within the scope of Eurocode 6.

### 1.1.1. *Sustainable constructions*

Here, we consider sustainable development as defined in [BRU 87] as "a development mode that meets the needs of present generations without compromising the ability of future generations to meet their own needs".

In this book, we will only consider the mechanical stability of masonry. However, in this introductory chapter, we consider some elements of thermal and hydric behavior, socio-economic aspects, and sustainability and environmental impacts of these structures. These elements will include references so that the reader, if he wishes, can further his knowledge of all these key aspects of sustainability.

Local materials are acquired from or near the construction site. Here, 'near' means a distance of about 20 km. Local materials used in construction

*Sustainable Masonry: Stability and Behavior of Structures,*
First Edition. Thierry Ciblac and Jean-Claude Morel.

have an impact due to their transportation. When a material is taken from on-site, as was often the case for earth, rubble stone masonry (rubble stone blocks and earth or sand lime mortar) and dry stone constructions, the impact is obviously reduced [HAB 12].

This precision concerning the implied proximity of the word "local" is important since it implies that the production of these materials cannot be completely industrialized. Materials therefore maintain a very variable composition, depending on the soil that is available locally and the geology. Therefore, it is not possible to give a standard composition of these materials. Local materials of interest here are: cut or uncut stone assembled with (rubble stone masonry) or without (dry stone) mortar, adobe and earth mortar and finally rammed earth. These materials are "earth" materials.

### 1.1.2. *Masonry structures*

By masonry structures, we refer to an arrangement of blocks hand-stacked by a mason, regularly or irregularly, with or without a mortar, over successive layers. We exclude "Cuzco rampart" type masonry or blocks exceeding one ton, quarry cut and assembled with a crane and Opus Incertum in general.

This masonry is done manually, thus is greatly dependent on the mason's skill, but following specific rules, which form part of the mason's skill set. We will also consider rammed earth as a part of masonry as they depend on a mason's art, even if they do not constitute a stack of small elements but rather layers of compacted earth.

In an industrial context, "sustainable development" can be interpreted as requiring structures to be designed based on criteria, taking all environmental consequences (in the broad sense of the word) induced by these constructions into account. However, the objects discussed here are the result of a systemic approach whereby an optimum is obtained according to environmental and sustainability criteria, amongst others, which revert to being current. Vernacular architecture was erected in a context of limited resources and energy shortages, thus respecting the criteria of minimum impact on the planet. Their age provides an obviously tangible guarantee of durability. However, we must also consider the innovation that characterizes sustainable masonry, as the use of old materials in a modern context can only be achieved through an adjustment that includes innovation.

## 1.2. Challenges of sustainable development in construction

The use of earth materials in construction allows a technological leap in terms of sustainability. A case study shows that for structural work of this type of construction, transport of materials (expressed in t.km), that is to say the amount of mass transported over a given distance, can be reduced five-fold, and embodied energy [MOR 01] can be reduced three-fold – embodied energy is the energy required to manufacture the "product" from its design to the end of its life. [HAB 10, HAB 12] presents an alternative method for quantifying the impact of construction using earth materials, which offer notable benefits in terms of their low impact. Moreover, another case study shows that work time on the construction site is tripled: this work has a positive impact upon the economy because it requires skills [MAR 09].

### 1.2.1. *Socio-economic aspects*

Our context concerns materials and therefore structures for which new constructions are few and far between in 21st Century Europe, as they are transformed and constructed primarily by manual labor. Society's choice of industrialization is reflected in the price of non-animal energy (electricity, oil, etc.), which is one to two hundred times cheaper than human labor [MAR 02]. Under these conditions, new constructions or restorations are hard to carry out with short term competitive costs, while the need to innovate increases; this also comes at a cost. However, there are hundreds of new structures and many more renovations carried out using masonry with earth materials. These sites provide some figures for numerical analysis. Socio-economic aspects are the least well-covered to our knowledge, however information on these challenges can be found in [MAR 02, MAR 09, RIG 02].

### 1.2.2. *Environmental impact*

Many more studies have been carried out on environmental impact than on socio-economic aspects. General tools currently used for calculating this impact are still being developed, but mature tools already exist for industrial materials and structures. These include lifecycle analysis (LCA). These tools, despite their complexity, are inadequate for technologies and architectures using earth materials [HAB 12]. In addition, the databases necessary for their use are not yet available in the case of earth materials.

The two best-covered areas in the published literature are embodied energy and energy expended during service (mainly for heating buildings). In France, thermal regulations (RT) only apply to the consumption of service energy. With increasing generalization of construction of "passive" buildings that do not consume "external" service energy or energy efficiency, the concept of embodied energy should become more important.

[HAB 12] covers works of art, particularly dry stone retaining walls, and the case study [BAU 12] covers rubble stone masonry bridges. For earth material buildings, see [MOR 01, MAR 02, MAR 09].

### 1.2.3. *Sustainability*

Sustainability is an important point in works on earth materials, but it depends on the geology of the site, and as for all structures, the quality of maintenance. It also depends on the design, the quality of implementation and therefore on cultural, economic or political criteria. However, it should be noted that paradoxically, the trend continues to favor conventional industrial approaches and therefore constructions with low durability by, for example, decreasing the thickness of concrete and the quantities of steel used.

Compared to current design criteria, monumental constructions such as Roman bridges appear to be oversized, while more vernacular structures are undersized, for example dry stone retaining walls used in farming. In the first case, the aim was to limit maintenance work in accordance with the available manual labor force; in the other case, it was to save manual labor on rebuilding collapsed parts after a storm, if necessary.

Unsuitable contemporary renovations have a more or less significant effect on reducing the lifecycle of earth materials and can even cause their sudden destruction. These consequences are the result of two main families of errors: coatings that are not sufficiently porous, and mechanical reinforcements that are too rigid to survive earthquakes. This last point is further detailed in [FER 05]. Further details concerning the case of industrial coatings which can not be applied to earthen material walls may be found in [ECO 13].

For sustainability issues concerning physicochemical actions, such as those caused by pollution or salt, readers may wish to consult the thesis [GRO 09] for the particular case of earthen structures. There are also many

publications in this field regarding stone constructions. Organizations such as ICCROM [ICC 14] (International Centre for the Study of the Preservation and Restoration of Cultural Property), the Paul Getty Trust [GET 13], have studied this area extensively.

### 1.2.4. *Recycling and reuse*

By definition, the non-industrial use of an earth material allows direct reuse (of rubble stone masonry, earth mortar and earth masonry). This practice has been used for thousands of years and is still widespread. Reuse of a material qualifies it as renewable, even if the resource is not infinitely renewable. This reuse of an earth material neither affects biodiversity nor does it tie down agricultural land, unlike intensive forestry, for example. This reusability aspect is a key advantage of these earth materials in terms of sustainability.

## 1.3. Past (civil engineering and architecture), present and future (design tools) practices

### 1.3.1. *Architectural heritage*

There is a rich heritage of masonry using earth materials from all over the world. We will limit ourselves to mentioning a few key works here. However, a large number of inventory documents are available, and are often produced by State agencies: ministries of agriculture, transport, and housing.

On the one hand, archaeologists and historians have carried out a lot of work in this area, see for example [BAR 08] for Roman bridges; architects [LOT 11] have worked on European vernacular earthen heritage. Studies coordinated by Ferrigni [FER 05] and Klein [DEC 03, DEC 07, DEC 11] take a trans-disciplinary approach, respectively in the fields of stone masonry and earthen construction.

Dry stone retaining walls are mainly found in France on county roads, rural roads, agricultural terraces and footpaths. Statistics relating to the national network only [ODE 00] include 2,100 studies unevenly distributed over three-quarters of the French departments. In the UK, studies emphasize the economic challenges: the road network is supported by dry stone walls over 2,000–3,000 km long [PRE 00]. It

would be economically unfeasible to replace these walls which, although often stable, no longer meet regulatory safety requirements. This has motivated renewed research into this field over the last twenty years.

Tunnels lined with stone, like bridges, are also currently being studied as part of new PhD theses because of their economic importance [DOM 06, STA 11].

### 1.3.2. *Cultural heritage*

Architecture is a natural part of culture. However, in the context of our chosen subject, it is interesting to highlight that there are two cultural components in masonry constructions with earth materials: the most obvious is the structure, once it is built, but there is also the skill set required for construction. These skills constitute an intangible heritage, leading toward a more sustainable dimension in our changing society.

This last point implies that regulations are not sufficient to ensure construction quality; we must also ensure that the skills of stakeholders are recognized. This requires special procedures, including training of masons (e.g. through apprenticeships), see section 1.5.

### 1.3.3. *Rehabilitation, strengthening*

Renovation of buildings include earth material masonry currently provides the largest bulk of work, while new buildings are rare. Intervention in these structures requires a thorough knowledge of the mechanical and hydrothermal behavior of these structures.

Interventions fall into three broad categories: modifications to suit current tastes (or the tastes of the client), maintenance or repair (Figures 1.1 and 1.2), and compliance with thermal or seismic regulations (resistance to horizontal stress).

**Figure 1.1.** *Dent repairs on two dry stone retaining walls. Left, repair in progress, granite (photo: Bruno Durand); right, after restoration, limestone (lighter part on the right) (photo: Paul McCombie)*

**Figure 1.2.** *Renovation of a rammed earth house, raising walls by the Nicolas Meunier company (photo: Nicolas Meunier)*

### 1.3.4. *New constructions*

New constructions with earth materials are still rare in Europe, but the last decade has seen a marked increase in interest in this subject, measurable by the increase in scientific publications concerning them. These constructions have found a place in the niche of 'green building' (eco-construction). This type of construction is carried out by clients and contractors involved in "pioneering" works (Figure 1.3). Other notable contributions have been made by self-builders.

**Figure 1.3.** *New constructions: load-bearing rammed earth and timber frame in Chasselay (France), contractor: Nicolas Meunier; right, rubble stone masonry bridge at St. Andeol de Clerguemort (France), contractor: Thomas Brasseur and Marc Dombres (photo: Paul McCombie)*

## 1.4. Durability, deformation and possible movement

Masonry that is sustainable over several decades, even centuries, often undergoes changes of use over time. These changes can create problems because they were not taken into account by the original designers. This type of pathology is similar to those relating to improper restoration, often coupled with a change of use. In the case of road works, dry stone retaining walls and arched bridges including stone masonry, the increased weight and speed of vehicles is a very common source of problems, as these structures were not designed to cope with these heavy weights. In the case of buildings, including earthen structures, changes in human behavior are associated with renovation. For example, the conversion of a barn into a house completely changes the hydrothermal transfers within the walls and can quickly (in less than 10 years) generate significant increases in the quantities of liquid water in the walls. Implementation of waterproof coatings, for example, can cause significant loss of strength, and may even lead to collapse (Figure 1.4).

Cultural aspects should also be taken into consideration, for example, the perception of cracks. Cracks occur systematically in old and new masonry, yet seem to be difficult for buyers to accept when purchasing a new house. The appearance of cracks is not necessarily a symptom of structural stability issues, but shows the masonry adapting to movement, for example at foundation level.

**Figure 1.4.** *Collapse of a rammed earth house wall due to excessive water content of the walls at the base as a result of capillary action which was then unable to evaporate*

In this book, we will not go into detail concerning the movement behaviors which precede perfect plasticity or fracturing, which can be understood using the material's behavior, that is to say, the relationship between stress and strain (rheology). Generally, inclusion of the behavior of the materials is limited to elasticity or elastoplasticity.

In this book, we have chosen only to take account of strength or stress stability, without consideration of movements and strains. This choice is based on the fact that, like the soils, "masonry" material exhibits a behavior that is close to perfect plastic behavior, and it resists very little, or not at all, to traction. This choice will be detailed in the following chapters. Of course, the designer should always remember that structural strains must remain below a certain limit.

## 1.5. Importance of expertise (complexity of cases and history of the structure, evolution over time)

The importance of experience and empirical knowledge of local masonry materials is essential for the reasons discussed above, that is to say, because of the variability of materials, architectures, heterogeneity of blocks and the strength of underlying assumptions. For complex structures, it is useful that the engineer, architect and mason cooperate to better understand the study of

the structure. This cooperation may also extend to other disciplines, such as anthropology, sociology and archaeology (see section 1.3).

## 1.6. Rationalization and calculation methods

We have therefore chosen to use strong hypotheses, which nevertheless seem realistic, and which, in any case, will provide rigorous results. In Part 3, we use yield design, which solves a stability problem with equilibrium equations and failure criterion of the material only. The resulting solution is correct if we assume a material behaves with perfect plasticity. We discuss yield design with, on the one hand, the mechanics of rigid bodies in the formalism of the point mass mechanics, and on the other hand, the formalism of continuum mechanics.

Local materials used for vernacular buildings have been largely ignored in academic research; our scientific approach focused on finding models in the literature that were adaptable to our study, then modifying or limiting their use as necessary. Our contribution will therefore make use of "rustic" models that have already been tested, allowing an initial interpretation of the mechanical stability of masonry using earth materials and the possibility of expanding to operational contexts.

The pragmatic approach taken in this book is the result of efforts to respond to a relatively urgent need. The skill sets of artisan builders are endangered and earth materials heritage is deteriorating. At the same time, the modern use of local materials constitutes a response to the challenges of reducing all kinds of industrial pollution.

Throughout this book, we borrow ideas or models from different fields of mechanics:

– from rigid body mechanics via graphic statics, a simple approach which gives quantitative results. This concept will be associated with yield design (defined in Chapter 9) to reach conclusions of the stability of masonry systems of elements that are considered dimensionally stable (Chapter 10);

– from soil mechanics for which yield design has been developed in a continuum mechanics formalism (Chapter 11). Masonry materials come from the soil (including rock), so obey complex material behavior for which much research is still ongoing. Under these conditions, yield design methods make it possible to obtain a good level of connection between theory and experiments;

– from studies on masonry structures using periodic regular blocks, which have been subject to a number of developments (Chapter 11).

## 1.7. Presentation of the outline of this book

In this book, we will follow the chronology of a masonry construction. We will begin by considering the blocks, then the mortar and finally, masonry. The quality of its components and their interaction will determine the quality of the structure they form.

This book is composed of three complementary parts: the first part deals with technologies and construction process (Chapters 1 to 4), the second with graphic statics (Chapters 5 to 8) and the third part deals with the implementation of yield design applied to masonry structures (Chapters 9 to 11).

## 1.8. Bibliography

[BAR 08] BARRUOL G., FICHES J.L., GARMY P., "Les ponts routiers en Gaule romaine", *Actes du colloque tenu au pont du Gard,* 8–11 October 2008.

[BAU 12] BAUMANN E., "Un pont en pierre du XXIe siècle fait école", *Le moniteur*, no. 5689, pp. 44–45, 2012.

[BRU 87] Notre avenir à tous, Rapport de la Commission mondiale sur l'environnement et le développement de l'ONU, présidée par Madame Gro Harlem Brundtland, Commission Mondiale sur l'environnement et le développement, April 1987.

[DEC 03] DE CHAZELLES C.A., KLEIN A., "Echanges transdisciplinaires sur les constructions en terre crue 1", *Actes de la table-ronde de Montpellier*, 17–18 November 2001, Edition de l'Espérou, 2003.

[DEC 07] GUILLAUD H., DE CHAZELLES C.A., KLEIN A., "Echanges transdisciplinaires sur les constructions en terre crue 2, Les constructions en terre massive, pisé et bauge", *Actes de la table-ronde de Villefontaine*, Isère, 28–29 May 2005, Edition de l'Espérou, 2007.

[DEC 11] DE CHAZELLES C.-A., KLEIN A., POUSTHOMIS N., "Echanges transdisciplinaires sur les constructions en terre crue 3, Les cultures constructives de la brique crue", *Actes de la table-ronde de Toulouse,* Edition de l'Espérou, 2011.

[DOM 06] DOMÈDE N., Méthode de requalification des ponts en maçonnerie, doctorat de L'Institut national des sciences appliquées de Toulouse, 11 July 2006.

[ECO 13] ECOBÂTIR R., *Enduits sur supports composés de terre crue: règles professionnelles – 63 fiches d'exemples de mise en œuvre*. Éditions du Moniteur: hors collection, 2013.

[GET 13] J. PAUL GETTY TRUST , http://www.getty.edu.

[FER 05] FERRIGNI F., HELLY B., MAURO A., *et al*., *Ancient buildings and earthquakes: reducing the vulnerability of historical built-up environment by recovering the local seismic culture: principles, methods, potentialities*, CUEBC di Ravello, EUR-OPA Major Hazards Agreement, 2005.

[GRO 09] GROSSEIN O., Modélisation et simulation numérique des transferts couples d'eau, de chaleur et de soluts dans le patrimoine architectural en terre, en relation avec sa dégradation, doctorat de l'Université Joseph Fourrier, 2009.

[HAB 10] HABERT G., CASTILLO E., MOREL J.C., "Sustainable indicators for resources and energy in building construction", *2nd International Conference on Sustainable Construction Materials and Technologies*, Ancona, Italy, 28–30 June 2010.

[HAB 12] HABERT G., CASTILLO E., VINCENS E., *et al*., "A new energy indicator for life cycle analysis of buildings", *Ecological Indicators*, vol. 23, pp. 109–115, 2012.

[ICC 14] http://www.iccrom.org/index_fr.shtml.

[LOT 11] LOTI G., MECCA S., Terra Europae, Earthen Architecture in the European Union, EdtETS, 2011.

[MAR 02] MARCOM A., Enquête sur la mesure de productivité dans les techniques de construction en terre, DPEA Terre, Ecole d'Architecture de Grenoble, 2002, http://www.atelierblanc.asso.fr/IMG/rtf/MEMOIRE_FINI_Alain.rtf.

[MAR 09] MARCOM A., FLOISSAC L., COLAS A.S., *et al*., "How to assess the sustainability of building construction processes", *Fifth Urban Research Symposium – Cities and Climate Change: Responding to an Urgent Agenda*, Marseille, France, 28–30 June 2009.

[MOR 01] MOREL J.C., MESBAH A., OGGERO M., *et al*., "Building houses with local materials: means to drastically reduce the environmental impact of construction", *Building and Environment*, vol. 36, pp. 1119–1126, 2001.

[ODE 00] ODENTN., "Recensement des ouvrages de soutènement en bordure du réseau routier national", *Ouvrage d'Art*, vol. 34, pp. 15–18, 2000.

[PRE 00] PRETTY J.N., BRETT C., GEE D., *et al*., "An assessment of the total external costs of UK agriculture", *Agricultural Systems*, vol. 65, pp. 113–136, 2000.

[RIG 02] RIGASSI V., SERUZIER M., Bilan économique, social et environnemental de 20 ans de filière blocs de terre comprimée à Mayotte, Direction de l'Equipement/Société immobilière de Mayotte, July 2002.

[STA 11] STABLON T., Méthodologie pour la requalification des ponts en maçonnerie, doctorat de l'Université Paul Sabatier, Toulouse 3, 4 October 2011.

# 2

# Earth and Stone Materials

## 2.1. Stone

Local geology, linked to human needs, is what determined the use of stones in vernacular masonry structures.

### 2.1.1. *Geological considerations*

From a geological point of view, there are three main types of stones. Sedimentary rocks (limestone and sandstone) are formed from the deposition and solidification of organic or mineral sediments. These rocks vary a lot because their creation depends on many factors (sediment type, transportation mode and deposition area). They are usually stratified deposits in layered beds. Limestone has a layered characteristic, which gives it a rectangular shape, while sandstones have more or less significant beds that, through their mode of erosion, give a rounded shape. Sedimentary rocks are spread over multiple territories.

Stones of magmatic origin (granite and basalt) form through crystallization of cooling magma. These stones are devoid of layers and have a more or less rounded shape due to erosion from wind and water. The units are obtained through yield due to shock, mass or peak. These rock formations are located in mountain chains that can be very eroded, as in Britain, for example.

Stones of metamorphic origin (shale and gneiss) result from the transformation of a rock due to a rise in temperature and/or pressure. Shales

*Sustainable Masonry: Stability and Behavior of Structures,*
First Edition. Thierry Ciblac and Jean-Claude Morel.

are in the form of plates which are easily broken down into layers. Gneisses have various shapes: some crumble into plates, while others are more granite-shaped.

Stones used in construction should have a high compressive strength. In general, compressive strength increases with the hardness and density of the stone. For stratigraphic stones, which can be compared to milfoil, we must also ensure that they do not disintegrate too easily. Finally, we should ensure the non-frost susceptibility of stones and retain those that resist best to water penetration cycles [AFN 06].

An atlas of construction stones from quarries especially updated for stone coating exists, see for example [ROC 98] for France. This atlas is obviously not exhaustive but provides comprehensive guidance on a wide variety of stones.

### 2.1.2. *Stone supply*

A large majority of materials used in various existing vernacular architectures are either from stones removed from cultivated plots, or from on-site extraction of the rock itself. Today, a supply of stone can be acquired by removing stones from fields, but it can also be acquired from the stones from road grading or demolition works, as well as from a quarry.

Construction or repair of masonry must not coincide with the dismantling of an existing structure, such as terraces of adjacent plots in the case of dry stone retaining walls. This type of degradation is not only damaging to the overall balance of cultures and landscape harmony but it provides, moreover, a disappointing performance of the stones (many of them are not reusable) and a lot of backfill. Similarly, looting of ruins that prevent future rehabilitation and that have proved to be minimally productive in terms of the damage, must be penalized.

#### 2.1.2.1. *Removing stones from fields*

This operation involves removing stones from a field in order to be able to work on the land more easily and enable better crop yields without damaging the tools. Once these “sterile” stones are sorted and cleaned of humus, they are placed into piles and are then directly usable for building walls. Today, we deplore the destruction of many hutches (piles of stones) that ruins reserves of materials and, therefore, the chances of conservation of

landscapes that are typical of limestone regions and the ecosystems that have adapted to them.

2.1.2.2. *Road grading works*

Road grading works also generate a large quantity of stones that could be used in construction. However, given the additional costs generated and the lack of will and organization from the client, this type of recovery is used infrequently.

2.1.2.3. *Rubble recovery*

Old buildings or civil engineering works in ruins, which are too altered to be rebuilt and are destined to be torn down by the owner, can also be sources of rubble. In this case, it is mandatory to obtain the owner's consent before any demolition, to ensure destruction of the work and see if it is subject to a demolition permit.

2.1.2.4. *Quarries*

Generally, only large boulders are extracted from quarries. Small stones or blocks that do not have the required qualities to be sold, as well as extraction and processing workshop scrap, are set aside and usually end up as granulate. We can negotiate with the quarry owner to recover stones or small blocks. Some operators also provide stones from natural quarries, such as rock outcrops, particularly for limestone or shale, which exhibit strata or layering and are therefore more easily detached from the rock. These stones can be extracted without backhoe explosives and instead simply using a crowbar and mass, corner and chisel.

The majority of stones that are kept are portable by two people, to facilitate implementation. All stones, whether from recovery or recent extraction, must be cleaned of earth (de-earthing).

### 2.1.3. *Rheology and mechanical strength*

We will restrict ourselves here to behaviors that are relevant to compression and shear between two carved stones. Even if there is tensile strength in blocks, in general the joints do not resist traction. Sticking mortar onto the block is a negligible effect. Moreover, we will see that the mechanical role of mortar is very limited in compression.

Literature on the mechanical behavior of stones is abundant in the field of rock mechanics. However, it involves studying the rock in a geological context with confining pressures above the megapascal and that has a significant macroscopic cracking problem. In this regard, the "stone" material follows the laws of Coulomb or Drucker Prager, meaning that it depends on confinement. In stone masonry construction, real confinements are rare because walls, arches or domes can usually be modeled by a two-dimensional approach. There is always a direction of the stone that is not confined. Therefore, we are happy enough to study the mechanical behavior by simple tests, such as those of simple compression and direct shearing of joints.

Let us note that some structures were correctly designed by only taking non-tensile strength into account, as discussed in the Part 3.

2.1.3.1. *Compressive strength*

Here, we give an example of a simple compression test. Figure 2.1 shows a test on shale that was used for the construction of a new arch bridge [TRA 14] Figure 1.3 right. If we consult the literature, the elastic modulus of shale ranges from 40 to 200 GPa, depending on its geological origin. It is likely that the tensile strength varies with the same proportion. The range in variation is very large, which can make it necessary to test the materials for each construction in advance if we need more precise values.

Cylindrical shape samples with a diameter of 59 mm were taken by coring blocks of stone on-site, therefore the height varies depending on the thickness of the block. It is important to keep an aspect ratio (height/diameter) close to two, to limit the end-effects due to friction during the test. During a compression test, as compressive stress increases, the test specimen expands laterally, however, due to friction along the interface between the plate and test specimen, lateral expansion of the specimen is confined.

A common way to measure the elastic modulus is by propagation of ultrasound; however the only way to get the compressive strength is to do a simple compression test (Figure 2.1). In this test, it is also possible to measure the elastic modulus either by sticking strain gauges directly onto the sample, or (like here) through the use of extensometers attached to the sample.

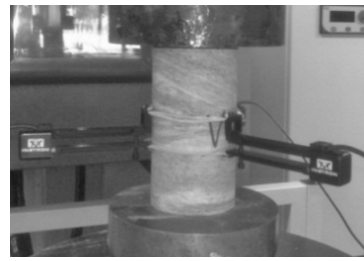

**Figure 2.1.** *Simple compression test of stone, with two vertical extensometers directly on the sample that measure strain (Photo: Stéphane Cointet)*

| Type of stone | Elasticity modulus in GPa (standard deviation) | Compressive strength in MPa (standard deviation) |
|---|---|---|
| Shale, Lozère, France | 60 (8) | 110 (30) |
| Sandstone, Vaucluse, France | 14 | 19 (3) |
| Limestone, St. Gens, Vaucluse, France | 18 | 23 (2) |

**Table 2.1.** *Variability of characteristics in compression of stones from the same site [VIL 04, TRA 14]*

The compressive strength of stones was determined and presented in Table 2.1. Let us note that the variation in the results, which relates to the variability of the material, is up to 30%. These differences are common in sustainable masonry, where the amount of material should not be reduced at any cost. A corollary feature is that these structures have very high safety factors (from 3 to 10).

2.1.3.2. *Friction between cut stones*

The study of block on block friction is generally not necessary in the arched structures because shear forces or stresses that are mobilized in the masonry joints are generally much smaller than the frictional resistance of joints. Therefore, this last value is generally not used to design structures. But, as for beam structures where bending is dominant, shear must be taken into account for specific cases.

Two particularly common cases are retaining walls of dry stone and rubble stone masonry that undergo horizontal forces, especially during earthquakes. Particularly for stones like shale, shearing can produce yield, which makes its study necessary.

Block on block shearing is a difficult mechanism to model as it involves varied and complex phenomena: attrition, physicochemical interactions and third body production. However, a simple and old law that provides a good match with experimental results is Coulomb's law of friction [COU 73].

It is this law that we will use in the model in Part 3. According to Coulomb's law of friction, the shear stress required to set a solid in motion is proportional to normal stress. At the slipping threshold, this stress defines the shear strength between the solid and the surface such that:

$$\tan\varphi = \frac{\tau}{\sigma} = \frac{T}{N} \qquad [2.1]$$

where $\varphi$ is the angle of friction, $N$ and $T$ are the normal and tangential forces at the shear surface, $\sigma$ and $\tau$ are normal and shear stresses (compression and shear respectively).

This is the angle of friction that will appear in the model. However, for a dry stone wall, the contact surfaces of blocks are not smooth and the arrangement of stones is not regular – this will be discussed in Chapter 3.

Studies on the mechanical behavior of dry masonry or mortar joints, conducted on shear boxes, are detailed in [RAF 00, VAS 05], including the link between displacement and shear stresses. However, here we will build on the work of [VIL 04] and [COL 09], who carried out a simplified study that only takes the extent of the angle of friction (yield) into account, without reliable measurement of displacement. We will see in Chapter 3 that this gives a sufficiently realistic feature to be used for designing.

This also gives a simplified characterization of block on block friction with simple shear boxes used in geotechnical engineering, called Casagrande boxes 6 × 6 cm and 30 × 30 cm on cut stone samples. A Casagrande box (Figure 2.2) is made of two half-boxes, the upper half-box is fixed while the other box can move horizontally relative to the former. For a shear test, a stone sample is placed in each of the half-boxes, then a confining pressure is applied to the upper half-box. We can then impose displacement of the lower half-box and gradually measure the tangential force generated by the upper

half-box as the lower half-box advances. Yield through shearing occurs when the shear stress reaches a maximum (peak) or a plateau. By performing several tests on identical samples with different confinement pressures, a point by point Coulomb plot can be made (Figure 2.3(b)).

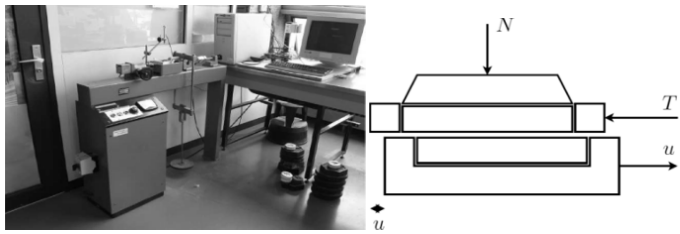


**Figure 2.2.** *Direct shear test on a Casagrande box a);and diagram of the principle b) (Photo and drawing by Anne-Sophie Colas)*

In theory, Coulomb's law does not depend on confinement, however it is best to carry out the tests in a confined value that corresponds to the level of stress actually encountered *in situ*. For a 2.5 m high retaining wall, assuming linear stress distribution on a horizontal section of the wall, the normal stress exerted by a wall (that is backfilled to its full height) on its foundation stones will be about 120 kPa.

Here, we present the results of tests carried out by [COL 09] on granite (Figure 2.4). By studying the evolution of tangential stress versus displacement $u$ (Figure 2.3(a)), we see that the four curves show similar behavior. The tangential forces increase rapidly until a displacement plateau between 0.5 and 1 mm. We note that this level of shear increases substantially at the end of the experiment. We can explain this phenomenon by assuming that, given the offset of the two boxes at the end of the experiment, there is a slight rotation of samples, which distorts measurements. Therefore, we choose to keep the beginning of the plateau as the tangential stress maximum.

For each test, normal and maximum tangential stress pairs are placed in the Mohr plane (Figure 2.3(b)). A Coulomb plot is obtained by linear regression. The angle of block on block friction is obtained using equation [2.1]:

$$\tau = 0.52\ \sigma \Leftrightarrow \varphi = 27° \qquad [2.2]$$

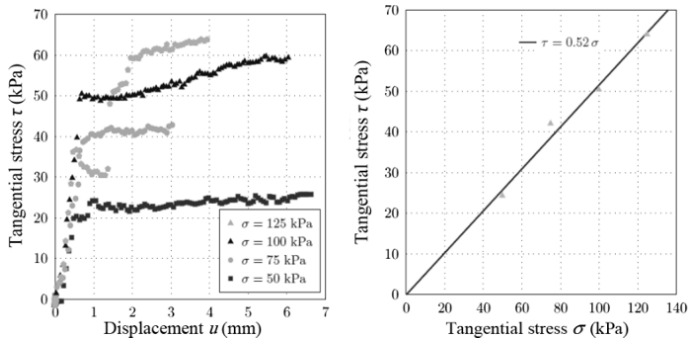


**Figure 2.3.** *Direct shear tests on granite samples [COL 09]*

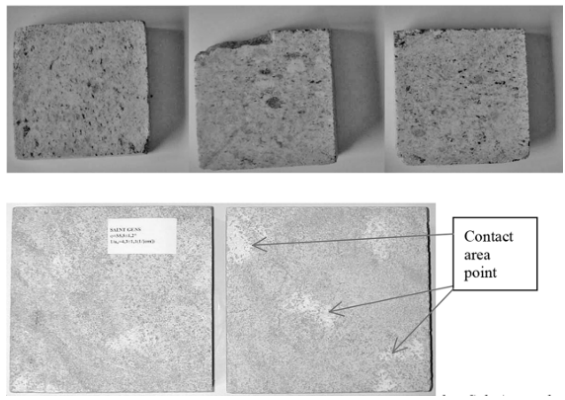


**Figure 2.4.** *Granite samples, 6 × 6 × 1 cm (top, photo Anne-Sophie Colas); molasse, 30 × 30 × 10 cm for Casagrande box tests (photo Boris Villemus)*

Let us note that we have chosen, based on the study [VIL 04], to impose a cohesion of zero. Without this condition, the angle of friction is φ = 26.5° and cohesion c = 0.6 kPa with:

$$\sigma = \tau . \tan \varphi + c \qquad [2.3]$$

Shear box tests showed that friction obeys Coulomb's law, meaning that friction is proportional to normal stress with a proportionality coefficient (angle of friction) that is not dependent of the contact surface at the joint. The tests also showed that despite the smoothness of joints, contact is localized to one, two or three areas of weak surface (Figure 2.4).

They also showed a bias due to the shearing device: the upper half-box rotates the lower half-box before reaching the slipping plateau level. Thus we obtain curves T = f(u) with a slope that corresponds to the bias of the device and not to shear stiffness Ks.

We have seen that [VIL 04] also measured the angle of block on block friction by a test on an inclined plane (Figure 2.5). The test consists of fixing a block of stone onto a plane that is connected to a pivot at one end. We then place a second block of stone on top of this first block and tilt the plane until the upper block slides: the angle made with the horizontal plane provides an estimate of the angle of friction. This test may be particularly interesting for practical use *in situ*, due to its ease of implementation and analysis.

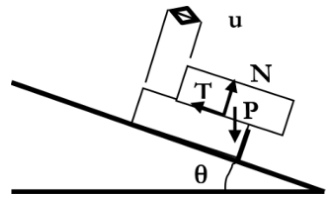


**Figure 2.5.** *Principle of the inclined plane test, P is the weight of the stone, N is the normal reaction and T the tangential reaction*

| Nature of stones | 6 × 6 cm box | 30 ×30 cm box | Inclined plane |
|---|---|---|---|
| Molasse from Vaucluse | 37 ± 1 | 35.5 ± 1.5 | |
| Molasse from St. Gens, Vaucluse | 36 ± 1 | 35.5 ± 1.5 | 38 ± 2 |
| Limestone from Vers | 35 ± 0.5 | 34 ± 1 | |
| Limestone from Espeil | | 37 ± 1 | |
| Hard limestone, Hautes-Alpes | | 26 ± 3 | |
| Limestone from Estaillades | 34 ± 1 | 34 ± 2 | |
| Limestone, Lozère | 35 ± 3 | | |
| Shale 1 | 28.5 ± 1 | | |
| Shale 2 | 25 | | |
| Granite | 27 | | |

**Table 2.2.** *Value of the angle of interface friction $\varphi_M$ depending on the type of interface of the shear test on cut stones*

In Table 2.2, we present a summary of tests done on cut stones. Despite the hardiness of tests, we found similar results for the three procedures. The inclined plane test overestimated the angle of friction by 2 degrees. Table 2.2 also gives the orders of magnitude of friction for different types of stones.

We consider here the angles of friction obtained by the Casagrande box and we will see in Chapter 3 that they can be used in design calculations. However, we must bear uncertainties about the influence of confinement and macro-roughness of blocks on the angle of friction in mind; this point will be discussed in Chapter 3.

## 2.2. Earth

### 2.2.1. *Geological and geotechnical considerations*

Unlike stone, which is directly taken from the bedrock and falls completely within the scope of geology, earth forms a part of regolith, which is outside the scope of geologists. The term regolith means the space between the soil that is enriched with organic matter (arable land or soil) and the bedrock. We should be able to distinguish between the layers, which have different names from one specialty to another (geotechnician, geologist, archaeologist, soil scientist), and which cover different things. To the geologist, the soil cover is something that hides what he wants to see, something valuable. The soil scientist distinguishes between rock (solid or soft), alluvium and colluvium, soil made from the weathering of bedrock and topsoil. We will discuss this material from the geotechnician's point of view in order to take his implementation into account, which arises from actual geotechnical techniques.

### 2.2.2. *Supply of earth*

Road grading work also generates a large amount of earth that can be used as a building material. However, this requires cooperation and organization from the developer.

The renovation of a building can provide reusable earth especially if openings are made. Unlike stone, there is virtually no waste recovery; a block of broken adobe will be as good as new after rewetting and molding.

We will discuss here the two main families of implementation of the material: the "dry" way, by compacting, and the "wet" way, by molding or shaping.

### 2.2.3. *Manufacturing of material by compaction (dry)*

Compaction has been studied for a long time [PRO 33]. The laboratory compaction geotechnical test is the Proctor test, used in the 20th century for granular soils (without clay). However, heterogeneity of the sample obtained by this procedure with a clay-like soil, makes it difficult to be used for specific laboratory studies.

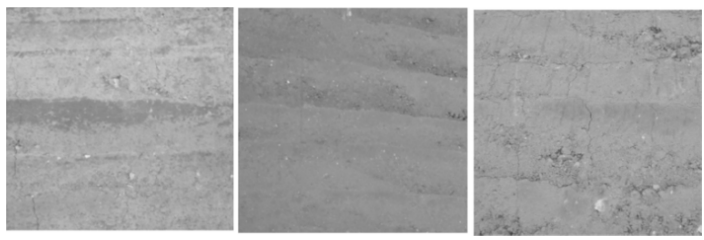

**Figure 2.6.** *Increasing density from bottom to top, for three modern rammed earth walls manufactured by Nicolas Meunier Ltd.*

Other tests have been developed [OLI 86,VEN 93, MOU 93] where compaction is quasi-static with a steady increase in axial compressive stress, as opposed to the dynamic compaction of the Proctor test. This test is closer to what happens during the manufacturing of blocks for use in construction.

In this section, we will use the static compaction test (SCT) to explain the process of manufacturing the "compacted earth" material in the form of blocks. All principles mentioned in this section are also applicable to rammed earth. In each layer of rammed earth, the dry density decreases from bottom to top (Figure 2.6). A layer of rammed earth can be compared to a bed of earth block masonry.

#### 2.2.3.1. *Manufacturing of earth blocks by compaction*

Firstly, it is important to know the different types of presses that exist for making blocks of compacted earth. The size of blocks is very variable; we use a common block size of $90 \times 140 \times 290$ mm$^3$.

Hydraulic presses allow us to apply a compaction stress of generally about 5 to 10 MPa, but may go up to 20 MPa for hyper-compressed blocks. These block presses are monitored by stresses, with hydraulic rams and thus compaction stress is known.

Mechanical presses impose the same compaction stresses as hydraulic presses. They are obtained by moving a piston through an imposed stroke. These presses are driven by displacement to obtain a fixed final volume. If the amount of earth in the mold is too much, there is a limitation on stress through a buffer system (springs) to avoid overloading the equipment, but unlike hydraulic presses, the stress limit is not known.

Finally, manual presses generally apply stresses of about 2 MPa. Compaction stress depends on the strength that the operator applies and will determine the maximum stress of compaction, if the press is properly used, that is, if enough soil is put in to completely fill the mold.

2.2.3.2. *Optimization of the material with the block press*

Proctor compaction test behavior shows that for a given compaction energy, there is a so-called "optimal" moisture level that allows us to obtain the maximum dry weight, which is a desired objective as it allows us to get the maximum strength at the given compaction energy. However, hydraulic presses set a compaction energy (through static compression stress) while mechanical presses are used to impose a final wet volume weight. Research into optimization of blocks' manufacture is therefore:

– for hydraulic presses: to investigate the (optimal) water content to obtain a static compaction stress giving the maximum dry density;

– for mechanical presses: to seek the optimal pair (wet weight of soil to place in the mold and water content) without exceeding the compression feasibility of the press, which is more delicate.

For this optimization phase, laboratory tests based on the SCT are a good approach. For convenience in the laboratory and accuracy reasons, we may also want to optimize this: the block press is not always available and sufficient quantities of samples are not always there. We can then use the SCT to find the optimum water content for a press and a given material. Let us first present the SCT.

2.2.3.3. *Static compaction test (SCT)*

The oedometric mold presented by [OLI 86] (Figure 2.7) is used to produce cylindrical samples under an axial stress that can vary from 0 to 10 MPa. It consists of two half-shells fixed to an outer axis and two pistons: lower (fixed) and upper (mobile). This mold can be displaced along its axis independently of the two pistons for symmetrical compacting relative to the median horizontal plane, and spread the friction between the material and the mold sides along the height of the sample. The reduction in static force imposed between the ends and the middle is approximately half of that between the top and bottom for a conventional compression from the top.

The parameters measured during a SCT are:

– axial stress $\sigma_{1h}$, issued by the press, applied to the top of the sample;

– axial stress $\sigma_{1b}$, measured by the fixed piston of the mold at the bottom of the sample;

– radial stress $\sigma_3$;

– vertical stacking of the sample $\Delta h = h_0 - h$ (radial strain $\varepsilon_3 = 0$, since this is an oedometric test), where $h_0$ = initial height of the sample corresponding to the height of the mold initially filled with excess material, $h$ = height of the sample at time "$t$".

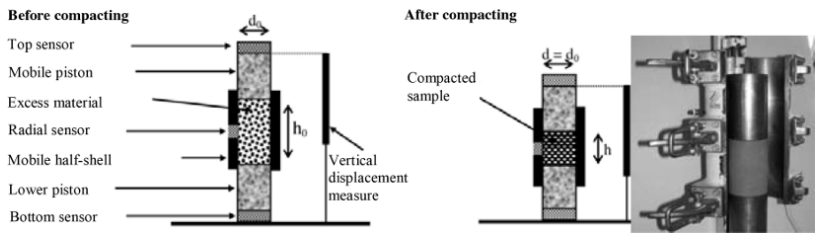


**Figure 2.7.** *Static compaction test (SCT) device, diagram (left) and photo drawing and photo: Ali Mesbah*

2.2.3.4. *Selection and characterization of the material: procedure*

Soils used as an earth construction material must contain a minimum of a few percent by weight of clay, and should not contain more than 10 or 20 mm grains, depending on the thickness of the blocks, which can vary from approximately 40 to 150 mm. For rammed earth, the space between two formworks varies between 30 and 50 cm (height of layers around 10 cm),

which allows the use of larger pebbles up to several kilograms in weight. However, we can sieve the soil to eliminate the large elements and get a finer material. A large quantity of this material is available on the planet, but depending on the type of soil used, it will have very different mechanical properties [OLI 94, WAL 96].

The material presented here must be considered as an example – it is not a "standard". It is defined in Table 2.3. The standard Proctor test is given in Figure 2.8: there is an optimum water content for a standard Proctor energy which is a dynamic compaction energy of SPE = 550 kJ/m$^3$, of 13.8%.

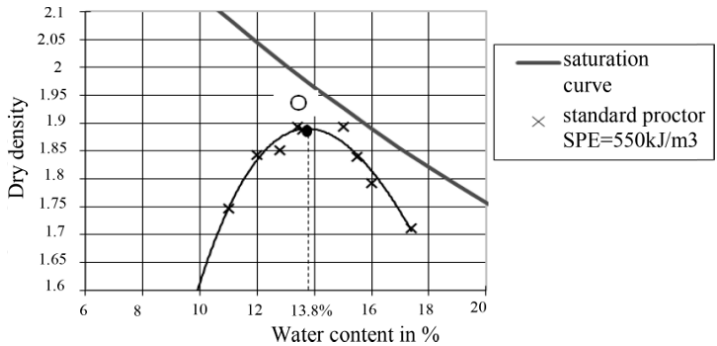


**Figure 2.8.** *Optimization of water content by Proctor test, SPE = Standard Proctor Energy*

For a compaction test, such as the Proctor test, soil is placed directly into the mold so that it is in contact with the steel walls. The "friction" surface corresponds to the lateral surface on which energy dissipation is created through friction during the movement of soil against the sides of the mold. At a given height h, friction losses are reduced when the diameter of the sample increases.

The amount of earth introduced into the mold is weighed to get a final aspect ratio after compaction between 1.4 and 1.6, or samples that are 112 mm in diameter and 160 to 180 mm in height. The samples are of small aspect ratio h/d to avoid having a large density gradient between the ends and the center. Blocks have an even smaller aspect ratio. The difference in dry density of the sample, measured by gamma densitometry, does not exceed 1% in the case of double compaction.

| Sand 10 mm–0.080 mm | Silt 0.080 mm–0.002 mm | Clay <0.002 mm | Liquid limit | Plasticity limit | Plasticity index | Methylene blue value of soil | Specific density |
|---|---|---|---|---|---|---|---|
| 36% | 52% | 12% | 31% | 21% | 12% | 1.3 | 2.71 |

**Table 2.3.** *Identification and composition of soil used in sections 2.2 and 2.3*

For manufacturing blocks, the $R_{s/v} = S_c/v$ ratio – contact area over compacted soil volume – is around 20 $m^{-1}$; for the cylindrical sample, it is around 36 $m^{-1}$. In both cases, the ratio of the contact area prior to compaction over the contact area after compaction is around 1.8.

[VEN 93] chose a static compaction laboratory test with set displacement to get a constant volume (final volume of the block) in order to be consistent with what happens in this type of block press. In this case, $R_{s/v} = 19$ $m^{-1}$ for the blocks and $R_{s/v} = 53$ $m^{-1}$ for laboratory samples. Friction has already been indirectly correlated with the size of the mold used in compaction since there is a dissipation of frictional energy of 30% in laboratory tests with respect to the block press. It is therefore necessary to use laboratory samples with an $R_{s/v}$ ratio that is as close as possible to that of blocks. For the SCT presented here with $R_{s/v} = 36$ $m^{-1}$instead of 20 for blocks, we will have increased compaction energy dissipation for cylindrical samples than for blocks.

Furthermore, by modifying the device, we can compress the top part and keep the base, which is no longer subjected to the same forces as the SCT, fixed; friction is evaluated through a differential measurement of the force between the top and the bottom of the sample. The energy dissipated through friction may result in a 50% decrease in compaction force at the base of the sample for old steel molds, and almost zero if the steel surface is new.

2.2.3.5. *Using the SCT for laboratory studies*

This is to manufacture cylindrical samples that have the same characteristics as blocks. In Chapter 3 (about blocks), we will consider the difficulty of finding procedures for laboratory testing of the strength of blocks themselves.

We have seen that the manufacturing simulation is correct if we assume that the friction on the sides of the mold during compaction is similar to that

of blocks or cylinders, because the friction surface ratio (=lateral surface) over volume is very similar in both cases. The surface of the mold must also be the same in both cases, which will depend on the level of attrition of the apparatus and will be variable with time.

Moreover, whatever the friction, we will get a similar decrease in density in the vertical direction (compaction), from the ends to the center of the sample, for blocks manufactured by a double compaction block press and cylindrical samples.

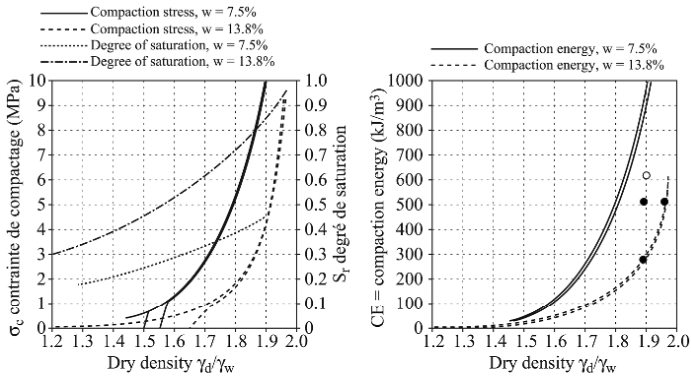


**Figure 2.9.** *Relationship between compaction stress a); energy absorbed by the densification of the material depending on the dry density b), $w_f$ = manufacturing water content (earth identified in Table 2.3)*

In Chapter 3, we will see that the dry density of the sample determines its mechanical behavior. We can easily measure the manufacturing water content of blocks and therefore calculate their dry density, knowing the volume. We consider that the laboratory sample obtained using SCT is representative of blocks obtained by a block press, if we get the same dry density for the same water content. This determines an equivalence between the static compaction stresses of SCT and the block press. To determine the equivalent stress, an SCT is done on the material until a sufficiently high (maximum stress of 10 MPa) compaction stress ($\sigma$c). Figure 2.9(a) is obtained for two water contents, $w$ = 7.5% and 13.8%. For each pair (dry density, water content), there is a corresponding static compaction stress $\sigma c$ (Figure 2.9(a)). For example, for blocks $\gamma_d/\gamma_w$ =1.9 manufactured with a water content of 13.8%, we refer to Figure 2.9(a) for $w$ = 13.8% and $\gamma_d/\gamma_w$ = 1.9 and we get $\sigma c$ = 4.3 MPa. Thus, by carrying out a static compression test up

to a stress of 4.3 MPa, we get a cylindrical dry density sample of 1.9 that is representative of the block. Instead of testing the blocks, it is then possible to test cylindrical samples.

2.2.3.6. *Optimization of manufacturing water content by SCT*

The energy spent during compaction is the parameter used to set the intensity of dynamic compaction in the Proctor test. Usually two intensities are used (Standard Proctor Energy SPE = 550 kJ/m$^3$and Modified Proctor Energy MPE = 2430 kJ/m$^3$), which are geotechnical engineering reference values. But the Proctor test principle can be used with other compaction energies: the number of strokes just needs to be changed. The energy in the SCT can then be compared to the energy spent during the Proctor test.

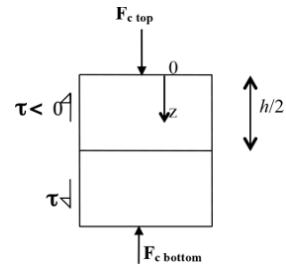


**Figure 2.10.** *Principle of static compaction test (SCT) Fcbottom is simplified in Fc*

For an SCT, the energy supplied per unit volume is (Figure 2.10):

$$E_{SCT} = \frac{F_{cb}\Delta h}{volume} \qquad [2.4]$$

where $F_{cb}$ is the compaction force measured by the sensor located beneath the fixed piston at the base of the sample.

$E_{SCT}$ does not include the energy provided by the press, which may be dissipated in friction and in any pressurized water.

However, this is not exactly the energy stored in the form of compaction by the sample. It is $E_{comp}$ energy per unit volume:

$$E_{comp} = \int_0^h F_z \varepsilon_z dz \times \frac{1}{volume} \qquad [2.5]$$

where *dz* being the compaction of the sample at any point thereof, we get:

$$\int_0^h \varepsilon_z dz = \Delta h \qquad [2.6]$$

and:

$$F_z = F_c + \int_0^z \tau dS \qquad [2.7]$$

with algebraic $\tau$, soil-wall friction stress, we obtain: $E_{SCT}$ is close to $E_{comp}$ if friction is negligible.

Static compaction was done with a load path of $\Delta F_{cb}/\Delta t$ = 0.5 kN/s or a stress rate of 0.05 MPa/s up to 10 MPa. Figures 2.10(a) and (b) compare, for the same material described in Table 2.3 for the two previous water contents, the degree of saturation, the stress and the compaction energy ($E_{SCT}$) depending on the dry density.

Stress is calculated as:

$$\sigma_c = \frac{F_{cb}}{S} \qquad [2.8]$$

The degree of saturation is calculated from:

$$S_r = \frac{\gamma_s}{\gamma_w} \times \frac{w}{\frac{\gamma_s}{\gamma_d} - 1} \qquad [2.9]$$

with $w = \frac{W_{water}}{W_{dry}}$ and $W_{water}$ = weight of water and $W_{dry}$ = weight of dry sample.

We find a classical result: the wettest material (w = 13.8% versus 7.5%) needs a lot less energy to achieve the same dry density, which emphasizes the lubricant role of water.

It is interesting to determine the equivalent energy for the Proctor dynamic compaction. If we consider the standard Proctor test energy $E_{SP}$, we

obtain two test results for the two water contents: $E_{SP}$ = 550 kJ/m$^3$ for w = 13.8% and $\gamma_d/\gamma_w$ = 1.89 (point O, Figure 2.9(b)).

These values are to be compared with the results of static compaction:

$E_{SCT} = E_{SP}$ for w = 13.8% and $\gamma_d/\gamma_w$ =1.96 (point A)

$E_{SCT}$ = 300 kJ/m$^3$ <$E_{SP}$ for w = 13.8% and $\gamma_d/\gamma_w$ = 1.89 (point B)

We defined the points A, B, O in Table 2.4 and Figures 2.9 and 2.11. The energy dissipated during the Proctor test outside of the sample (in the vibrations of the frame, friction against the walls of the mold) is 250 kJ/m$^3$(energy difference of points O and B) or 45% of the total energy that is not used for compaction. This difference justifies the use of (non-vibrating) static compaction machines for these materials.

| Definitions | w: water content (%) | $\gamma_d/\gamma_w$: dry density | Energy (kJ/m$^3$) |
|---|---|---|---|
| O: Optimum standard Proctor | 13.8 | 1.89 | 550 issued |
| A: static compaction | 13.8 | 1.96 | 550 provided |
| B: static compaction | 13.8 | 1.89 | 300 provided |

**Table 2.4.** *Identification of points A, B and O (earth identified in Table 2.3)*

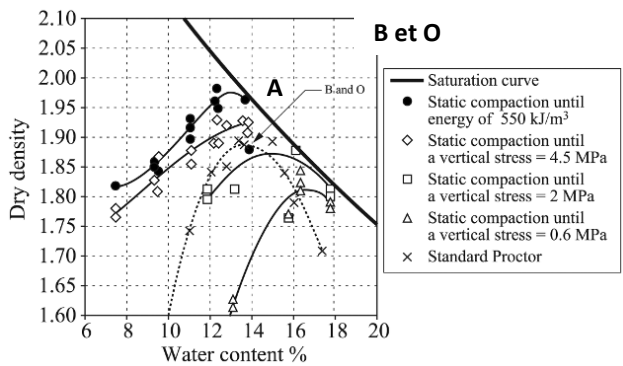


**Figure 2.11.** *Tests for optimization of water content (earth described in Table 2.3)*

There are large differences in behavior during compaction between a material containing clay and powdery material. Clay soil will be very sensitive to water and will have a very different internal and interface friction behavior (on the mold sides in the Proctor test, for example) compared to powdery soil.

We verify that, when approaching saturation ($S_r$ > 90%), the dry density tends to a limit as energy increases: when air bubbles have disappeared (or are under high pressure), density barely varies, the saturation is reached and swelling may occur.

Figure 2.12 shows the relationship between stress and energy. For relatively dry soil (w = 7.5%), the relationship is linear up to a stress of 10 MPa.

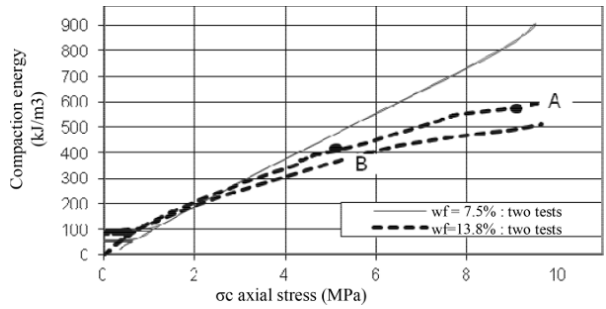


**Figure 2.12.** *Relationship between stress and compaction energy (earth identified in Table 2.3)*

In the case of "wet" material w = 13.8%, the $E_{SCT}$–σc relationship (Figure 2.12) is no longer linear; we cannot use the stress-compaction energy equivalence. However, we may consider this relationship linear, as the compaction stress is less than 3 MPa for w = 13.8%. Beyond this level, compacting "wet" soil consumes less energy relative to compacting a drier soil. This is explained by the fact that the dissipation by friction of dry soil is more significant (internal friction within the material and between the mold and the sample).

For mechanical or manual block presses, we must find the applied stress in order to perform the optimization procedure with an SCT. This stress can be directly measured by a force sensor placed in the same position as the block, or indirectly, for example, by the procedure described above. However, in both cases, this measurement is difficult.

For different types of block presses, it is possible to optimize the manufacturing process (finding the optimum water content) through SCT, but this implies that the rate of compaction does not affect the final result.

We must have a laboratory compaction test to get at least the applied compaction stress and not just energy. In this case, we seek the dry density of the blocks according to their manufacturing water content for a given press, i.e. for a given energy or compaction stress.

2.2.3.7. *The role of water during compaction*

A material is compacted from a bulk state with a certain water content. During compaction, the material passes from an unsaturated state to, in extreme cases, a saturated state.

During the SCT, the material is compacted for a few seconds so the water does not have time to escape. The mass water content $w$ does not change but the degree of saturation will change as well as the volumetric water content. Suction will therefore also vary.

Without measuring suction during compaction, it is possible to obtain an estimation of the variation of suction depending on the degree of saturation. Figure 2.13 was obtained by measuring the suction (filter paper and desiccator method) on samples that were statically compacted then dried in order to get the desired water content. From this water content, we calculate the degree of saturation.

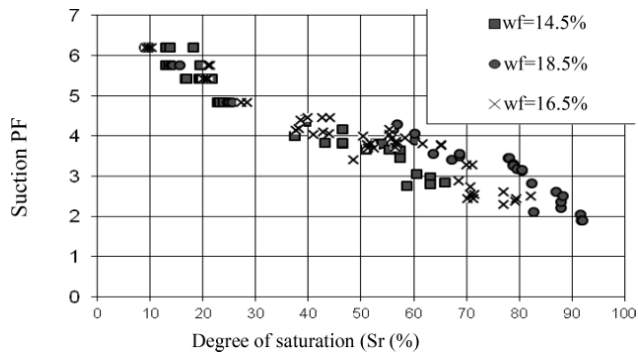


**Figure 2.13.** *Variation of suction depending on the degree of saturation, by drainage (drying) after the compaction operation for a water content of $w_f$ (earth identified in Table 2.3)*

If we consider that the "history" of the material begins at the end of compaction, knowledge of the stress tensor at that time may be useful for determining an accurate behavior of the material.

### 2.2.4. *Implementation of earth in plastic state (wet)*

We just discussed the case of compacted earth, including compressed earth blocks (CEB) and rammed earth, for which the literature is now more abundant and older than any other construction technique using earth. CEB and rammed earth are implemented dry (mass water content <20%). This leaves us to now examine the other "wet" way, which includes adobe and cob. We will see that the border between the two channels is progressive, although for convenience, we can set a transitional value of 20%. However, adobes are often composed of a material containing more clay than rammed earth or CEB. Adobes are manufactured in a plastic state (mass water content > 20%). Many types of earth contain more than 20% clay and were used for the construction of the first cities of Mesopotamia and Egypt nearly five thousand years ago. Thus, earth is probably one of the oldest construction materials. Adobe was also used in the Hadramout valley in Yemen for building eight floor houses. We will first describe the traditional way and the modern process of developing adobes. In the book [DEC 11], much scientific information on adobes can be found.

#### 2.2.4.1. *Manufacturing samples of blocks*

By way of example, here we use earth from the village of Rochechinard in the lower valley of the Isère (Hostun, France). Figure 2.14 gives its granulometric curve. Its geotechnical properties are: liquid limit of 38%, plastic limit of 20%, plasticity index of 18%, methylene blue value of 2.5 and clay activity of about 10. Kaolinite clay forms the majority and smectite the minority.

The traditional technique for producing molded adobe requires a water content that is generally greater than 20% ("wet"). Adobes are made in molds of wood or metal and sun-dried on the ground after removal from the mold. Their method for shaping requires preparation in the plastic state, therefore a high manufacturing water content (earth). However, this preparation should have enough consistency not to flow under its own weight. To our knowledge, there are no methods in the literature for determining this water content, but in general, adobes are made at sites with water contents near the plasticity limit.

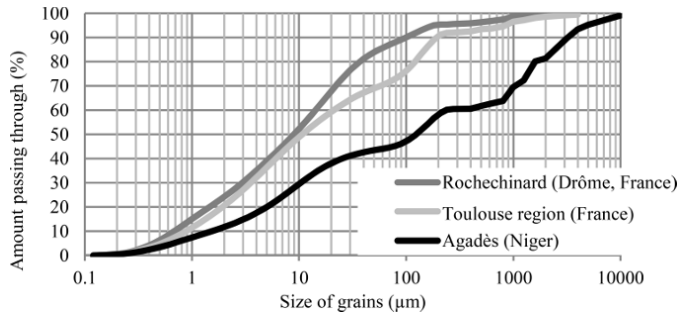


**Figure 2.14.** *Granulometric curves of three types of adobe earth used*

For the production of adobes presented here, Rochechinard earth is mixed at different water contents. The first manufacturing water content was arbitrarily selected at 24%, a value close to the plasticity limit, then it was lowered for the other samples. This earth is mixed until a visibly homogenous mixture is acquired. Then this homogeneous earth–water mixture is poured into a wooden mold (of dimensions $310 \times 152 \times 71$ mm$^3$) on the ground. Using hands or fists, this mixture is compacted or molded into the corners and the surplus is removed with a wooden ruler. Finally, the adobes are dried at room temperature in the laboratory until they reach a constant weight (about 3 weeks). During this period, they are frequently turned.

It is possible to make blocks with a lower water content, but their shaping cannot be done manually. Indeed, the earth–water mixtures used for making adobes have an higher consistency with decreasing water content. Molding becomes difficult. It was also necessary to do the compaction with a manual block press, used for the production of CEB.

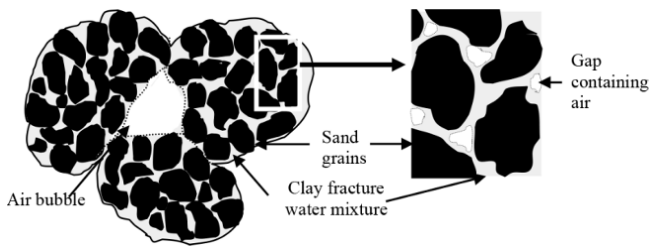


**Figure 2.15.** *Different fractions contained in the adobe during its manufacture*

Mechanical compaction is used not only to facilitate the shaping of blocks, but also to evacuate air bubbles trapped inside the wet mixture (Figure 2.15). In this respect, it is similar to extrusion. To differentiate these blocks from conventional CEB, with low water content (around 13%), we propose to call this wetter paste element "pressed blocks" (PB).

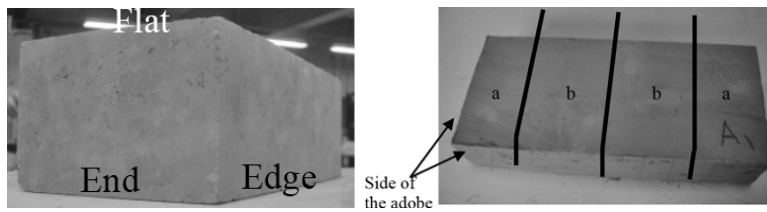


**Figure 2.16.** *PB on the left; adobe before being cut into four on the right*

After mixing and kneading, a mass of 8.7 kg of earth–water mixture is introduced into the press mold, of dimension 295 × 140 × 95 mm$^3$. This quantity is determined by gradually varying the molded mass until the surface of the block no longer presents manufacturing defects due to inadequate quantities of earth–water in the mold. After pressing and removal from the mold, the blocks obtained (Figure 2.16) are dried as adobes at laboratory room temperature.

2.2.4.2. *Influence of the sample preparation method on their dry density*

To assess the influence of the two block-shaping methods, we measured the manufacturing water content of the adobes and PBs, as well as their dry density.

The dry density has a direct influence on the compressive strength, hence it is a parameter to be checked in the quality control process. It is calculated based on the change in mass of the samples after desiccation in an oven at 105°C until constant mass. The temperature of the oven may also be 50°C, which will change the value of water content; this latter value being better suited to earth construction water content definition. Adobes were cut (Figure 2.16) in order to get samples with an aspect ratio of 2, and reduce the risk of confinement due to friction on the side of the mold during the compression test (see Chapter 3). PB, in turn, are tested uncut.

For adobes, Figure 2.17 shows that the dry density of adobe samples (samples *a* and *b*) vary greatly from one sample to another, within the same

unit, although it has been manufactured with the same earth–water mixture and dried under the same conditions. The adobes are therefore not homogeneous. This disparity is partly due to manual molding, which becomes increasingly difficult with a less wet earth–water mixture (Figure 2.17). Dry density values are more dispersed with decreasing water content of the mix, which results in the enlarged scattering of points toward the left. The dry density values of samples *a* and *b* become less heterogeneous with increasing water content. This regularity is much better for test sample *b* that is cut in the middle part of adobes. Indeed, 20% of the surface of sample *b* is in contact with the mold throughout manufacture, while this figure is 40% for sample *a* (Figure 2.16). Thus, the molding and demolding procedures are less harmful for sample *b* than for sample *a*, because the friction and adhesion of the wet mixture to the mold walls generate defects on the surface of the blocks. The material composing the adobe appears heterogeneous and is therefore difficult to study.

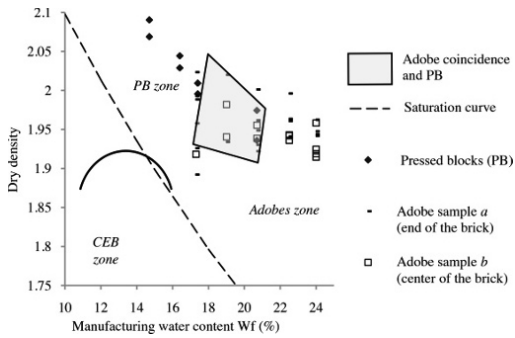


**Figure 2.17.** *Dry density depending on the manufacturing water content*

For PB, Figure 2.17 shows (with good correlation) that the dry density of PB increases as water content in the mix decreases. Thus, the process of making PB would allow the production of more homogeneous blocks. However, when the water content in the mix is further reduced (by 14–15%), the PB become heterogeneous and it is not possible to produce them with a lower value than this. This heterogeneity can be explained by the difficulty of mixing earth–water. The quantity of water in the mix is not sufficient for an adequate consistency. Therefore, blocks thus obtained have a structure formed by irregular aggregates, which weakens them and prevents their study as a homogeneous material. The critical amount of water that leads to this structure is approximately 15% for the example of earth chosen here. This threshold varies depending on the clay content.

Let us now draw a comparison of manufacturing water contents (Wf) between adobes and other earthen blocks (CEB and PB). For the manufacture of CEB produced with a different earth that contains less clay, we get a classic bell curve on the left side of Figure 2.17. This bell curve is similar to the Proctor test curve, for which the right side approaches the saturation curve without crossing it (see section 2.2.3). For a given soil (with a clay content of about 20%, for example), it is possible that its compaction curve is intermediate between the bell curve and the Rocheninard earth curve.

Figure 2.17 can be divided into three areas: the area of the adobe, the area of PB and the CEB area. The separation between each area is not abrupt. Passing from the adobe area to the PB area is accompanied by an increase in dry density caused by the use of a mechanical densification process: compaction or extrusion. However, this PB increase in density with decreasing water content of the mix is also due to shrinkage during drying. Clay minerals have the ability to adsorb water and swell [VAN 13]. The greater the amount of water applied to the soil, the greater the adsorbed water layer and the greater the volume of the earth (Figure 2.18). Thus, when water content in the mix is high, compaction, which has effect of bringing grains closer to each other, is not efficient because part of the compaction energy is dissipated by the pressurization of water. The volume taken by water is high, then when drying, the voids are high too, leading to low dry density value. However, when the quantity of water in the mix is low, the compaction energy is entirely used to force the grains closer to each other, wherefrom the high density value.

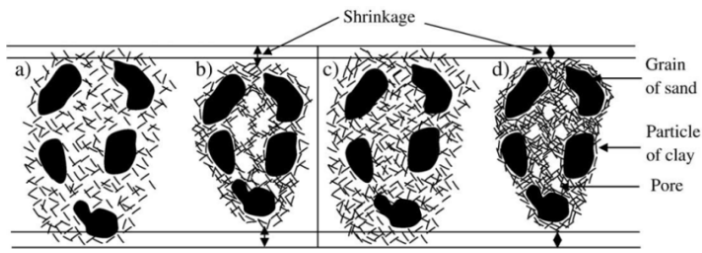


**Figure 2.18.** *Diagram of the structure of the material during drying. The material in the wet state: a) $W_f$ = 20%; b) $W_f$ = 20%, predominance of macropores; c) $W_f$ = 16%, the clay particles are closer together. Material after drying, appearance of macro and micropores; d) $W_f$ = 16% predominance of micropores*

A block with a high $W_f$ value will shrink and exhibit more significant porosity (Figure 2.18), and its dry density will be lower (Figure 2.18(b)).

That is why PB and adobe points are above the saturation of Rochechinard earth (Figure 2.17), which does not happen in the case of CEB with a bell curve (while the shrinkage is negligible). Moreover, the increasing gap between the points and the saturation line, as the manufacturing water content increases, confirms this influence of shrinkage during drying.

Furthermore, we propose to continuously classify the techniques used today for the production of earth blocks depending on the manufacturing water content ($W_f$) in two ways: dry (8% <Wf<20%) and wet (20% <Wf<35%). The dry method is that of CEB or rammed earth while wet includes adobe, earth and straw mortar, and cob. The method developed by "extrusio-compaction" of PB is classified in the hinge between the two channels (semi-dry, semi-wet), as seen in Figure 2.17. Thus, the progressive decrease of water content in the mix from the liquid limit leads to the determination of the best suited technique for the densification of a given earth (without added stabilizer or modification of the soil texture).

The comparison of manufacturing water contents of CEB, PB and adobes shows that these earth shaping processes are categorized into dry (CEB, rammed earth) and wet (adobe, clay and straw mortar). Moreover, for a given soil, an "ideal" technique leads to the highest dry density and so greatest compressive strength.

### 2.2.5. *Physicochemical considerations*

The cohesion of earth structures begins in the capillary and electrostatic forces acting within the clay. Capillary forces are well-known to all since it is they who hold sand castles up. They are apprehended by the mechanics of soils by the concept of suction used in the mechanics of unsaturated soils [OLI 95]. Electrostatic forces are variable depending on the mineralogy of clays, in particular in two main families of clays: kaolinites and chlorites on one side, and smectites and illites on the other. To further explore these ideas, the reader can consult the work of [VAN 13].

## 2.3. Measurement of dry density

### 2.3.1. *Hydrostatic weighing*

The hydrostatic weighing method is used to measure the dry density of material when it is not possible to get the accurate volume of the sample by

measuring its dimensions. This applies to stone and earth which, as we have seen, are not standard materials when it comes to their composition and also the size of blocks (the latter is discussed in Chapter 3). Moreover, it is often easier to take a sample of material by breaking a piece of a wall or a block than to get a complete block or wall.

Hydrostatic weighing involves weighing the same sample in air and then plunged into a water bath (Figure 2.19). Based on the Archimedes principle, we know that the apparent weight (weight of the material sample when immersed in water) $P^{(w)}_e$ is equal to the weight of the measured dry material, $P_e$, from which Archimedes thrust $P_a$ (which is itself equal to the product of the unit weight of water $\gamma_w$ and sample volume $V_e$) is subtracted.

$$P_e^w = P_e - P_a = P_e - \gamma_w V_e = P_e - \gamma_w \frac{P_e}{\gamma_e} \quad [2.10]$$

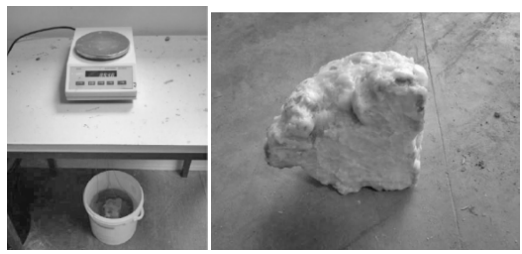

a) b)

**Figure 2.19.** *Hydrostatic weighing a), and waxed sample material b)*

We therefore deduce the unit weight of the sample:

$$\gamma_e = \gamma_w \frac{P_e}{P_e - P_e^w} \quad [2.11]$$

In Table 2.5, we present examples of measurements of three types of stone (granite, shale and limestone), several samples weighing between 100 g and 1.3 kg were thus tested.

| Type of stone | Granite | Shale | Limestone |
|---|---|---|---|
| Number of samples | 3 | 4 | 20 |
| Dry density (kN/m$^3$) | 24.9 | 26.4 | 26.0 |
| Standard deviation (kN/m$^3$) | 0.3 | 0.2 | 0.3 |

**Table 2.5.** *Example of measured unit weights of three stones*

The unit weight of the material of blocks does not directly give the unit weight of the masonry since we must consider the volume of the masonry joints. For stones, based on empiricism and measurements [VIL 04, COL 09, MUN 09], we can estimate this rate to be 25% for masonry using rubble blocks (or dry stone). For masonry using earth blocks, the average thickness of joints must be measured.

For very porous stones and earthen material, samples must first be waterproofed by dipping them in hot wax, for which the weight is known. The procedure is then identical but includes consideration of the wax coating in the calculation of the weight and volume of the sample.

In this case, it is sufficient to calculate $V_e$ by the following formula:

$$Ve = \frac{m_{sample} - m_{sample}(water)}{\rho_{water}} - \frac{m_{\text{wax}}}{\rho_{\text{wax}}} \quad [2.12]$$

with:

$m_{sample}$: mass of waxed sample (kg)

$m_{sample}(water)$: mass of waxed sample when immersed in water (kg)

$m_{\text{wax}}$: mass of wax coating the earth sample (kg)

$\rho_{wax}$: density of wax ($\rho_{\text{wax}} = 0.88 kg/m^3$)

Dry density is deduced from:

$$\rho = \frac{m_{earth}}{Ve} \quad [2.13]$$

The results are shown in Table 2.6. The values presented here are the averages of several samples tested with the method described above. For St Antoine earth, no significant difference was found between the upper and lower parts of beds (or blocks); the value shown is the average of all samples. St Antoine earth consists of a wide granular range (up to 5 cm). Therefore, it was necessary to test a larger sample (7 kg) to be as representative as possible. For other samples, measurements were carried out on samples without specifying the sample removal location.

| Origin of earth | St Antoine | Monseveroux | Lyon | Dolomieu |
|---|---|---|---|---|
| Dry density ($t/m^3$) | 1.73 | 1.62 | 1.62 | 1.91 |
| Standard deviation ($t/m^3$) | 0.04 | 0.05 | 0.07 | 0.06 |
| Porosity (%) | 35 | 39 | 39 | 28 |

**Table 2.6.** *Measurement of densities of four rammed earth from 4 sites*

### 2.3.2. *Gamma densitometer weighing*

Depending on the apparatus, samples that are up to 900 cm long, 35 cm wide and 25 cm high can be measured. The sample must have a bearing surface that is as flat as possible with surface roughness limited to a few mm high. The height depends on the measuring range of the sensor so that the height of the sample can be measured in real-time.

To calculate the apparent density, the density of solid grains of the material (which can be found with a pycnometer) and the mass absorption coefficient of the material to Cesium 137 must be known. We can estimate the coefficient depending on the chemical composition of the material, which involves a measurement method validation phase.

This device has severe limitations compared to hydrostatic weighing after wax coating of the sample, but it can measure density gradients within a layer of earth, or within a block of earth.

## 2.4. Bibliography

[AFN 06] Produits des carrières – Pierres naturelles – Prescriptions générales d'emploi des pierres naturelles, NF B10-601, July 2006.

[COL 09] COLAS A.-S., Mécanique des murs de soutènement en pierre sèche: modélisation par le calcul à la rupture et expérimentation échelle 1, Thèse de l'ENTPE-ECL, 2009.

[COU 73] COULOMB C.A., Sur une application des règles de maximis et minimis à quelques problèmes relatifs à l'architecture, Mémoire, Académie Royale des Sciences, 1773.

[DEC 11] DE CHAZELLES C.-A., KLEIN A., POUSTHOMIS N., "Echanges transdisciplinaires sur les constructions en terre crue 3, Les cultures constructives de la brique crue", *Actes de la table ronde de Toulouse*, *May 2008*, Editions de l'Espérou, 2011.

[HOU 94] HOUBEN H., GUILLAUD H., *Earth Construction: A Comprehensive Guide*, IT Publications, London, 1994.

[LOT 11] LOTI G., MECCA S., *Terra Europae, Earthen Architecture in the European Union*, EdtETS, 2011.

[MOU 93] MOUSSAI B., DIDIER G., "Etude d'un appareillage de compactage statique et de mesure de la perméabilité des sols fins argileux", *Bull. Liaison Labo. P. et Bulletin de Liaison des laboratoires des ponts et chaussées Ch.*, 188, pp. 15–22, 1993.

[MUN 09] MUNDELL C., Large scale testing of drystone retaining structures, Doctor of Philosophy (PhD) Thesis, University of Bath, 2009.

[OLI 86] OLIVIER M., MESBAH A., "Le matériau terre: Essai de compactage statique pour la fabrication de briques de terres compresses", *Bulletin de Liaison des laboratoires des ponts et chausses Bull. Liaison Labo. P. et Ch*., 146, pp. 37–43, 1986.

[OLI 94] OLIVIER M., Le matériau terre, compactage, comportement, application aux structures en bloc de terre, Thèse de 3e cycle, INSA de Lyon, 1994.

[OLI 95] OLIVIER M., MESBAH A., "Modèle de comportement pour sols compactés", *Proceedings of the First International Conference on Unsaturated Soils*, France, 6–8 September 1995.

[PRO 33] PROCTOR R.R., "Field and laboratory verification of soil suitability", *Engineering News-records*, vol. 111, no. 12, pp. 245–248, 1933.

[RAF 00] RAFFARD D., Modélisation de structures maçonnées par homogénéisation numérique non linéaire: Application aux ouvrages d'intérêt archéologique, Doctoral thesis, Institut National Polytechnique de Lorraine, 2000.

[ROC 98] PRO ROC, *Roches de France: pierres, marbres, granits, grès et autres roches ornementales et de construction*, Edition PRO ROC, 1998.

[TRA 14] TRAN V.H., VINCENS E., MOREL J.C., *et al.,* 2D-DEM modeling of the formwork removal of a rubble stone masonry bridge, Engineering Structures, 2014.

[VAS 05] VASCONCELOS G., Experimental investigations on the mechanics of stone masonry: characterization of granites and behavior of ancient masonry shear walls, Doctoral thesis, Universidade do Minho, 2005.

[VIL 04] VILLEMUS B., Etude des murs de soutènement en maçonnerie de pierres sèches, Thèse de Doctorat, ENTPE–INSA de Lyon, 2004.

[VAN 13] VAN DAMME H., "La terre un béton d'argile", *Pour la Science*, no. 423, pp. 50–57, January 2013.

[VEN 93] VENKATARAMA REDDY B.V., JAGADISH K.S., "The static compaction of soils", *Géotechnique*, vol. 43, no. 2, pp. 337–341, 1993.

[WAL 96] WALKER P., "Specification for stabilized pressed earth blocks", *Masonry international*, vol. 10, no. 1, pp. 1–6, 1996.

# 3

# Blocks: The Elements of Masonry

## 3.1 Compression of blocks of uncut stone, dry stone masonry

Compressive stresses are low in weak jointed masonry (earth or lime mortar, or dry stone), but the irregular geometry of blocks could induce stress concentrations that exceed the limits of the strength of the material. In practice, yield due to compression is observed. In this section, we will study this aspect.

### 3.1.1. *Cylindrical samples with dry joints*

To simplify the problem, first we will investigate the effect of the number of joints on the compressive strength and stiffness. The same device as for the simple compression test is used, with a cylindrical sample made of identically-sized disks stacked in two, three, four or five layers.

| Number of joints | 0 | 1 | 2 | 3 | 4 |
|---|---|---|---|---|---|
| Compressive strength (MPa) | 19 | 3 | 3.2 | 8 | 4.3 |
| Modulus E (MPa) | 14,300 | 10,200 | 9,800 | 11,300 | 8,300 |

**Table 3.1.** *Results of compression tests of cylindrical samples of molasses [VIL 04]*

The presence of joints weakens the compressive strength of the sample (Table 3.1). Yield occurs by splitting, because the joints are not perfectly flat.

*Sustainable Masonry: Stability and Behavior of Structures,*
First Edition. Thierry Ciblac and Jean-Claude Morel.

This gives us an idea of the brittleness to splitting of stones in a dry stone wall that is built with rubble stones in point contact with each other.

### 3.1.2. *Compression of rough blocks*

The test consists of compressing various rubble stones by means of a press system with a ball joint, such as those used in masonry (Figure 3.1). This test may be analogous, in the case of compact blocks, with the split test also called the Brazilian test.

As an example, we took sandstone from Luberon (France) as studied in [VIL 04]. Three series of tests were carried out for three different sizes of stones. The loading system was monitored by a displacement rate. The stones have two types of fracture behavior: one or two stages. In two stages, the first rupture occurs by bending (Figure 3.1(a)) and the second by splitting or compression (Figure 3.1(b)).

Contact areas are assessed by placing a sheet of paper between the stone and the press, in order to estimate the actual contact surface Sc of the total joint surface S. The purpose of this test is to assess limitations of the use of these stones in weak joint masonry (earth mortar, lime mortar or dry stone). However this test may underestimate the compressive strength of the same stone used within a wall. Indeed, in the least favorable scenario with dry stone (no mortar to distribute stresses), an experienced mason has to smooth coarse roughness using a hammer and wedge stones amongst each other using smaller stones or debris (see Chapter 4). These knappings should avoid flexion in stones. Some masons use sand to fill gaps and to better distribute the forces by avoiding hard spots. In the test, stones were subjected to a relatively large flexion because of the obvious non-compliance with the rules of the art of building, as defined above.

Table 3.2 gives the results of tests, on which we can comment:

– the actual measured contact surface Sc is estimated at about 5% of surface S of the stone, which is the cause of localized stresses $\sigma c$;

– because of the localization of stresses, the first yield generally occurs through bending, at a fictional averaged stress level of 800 kPa, which corresponds to a stress level of $\sigma c$ = 15 MPa for estimated contact levels. This should be compared to the average stress level of 200 kPa for a 10 m high wall under its own weight. If there is an eccentricity, this level can be doubled or tripled. This yield is not complete, and stone can support an

additional normal force until a second yield, which is the majority (crushing of the sample);

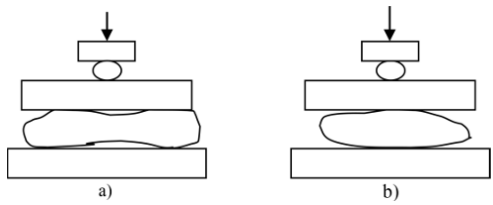


**Figure 3.1.** *Principle of the compression test on raw sandstone samples; a) failure by bending; b) failure by splitting or compression*

– the second yield occurs by crushing the stone at a fictional stress level of 1 MPa on average, which corresponds to a local stress level of $\sigma c$ = 23 MPa for estimated contact levels. This is very consistent with the simple compressive strength value Rc = 19 MPa of this stone.

[VIL 04] showed that the compressive strength of a dry stone retaining wall, that is less than 8 m high, seems sufficient in the context of a classic design and so that cracking of some stones does not change the behavior of the wall. The load bearing retaining walls are primarily stressed structures under compression and horizontal loading, which generates significant eccentricity.

| | Yield through flexion | | | Yield through compression | |
|---|---|---|---|---|---|
| | Sc/S (%) | $\sigma$ (Mpa) | $\sigma_c$ (Mpa) | $\sigma$ (Mpa) | $\sigma_c$ (Mpa) |
| Average | 4.9 | 0.81 | 15 | 1.1 | 23 |
| Standard deviation | 1.9 | 0.4 | 8.4 | 0.4 | 5.0 |

**Table 3.2.** *Compression tests of raw samples of sandstone across 17 tests*

### 3.2. Shear strength of rubble stones

In section 2.1.1, we described the interface behavior between two cut stones. We will now study uncut stones in order to qualify the effect of macro-roughness, compared to cut stones.

### 3.2.1. *Shear tests of one bed of stone on another*

To correctly find out what happens *in situ*, shear tests with a "very large" Casagrande box must be done. Large dimensions allow consideration of interactions between the stones, in particular the presence of joints as well as macro-roughness.

We use a prototype shear box of 100 × 100 cm², which was originally designed to shear household waste [ABO 99]. This size allows mounting of a bed of dry stones in the lower box, and shearing by a second bed, mounted in the top box (Figures 3.2 and 3.3).

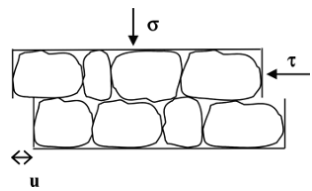


**Figure 3.2.** *Principle of interface shear between two beds of stones in a 100 cm x 100 cm box from the Joseph Fourier University of Grenoble drawing by Boris Villemus*

To completely fill the lower half-box, stones are selected to ensure relative flatness of the upper surface of the bed of stones. This surface is the closest possible to the shear plane of the box. The stones, once arranged, are blocked in place using small sharp stones (knappings), as mentioned in Figure 3.3.

For the partial filling of the upper half-box, the joints are crossed by blocking many stones against each other. Wooden knappings and fairly rigid polymer pin geomembranes are placed on top of the upper half-box to distribute the confinement over all the stones of the upper bed. This distribution of confinement is not uniform but all the stones have at least one contact point with the loading plate.

Confinement (vertical load of 30 to 130 kPa) is applied using four rams that are connected to a manometer. The speed of the horizontal ram is less than 3 mm/min. The test is performed at a defined displacement until there is a displacement of three to four centimeters per load. The friction between the two beds of stones is directly related to the construction method of the sample. We chose to keep the same sample for the four shear tests with increasing confinement. Between loads, the sample is "deconfined" to unblock the stones. This procedure changes the displacement response,

because after the first load, we do not have the necessary displacement to set stones in relation to the horizontal shear stress. However, this has no impact on the calculation of cohesion and angle of friction parameters c and φ.

During the test, we can sometimes hear stones cracking especially under highest level of confinement. After opening the cover, two to three stones of the upper bed were broken in two (out of a total of 13 stones), and five to six of the lower bed (from a total of 13 stones).

After a test, the surface of stones is damaged, including the creation of sand from friction, broken angles, crushing of knapping.

To exploit the results, a correction of the shear surface is applied depending on the displacement. Parasitic friction forces of the box were calibrated and removed from the measured forces.

Out of five tests, cohesion had an average of 5 kPa and will be ignored, especially since it can be induced by the very big shear box itself; cohesion particularly depends on the spacing between the two half-boxes [SHI 98]. The angle of friction obtained is similar to that found through other shear boxes, see Table 3.3.

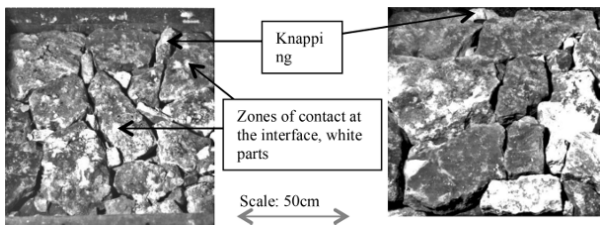


**Figure 3.3.** *Views after completion of the interface shear test between two beds of stones of 100 cm × 100 cm (sandstones): lower bed of stone on the left, view of the interface with the upper bed; on the right, reconstituted view of the interface with the upper bed*

### 3.2.2. *Shear tests on rubble stone (uncut) on an inclined plane*

The idea of these tests is to know whether it is possible to use a simple device on-site to evaluate the friction of a given stone, and avoid expensive shear box laboratory tests or not. These tests are also used to measure the displacement required to mobilize friction, given the parasitic effects induced by shear boxes on forces and displacements. The procedure of this test is described in section 2.1.3.2 of Chapter 2 about cut stones.

Table 3.3 shows that tests on raw uncut stones from St. Gens on an inclined plane, give an angle of friction that is greater than two degrees for cut stone compared to uncut stones. Overestimation is about four degrees for cut stone and the shear box. Dispersion comes from the heterogeneity of samples: under low stresses, interface roughness is expressed by an angle of dilatancy. This angle is added to the measured angle of friction for a smooth interface. Under high stresses, roughness is generally smoothed, reducing the angle of dilatancy to a negligible value.

| Nature of stones | 6 cm × 6 cm box cut sample | 30 cm × 30 cm box cut sample | 100 cm × 100 cm box raw sample | Inclined plane cut sample | Inclined plane raw sample |
|---|---|---|---|---|---|
| Molasse | 37 ± 1° | 35.5 ± 1.5° | 38 ± 2° | | |
| Molasse from St. Gens | 36 ± 1° | 35.5 ± 1.5° | | 38 ± 2° | 40 ± 2° |
| Limestone from Vers | 35 ± 0.5° | 34 ± 1° | | | 36 ± 2° |
| Limestone from Espeil | | 37 ± 1° | | | 40 ± 2° |
| Limestone from Caberan | | 37 ± 0.5° | | | 39 ± 1° |
| Hard limestone Hautes-Alpes | | 26 ± 3° | | | 30 ± 4° |
| Limestone from Estaillades | 34 ± 1° | 34 ± 2° | | | 39 ± 2° |

**Table 3.3.** *Value of the interface angle of friction according to the type of interface shear test and depending on the nature of interfaces (type of stones and interface dimensions) [VIL 04, COL 09]*

### 3.2.3. *Conclusion*

Friction is theoretically intrinsic data that does not depend on contact surface value in the field of small normal stresses (30 to 200 kPa), which is a classical result known from the works of Amonton and Coulomb [COU 21].

In this same case of low stresses, (apparent) cohesion is negligible.

The displacement required to mobilize friction cannot be properly evaluated by "classical" shear box tests as they induce parasitic effects for displacement but also for apparent cohesion. We obtained angle of friction values (Table 3.3) that were very consistent with those of [RAF 00], who used a sophisticated shear box adapted to the characterization of the behavior of rock joints. [RAF 00] found an angle of friction for the Estaillades stone of 32° to 37° and a shear stiffness value between 500 and 9,000 MPa/m, which can be roughly estimated through inclined plane tests, but not with Casagrande box tests.

Tests on an inclined plane realistically measure the movement required to mobilize friction, but they are very limited because they involve very low stresses (a few kPa). These low stresses induce a certain dispersion and overestimate the interface angle of friction due to dilatancy.

### 3.3. Compression of earth blocks

Compressive strength tests of compressed earth blocks have often followed the procedures developed for terracotta and concrete blocks [WAL 96]. However, the compressive strength of compressed earth blocks is approximately five times smaller than that of baked bricks. Strength is also heavily influenced by water content.

Studies on the compressive strength of the earth blocks include [LUN 80, OLI 86, OLI 97, WAL 95, WAL 97, PKL 02, VEN 03]. Strength is improved by compaction (higher density) and cement content (usually linear correlation), but is reduced when the water and clay contents increase (see Chapter 2). National and international standards have also developed for compressed earth block test procedures [WAL 96, NEW 98, CDE 00]. However, unlike other masonry elements, there is no general consensus on compressed earth block test procedures. Questions on whether to test blocks dry or wet, or the dimensions that samples must have (block sizes are very variable), have not been solved.

Experimental determination of the compressive strength of materials such as concrete, stone, burned clay brick and earth depends on the dimensions of the sample, because it is not possible to completely avoid the end effects. Load is normally applied uniformly by two rigid steel plates. As compressive stress increases, the sample expands laterally. However, because of friction along the interface between the plates and the sample, lateral expansion of the

sample is prevented. Therefore, confinement of samples is generated by the friction exerted by the rigid steel plates of the press that are in contact with the samples. This confinement increases the apparent strength of the material. This induced strength decreases when the aspect ratio of the sample (height divided by width) increases.

In materials such as concretes and mortars, overestimation of compressive strength is determined by specifying a standard sample size, parallelepipoid or cylindrical. While measured compressive strengths are overestimated, geometry being standard between different samples, it is possible to compare them to each other. We will first look at approaches used in testing burned clay bricks and concrete.

### 3.3.1. *Compressive strength tests of clay bricks and concrete masonry units*

The compressive strength of stone blocks, concrete or burned clay is determined by a simple compression test on a unit in a similar manner to the concrete material or mortar cubes test. To overcome surface irregularities, the blocks are capped, either by a 3 to 4 mm thick plywood or similar sheet, or covered with a thin layer of cement mortar or plaster. Bricks containing recesses are usually tested uncapped and the obtained force is expressed in terms of the gross section rather than net.

In countries where terracotta bricks are generally manufactured in a standard format, such as in the UK where almost all bricks are nominally $215 \times 102.5 \times 65$ mm$^3$, the geometric effects on the strength of brick are ignored because the geometry of the sample is always the same, as is the case for concrete cubes or cylinders.

Concrete masonry blocks exist in a much wider variety of sizes and formats (full, cellular and hollow). Consequently, in the British standard for masonry [BRI 92], the effects of geometry of blocks are taken into account in the determination of the compressive strength of the masonry. Otherwise, in Eurocode 6 (on masonry) [CEN 96], the strength of blocks is normalized by applying a shape factor to account for the effects of aspect ratio [BRI 96]. In Australia, geometric variations for both clay and concrete blocks are also supported by the application of a geometrical correction factor. The empirical correction factor [KRE 38] is designed to eliminate the influence of geometry by converting compressive strength values to obtain “unconfined” strength, like those obtained for a sample with an aspect ratio of 5. For example, for the French standard for baked bricks (measuring $230 \times 110 \times 76$ mm), the aspect ratio correction factor is 0.60.

### 3.3.2. *Test on directly flat earth block*

The procedure adopted by many national standards is similar to that used for terracotta and concrete blocks [WAL 96]. The surfaced blocks are tested directly between the plates of the press. Block surfaces are generally sufficiently flat and parallel so that only a thin sheet of plywood is needed to make a surface. The blocks are generally tested in the direction in which they have been manufactured, which is also the direction in which they are generally positioned within the masonry. Generally, between 5 and 10 blocks are tested to get a characteristic strength.

There are some internationally recognized sizes, such as 295 × 140 × 90 mm for CEB. However, in general, block sizes are variable [HOU 94, STA 02]. The production method, which is generally non-industrial, allows the manufacturer to vary the size and geometry of the block depending on the need by using inserts in the mold.

The effects of geometry on the compressive strength of blocks are generally treated in two ways. In some cases, standard test procedures make no attempt to correct the results of press plate friction (see [VIL 10], for example).

In other cases, compressive strengths are simply expressed by a statistical analysis of the results of tests on several blocks [WAL 96]. In another approach, applied in Australia [STA 02, MID 92], the effects of friction are taken into account by reducing the strength values through an aspect ratio correction factor. Correction factors in these studies are given in Table 3.4; they are generally the same as for clay bricks. Other studies have suggested more appropriate correction values for compressed earth blocks [HEA 92].

| Aspect ratio | 0 | 0.4 | 0.7 | 1.0 | 3.0 | ≥5.0 |
|---|---|---|---|---|---|---|
| [KRE 38] correction factor (using linear interpolation) | 0 | 0.50 | 0.60 | 0.70 | 0.85 | 1.00 |
| [HEA 92] correction factor (non-linear) | 0 | 0.25 | 0.40 | 0.58 | 0.90 | 1.00 |

**Table 3.4.** *Aspect ratio correction factors for earth blocks*

In some cases, cubes were cut from blocks then tested under direct compression. However, comparative strength tests of blocks and cubes of the same material showed poor correlation. Cubes were manufactured separately rather than by cutting blocks [VEN 03]. By testing cubes with constant geometry, confined compressive strengths can be compared between themselves. However, the effects of heterogeneity of the material within the cube resulting from the manufacturing process require further investigation (see also section 2.2.3).

### 3.3.3. *Test developed under RILEM*

In an attempt to indirectly measure the compressive strength of compressed earth blocks, the Technical Committee 164 of the RILEM (International union of laboratories and experts in construction materials, systems and structures) proposed the use of the test shown in Figure 3.4. To double the aspect ratio of the sample, blocks were cut in half and stacked using an earth mortar joint. The earth mortar joint reproduces the masonry configuration and allows the uniform transfer of stresses between the two masonry blocks. To enable uniform transfer of stresses between the plates of the press and the blocks, a neoprene layer is inserted between the steel plate and the block. A sheet of Teflon is also placed between the plate and each end of the sample to minimize friction (Figure 3.4(b)). Half-blocks can be prepared following a splitting test, which is an indirect tensile test, similar to the Brazilian test (primarily used on cylinder samples of rock or concrete).

Tests done by this procedure were compared to tests done on cylindrical samples manufactured by dual compaction of a same material (see Chapter 2 also section 2.2.3). These validation tests were independently verified by three research laboratories in France and North Africa [OLI 97, PKL 02, HAK 96], (Figure 3.5).

All blocks are made with a CEB manual press. That is why the compression strength is around 2 MPa. Higher values would have been obtained with a hydraulic press or a higher cement content. The materials are used with or without cement, each point representing an average of between 2 and 13 repeated tests. On average, the RILEM test underestimates the compressive strength of blocks or cylinders. Differences between the two procedures are partly due to variations in the dry density of the material depending on the two manufacturing methods.

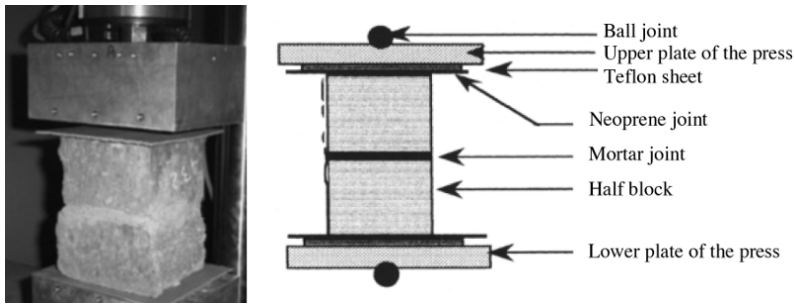


**Figure 3.4.** *Experimental device developed by [OLI 97], adopted by the RILEM TC164 photograph and drawing by Ali Mesbah*

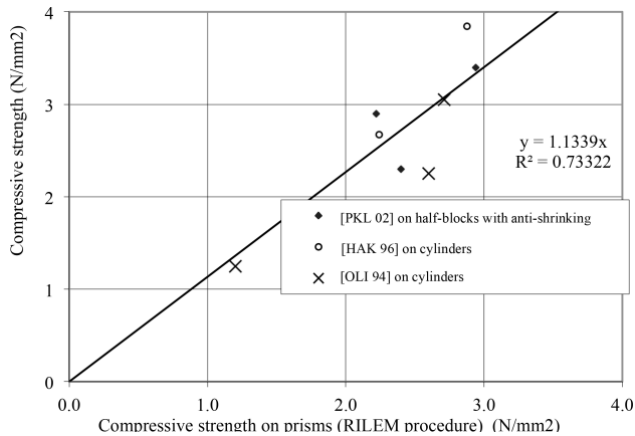


**Figure 3.5.** *Comparison between tests on a cylinder and prism according to RILEM procedure trials with anti-friction, blocks made with a manual press*

The inclusion of a mortar joint between the two tested half-blocks changes the format of the sample. The mortar joint, even if it is made of a material that is identical to the blocks, is less rigid than the blocks. This is due to its high initial water content and the absence of compaction. The presence of the mortar joint has a further variable that depends on the quality of its implementation work. On an average, there is a difference of 15% between the RILEM procedure and other procedures that are more representative of the material. This small difference entirely justifies the feasibility of using this test in practice.

### 3.3.4. *Indirect tests*

Other strength tests than compression may give an indirect measurement of compressive strength. These indirect tests have been primarily developed to allow *in situ* quality control of materials when laboratory tests are not possible. The most widely used method is the "three points bending test". The blocks are subjected to a load at their center while they are placed on two supports. The force required to cause yield in this manner is usually 80 to 150 times lower than that required to cause yield under simple uniform compression. This level of load is normally quite feasible on-site, without requiring sophisticated equipment. For example, it can be obtained through the weight of construction materials (10 blocks can weight 80 kg). The strength is calculated assuming that the block is a beam in pure bending in the strength of materials' theory. Other potentially mobilized effects, such as shear and compression through struts, due to the aspect ratio of the "beam" are ignored, which biases the results, as shown in section 3.3.5.6.

The correlation between compression and three point bending strength was established empirically by a number of studies. The results show considerable scatter, although they are commonly used for a summary assessment of compressive strength [VEN 90]. A disadvantage of this test method is its sensitivity to defects in blocks (shrinkage cracks, for example).

Another less common test is the splitting test, related to the Brazilian test used on rocks, wherein a block is loaded under compression by two steel bars along opposite sides. This induces a tensile stress, which causes the yield of the block along the line of the load. The blocks obtained from this test can also be used in the RILEM compressive strength test, which allows a direct correlation between the two measurement results.

### 3.3.5. *Features of the compressive strength of earth blocks*

#### 3.3.5.1. *Influence of sample geometry*

As previously discussed, the geometry of blocks has a significant influence on the measured compressive strength value depending on the test method. The increase in confined strength due to friction depends on the ratio between the height and width (aspect ratio) of the block. As indicated above, one approach is to correct the strength measured by an aspect ratio correction factor. The advantage of this approach is that it takes the variety of block sizes into account.

To date, correction factors were set up for masonry burned clay. The effects of the geometry of earth blocks on their compressive strength come from friction, but also from the effects of friction during the manufacturing of blocks (see Chapter 2 section 2.2.3). The dry density of blocks produced through simple compacting presses (on one side) is not constant, but decreases with increasing height of the block. Experimental studies have confirmed that a realistic value of compressive strength is obtained when the aspect ratio of blocks is 5 [WAL 97, KRE 38]. However, with such a high aspect ratio, the material within the block gradually loses its homogeneity (see Chapter 2 section 2.2.3).

The influence of geometry of the block on RILEM test results is expected if we refers to classical masonry behavior [HEN 81]. When the thickness of the blocks decreases, 10 mm mortar joints have a proportionally greater effect on measured strength, (Figure 3.6). Direct compression tests were corrected by the factor given by [HEA 92], (Table 3.4). Although there is no correction for the thickness of the mortar joint in Figure 3.6, the effect of the geometry could be alleviated by adjusting the thickness of mortar joints, depending on the height of the block. The best correlation in Figure 3.6 obtained using the correction factor shows that even with the RILEM procedure, the size of the block has a measurable effect.

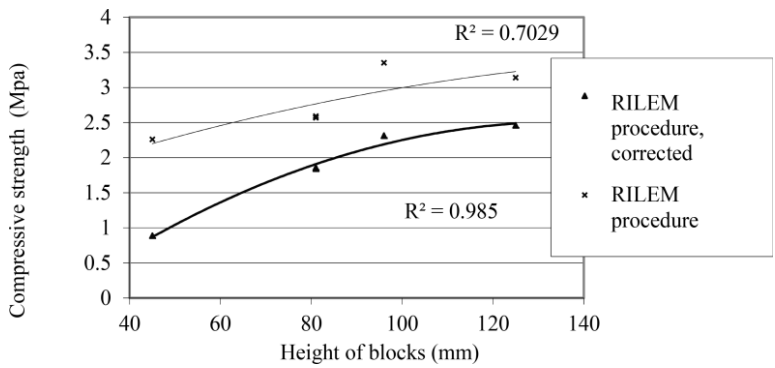


**Figure 3.6.** *Effect of the height of blocks on the RILEM procedure, the correction is made based on data from [HEA 92] (Table 3.4)*

3.3.5.2. *Influence of the test procedure*

In Figure 3.7, we show that there is no correlation between the results obtained with the RILEM procedure and strength values obtained from whole

blocks tested under direct confined compression and corrected with the [KRE 38] coefficients from Table 3.4. As Figure 3.5 showed that the RILEM test was representative of blocks, this shows that the Krefeld correction factors are not applicable to earth blocks.

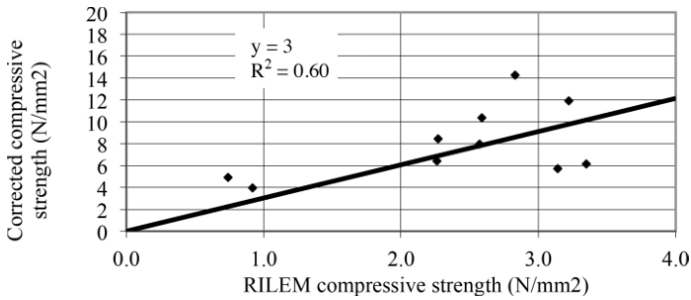


**Figure 3.7.** *Comparison between the RILEM procedure and corrected confined strength*

3.3.5.3. *Influence of the dry density*

The compressive strength of earth blocks is linked to the dry density and increases with increasing dry density as shown in Figure 3.8 for CEB and Figure 3.9 for adobes. This property is exploited for on-site quality control.

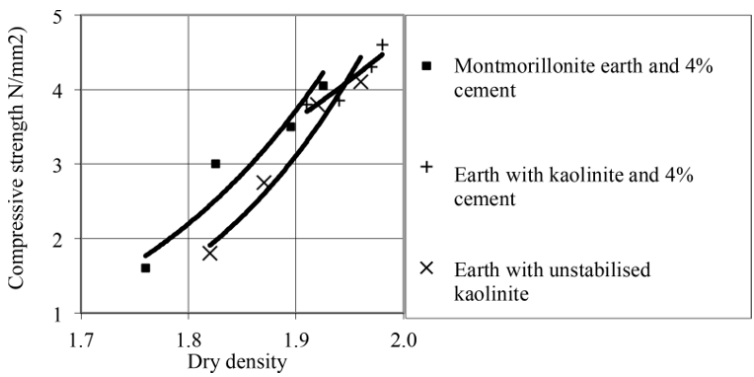


**Figure 3.8.** *Relationship between the dry density and compressive strength for CEB*

For adobes, cutting them into four (Figure 2.16) resulted in samples of dimension 70 × 60 × 140 mm, so an aspect ratio of 2. We assume that this procedure does not affect the quality of the fragments, because of the fineness of the soil used and the absence of visible cracks on the surface. Similarly, pressed blocks (PB, see Chapter 2 for the definition, 310 × 152 × 71 mm) were tested at their ends, in order to keep the same aspect ratio of 2 to compare the compressive strength value to that of adobes (Figure 3.9).

Figure 3.9 also shows that the curve has an area where the strength and density of adobes and PB overlap. This coincidence is explained by the compaction nulling effect, since the material is close to saturation (Chapter 2). We get dispersion of values of adobes discussed in Chapter 2, but this could also be because they have been cut, while PB are whole. PB may have a slight anisotropy, because they have not been tested in the direction of compaction.

Table 3.5 shows a comparison of adobes from different places. Adobes from the Toulouse region were probably made in the 19th century, those from Agadez (Niger) at the end of the 20th century and those from Rochechinard in 2008. There is a direct relationship between the amount of binder (clay, here) and compressive strength. Indeed, according to Figure 2.14, the two Rochechinard and Toulouse region adobes contain twice as much clay as the one from Agadez, which translates into 2–5 times better strength.

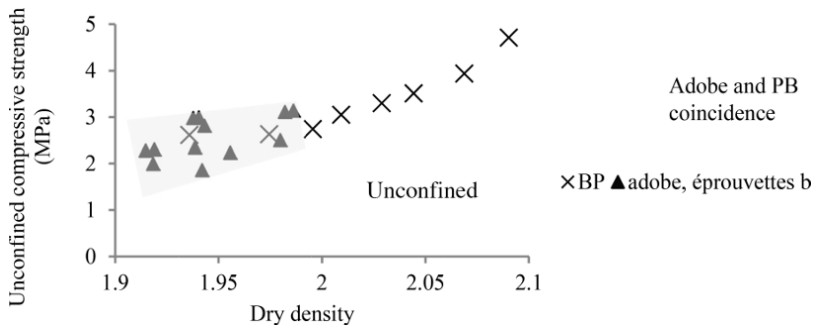


**Figure 3.9.** *Relationship between dry density and compressive strength for adobe*

| Origin of adobes | Number of samples | Dry density in g/cm$^3$ (standard deviation) | Compressive strength in MPa (standard deviation) |
|---|---|---|---|
| Toulouse region (France) | 3 | Non-measured | 4.4 (0.13) |
| Rochechinard (Drôme, France) | 12 | from 1.9 to 2.1 | from 2 to 4.5 |
| Agadès (Niger) | 2 | 1.89 (0.03) | 0.9 (0.07) |

**Table 3.5.** *Compressive strength of adobe blocks*

3.3.5.4. *Influence of cement content on CEB*

Cement acts as a stabilizer of compressed earth blocks by improving their resistance to water and, indirectly, their durability. Data produced by various researchers show a correlation between compressive strength and cement content. The data presented in Figure 3.10 are characteristic of the relationship between compressive strength and cement content.

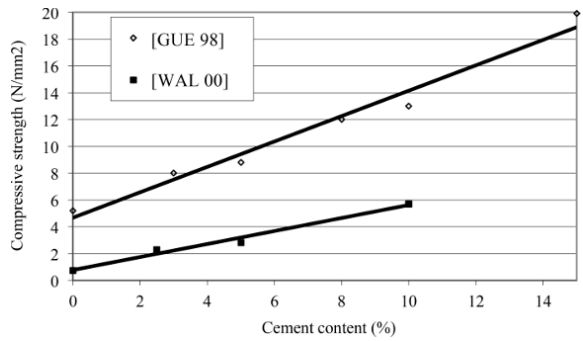


**Figure 3.10.** *Relationship between compressive strength and cement content according to data from [GUE 98] and [WAL 00]*

3.3.5.5. *Influence of the water content of the block during a test*

The water content of blocks has a significant influence on their compressive strength. Blocks are usually tested either after oven drying or drying at ambient humidity, reflecting service conditions. As water content increases the suction decreases, clays gradually plasticize, which reduces their mechanical strength. For a unstabilized earth block, clay is the sole binder and the compressive strength of blocks in the event of saturation is zero. The water content of unstabilized tested materials should ideally reflect

service conditions. Tests on saturated stabilized blocks enable a minimum controllable strength that is easy and reproducible, even if these conditions are unlikely to be achieved in practice unless in case of a flooding episode. The inclusion of the mortar joint in the RILEM test causes determination of strength under conditions of saturation difficult.

3.3.5.6. *Three-point bending test*

The three-point bending test was recommended and used as a simple but indirect measure of the compressive strength of earth blocks [VEN 90, WAL 96, MOR 02, MOR 03] from a calculation in pure bending.

There is an interpretation other than pure bending given by [MOR 02, MOR 03] where the compressive strength $\sigma_c$ is given by equation [3.1]:

$$\sigma_c = \frac{-PL}{2h_o el}\sqrt{1+\frac{L^2}{4e^2}} \qquad [3.1]$$

where $P$ is the yield load of the three-point bending test, $L$ is the distance between the two supports (hinges), $e$ is the height of the block, $l$ is the width of the block and $h_o$ is a parameter (the height of a fictive strut), taken to be 23 mm for the compressed earth blocks tested by [MOR 02, MOR 03].

In both cases (the conventional formula for pure bending [VEN 92] or formula [3.1]), there is a linear relationship between compressive strength and the strength given by the three-point bending test. The correlation between the two calculations is shown in Figure 3.11. The best correlation obtained with the RILEM procedure tests also shows that the correction of confined compressive strength does not work for any random block.

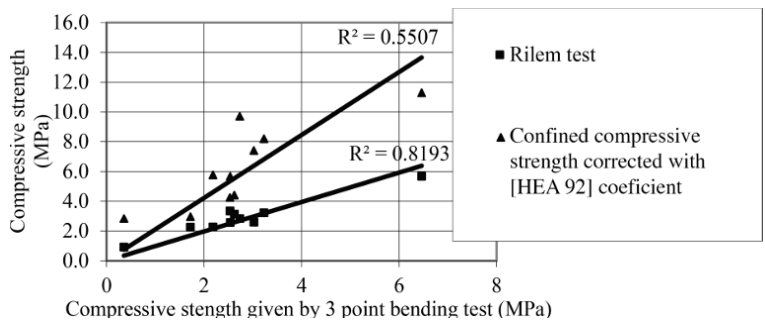


**Figure 3.11.** *Comparison of RILEM tests and corrected confined compressive strength correlated with compressive strengths calculated with formula [3.1], derived from [MOR 02]*

### 3.3.6. *Conclusion*

Many research works were interested in determining the compressive strength of earth blocks from a simple compression test and advocate to reduce friction of the sample through the plates of the press by using an anti-friction system (latex membrane coated with silicone grease, for example), for an aspect ratio of elements that is less than 1.5 or even 2. An aspect ratio (height/width ratio) of 2 reduces the risk of overestimating compressive strength due to friction.

However, if we want to do the test directly on the block and not on a sample made specifically for the test, we must consider that earth blocks are produced in a large variety of sizes.

The RILEM Technical Committee 164 proposed a method that tests two masonry half-blocks by a mortar joint. This test eliminates the problem of the low aspect ratio of blocks, but not for very flat blocks (aspect ratio less than 0.6), which is often the case for adobes. This procedure underestimates the strength of blocks by a few percent and is therefore closer to the behavior of the masonry than that of the block. But this last point is not detrimental in practice since the block will actually by masoned to make a wall.

An indirect test, such as the three-point bending test, may also provide an indication of the compressive strength.

## 3.4. Bibliography

[ABO 99] ABOURA A., Etude expérimentale et mise au point d'une boîte de cisaillement pour caractériser les déchets ménagers, Thèse de l'UJF, 1999.

[BRI 92] BRITISH STANDARD 5628-1:1992. Code of practice for use of masonry – Part 1: Structural use of unreinforced masonry, BSI, 1992.

[BRI 96] BRITISH STANDARD PREN 1996-1-1:2003. Eurocode 6. Design of masonry structures, BSI, 1996.

[CDE 00] CENTRE FOR THE DEVELOPMENT OF ENTERPRISE, Compressed earth blocks testing procedures, CDE, Bruxelles, Belgique, 2000.

[CEN 96] COMITÉ EUROPÉEN DE NORMALISATION, Eurocode 6: Calcul des ouvrages de maçonnerie -partie1-1: Règles générales- Règles pour la maçonnerie armée et non armée, ENV 1996-1-1.

[COL 09] COLAS A.-S., Mécanique des murs de soutènement en pierre sèche: modélisation par le calcul à la rupture et expérimentation échelle 1, Thèse de l'ENTPE-ECL, 2009.

[GUE 98] GUETTALA A., GUENFOUD M., "Influence des Types d'Argiles sur les Propriétés Physico-mécaniques du Béton de Terre Stabilisée au Ciment", *Annales du Bâtiment et des Travaux Publics*, vol. 1, pp. 15–25, 1998.

[HAK 96] HAKIMI A., YAMANI A., OUISSI H., "Rapport: Résultats d'essais de résistance mécaniques sur échantillons de terre comprimée", *Materials & Structures*, vol. 29, pp. 600–608, 1996.

[HEA 92] HEATHCOTE K., JANKULOVSKI E., "Aspect ratio correction factors for soilcrete blocks", *Australian Civil Engineering Transactions, Institution of Engineers Australia*, vol. CE34, vol. 4, pp. 309–312, 1992.

[HEN 81] HENDRY A.W., *Structural Brickwork*, Macmillan, London, 1981.

[HOU 94] HOUBEN H., GUILLAUD H., *Earth construction: a comprehensive guide*, IT Publications, London, 1994.

[KRE 38] KREFELD W.J., "Effect of shape of specimen on the apparent compressive strength of brick masonry", *Proceedings of the American Society of Materials*, Philadelphia, PA, pp. 363–369, 1938.

[LUN 80] LUNT M.G., Stabilised soil blocks for building, Overseas Building Notes, Building Research Establishment, Garston, 1980.

[MID 92] MIDDLETON G.F., (revised by SCHNEIDER L.M.), Earth-wall construction, Bulletin 5, CSIRO Division of Building, Construction and Engineering, 4e édition, Sydney, 1992.

[MOR 02] MOREL J.C., PKLA A., "A model to measure compressive strength of compressed earth blocks with the three point bending test", *Construction & Building Materials*, vol. 16, pp. 303–310, 2002.

[MOR 03] MOREL J.C., PKLA A., DI BENEDETTO H., "Interprétation en compression ou traction de l'essai de flexion en trois points", *Revue Française de Génie Civil*, vol. 7, pp. 221–237, 2003.

[OLI 86] OLIVIER M., MESBAH A. "Le matériau terre: Essai de compactage statique pour la fabrication de briques de terres compresses", *Bull. Liaison Labo. P. et Ch*., 146, pp. 37–43, 1986.

[OLI 97] OLIVIER M., MESBAH A., EL GHARBI Z., MOREL J.C., "Mode opératoire pour la réalisation d'essais de résistance sur blocs de terre comprimée", *Mater. Struct.*, vol. 30, pp. 515–517, 1997.

[PKL 02] PKLA A., Caractérisation en compression simple des blocs de terre comprimées (btc): application aux maçonneries btc-mortier de terre, PhD, INSA, Lyon, 2002.

[PRO 33] PROCTOR R.R., "Field and laboratory verification of soil suitability", *Engineering News-records*, vol. 111, no. 12, pp. 245–248, 1933.

[RAF 00] RAFFARD D., Modélisation de structures maçonnées par homogénéisation numérique non linéaire: application aux ouvrages d'intérêt archéologique, Thèse de Doctorat, Institut National Polytechnique de Lorraine, 2000.

[SHI 98] SHIRDAM R., FAURE R.M., MAGNAN J.P., *Caractérisation des éboulis de pente à l'aide d'une grande boîte de cisaillement*, The Geotechnics of hard soils, Soft Rocks, Evangelista and Picrelli, Rotterdam, 1998.

[STA 84] AUSTRALIAN STANDARD 2733, Concrete masonry units, Standards Australia, Sydney, Australia, 1984.

[STA 02] STANDARDS AUSTRALIA HANDBOOK 194, *The Australian Earth Building Handbook*, Standards Australia, Sydney, Australia, 2002.

[VIL 04] VILLEMUS B., Etude des murs de soutènement en maçonnerie de pierres sèches, Thèse de Doctorat, ENTPE, INSA de Lyon, 2004.

[VIL 10] VILANE B.R.T., "Assessment of stabilisation of adobes by confined compression tests", *Biosystems Engineering*, vol. 106, no. 4, pp. 551–558, 2010.

[VEN 90] VENKATARAMA REDDY B.V., JAGADISH K.S., "Field evaluation of pressed soil-cement blocks", *Proceedings of the 4th International Seminar on Structural Masonry for Developing Countries*, Madras, pp. 168–175, 1990.

[VEN 03] VENKATARAMA REDDY B.V., SUDHAKAR M.R., ARUN KUMAR M.K., "Characteristics of stabilised mud blocks using ash-modified soils", *The Indian Concrete Journal*, pp. 903–911, February 2003.

[WAL 95] WALKER P., "Strength, durability and shrinkage characteristics of cement stabilised soil blocks", *Cement & Concrete Composites*, vol. 17, no. 4, pp. 301–310, 1995.

[WAL 96] WALKER P., "Specification for stabilized pressed earth blocks", *Masonry International*, vol. 10, no. 1, pp. 1–6, 1996.

[WAL 97] WALKER P., "Characteristics of Pressed Earth Blocks in Compression", *Proc. 11th International Brick/Block Masonry Conference*, Shanghai, China, pp. 1–10, 14–16 October 1997.

[WAL 00] WALKER P., "Strength and durability testing of earth blocks", *Proc. 6th International seminar on Structural Masonry for Developing Countries*, Bangalore, India, pp. 111–118, 2000.

# 4

# Arrangement of Blocks

## 4.1. Dry assembling, or the art of arranging irregular blocks to make a wall

Although the expertise of the dry stone mason is described in many books [GUI 08, DSW 04, LAS 08], the working method is still *transmitted* through the practice of dry stone building. Here, we will only consider the outlines that underline this expertise. In addition, these outlines will be explained for the case of a dry stone retaining wall construction, to illustrate taking the whole constructive system into account and not merely the arrangement of stones. This section draws directly on the work of Philippe Alexandre (PETRA TERRA) in the ASCNI project [ASC 07].

The arrangement of stones for stone masonry construction (with mortar) follows the rules of dry stone masonry since the mortar has a poor mechanical role, as discussed later in this chapter (section 4.4). Only the arrangement of stones provides stability. The mortar has mainly an air sealing role and eventually also a water sealing role.

### 4.1.1. *The area of influence of a dry stone retaining wall*

Whether for a creation or repair, we must evaluate the role (or not) of natural elements and construction elements in the stability of the structure for a zone extending to an equal distance, at all points, of up to three times the maximum height of the wall.

The area of influence may include adjacent slopes (upstream and downstream), vegetation (root paths or surface, etc.), construction works

*Sustainable Masonry: Stability and Behavior of Structures,*
First Edition. Thierry Ciblac and Jean-Claude Morel.

(buildings, fences, etc.), various networks, a stream bed, a developing ravine, etc.

For the reconstruction of a structure, we must identify in advance what caused the collapse of the wall:

– overturning from pressure;

– sliding of stones;

– exuberant vegetation;

– deterioration of the material;

– scouring of the foundation;

– a sudden, unusual event;

– poor workmanship.

### 4.1.2. *Quality of the material*

Whether for reconstruction or creation, material that is local or found nearby should be used. Recovery of on-site material should be equally distributed according to particle size all along the length of the gap (in the case of repair of an existing wall), leaving a passage of sufficient width (from 0.50 to 1.00 m) to avoid cluttering the foot of the structure. Earth should be collected and placed above and behind the collapsed area. All areas that do not respect the initial construction and those that are unstable should be dismantled.

Each stone is selected according to its position in the wall, its size, shape and density.

Evaluation of the interface angle of friction is based on an inclined plane test (see Chapters 2 and 3). This test will give an approximate value of the angle of friction under low stress.

Stones with a large longitudinal axis will be kept as through stones, to link or join the two sides of the wall. This means that the largest dimension of the stone is perpendicular to the external facing of the wall in order to give it overall cohesion.

### 4.1.3. *Elevation*

Elevation is the act of constructing the wall from the bottom upwards.

4.1.3.1. *Excavation*

This is excavation into the ground in which the foundation is built. Sometimes non-existent (on rock), and often reduced, it should be of sufficient depth and width in relation to the quality of the earth (presence of non-loose soil) and the height of the structure. The base of the excavation will be tilted downwards toward the inside face of the future wall.

On a rock base, an inclined plane should be created by dressing the stone with the same downward inclination and minimum width of the first stone to be placed on the rock, to facilitate the installation of the first row of facings.

4.1.3.2. *Foundations*

Foundations distribute the wall load over a wider surface toward the outside by about a quarter of the thickness of the wall. This enables the laying of the first course. The foundation consists of a stable base made up of large stones, which defines the inclined plane of the coursing to follow. The size of the stones selected allows the foundation to emerge from the ground level by few centimeters.

The installation of these large and roughly shaped stones is carried out according to the same rules as specified for "elevation", see below.

4.1.3.3. *Laying the first course*

The wall body consists of elements for which the visible face, the "facing", is aligned along the external side of the wall (Figure 4.1).

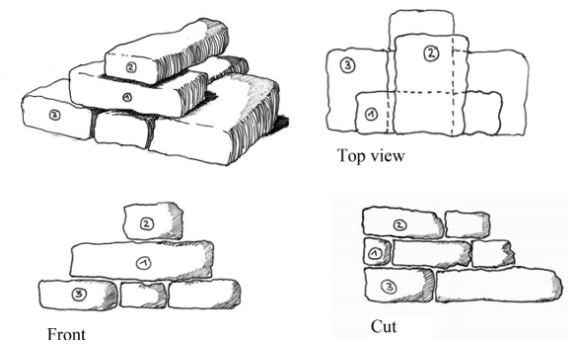


**Figure 4.1.** *Horizontal and vertical cross joints, drawing by Rabia Charef-Morel from [GUI 08]*

Stones are positioned side by side and fully stabilized to create the external wall facing, often using “pins” (stone wedges) placed at the heel of the stone (Figure 4.2). The course is laid with stones placed as tightly as possible one against another, sometimes using a specially-shaped hammer (for example with a square, concave head on one side and a point on the other for shaping, sizing and dressing hard stones). Small stones may be placed between certain larger joints, although these should be wedged very tightly if they are to serve a purpose other than aesthetic.

The wall body is supplemented with non-faced stone elements, the “hearting or packing”, placed throughout its thickness, filling the gaps as much as possible (Figure 4.3). The type of packing may depend on the quality of contact points of the facing stones and the number of throughstones.

4.1.3.4. *Laying the second course*

At this degree of elevation, care should be taken to install an appropriate device to enable the waller to follow the line and plane of the wall, if this has not already been done. This is defined in advance by a cord that runs between both wall ends, attached to a guide frame that delineates the batter of the wall. The second course of facing stones systematically covers the joints and contact points of the previous course. It has the same characteristics as the previous course and is laid according to the same rules.

Packing is installed like the facing, to cover the previous level of stones, particularly in the thickness of the wall. The filling between the wall and the ground behind (the drain) can be done using improper construction elements: chips, waste excavation, unsuitable elevation stones.

**Figure 4.2.** *Packing wedges, drawing by Rabia Charef-Morel from [GUI 08]*

4.1.3.5. *Laying the third course*

This is a repetition of the previous operation. If the wall has reached a third of its height, a drain should be installed behind the wall using stone chips and other small stones.

The height of the wall is now sufficient to allow the occasional laying of stones that, with a facing, are not throughstones or headers, but traced stones or "stretchers". The length of their axis in the wall is shorter than the length of the facing.

A sufficient number of "throughs" should be placed from the first quarter to about half the height of the wall (Figure 4.3).

Construction progresses by alternating traced stones, building stones and occasionally throughstones which, if they cover both the external face of the wall and the internal packing, will feature as "binders".

The installation of the drain behind the wall continues up to 20 to 25 cm below the ground level retained by the wall.

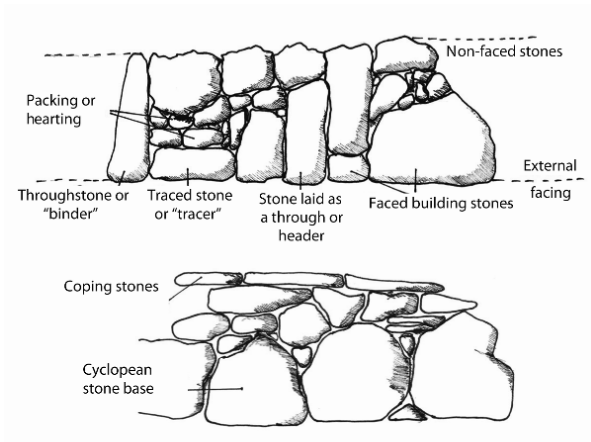


**Figure 4.3.** *Stones arranged in a wall: elevation (top) and horizontal section (below), drawing by Rabia Charef-Morel from [GUI 08]*

4.1.3.6. *Covering or coping*

This involves blocking the last row of wall stones to maintain the wall head in place, enabling circulation on the terrace. Several types of finish are possible, depending on the characteristics of the stone.

Whether the coping is created using thick, large stones laid horizontally or smaller stones placed vertically on their edge ("*en délit*"), it will be aligned to the surface of the soil that is to be retained.

The wall is finished by presenting a copestone that will be aligned to the upper cord and the last stone course will be placed under these thick, heavy stones according to the same installation rules as before.

4.1.3.7. *Finishing the construction*

A final sorting of granulates separates the stones that will be part of the drain from the earth that will be raised on the terrace to finish the job.

### 4.1.4. *Conclusion*

In this book, we will not discuss the different types of arrangement that have already been described in many books, see for example [GUI 08] and [ACA 01]. Dry stone arrangements are the most difficult to implement, compared to arrangements with cut stones where the mortar can be used to correct errors in the geometry of blocks and their placement. The quality of the masonry is directly dependent on the expertise of the mason, and even if this knowledge is empirical, it is quite sufficient to obtain stable structures which can be modeled by an engineering deterministic approach. This expertise may even allow us to consider masonry as a homogeneous material in the first approximation and on a certain scale (see Part 3, Chapter 11).

## 4.2. Mortars of earth blocks and rubble stone masonry

For stone masonry, the first role of mortars is to provide an air seal, which is necessary in the case of residential buildings. The second role is to transmit and distribute compressive loads between blocks of irregular geometry. In some cases of excellent compatibility between the mortar and the block, the mortar can provide tensile strength to the joints and thus to the masonry. The tensile strength of the mortar and the joint can be approximately equal to a maximum of <0.4 MPa, which is highly dependent on the implementation, without knowledge of its evolution over time. That is why it will not be considered in this book. Let us note that ignoring this strength is not in the interest of safety.

In this chapter, we will consider earth mortars but the presented works are transposable to low-content lime-based mortars. The main macroscopic difference is less shrinkage for the latter. There are very few studies on these mortars and testing procedures are different according to various authors. All procedures used for conventional sand:lime:cement mortar are not directly

applicable because of clay activity (clay affinity with water) and low stiffness of earth mortars [PKL 03]. In this section, we present some test procedures and their influences on the characteristics of some earth mortars. The results form the basis for a discussion on the choice of test procedures.

| Soil | Magagnosc | Rochechinard | Tassin | Tamée | TR |
|---|---|---|---|---|---|
| Amount of clay by weight (particles <2 μm) | 12 | 26 | 18 | 6 | 15 |
| Liquid limit (%) | 29 | 38 | 30 | 60 | NM |
| Plasticity index (%) | 9 | 18 | 9 | 31 | NM |
| VBS = Methylene blue value of the fragment 0/D (total) | 1 | 2.5 | 1.4 | 2.2 | <1 |
| $Ac_B$ Methylene blue activity =100 × VBS/C2% | 8 | 10 | 8 | 37 | <3 |

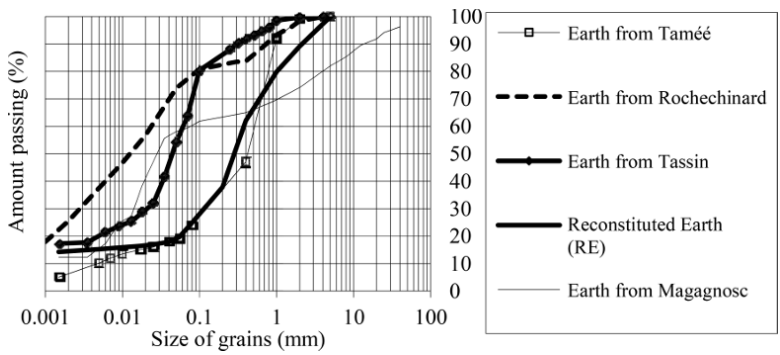


**Figure 4.4.** *Geotechnical characteristics of soils used for earth mortars, origin: South-East France*

Just like block materials, it is impossible to give a standard composition of earth mortar as can be done for sand:lime:cement mortar for which knowledge of the proportions of each component is sufficient to ensure mechanical behavior. One reason for using earth mortar is for the constraint

or choice of using soil from (or nearby) the site, which is naturally very variable depending on the site. To illustrate our point, we arbitrarily choose given earth as an example (Figure 4.4).

There are two approaches for determining the properties of mortar: direct tests on the mortar, or masonry element (block + mortar). Measurement of consistency is obviously done on the mortar alone and the measurement of the shear strength of the block-mortar interface is obviously done on a masonry element. The compressive strength of mortar can be studied through two approaches [SHR 95, WAL 97]. But to our knowledge, there is not yet correlation between the compressive strength of earth mortar and that of masonry.

In section 4.3, we will consider block–mortar interactions. Here, we will study tests on mortar alone and not within the masonry.

### 4.2.1. *Measurements in the fresh state*

There are usually five quantities measured in this state for conventional mortars (sand:lime:cement): workability, consistency, water retention, air content and water content. All these quantities are related to each other, which makes their measurement difficult because different procedures can be used to measure the same parameter.

#### 4.2.1.1. *Measuring air content*

We used the alcohol method according to the [CEN 94b] standard on three different earths with a cement content (which we will always express in dry weight) of 25:2, which means 25 parts soil, sand or granulate for 2 parts cement (see Table 4.1).

Apart from unstabilized reconstituted earth (1:0), all air content levels are less than 7%. This is a characteristic for earth mortar and is due to the ability of clay to adsorb water. Earth mortars therefore have higher water contents than lime:sand:cement mortars, thus smaller air contents (air cannot dispel away adsorbed water).

| Mortars | Water content (%) | Air content (% in volume) | Water retention (%) | Consistency, slump test, NF P 18-451 1981 | | Workability NF EN 413-2 | |
|---|---|---|---|---|---|---|---|
| | | | | Slump (cm) | Sample diameter (cm) | 1st trial | 2nd trial |
| Standardized mortar MC5 | 12 | 8 to 20 | 80 to 95 | | | 5 to 30 s | |
| Reconstituted Earth (1:0) | 13 | 9.8 | 98 | 12.5 | 30 | 8 s | 10 s |
| Reconstituted Earth: cement (25:2) | 17 | 5.9 | 99 | 0 | 20 | >5 mn | >5 mn |
| Reconstituted Earth: cement (25:2) | 21 | 4.8 | 98 | 4.5 | 22 | 45 s | 30 s |
| Tamée (1:0) | 22 | 6.5 | 99 | 1.5 | 22 | >5 mn | >5 mn |
| Tamée:cement (25:2) | 23 | 6.0 | | 0.5 | 21 | >5 mn | >5 mn |
| Tamée:cement (25:2) | 25 | 4.1 | | 1.5 | 22 | >5 mn | >5 mn |
| Tamée:cement (25:2) | 29 | 2.4 | 95 | 7 | 23 | >5 mn | >5 mn |
| Tassin (1:0) | 25 | 3.9 | 98 | 0.5 | 21 | >5 mn | >5 mn |

**Table 4.1.** *Water content (by dry weight) Air content (alcohol method NF EN 413-2), water retention, slump test consistency, workability of earth mortars*

In the case of reconstituted earth, poor quality of mix could explain a higher value. The air would not have been dispelled as much by the water added during the procedure. For reconstituted earth (clay–sand mixture), it is best to allow a reaction time for the plastic mixture of 24 h to 1 week to ensure good homogeneity.

4.2.1.2. *Measuring water retention*

To our knowledge, the first water retention measurements on earth mortar were published by [WAL 97]. These measurements provide a more significant water retention capacity than conventional mortar (sand:lime:cement). In light of the variability of earth use on sites, we carried out further tests. The [WAL 97] tests were carried out on reconstituted earth containing only kaolinite. This water retention capacity is only relevant when

correlated with masonry earth blocks as the migration of water and particles will depend on the two media involved. There are very few studies on this aspect of earth masonry [VEN 96, WAL 99]. This is also still in the field of research of masonry using baked bricks and sand:lime:cement mortars [GRO 00].

This improved water retention capacity will usually promote adhesion to the block–mortar interface [WAL 99] because it slows down overly-rapid migration of water toward blocks and the atmosphere. This is accentuated by the nature of earth blocks that are generally less absorbent than baked bricks.

For all the earth mortars in Table 4.1, water retention measured according to [CEN 94b] is greater than 95% and therefore greater than that of conventional standardized MC5 mortar, which varies between 80 and 95%. These results of natural earths confirm those from [WAL 97] for reconstituted earths containing kaolinite.

4.2.1.3. *Measuring rheology of fresh mortar*

Here, we will discuss in a little more detail how to describe the rheology of fresh mortar paste. A lot of research is being done on this topic on concrete mortars, having had interest in it be revived through the increasing use of self-leveling concrete [SED 95] and sand:lime:cement mortar in masonry. The complexity of this field arises from the fact that earth mortar is:

– a multi-phase medium (clay–sand–water–cement/lime–air);

– these phases act strongly on its rheology over time;

– interacting with blocks (themselves also with very different characteristics);

– interacting with ambient air and therefore subject to climatic conditions during laying.

The first attempts to measure the rheology of earth mortars are detailed in [AZE 05] and partly published in [AZE 08]. Tests done using a rheometer showed that earth mortars followed a Bingham fluid-like behavior as described in Figure 4.5. As a first approximation, three parameters are needed to describe this behavior: the shear threshold $\tau_o$ and the two Bingham flow line parameters ($\eta$ and $\tau_B$).

Despite this complex behavior, experienced masons naturally find a compromise between all these constraints and therefore the appropriateness

of a mortar is foremost an appreciation of the mason before it is a laboratory measurement. An easily-implemented mortar must hold without sticking to the trowel, must spread well and adhere to a vertical surface when it is thrown on. However, knowledge of rheology may be useful, at least for determining the number of parameters needed to define the behavior of fresh mortar.

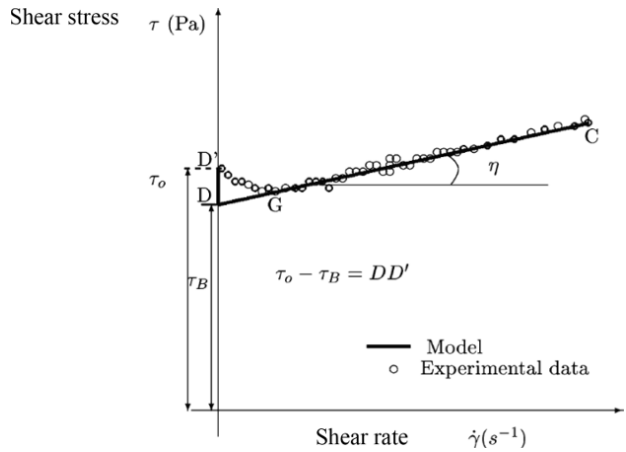


**Figure 4.5.** *Behavior law of earth mortar in the fresh state*

These properties are divided into two measurements called [BOW96]:

– consistency (resistance to deformation), measured by a penetrometer type test called cone impression. The use of a flow table and the dropping ball test is also possible. If using a flow table, one must calibrate the table using a mortar that satisfies the right consistency criteria for the cone, otherwise this test gives a workability value;

– workability (static or dynamic), measured by a slump or flow test. The standard [SAA 84] does not differentiate between workability and consistency.

[CEN 94a] standards specify the consistency that will determine a suitable water content for the mortar. The workability of mortar is then measured for this given consistency.

The "two points: consistency and workability" approach is justified by the fact that for years, the behavior of conventional mortars (sand:lime:cement) was considered to follow a Bingham fluid model [TAT 91] with two physical parameters called Bingham constants (threshold shear stress and plastic viscosity ($\tau_B$,$\eta$)). To fully qualify a mortar under this behavior, these two parameters must be measured. Therefore at least two different experimental measurements are required, including a time-dependent measurements (rate, for example), for measuring plastic viscosity. [TAN89] [HU 95] admit that the value of the slump test indirectly gives the stress threshold.

We can find the second parameter (plastic viscosity) using rheometers that are adapted to mortars or by measuring an intermediate slump time with a modified slump test [DEL 98]. These recent developments are applied to "fluid"concretes with a slump of over 10 cm for which [DEL98] proposes a Herschel–Buckley behavior law with three parameters. In this case, we must measure three parameters as defined by [AZE 08] for earth mortars.

While waiting for progress in this field, we must focus on practical tests that are already used *in situ* and integrate them into a larger-scale practice.

#### 4.2.1.3.1. Measuring consistency

Consistency was measured through two tests by [WAL 97] on reconstituted earths (sand–kaolinite) with clay contents of 10–40%. The two tests, plunger and flow table give very scattered results for mortars that are, according to the subjective opinion of a mason, of good consistency.

#### 4.2.1.3.2. The slump test

The slump test measures workability and is only used for concrete in France. Its use on mortars is nonetheless common for the British who then measure consistency. [WAL 97] shows that a smaller slump test [SAA 84] than one for concrete is more suitable than the previously described tests for reconstituted earth mortars containing kaolinite only.

Slump tests for concrete [NFP 81] gives lumps of 1.5 to 7 cm for the most acceptable mortars from the perspective of their fresh state implementation, see Table 4.1. Tests with a smaller cone (adapted to the mortar) require lubrication of the cone with oil [WAL 97].

4.2.1.3.3. Measuring workability

According to standards for conventional mortars, we present two tests for quantifying the workability:

– the flow table, used for earth mortars by [BEI 96] depending on the [AST 98] standard for the number of strokes. The diameter of the sample paste giving adequate workability is determined by the experience of a mason;

– the maniabilimeter [CEN 94] that measures flow time.

These tests have been developed for conventional mortar (cement:lime:sand) and give cohesivity. We have seen (Table 4.1) that the values given by the standards do not apply to earth (see also [WAL 97]).

The dynamic workability measured by a maniabilimeter seems inappropriate for masonry mortars. Indeed, unlike concrete, these mortars are not vibrated during their implementation. Moreover, it is for concrete mortars that the maniabilimeter NF EN 413-2 [CEN 94b] was designed. We have a lot of information about dynamic workability so it therefore seems interesting to carry out research in this direction. In addition, the French standard [CEN 94a] gives requirements for this workability for mortars.

Previous studies with the maniabilimeter on earth mortars [OLI 95] showed that adding:

– Sisal fiber increases water content and decreases flow time. The amount of extra water depends on the specific surface of the fibers;

– a plasticizer does not change flow time but reduces water content. Shrinkage decrease with decreasing water content is a way to stop the appearance of shrinkage cracks.

Maniabilimeter values of flow in Table 4.1 show that the device is not suitable for all earth mortars because three mortars (suitable for earth construction) out of 4 give an infinite flow time. We simply propose to abandon the use of this device rather than modify it. It is indeed necessary, in the present state of knowledge, to use simple and inexpensive measuring devices (for example, non-electric).

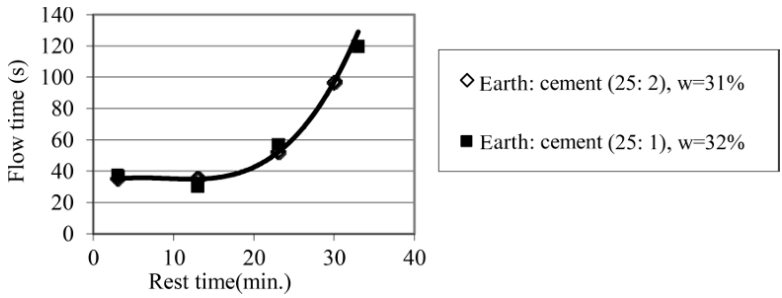


**Figure 4.6.** *Variation of dynamic workability versus time, earth (Tassin) described in Figure 4.4*

In the field, mortar is not immediately used. Part of the mix remains at rest before progressively being used to mason blocks. If the mortar contains a hydraulic binder, it should not be remoistened. In Figure 4.6, we see that even earth mortars with little cement content (here with a high clay content of C2% = 18% and a rather fluid consistency according to Table 4.1) lose their workability significantly from 20 min onwards and after 35 min the mortar is no longer usable. This is in temperate conditions (France), so in the shade and at a temperature of about 20°C.

4.2.1.4. *Water content*

We compared water contents, considered to be adequate, for different earths and by different authors. Proper workability is either determined by different masons or by a flow time of 16 s on the EN 412-2 maniabilimeter for data from [UNI 82]. Figure 4.7 shows the influence of the amount of clay (a kaolinite for all reconstituted earths; for Tassin, which is a natural earth, there are more active clays but kaolinite remains the majority, see $A_{cB}$ Figure 4.4) on the water content of earth mortars. Water content is less dependent on the amount of cement than the amount of clay and the mineralogical nature of the clay. Data from [UNI 82] are obtained with a cement content that is too high for earth construction.

We also note that for the same earth, the manufacturing water content increases with the amount of cement as well as with clay activity (see Table 4.1); this is the case for reconstituted earth containing kaolinite, as well as for Tamee earth, which mainly contains smectite.

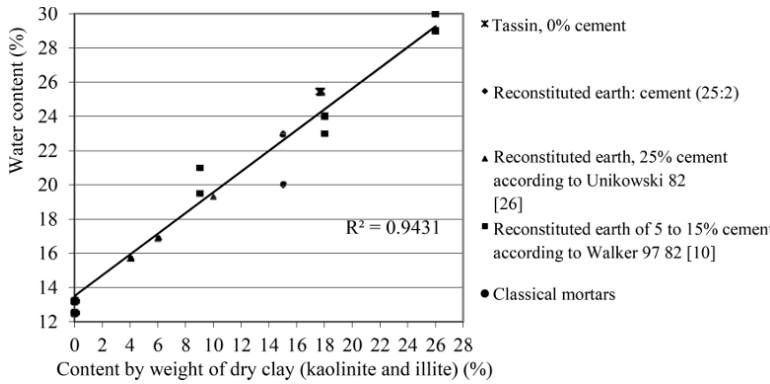


**Figure 4.7.** *Water content of the mortar for acceptable workability according to different authors, Tassin earth mainly contains illite and very little kaolinite*

4.2.1.5. *Conclusion*

Direct measurements of the rheology of earth mortars show that they have a Bingham fluid type behavior with three parameters. In this case, we must carry out three experimental measurements, which remain to be defined. While awaiting direct rheological measurements, it seems that the slump test is usable for many earths. The maniabilimeter test is not suitable for earth mortars.

### 4.2.2. *Drying shrinkage measurements*

One of the main problems with earth mortars, especially with unstabilized mortars (100% earth), is the appearance of shrinkage cracks. If there is no coating, these cracks can affect the homogeneity of masonry and its durability, as water can penetrate through the cracks.

Shrinkage greater than 10% is also a problem for obtaining homogeneous cylindrical samples with an aspect ratio of 2. The mold wall–sample interaction during the procedure can destroy it.

Another method to reduce drying shrinkage is to add sand (optionally in addition to cement) or natural fibers [BEI 96]. But in the case of addition of sand alone, compressive strength will decrease as the amount of binder (clay) decreases.

### 4.2.3. *Tests on hardened mortars*

Four procedures using the following test samples can be found in the literature:

– $4 \times 4 \times 8$ cm$^3$ prism with an aspect ratio of 2 with friction when the sample is in contact with the press [BEI 96] (confined test);

– cylinder (diameter 7 cm, height 14 cm) aspect ratio of 2 without friction [AZE 05] (unconfined test);

– 7 cm cubes with friction [SHR 95, VEN 96] (confined test);

– 5 cm cubes with friction [WAL 97] (confined test).

As for earth blocks, samples with an aspect ratio of 2 will always be given priority. The results obtained from cubes without anti-friction cannot describe the material behavior.

We will not further develop this section because it is either not necessary to quantify the strength of hardened mortar because they have no important structural role, or we recommend directly testing the mortar block masonry. If we still wishes to do tests on mortar alone, for example to compare two mortars, we may refer to procedures developed for adobes (Chapter 2). It is possible to treat adobes and fresh state earth mortars in the same frame because their manufacture follows the same "wet" process, contrary to compaction, which is "dry". The material is shaped or "masoned" when it reaches the consistency of a paste with a water content of about 17–30%. However, the composition of these two materials may be different when it comes to proportion and quality of clay; adobe may therefore contain more clay. Indeed, adobe remains a small element that is dried alone, while mortar creates a joint that dries under very different conditions by interacting with blocks and the atmosphere.

## 4.3. Masonry of earth blocks

When assessing the compressive strength of masonry, Eurocode 6 [CEN 96] correlates compressive strength values of mortar and block samples obtained in a laboratory with those of masonry strength. Because of its inaccuracy due to the difficulty of finding the mechanical characteristics of masonry based on knowledge of its components alone without taking their interactions into account, this approach is relatively open to criticism. We recommend carrying out tests on the masonry elements to directly get the

compressive strength of the masonry, namely on triplets for which examples will be given in the next section. With tensile strength being ignored, shear strength is generally not useful.

### 4.4. Stone blocks and mortars

To show that the very low strength of hand friable mortar (less than 1 MPa) is compatible with masonry stability, tests on triplets were carried out.

The configuration of three blocks/stones with mortar ("triplet") is generally considered to be representative of the stone/mortar interaction within the masonry. Triplets are used as samples subjected to compressive stress to assess the strength of the stone/mortar composite under loading.

Here we present results matching three different sources (Table 4.2). [VEN 97] used a low binder content sand:cement mortar (1:8). Tests on mortars alone were on cubic samples without anti-friction such that their real strength is probably below 1 MPa. [ASC 07] measured unconfined compressive strength on samples with an aspect ratio of 2 (Figure 4.8), for two earth mortars.

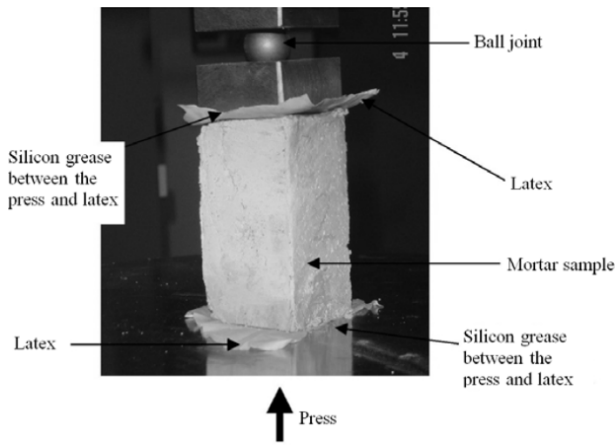


**Figure 4.8.** *Anti-friction compression (unconfined) test on an earth mortar sample*

[TRA 14] used a sand:lime mortar with hydraulic lime NHL5 for unconfined compression tests on samples with an aspect ratio of 2, as shown in Figure 4.8.

Tests on triplets were done as described in Figure 4.9. As the stone has significant stiffness, the influence of friction between the steel press and the stone is relatively low. In addition, the aspect ratio of the sample is 3, which justifies not using the anti-friction system. In addition, we are only interested in the central part, so the intermediate rubble stone (see Figure 4.9).

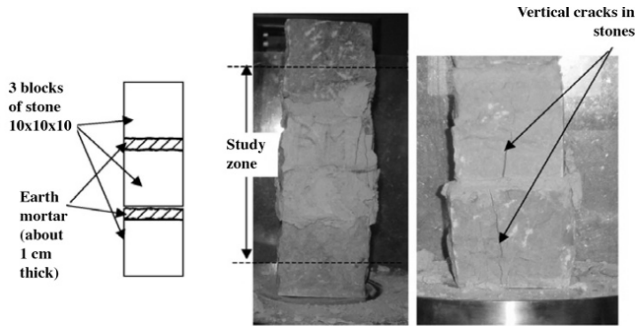


**Figure 4.9.** *Simple compression test on stone earth mortar triplet [ASC 07]*

Crushing of triplets is achieved by breaking stones through vertical cracks. The three sources in Table 4.2 have consistent and similar results. The strength of the triplet is far greater than that of the mortar. Even the smallest triplet strength of 11 MPa leaves a substantial coefficient of safety relative to the load distribution, which is around 0.25 MPa for a stone house of 2 storeys. These results show that mortar does not play a significant mechanical role in masonry that is correctly made.

However, one can see that the strength of mortar has an influence on the strength of the masonry: with a mortar of 3 MPa instead of 0.85 MPa, the brick work has greater strength (about 15 MPa instead of 11 MPa).

From the results of tests on triplets, we see that the strength of a wall depends on the stones first and secondarily on the strength of the mortar. Whatever the composition of the earth mortar, the wall will have a compressive strength safety coefficient of around 4 if the masonry is well made. This last point therefore has a greater impact on the performance of the wall.

| Materials | Compressive strength of stones (MPa) | Compressive strength of mortar (MPa) | Compressive strength of the triplet (MPa) |
|---|---|---|---|
| Granite [VEN 97] | 105 (3) | 2.8 | 33 (3) |
| Granite [VEN 97] | 86 (10) | 2.8 | 30 (3) |
| Limestone [ASC 07] | 96 | 0.85 | 11 (0.9) |
| Limestone [ASC 07] | 96 | 3 | 15 (0.4) |
| Shale [TRA 14] | 110 (30) | 0.7 | 47(2) |

**Table 4.2.** *Compressive strength of stones, mortars and triplets (standard deviation in brackets)*

## 4.5. Bibliography

[ACA 01] ACARY V., Contribution à la modélisation mécanique et numérique des édifices maçonnés, Doctoral thesis, LMA Marseille, 2001.

[ASC 07] Analyse des systèmes constructifs non industrialisés, ECOBATIR-CSTB-ENTPE-FFB-CAPEB, projet financé par l'ADEME dans le cadre du PUCA, 2007.

[AST 98] ASTM Specification C230/C230M-98e1 Standard Specification for Flow Table for Use in Tests of Hydraulic Cement, 1998.

[AZE 05] AZEREDO G., Mise au point de procédures d´essais mécaniques sur mortiers de terre, application à l´étude de leur rhéologie, Doctoral thesis, Génie Civil, ENTPE/INSA, 2005.

[AZE 08] AZEREDO G., MOREL J.C., LAMARQUE C., "Applicability of rheometers to characterizing earth mortar behavior. Part I: experimental device and validation", *Materials and Structures*, vol. 41, pp. 1465–1472, 2008.

[BEI 96] BEI G.E., Raw earth, an ancient and modern building material, Master thesis, Katholieke Universiteit Leuven, 1996.

[BOW 96] BOWLER G.K., JACKSON P.J., MONK M.G., "The measurement of mortar workability", *Masonry International*, vol. 10, no. 1, pp. 17–23, 1996.

[CEN 94a] COMITÉ EUROPÉEN DE NORMALISATION, NF EN 413-1, ciment à maçonner, partie 1: Spécifications, 1994.

[CEN 94b] COMITÉ EUROPÉEN DE NORMALISATION, NF EN 413-2, ciment à maçonner, partie 2: Méthodes d'essai, 1994.

[CEN 96] COMITÉ EUROPÉEN DE NORMALISATION, Eurocode 6: Calcul des ouvrages de maçonnerie -partie1-1: Règles générales- Règles pour la maçonnerie armée et non armée, ENV 1996-1-1.

[DEL 98] DELARRARD F., FERRARIS C.F., "Rhéologie du béton frais remanié, III – L'essai au cône d'Abrams", *Bull. des Labo. P. et Ch*., 215, pp. 53–60, 1998.

[DSW 04] Dry Stone Walling Techniques and Traditions, The Dry Stone Walling Association, 2004.

[GUI 08] Ouvrage collectif, Guide des bonnes pratiques de construction de murs de soutènement en pierre sèche, ENTPE, Paris, 2008.

[HEA 92] HEATHCOTE K., JANKULOVSKI E.,"Aspect ratio correction factors for soilcrete blocks", *Australian Civil Engineering Transactions, Institution of Engineers Australia*, vol. CE34, no. 4, pp. 309–312, 1992.

[HU 5] HU C., Rhéologie des bétons fluides, études et recherches des LPC, OA 16, 1995.

[LAS 08] LASSURE C., *La pierre sèche, mode d'emploi*, Eyrolles, Paris, 2008.

[GRO 00] GROOT C.J.W.P., LARBI J.A., "The influence of interfacial moisture exchange on mortar-brick bond strength", *6th International Seminar on Structural Masonry for Developing Countries*, Bangalore, India, pp. 148–156, 11–13 October 2000.

[NFP 81] NORME FRANÇAISE HOMOLOGUÉE, Béton essai d'affaissement, NF P 18-451, 1981.

[OLI 95] OLIVIER M., EL GHARBI Z., "Sisal fibre reinforced soil block masonry", *4th International Masonry Conference*, The British Masonry Society, London, UK, pp. 55–58, 26–28 October 1995.

[PKL 03] PKLA A., MESBAH A., RIGASSI V., MOREL J.C., "Comparaison de méthodes d'essais de mesures des caractéristiques mécaniques des mortiers de terre", *Materials and Structures/Matériaux et Constructions*, vol. 36, pp. 108–117, March 2003.

[SED 95] SEDRAN T., "Les bétons autonivelants", *Bulletin de Liaison des Ponts et Chaussées*, vol. 196, pp. 53–60, March–April 1995.

[SAA 84] STANDARDS ASSOCIATION OF AUSTRALIA, AS 2701.5, method for determination of constency-slump test, 1984.

[TAT 91] TATERSALL G.H., *Workability and Quality Control of Concrete*, E&FNSPON, London, 1991.

[UNI 82] UNIKOWSKI Z.R., Influence des argiles sur les propriétés des mortiers de ciment, Rapport de Recherche LPC, no. 110, February 1982.

[SHR 95] SHRINIVASA RAO S., VENKATARAMA B.V., JAGADISH K.S., "Strength characteristics of soil-cement block masonry", *The Indian Concrete Journal*, pp. 127–131, February 1995.

[TRA 14] TRAN V.H., VINCENS E., MOREL J.C., *et al.*, "2D-DEM modelling of the formwork removal of a rubble stone masonry bridge", *Engineering Structures*, to be published in 2014.

[VEN 96] VENU MADHAVA RAO K., VENKATARAMA B.V., JAGADISH K.S., "Flexural bond strength of masonry using various blocks and mortars", *Mater. Struct.*, vol. 29, pp. 119–124, 1996.

[VEN 97] VENU MADHAVA RAO K., VENKATARAMA B.V., JAGADISH K.S., "Strength characteristics of stone masonry", *Materials and Structures/Matériaux et Constructions*, vol. 30, pp. 233–237, May 1997.

[WAL 96] WALKER P., "Specification for stabilised pressed earth blocks", *Masonry International,* vol. 10, no. 1, pp. 1–6, 1996.

[WAL 97] WALKER P., STACE T., "Properties of cement stabilised compressed earth blocks and mortar", *Mater. Struct*., vol. 30, pp. 545–551, 1997.

[WAL 99] WALKER P., "Bond characteristics of earth block masonry", *Journal of Materials in Civil Engineering*, pp. 249–256, August 1999.

PART 2

# Graphic Statics

# 5

# The Foundations of Graphic Statics

## 5.1. Introduction

Graphic statics is a method for determining the equilibrium of solids using solely geometric constructions. Research on purely geometrical methods for designing structures was a practice that marked construction history [HUE 04]. Initial attempts involved developing empirical approaches on more or less complex systems. It is only through developments supporting the principles of statics that rational graphical approaches have been developed in parallel or in conjunction with analytical approaches. Thus, the same principles of statics allow a purely analytical or purely geometrical approach.

Analytical approaches are based on analytical geometry and equilibrium equations of a structure. These equations reflect the nullity of the sum of forces and moment applied to a balanced solid. Graphic statics is a way to graphically solve a static problem without analytical calculation. This type of approach is a full part calculation method (graphical calculation) as it gives numerical results by measuring graphical lengths. It is therefore an effective method for precisions considered acceptable by the user. The graphical method has an advantage for problems where systems have a large number of equations and for which there is no computational assistance. So long as calculations could not be automated by a computer, graphic statics were an effective calculation method for engineers. The precision of lines on paper is limited but sufficient if the margin of error can be estimated. Thus, graphic statics were an effective and widely used method in the 19th and early 20th Centuries. For example, the Eiffel Tower was calculated by graphic statics. Today, they have a pedagogical value for direct visualization of values in a graphical context, rapid implementation, and the direct link between

*Sustainable Masonry: Stability and Behavior of Structures,*
First Edition. Thierry Ciblac and Jean-Claude Morel.

geometric operations and physical phenomena. They are also a quick way to control the consistency of results if an analytical approach is also adopted. Dynamic geometry tools allow computational implementation of graphic statics for geometric configurations that change interactively, which has sparked a renewed interest in this method, especially for structural design problems for architects or engineers [CIB 08, FLE 08, ALL 10]. Applications for studying masonry structures using these tools are also the subject of contemporary developments [BLO 06].

Graphic statics are based on the principle of statics with a vector formalism of point mechanics for non-deformable solids. These principles are reflected graphically as they establish relationships between forces represented by vectors and their points of application. This makes it easy to translate the zero-sum applied to a solid in equilibrium by a geometric structure which consists of drawing a *polygon of forces* that must be closed. This chapter will only concern coplanar forces. Thus, construction of the polygon is done on a specially selected plane, called the *force plan*, which is independent of the figure representing the body and forces applied to it. The *layout plan* is the plane in which the solid and the forces applied are represented. The zero-sum of forces, which is necessary for the equilibrium of a solid, is not sufficient since the sum of the moments must also be zero. For this condition on moments to be taken into account geometrically, we proceed to the *reduction* of the system of forces, which can only be done in the *situation plane*. If the sum of forces is zero, or the system can be reduced to a couple, then the sum of the moments is clearly not zero, or it is reduced to zero force, in which case equilibrium is ensured. The basic concepts of graphic statics are described in detail in this chapter.

## 5.2. Concepts and principles of statics

### 5.2.1. *Hypotheses and basic concepts*

The purpose of statics is to study the mechanics of the body at rest, so immobile material points systems in a particular Galilean observation referential (the general movement of a body at rest in a Galilean referential is a rectilinear uniform translational movement). We are particularly interested in statics of solids, meaning bodies on which there are little strains. With this assumption, we can assume that strains on a solid are negligible under the effect of the actions applied to it. Thus, we base our reasoning on supposedly non-deformable solids. We will present concepts generally, particularly three dimensional aspects, then apply them to planar cases.

5.2.1.1. *Force*

For material statics, Galileo's first principle of inertia or Newton's first law (1642–1727) state that *a single material point has a constant speed of linear motion*. Thus, if a material point has no external action on it, its movement is not changed over time. We notice that immobility of the point relative to the observation referential only corresponds to the particular case where the velocity is zero. If the material point is not isolated, it may be influenced by other bodies that exert their forces upon it. Therefore, we can define the concept of force as the cause that modifies the movement of a material point. The concept of force is used to express the action exerted by one body on another with respect to its change in motion. For example, a pebble on the ground undergoes the influence of gravity in the form of its weight and its fall reflects its change in motion (constant acceleration) under the action of its own weight force.

A force is defined by:

– its point of application;

– its line of action;

– its direction;

– its magnitude, expressed in N (Newtons) in the ISU (International System Units).

When a force is applied to a solid, it will exert an action that modifies its overall movement in a translational direction with the same direction as the force.

The graphical representation of a force must be completely defined. Its point of application, line of action, magnitude and direction must therefore be characterized. Several equivalent representations exist, depending on whether we prefer to use vector or scalar (real number) on the oriented action line.

5.2.1.1.1. Vector representation of a force

The vector of force **F** (vectors are denoted in bold) is associated with a vector representation in the plane containing it (Figure 5.1). Magnitude $F$ of the force is equal to vector length **F** ($F$=||**F**||), therefore it is positive and is measured on the graph knowing the scale of associated forces. The direction of the vector directly gives the direction of the force. Application point A and force vector **F** are used to characterize and thus draw the line of action. In the example of Figure 5.1, a force representation scale is given by the length of a

segment associated with a magnitude of 10 N. This vector representation allows the graphical addition of vectors, which is why we adopt it as part of graphic statics.

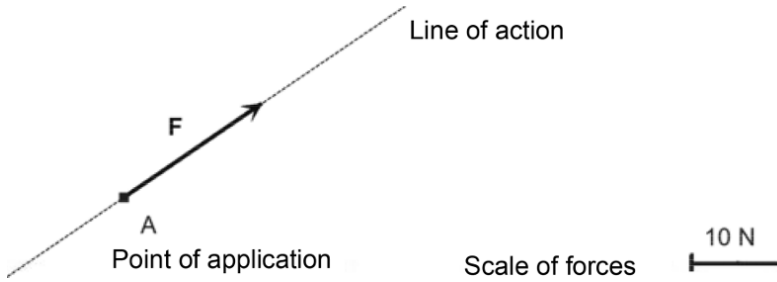


**Figure 5.1.** *Vector graphical representation of a force in a plane*

5.2.1.1.2. Scalar representation of a force

This is another graphical convention, often used for practical reasons. It involves representing force through the association of a number $F$ (scalar) equal to the magnitude of force with an arrow indicating the direction of its oriented line of action (axis). This representation has the advantage of not being associated with a force representation scale, as the value of $F$ gives its magnitude.

In this representation, if the direction of the force and its magnitude value are known, we can very easily switch to vector representation by using a force representation scale. For example, Figure 5.2 shows the graph representation of force $F$ applied at A in a plane. Scalar representation indicates a value of $F$ equal to 20 N, and the arrow shows the direction of the vector. In the example, the corresponding vector graph representation uses a force representation scale given by the length of a segment associated with a magnitude of 10 N. Vector **F** is oriented in the direction indicated by the scalar representation, and has a length that is double that of the segment fixing the forces representation scale.

The force component is equal to magnitude and is assigned a + or – sign depending on the direction of the axis. For the force shown in Figure 5.2, the **F** component on the axis is equal to –20 N.

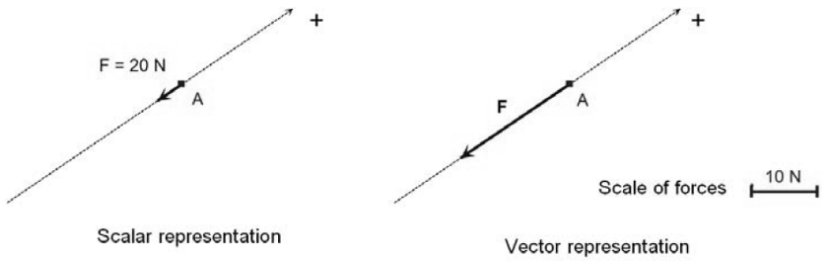


**Figure 5.2.** *Scalar and vector representations of a force F applied at A in a plane*

This convention also allows us to represent forces for which direction and magnitude are not known. For this, we give the arrow an arbitrary direction and carry out the force component calculations using this direction, the axis orientation and unknown magnitude *F*. The component sign obtained through calculation gives the actual direction of the force. We will see in what follows that in graphic statics, a static problem with an unknown line of action, magnitude or direction of force may be solved without analytical calculation.

A same force can be identified by its magnitude *F* or vector **F**. For notation homogeneity reasons and to present vector operations used in graphic statics, we denote forces by vectors.

5.2.1.2. *Moment*

We have seen that a force has the ability to produce a translational motion for a solid in the direction of its line of action and in the direction of its action. However, a force may also have the ability to rotate the solid about an axis, as in the case of a lever or a wheel. This ability is measured using the moment of this force with respect to a point.

The moment of force **F** relative to point O (Figure 5.3) is characterized by:

– its magnitude *M*, calculated by the following formula: $M=F.d$ expressed in N.m (Newton meter) in ISU where *F* is the magnitude of force and *d* is the distance from point O to the line of action of the force. Distance *d* is referred to as the *lever arm*;

– the slope of the axis and direction of rotation that the force may cause. The direction of the axis is perpendicular to the plane containing the force

and O. The sign of the moment is defined relative to a positive direction of rotation assigned by convention to the same plane.

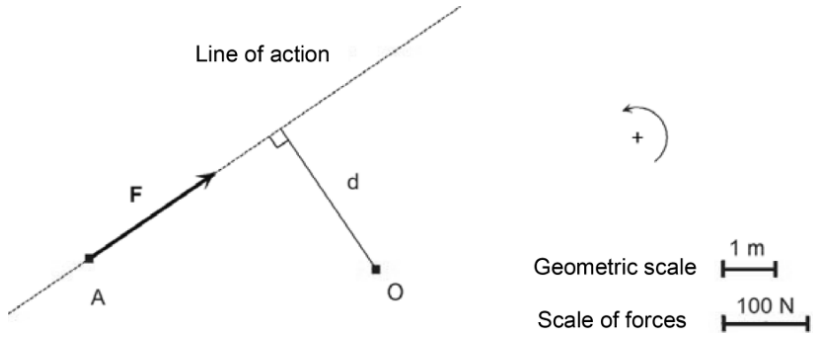


**Figure 5.3.** *Graphical representation of the characteristic elements of the moment of a force relative to point O in a plane and definition of conventional direction*

From the expression $M=F.d$, we notice that the moment of force depends on the position of point O from which it is calculated and is proportional to the lever arm $d$. That is why the notation of moment can be specified by writing $M_O\mathbf{F}$ to indicate that this is the moment of force **F** relative to O. Another consequence of this expression is that the ability of a given force to turn a solid is zero if the point from which it is calculated is on the line of action. In this case, the axis and the direction of rotation are not defined.

We may graphically represent force **F** in the plane containing O and **F**. Thus, the rotational motion that tends to cause force **F** is about an axis of rotation passing through O and perpendicular to this plane. On this plane, we must give a positive conventional direction of rotation and a geometric scale of representation in order to evaluate the sign of the moment and distances, especially the lever arm. For example, Figure 5.3 vectorially represents a force **F** in the plane containing O and **F**. In this case, the positive conventional direction of rotation is the inverse direction to clockwise. Force **F** tends to produce a rotation relative to O in the opposite direction of the positive direction, so the moment will be negative with the chosen convention. The sign of the moment of **F** is negative relative to all the points lying on the same side as O in relation to the line of action, and positive on the other side. In the example, the force representation scale is given by the length of a segment associated with magnitude 100 N and the geometrical representation scale by a segment associated with a length of 1 m.

5.2.1.2.1. Vector representation of moment

The definition of moment shows that it can be fully characterized by a free vector. Indeed, a vector may: by its length, indicate magnitude $M$ of the moment; by its direction, indicate the direction of the axis of rotation, and by its rotation indicate the direction of rotation. We denote by **M**, the moment vector for which the physical significance is very different from the force vector, since the unit is not the same (N.m) and the arrow indicates the direction of rotation and not a translation. Thus, it is impossible to add a force vector to a moment vector. To mark this difference in nature, it is sometimes useful to draw a curved arrow instead of a straight arrow on the letter designating the moment vector. In the example of Figure 5.3, the moment vector of force **F** relative to O must be perpendicular to the plane of the figure and the arrow should point to the observer if the convention that the direction of rotation in the clockwise direction is associated with the direction of the arrow oriented toward the observer. Analytical relationships between **M** and **F** are beyond the scope of this section on graphic statics, but they allow demonstrations and elegant calculations in three dimensional space (see for example [FRE 98]).

5.2.1.2.2. Scalar representation of moment

The scalar graphical representation of moment is mainly useful for setting planes into equations, but it can describe the moment of a force relative to a point in the plane containing the force and the point perfectly. This convention involves representing moment by the association of a number $M$ (scalar), able to be positive or negative, for which the absolute value is equal to the absolute value of $F.d$, and a curved arrow indicating the *positive conventional rotation direction assigned to the moment in question*. Thus, if the direction given by the arrow of force **F** induces a rotation in the same direction as the curved arrow, then $M = +F.d$ (as in Figure 5.4). If the direction of rotation is in the opposite direction to that of the curved arrow, then $M = -F.d$.

With this convention, the positive conventional direction of rotation defined for the plane is not useful for characterizing the direction of rotation of moment but it is used as a common convention to all force moments belonging to this plane and thus for algebraically summing moments. It is always important to use the graphically defined convention to define the sign of moment and only consider the overall direction for the algebraic sum.

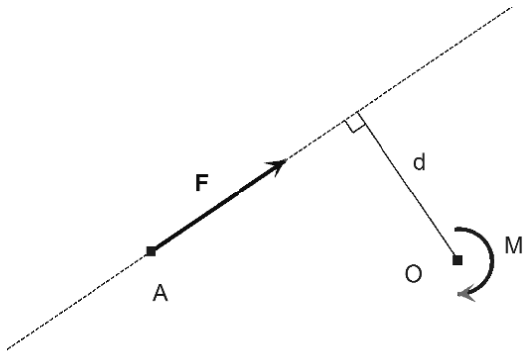


**Figure 5.4.** *Scalar graphical representation of moment M of a force F relative to a point O in a plane*

5.2.1.2.3. *Planar case*

Definitions of force and moment were given in full generality of space. The proposed representations in the case of a force are *in a plane containing it* and in the case of moment relative to a point O, in *the plane containing the force and point O*. Thus, scales and geometrical forces can be used in these planes. These representations are useful for a set of forces contained in the same plane, called *planar case*. If we wish to study a problem in space, graphical representations can only be simple to use in special cases where we consider spatial symmetries, for example.

*Planar case* is a solid plane subjected to a system of forces within this plane. For the planar case, point O, from which the moment of a force is calculated, is in the plane and the axis of rotation passes through O and always has the same direction, perpendicular to the plane, regardless of force. Thus, rotation may be defined relative to point O and not relative to an axis. In this case, the notion of moment relative to a point coincides with notion of moment relative to an axis that is perpendicular to the plane.

For the planar case, moment relative to a point of any force reflects the ability to rotate the solid around the same perpendicular direction to the plane. This is why we can calculate the algebraic sum of moment, relative to a reference direction of rotation, to assess the overall ability of the set of applied forces to rotate the solid about this direction. The equilibrium condition on the nullity of the sum of moments about a point reflects the nullity of the overall action of forces to produce a rotational movement.

5.2.1.3. *Degrees of freedom of a point or a solid*

The focus here is on the number of parameters, called degrees of freedom, which indicate the position of a point or a solid in space. We therefore focus on the only possible movements without addressing the causes of their modification.

Degrees of freedom of a point: the position of a point in space depends on three parameters ($x$, $y$, $z$ for example) so it has three degrees of freedom in space. If the point is in a plane (planar case problems), it only has two degrees of freedom ($x$ and $y$ for example).

Degrees of freedom of a solid: a free solid can have an overall translational movement in any direction in space and rotational movements, corresponding to 6 degrees of freedom: 3 for translations in the three directions $x$, $y$, $z$ in space, and 3 for rotations about $x$, $y$ and $z$. A solid plane moving freely in the plane has three degrees of freedom: 2 for translations in both directions $x$, $y$ of the plane, and 1 rotation about the orthogonal $z$ direction of the plane.

5.2.1.4. *Connecting elements and contact surfaces*

The interaction of a solid with its environment can be achieved through connecting elements or contact surfaces.

A connecting element is a device connecting two solids by blocking a number of degrees of freedom of one relative to the other. If a solid is influenced by the external environment that is assumed to be fixed, for example to rock, the connection is called an *external connection*. If a solid is part of a system of interconnected solids, a connection between the two solids is called *internal connection* (implying the internal connection to the system of solids). Internal connections ensure the assembly of elements of the structure while external connections ensure the connection of the whole structure to the external environment.

The connecting elements can be classified according to the movements they allow. Thus, the following connections are presented in descending order of the number of degrees of freedom allowed. We describe conventional connections below:

– a *simple support* allows rotation of the solid in each of the three axes of rotation and blocks a single translation in any particular direction, so it allows 5 degrees of freedom (3 rotations and 2 translations) and only blocks 1. In the

planar case, a single axis of rotation is possible (perpendicular to the plane), therefore there are 2 possible degrees of freedom and a single degree is blocked (1 translation);

– a *ball joint* permits rotation of the solid in each of the three axes of rotation, it allows 3 degrees of freedom and therefore blocks 3 (3 translations in $x$, $y$ and $z$). A physical device that ensures a connection between two solids A and B can be considered as a sphere attached to solid A and inserted into a spherical cavity in solid B. We must of course avoid any friction so that this system allows rotational movements. The gimbal is a mechanical device that also provides the same type of connection. In the *planar case*, a single rotation axis is possible (perpendicular to the plane), therefore there is only 1 degree of freedom possible and therefore 2 degrees are blocked (2 translations in $x$ and $y$);

– a *hinge* permits rotation of the solid in a single axis of rotation, it allows 1 degree of freedom and therefore blocks 5 (2 rotations and 3 translations in $x$, $y$ and $z$). In the *planar case*, the single axis of rotation possible for the hinge is perpendicular to the plane, so there is only 1 degree of freedom possible and therefore 2 degrees are blocked (2 translations in $x$ and $y$). In the planar case, the ball joint and hinge are equivalent but they are no longer in space;

– a fixed joint neither allows any rotation nor translation of the solid. It blocks the 6 degrees of freedom in space and 3 degrees of freedom in the planar case. Thus one fixed joint is sufficient to block all relative movements of both solids.

In any case, blocking a degree of freedom does not translate as the capacity of an element to resist relative movement from the two connected solids. This is characterized by a certain type of interaction between solids that we will described in section 5.2.4.

The contact surfaces between solids (interfaces) meet at, for example, foundations, structure supports and of course in masonry. The connecting elements described above cannot precisely model the behavior of these assemblies, as resistance criteria occur at these interfaces. These criteria are important because they allow us to define whether the connection can be ensured at the interfaces. The definition of criteria and their uses are described in the third part of this book.

5.2.1.5. *What is a principle of statics?*

Once the basic concepts are established, we should be able to use them to model real cases. Principles of statics are involved in real simple and general cases and establish relationships between quantities defined by concepts (forces, moment, distances, etc.). A principle in physics is only valid as long as experiments do not invalidate it. Together, these principles form a necessary and sufficient coherent system for the study of equilibrium of a solid. They allow mathematization of the problem and in the case of graphic statics, geometric mathematization. For statics, principles justify and characterize mathematical operations on the forces and moments applied to a solid.

### 5.2.2. *The principle of the parallelogram of forces*

The principle of the parallelogram of forces is attributed to Simon Stevin (1548–1620).

PRINCIPLE OF THE PARALLELOGRAM OF FORCES.– Two forces acting on a same point have the equivalent action of a single force acting on the same point, represented by the diagonal of the parallelogram based on these two forces.

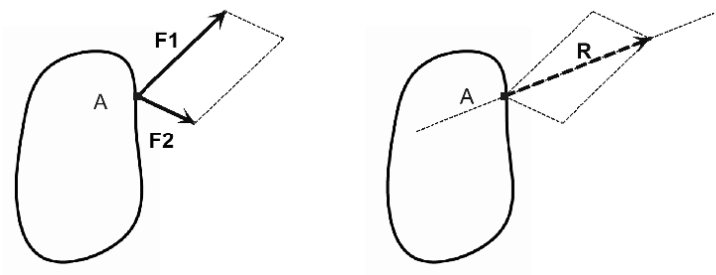


**Figure 5.5.** *Principle of the parallelogram of forces*

This principle *reduces* two forces applied at a point into a single force. Figure 5.5, left, shows a solid on which forces $\mathbf{F_1}$ and $\mathbf{F_2}$ are applied at point A. The right figure shows the equivalent force **R** applied in A.

Force **R** can be calculated vectorially: $\mathbf{R}=\mathbf{F}_1+\mathbf{F}_2$ and can be constructed graphically independently from the solid (Figure 5.6). But it should also be applied at point A to define the position of the line of action of the resultant force **R**.

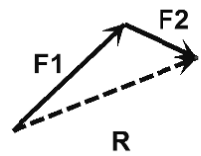


**Figure 5.6.** *Vector sum of forces*

COMMENT 5.1.– This principle can be verified experimentally using devices made of pulleys and weights. Very flexible wires that are assumed to be massless transmit force intensities equal to the suspended weights, while controlling the orientation of forces. Such devices have been used extensively in Stevin processes.

### 5.2.3. *The principle of equilibrium and its consequences*

#### 5.2.3.1. *The principle of equilibrium*

The principle of equilibrium is based on Galileo's principle of inertia (1564–1642) or Newton's first principle. Below, we summarize the formulation of [FRE 98].

PRINCIPLE OF EQUILIBRIUM.– A system of forces is in equilibrium if, when applied to a solid, it does not change the state of movement or rest of the solid.

This principle results in the nullity of the sum of forces and the sum of moments applied to a solid. Analytically, this principle is reflected by a written system of equations. The graphical approach is based on this principle, but breaks it down into two corollary principles that can be applied purely graphically: the principle of equilibrium of two forces and the principle of adding a system of forces in equilibrium.

5.2.3.2. *Two corollaries of the principle of equilibrium*

The two following principles, for which we took formulations by Pirard [PIR 67], can graphically represent the principle of equilibrium.

COROLLARY 5.1.– PRINCIPLE OF EQUILIBRIUM OF TWO FORCES.– Two forces can only be in equilibrium if they are equal and directly opposing.

Let us analyze this principle by considering two forces **F** and **F′** (Figure 5.7) that are directly opposed (**F=-F′**). The fact that the forces are equal and opposite results in the sum of forces being zero (**F+F′=0**). The fact that they are directly opposite implies that they are on the same line of action; the lever arm is therefore zero, the sum of moments is therefore also zero. Equilibrium of the solid is confirmed.

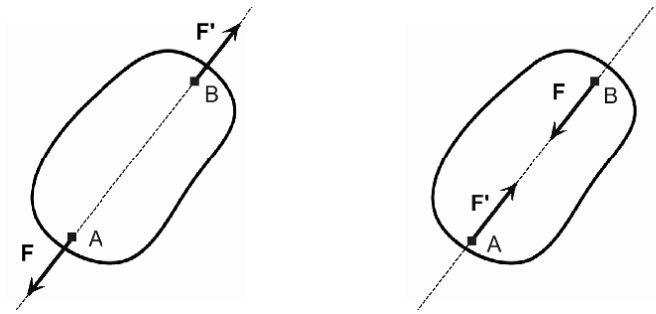


**Figure 5.7.** *Solids subjected to two forces in equilibrium*

This principle is illustrated in Figure 5.7 with application points A and B, of **F** and **F′** inverted in their common line of action. Thus, on the left, the equilibrium of a solid subjected to tensile forces, and on the right, a solid subjected to compressive forces. Both cases are statically equivalent, since both solids are in equilibrium. It is important to note, however, that stresses on the solid are of different types, and this has implications in terms of the resistance of the solid. Masonry has a capacity of resistance to compression but not to tension (see first part of this book). This implies that equilibrium conditions alone are not sufficient to ensure the stability of a structure. Herein the term “stability” in the sense of resistance, and not in the sense of stability theory. The third part of this book will focus on the inclusion of these criteria in the context of calculating yield design.

COROLLARY 5.2.– PRINCIPLE OF ADDING A SYSTEM OF FORCES IN EQUILIBRIUM.– The action of a given force system is in no way altered if one adds or subtracts any other system of forces in equilibrium.

This equivalence principle is valid in terms of equilibrium, but not in terms of the behavior of the solid. Adding a system of forces in equilibrium can cause transformations and reductions of force systems by judicious addition of systems in equilibrium. For example, it is easy to prove the theorem of sliding forces using this principle.

5.2.3.3. *Theorem of sliding forces*

THEOREM OF SLIDING FORCES.– Nothing changes on the action of a force acting on a solid when this force slides on its line of action.

The proof of this theorem is easily shown using the principle of adding a system of forces in equilibrium consisting of only two forces. Figure 5.8(a) shows a solid subjected to a force **F** applied at A. The system of two forces in equilibrium **F′** and **F″** applied at A and B respectively is added, with B on the line of action of **F** and is added such that **F′**=-**F** (Figure 5.8(b)). It follows that **F″**=**F**. By noticing that the system formed by **F** and **F′** is in equilibrium, it can be removed. We then get the configuration in Figure 5.8(c), where the single force **F″**=**F** is applied at B. We see that force **F** has slid on its line of action from A to B without changing the action of the force on the solid, at least as regards its equilibrium conditions.

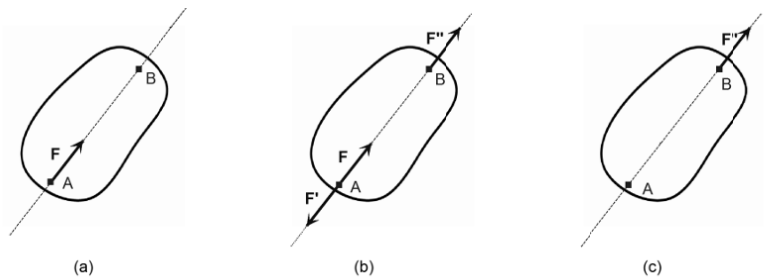


**Figure 5.8.** *Proof of the theorem of sliding forces*

5.2.3.4. *Couple*

A *couple* is a set of two forces of the same magnitude, in opposite directions and with parallel lines of action. The distance between the lines of action of the two forces is referred to as the *couple lever arm*.

A consequence of defining the couple is that the sum of forces is zero but the resultant moment with respect to a point is not.

We will now consider the *planar case*. Figure 5.9 represents a couple consisting of two forces **F** and **-F** in their plane. The lever arm is denoted as *d*. We can try to determine the resultant moment relative to point O in the plane of the couple. The lever arm of forces are respectively denoted as *da* and *db*. Thus, following the sign convention shown in the figure by the conventional positive direction of moment calculated in O and the position of point O relative to the lines of action, we get $M = F\,da - F\,db = F\,(da-db)$. But $d = da - db$. Wherefrom $M = -F.d$.

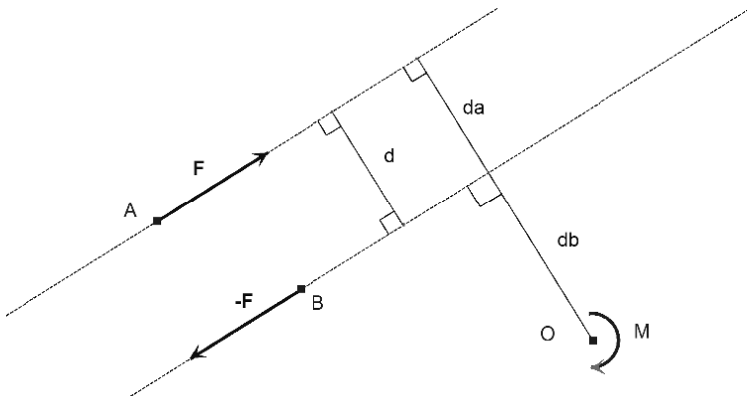


**Figure 5.9.** *Couple and determination of moment relative to point O in the plane containing the couple*

We get the same expression regardless of the position of O relative to the lines of action of forces. The expression of *M* is independent of the position of O because *d* does not depend on O. In the example, moment is negative, which corresponds to the direction of rotation that the couple causes. Thus we can deduce a very peculiar feature of a couple:

FEATURE 5.1.– The resultant moment of a couple is independent of the point from which it is calculated. The moment of force **F** and of lever arm d, has magnitude:

$$Mc = F\,d \qquad [5.1]$$

This feature illustrates the fact that *moment is a free vector that can be replaced by a couple*. In addition, this property shows that couples with different magnitude forces can have the same moment if the product *F.d* is retained. A couple of forces **F′** and **-F′** must have a lever arm $d'=Mc/F'=F/F'd$, for a moment with the same magnitude as the previous one.

This property, which is easily proven in the planar case, is also true in three dimensional space. Its demonstration in three dimensional space is facilitated by the use of vector calculus.

5.2.3.5. *Reduction of a force at a point*

The reduction of a force at a point involves determining a simple system consisting of a force and an equivalent moment applied at that point.

FEATURE 5.2.– A force F applied at point A is equivalent to a force of the same direction, slope and magnitude applied on another point B, with the moment of the force relative to point B.

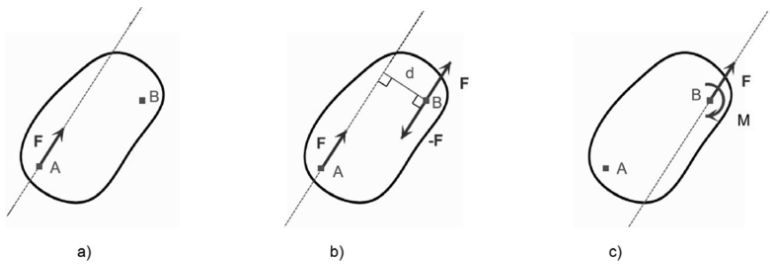


**Figure 5.10.** *Stages for reduction of a force at a point represented in its plane*

Proof of this property is done by adding two forces in equilibrium to point B: **F** and **-F**. Thus, according to Corollary 5.2, this new system (shown in Figure 5.10(b)) is statistically equivalent to the initial system (a). We then recognize a couple (**F** applied at A and **-F** at B) for which (free) moment can be applied at B (shown in (c)). Also, the moment of the couple corresponds to the moment of **F** (applied at A) with respect to B.

The theorem of sliding can be seen as a direct application of this property.

5.2.3.6. *Torsor*

The reduction of a force at a point is characterized by the set consisting of a force and the moments applied at this point. Moment is applied at this point but it is still a free vector. This set, consisting of a force and moment applied at a point, is called *torsor*.

### 5.2.4. *The principle of reciprocal actions (or action and reaction)*

The principle of reciprocal actions, also known as the principle of action and reaction, is none other than Newton's third law.

THE PRINCIPLE OF RECIPROCAL ACTIONS.– A solid A that exerts action $\mathbf{F}_{A/B}$ on solid B, receives action $\mathbf{F}_{B/A}$, which has the same support and magnitude as the first action but in the opposite direction.

We get the relationship:

$$\mathbf{F}_{B/A} = -\mathbf{F}_{A/B} \qquad [5.2]$$

Reciprocal actions between solids can be forces and moment. They can take place remotely (gravitational forces) or through contact. Solids can be connected by connecting elements characterizing the types of eligible reciprocal actions (forces, moment and direction).

To illustrate this principle, let us consider the example of two solids connected at their point of contact by a *ball joint* (Figure 5.11). At this contact point, solid A exerts the force $\mathbf{F}_{A/B}$ and solid B exerts the force $\mathbf{F}_{B/A} = -\mathbf{F}_{A/B}$ on solid B. In space, all relative movements of rotation between the two solids are permitted by the ball joint, so no moment can occur between the two solids and only forces passing through the ball joint and from such directions are involved. In the planar case, Figure 5.11 may be viewed as representing two planar solids connected by a *hinge*. In this case, the only relative movement between the solids is a rotational movement and as such moment cannot occur between the two solids and only forces passing through the hinge are involved. If there was a *fixed joint* at the point of contact, no relative movement could take place, and reciprocal actions could include forces and moment.

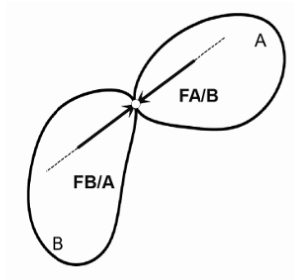


**Figure 5.11.** *Reciprocal actions of two solids connected by a ball joint*

COMMENT 5.2.– If solid A was chosen as a reference solid, the action of solid A exerted on solid B may be simply called an *action* (implying the action of A on B), while the action undergone by solid A from solid B is called *reaction* (implying the reaction of B on A), wherefrom the former name of the principle: "action and reaction". But beware, it is not that one solid "acts" and the other "reacts" but rather that two solids that interact. That is why we currently prefer to call this principle 'the principle of reciprocal actions', because the choice of a reference solid is purely arbitrary. However, we do use the term reaction, as it is commonly used for many readers and is present in many texts.

## 5.3. Layout plan and force plan

Graphic statics is based on the principles of statics, but also on a method of graphical representation separating information relating to the vector sum of forces and those of moments. This separation is made possible by the simultaneous use of two plans, one for layout the other for forces.

### 5.3.1. *Layout plan*

DEFINITION OF THE SITUATION PLAN.– *The layout plan is the plan in which the solid and the forces applied to it are represented. Two levels of representation are necessary: a geometric scale and a scale representation of forces.*

The layout plan allows the representation of forces and the positioning of their lines of action relative to the object. The object of study must be

represented at a scale called geometric scale, which we denote as $e_g$. This number is dimensionless since it represents the ratio of length measurements of the object and the figure. Thus, 1 m on the object measures $e_g$ m (for example, 1 cm if $e_g = 1/100$) on the layout plan figure. Forces applied to the object are represented by a scale called the scale of forces, which we denote as $e_f$. This number is dimensional since it represents the ratio between the measurement of a force and its graphical representation in terms of length in the plane. The scale of forces $e_f$ is expressed in N/m if SI units are selected. Thus, a length of 1 m in the figure represents a force of $e_f$ N (for example, a vector of length 1 cm represents a force of 50 N if $e_g = 5000$ N/m) on the layout plan figure. Given the usual dimensions of figures measured in cm, it may be convenient to express $e_f$, as appropriate, in N/cm or kN/cm.

For reasons of clarity in the graphical troubleshooting of statics, it is important to dedicate the layout plan to the determination of lines of action and positioning of forces only. Thus, in the layout plan, no operations on vectors should be performed. For this, a special plane is used – the force plan. This approach allows the use of a scalar representation of forces in the layout plan and vector representation in the force plan. In the latter case, only the geometric scale is useful in the layout plan.

EXAMPLE 5.1.– SUM OF TWO CONCURRENT FORCES.– Determination of two concurrent forces in graphic statics reflects the theorem of the parallelogram of forces. Figure 5.12 shows an illustration of the initial data of the parallelogram theorem. The resultant of the two forces will be built in terms of the force plan and positioned in the layout plan.

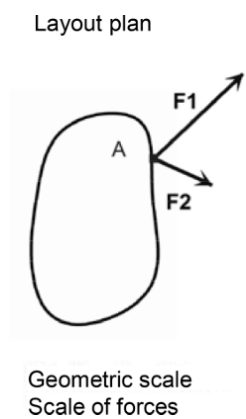


**Figure 5.12.** *Layout plan in the example of the theorem of the parallelogram*

### 5.3.2. *Force plan*

DEFINITION OF THE FORCE PLAN.– *The force plan is a separate plane from the layout plan where only vector operations on forces are built.*

The force plan allows visualization of the conditions relative to the sum of forces, including nullity of equilibrium. Thus, only the scale of forces is necessary in terms of forces. Conditions for the sum of moments are only seen in the layout plan. Indeed, lines of action can only be placed in the layout plan.

EXAMPLE 5.2.– SUM OF TWO CONCURRENT FORCES (CONTINUED).– To continue Example 5.1, Figure 5.13 shows the resultant of two forces by vector sum.

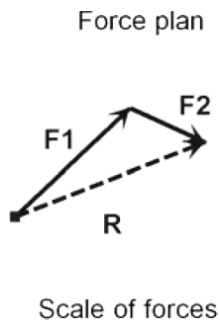


**Figure 5.13.** *Force plan in the example of the sum of two concurrent forces*

To complete the representation, the resultant vector built in the force plan is used, and is positioned in the layout plan in A (Figure 5.14). This last step is used to represent the line of action of the resultant.

The initial forces are shown as solid lines and the resultant as a dotted line in order to avoid ambiguity about the forces that really act on the solid.

We notice in this simple example that there is to-ing and fro-ing between the structures of the layout plan and the force plan. This will be a constant in graphic statics methods.

This basic example, the dissociation of layout plans and planes of forces, does not seem very useful and even seems somewhat artificial. Its utility will be revealed for more specific configurations like the determination of the

resultant of two parallel forces, or more complex events such as the resultant of *n* forces. These aspects will be developed in the following chapters.

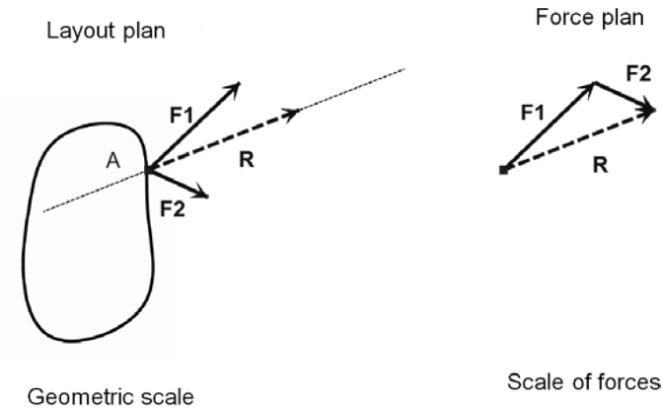


**Figure 5.14.** *Representation following the conventions of graphic statics of the sum of two concurrent forces*

## 5.4. Bibliography

[ALL 10] ALLEN E., ZALEWSKI W., *Form and Forces: Designing Efficient, Expressive Structures*, John Wiley & Sons, New York, 2010.

[BLO 06] BLOCK P., CIBLAC T., OCHSENDORF J., "Real-time limit analysis of vaulted masonry buildings", *Computers and Structures*, vol. 84, pp. 1841–1852, 2006.

[CIB 08] CIBLAC T., "Structure computation tools in architectural design. Teaching experimentations" *Proceedings eCAADe 2008* (Education and research in Computer Aided Architectural Design in Europe), Antwerp, Belgique, September 2008.

[FLE 08] FLEURY F., *Nouvelles perspectives pour la statique graphique*, Complément Technique des éditions Le Moniteur, Hors série, September–October 2008.

[FRE 98] FREY F., *Analyse des structures et milieux continus, Statique appliquée,* Presses polytechniques et universitaires romandes, Lausanne, vol. 1, 2nd ed., 1998.

[HUE 04] HUERTA S., *Arcos, bóvedas y cúpolas. Geometría y equilibrio en el cálculo tradicional de estructuras de fábrica,* Instituto Juan Herrera, Escuela Técnica Superior de Arquitectura de Madrid, 2004.

[PIR 67] PIRARD A., *La statique graphique*, 3rd ed., Dunod, Paris, 1967.

# 6

# Reduction and Equilibrium of a System of Forces in a Plane

## 6.1. Goals for the reduction of a system of forces

In this chapter, we consider a solid subjected to a system of forces in a plane. We can use graphic statics methods to study the equilibrium of these systems. In this chapter, we do not portray solids on which forces are applied.

The reduction of a system of forces involves seeking a system, usually the simplest possible, that is equivalent to the first, from the point of view of statics. Thus, the overall effect on the equilibrium of the solid is retained in the reduction procedure. For example, in the principle of the parallelogram of forces, finding the result involves reducing two concurrent forces into one.

To shift from a system of forces to an equivalent system from the perspective of statics, we must rely on the principles of statics. Thus, some operations on a system of forces that directly arise from these principles are:

– *addition or removal of a system of forces in equilibrium* (in view of Corollary 2 of the principle of equilibrium). This can be a very simple system such as two forces in equilibrium (used in the case of reduction of a force at a point, see section 5.2.3.5) or it can be more complex but carefully chosen systems;

– *reduction of two concurrent forces into one* using the principle of the parallelogram of forces and the theorem of sliding forces (see section 6.2.1.1).

*Sustainable Masonry: Stability and Behavior of Structures,*
First Edition. Thierry Ciblac and Jean-Claude Morel.

Reduction of a system of forces can be used to simplify a problem, but it is also a tool for determining the equilibrium conditions of a solid. Indeed, if the system is reduced by a torsor, all external environment reactions must balance this torsor.

To study the reduction of systems of forces, we first consider the case of concurrent forces, then the case of arbitrary forces and deduce equilibrium conditions from these.

## 6.2. Concurrent forces in the plane

Cases of concurrent forces are frequently encountered in construction systems, for example in tensile cable systems, stayed masts and reticulated structures consisting of rods connected by hinges. For masonry, the forces applied to a block can be seen as the resultant of stresses at the interfaces. In the case of equilibrium of a block connected to the rest of the structure by two interfaces, we consider equilibrium of three forces (weight of the block and the resultant at the two interfaces), which can only be concurrent, as will be discussed in section 6.2.4. If there are more than two interfaces, the forces in equilibrium are generally not concurrent.

### 6.2.1. *Reduction of concurrent forces*

Concurrent forces are forces for which the lines of action are concurrent. In Euclidean geometry, in which we usually place ourselves, such forces are distinguishable from parallel forces for which the lines of action do not intersect. Reduction of this system can be done very simply using the principle of the parallelogram and the theorem of sliding forces.

#### 6.2.1.1. *Reduction of two concurrent forces*

Here, we consider the case of two concurrent forces. Reducing this system uses the principle of the parallelogram and the theorem of sliding forces. There are four stages based on these principles (Figure 6.1):

1) in the force plan, the *vector sum of the two forces* is determined by the construction of a force polygon and the resultant vector **Fr**;

2) in the layout plan, the *sliding of the two forces to the point of intersection* I of their lines of action is used (application of theorem of sliding forces with two forces);

3) in the layout plan, we *construct the line of action of the resultant force* by drawing the line parallel to **Fr** through I (application of the principle of the parallelogram of forces);

4) in the layout plan, *the resultant force* **Fr** *is positioned on the previously determined line of action*. The theorem of sliding forces implies that the point of application of the resultant can be any point on the previously determined line of action. The force **Fr** is placed in the layout plan in Figure 6.1, shown as dotted lines to distinguish it from the initial system.

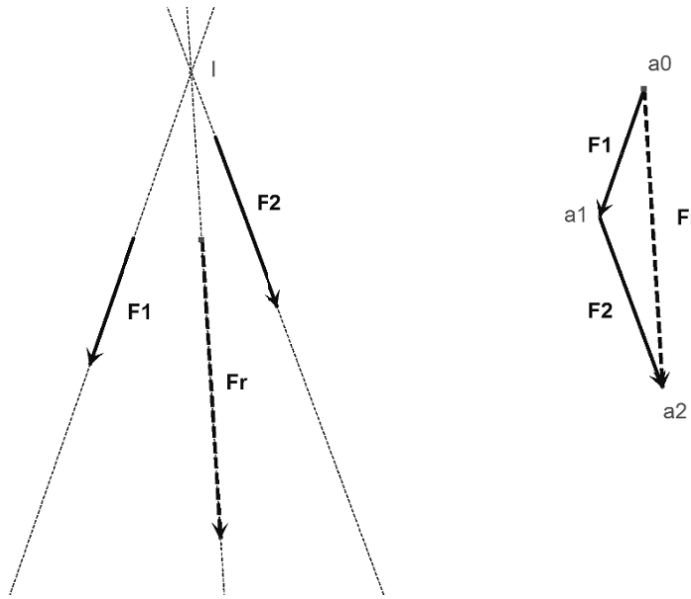


**Figure 6.1.** *Reduction of two concurrent forces*

In practice, the construction boils down to two steps:

1) in the force plan, determining the *vector sum of the two forces* through the construction of a force polygon and deduct the resultant vector **Fr**;

2) in the layout plan, placing the resultant **Fr** on a line parallel to the force passing through the point of intersection I.

This method cannot be applied to the case of two parallel forces of distinct lines of action, since in this case, the point of intersection of forces

does not exist (in Euclidean geometry, two distinct parallel lines do not intersect).

In the force plan, it may be useful to consider the points of origin and extremities of successive vectors in the vector sum. Thus, $\mathbf{F_1}=\mathbf{a_0a_1}$ and $\mathbf{F_2}=\mathbf{a_1a_2}$ and the resultant force $\mathbf{Fr}=\mathbf{a_0a_2}$. Thus, the line of action of force **Fr** is parallel to the line ($a_0a_2$) that passes through I.

We chose to carry out the vector sum starting with $\mathbf{F_1}$, but as the order does not matter in vector addition, the resultant force is of course the same if we start with $\mathbf{F_2}$.

6.2.1.2. *Reduction of n concurrent forces*

We can generalize the previous method to the case of *n* concurrent forces in I (Figure 6.2). To do this, in a first instance, we apply the method above for the first two forces $\mathbf{F_1}$ and $\mathbf{F_2}$. We get the resultant for $\mathbf{a_0a_2}$ in the force plan, which passes through the layout plan at the point of intersection I. Force $\mathbf{F_3}$ is then added to this force and the resultant force $\mathbf{a_0a_3}$ is obtained in the force plan. This force is then positioned on the line of action parallel to $\mathbf{a_0a_3}$ and passing through I. This process is continued each time until the last resultant force $\mathbf{Fr}=\mathbf{a_0a_5}$ and it is positioned in the layout plan on the line parallel to that of the force through I.

Finally, the only practical operation to identify and locate the resultant force of *n* concurrent forces results in:

1) the force plan, determining the *vector sum of n forces* through the construction of a force polygon and deducting the resultant vector **Fr**;

2) the layout plan, *placing the resultant **Fr** on a line parallel to the force passing through the point of intersection I.*

We note once again that the order of forces is chosen arbitrarily (we could have, for example, added the forces in the following order $\mathbf{F_2}+\mathbf{F_5}+\mathbf{F_3}+\mathbf{F_1}+\mathbf{F_4}$) and it would not affect the resultant.

We further note that the case of concurrent forces is a simple special case, as the resultant passes through the point of intersection of forces. Generally, there is no common point of intersection, and we must therefore determine the position of the line of action of the resultant in the layout plan.

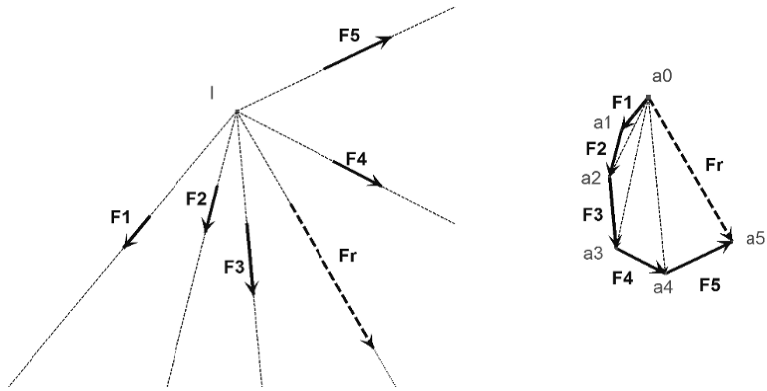


**Figure 6.2.** *Reduction of n concurrent forces*

### 6.2.2. *Equilibrium condition of n concurrent forces*

The study of the reduction of *n* concurrent forces discussed previously shows that the system is reduced to a resultant force **Fr** that passes through the point of intersection of *n* forces. Thus, if this resultant is zero, the force polygon is closed and the system is in equilibrium. Conversely, if the system is in equilibrium, the resultant is zero. *We therefore conclude that the equilibrium of n concurrent forces is equivalent to the closure of the force polygon.*

This necessary and sufficient equilibrium condition, which is only valid for concurrent forces, only corresponds to nullity of the sum of forces. Nullity of the sum of moments follows because the system of concurrent forces can always be reduced to a single resultant force **Fr**. In other words, it is not possible to reduce a system of concurrent forces to a single couple that could lead to a zero-sum of moments.

If *n* forces are not in equilibrium, to balance a system of *n* concurrent forces, a force must simply be applied directly opposite **Fr**. Thus the force polygon closes, so there is equilibrium of forces, and by placing the force **-Fr** on the line of action of **Fr** (passing through the point of intersection of forces), equilibrium of moments is ensured.

### 6.2.3. *Decomposition of a force into several concurrent forces*

6.2.3.1. *Decomposition of a force into two concurrent forces*

The problem involves determining two concurrent forces, for which the lines of action are given, that are statically equivalent to a given force. Using the principle of the parallelogram in the opposite direction, we see that the only condition on the lines of action of the two forces is that they are concurrent with the line of action of the initial force. Thus, the plot is started in the layout plan using two lines of action of forces $\mathbf{F_1}$ and $\mathbf{F_2}$ which must decompose **F**. These lines of action intersect at I (Figure 6.3). We wish to determine the magnitude and direction of forces $\mathbf{F_1}$ and $\mathbf{F_2}$. To do this, we know that the vector sum of $\mathbf{F_1}$ and $\mathbf{F_2}$ is equal to **F**. Therefore, we plot the lines parallel to the line of action of $\mathbf{F_1}$ and $\mathbf{F_2}$, respectively passing through the origin $a_0$ and end point $a_1$ of vector **F**, in the force plan. Thus point $O_1$, the intersection of these two lines corresponding to the end point of $\mathbf{F_1}$ and the origin of $\mathbf{F_2}$, is determined. $\mathbf{F_1}$ and $\mathbf{F_2}$ vectors are perfectly determined and we only need to place these forces in the layout plan on their line of action to get the layout decomposition.

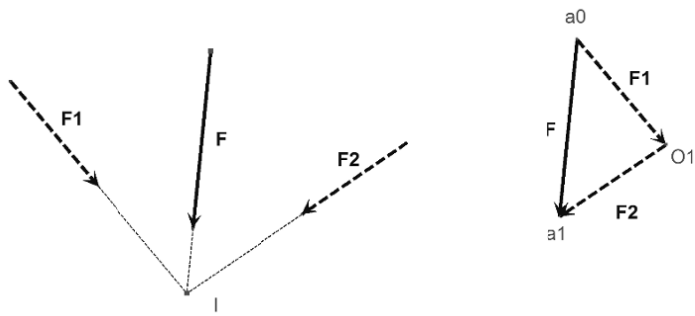


**Figure 6.3.** *Decomposition of a force into two concurrent forces*

Let us note that the decomposition of **F** could have been done starting with $\mathbf{F_2}$. In this case, the intersection point of lines parallel to the lines of action would be different, but vectors $\mathbf{F_1}$ and $\mathbf{F_2}$ would obviously be identical, because the complete parallelogram is constructed.

This method does not decompose a force into two parallel forces. To do that, the funicular polygon method must be used, as will be discussed later.

EXAMPLE OF USE 6.1.– Weight hanging from a wire attached to two anchor points, to a triangular frame, or to a triangular bracket. The equilibrium conditions of the three devices can be studied through decomposition of a force (weight) in two directions to determine the three forces in equilibrium at the point of application of a weight. This initially involves determining the tension in the infinitely flexible wire fixed at two anchor points, A and B, from which a weight **P** is suspended at I (Figure 6.4). A similar device could be formed of two rods hinged at I and at anchor points A and B. The direct application of the decomposition of forces shows that if the weight **P** and the shape taken by the wire (triangle AIB) is known, then the lines of action of tension are also known and these are the lines (IA) and (IB). Their magnitude and direction are uniquely determined ($\mathbf{T_1}$ and $\mathbf{T_2}$) by decomposing the weight **P** in the directions of both wires and writing the equilibrium of node I. $\mathbf{T_1}$ and $\mathbf{T_2}$ are the respective actions of AI and BI at point I. This is an isostatic case.

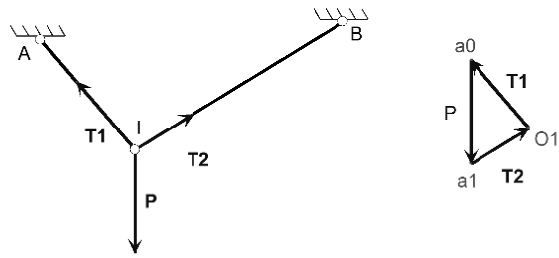


**Figure 6.4.** *Decomposition of a force applied to a weight hanging from a wire fixed at two anchor points*

A similar case in terms of resolution is that of a weight applied to the central joint of a triangular three-hinged gantry (Figure 6.5). In this case, the two rods are compressed. This configuration, unlike the previous one, is suitable for materials that are resistant to compression and not to tension, such as masonry. However, we must not forget that the weight of the rods is ignored here, which is not an acceptable assumption for masonry constructions for which the weight is a predominant load. We can pass from a tensile structure to a compressed structure through a horizontal symmetry axis, and for the same sum of forces $\mathbf{T_1}$+$\mathbf{T_2}$ in the force plan, the position of the point $O_1$, in the case of compressed rods, is to the left of **P** (Figure 6.5), while it was on the right for tensile rods (Figure 6.4). The generalization for multiple weights will be discussed in section 7.4.1.

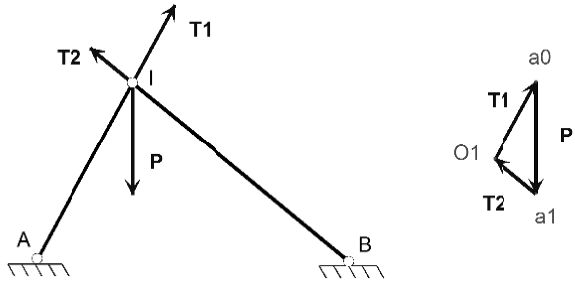


**Figure 6.5.** *Decomposition of a force applied to a triangular gantry*

A third case (that is equivalent in terms of statics) is that of a bracket formed of two hinged rods fixed at the ends to a vertical wall and loaded at a central node (Figure 6.6). In this case, one rod is compressed (AI) and the other is tensed (BI).

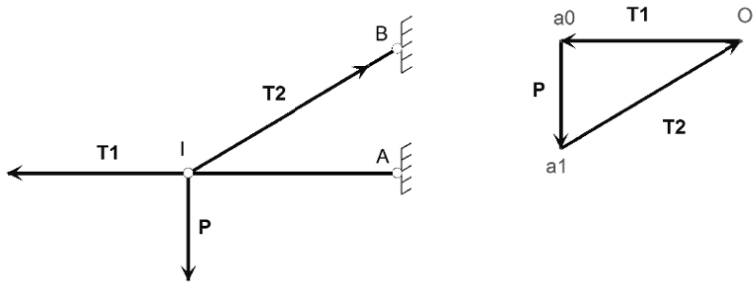


**Figure 6.6.** *Decomposition of a force applied to a triangular bracket*

6.2.3.2. *Decomposition of a force into n concurrent forces*

If we generalize the above problem to the case of *n* concurrent forces for which lines of action are known, we can easily realize that there is no more uniqueness of decomposition once $n > 2$. Indeed, closing the circuit of forces requires that, for an order of directions with given forces, the directions of the initial and final vectors respectively pass through the origin and end point of vector **F**. Thus, in the force plan (Figure 6.7), we construct lines parallel to the line of action of $\mathbf{F_1}$ passing through the origin of **F** and the line parallel to the line of action of $\mathbf{F_n}$ ($\mathbf{F_3}$ in the example where $n = 3$ in Figure 6.7). In the case of three forces, to close the circuit of the sum of vectors ($\mathbf{F_1}+\mathbf{F_2}+\mathbf{F_3}$), it suffices to position a line parallel to $\mathbf{F_2}$. To do this, we can take an arbitrary

point $O_1$ on the line passing through origin $a_0$ of **F**. $O_1$ corresponds to the end point of $\mathbf{F_1}$ and origin of $\mathbf{F_2}$. This arbitrary choice of $O_1$ fixes the arbitrary magnitude and direction of force $\mathbf{F_1}$. Point $O_2$, end point of $\mathbf{F_2}$ and origin of $\mathbf{F_3}$, is then obtained through the intersection of the line parallel to $\mathbf{F_2}$ passing through $O_1$ with the line passing through the end of **F** ($a_1$). Another option for the position of $O_1$ (Figure 6.8) on the line passing through $a_0$ would lead to another circuit and therefore to a different system of forces equivalent to **F**.

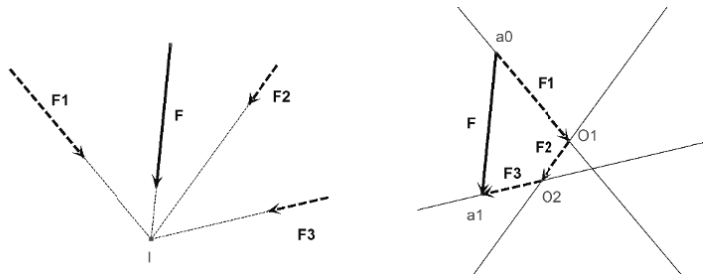


**Figure 6.7.** *Decomposition of a force into three concurrent forces*

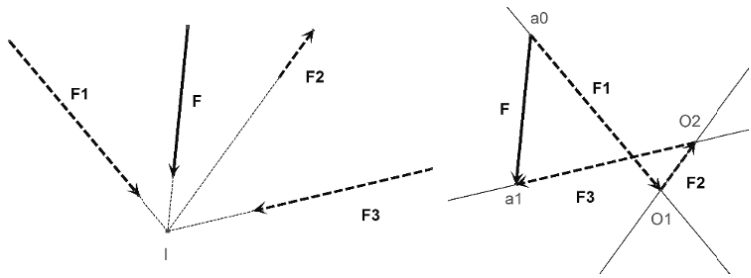


**Figure 6.8.** *Another decomposition of a force into three concurrent forces obtained by changing the position of $O_1$*

For *n* concurrent forces, the number of arbitrary choices of points ($O_1$, $O_2$, etc.) on the lines parallel to the corresponding forces is equal to *n-2*. Thus, to establish a decomposition of *n* concurrent forces defined by their lines of action, we must arbitrarily fix *n-2* forces.

EXAMPLE OF USE 6.2.– Weight attached to n tensile wires. This involves determining the tensions of *n* infinitely flexible wires connected to a weight at one end (I) and fixed at their other end attached to an anchor point (A, B, C…). Direct application of the decomposition of forces shows that if the

weight (**P=F** assumed to be vertical) and the shape taken by the wire (AI, BI, CI…) is known, the tensions cannot be determined by initial data only, because there is an infinite number of possible solutions for tensions ($\mathbf{T_1}$=-$\mathbf{F_1}$, $\mathbf{T_2}$=-$\mathbf{F_2}$, $\mathbf{T_3}$=-$\mathbf{F_3}$...). This is a hyperstatic case. To get the real equilibrium state of the structure, we must know the law of behavior of materials that defines the relationship between the applied strains and stresses. We may notice that in the case of the geometry of Figure 6.7, wires are tensed under the action of force **F**, but in the case of Figure 6.8, wire number 2 should be compressed, which cannot be the case (a wire can only absorb tension forces). Physically, a similar device formed of hinged rods and not wires forms a hyperstatic system that can absorb tension and compression forces of the case in Figure 6.8.

### 6.2.4. *Theorem of three forces*

The theorem of three forces, of particular practical use, gives a geometric condition necessary for the equilibrium of three forces.

THEOREM OF THREE FORCES.– Three non-parallel forces in a plane can only be in equilibrium if they are concurrent.

This theorem can be easily deduced from the reduction of two concurrent forces. Let us suppose three forces $\mathbf{F_1}$, $\mathbf{F_2}$ and $\mathbf{F_3}$ that are non-parallel and in equilibrium: $\mathbf{F_1}$ and $\mathbf{F_2}$ are concurrent by assumption and can therefore be reduced to a force **Fr** through their point of intersection. Force $\mathbf{F_3}$ must balance **Fr** and be equal and directly opposite to it. The line of action of $\mathbf{F_3}$ must therefore pass through the point of intersection of forces $\mathbf{F_1}$ and $\mathbf{F_2}$. Thus, the three forces are concurrent.

COMMENT 6.1.– We can generalize this theorem to the case of parallel forces by considering that the lines of action of forces have their point of intersection at infinity. The proof then uses the notion of the funicular polygon.

COMMENT 6.2.– This theorem in the plane is a special case of a more general theorem in three-dimensional space that says that *the lines of action of three forces in equilibrium are concurrent and coplanar*. Proof is given in [FRE 98].

## 6.3. Arbitrary forces in a plane

Here we will discuss the reduction of arbitrary forces in a plane by generalizing the approach used for concurrent forces, namely the successive application of the theorem of the parallelogram of forces. From this approach, we deduce various possible circumstances of reduction of these systems of arbitrary forces.

### 6.3.1. *Method of successive applications of the theorem of the parallelogram of forces*

Let us consider a system of *n* arbitrary forces ($\mathbf{F_1}$, $\mathbf{F_2}$ …$\mathbf{F_n}$) in a plane. We wish to reduce this system. To do this, we seek to successively reduce the forces starting with two that are not parallel (for example, $\mathbf{F_1}$ and $\mathbf{F_2}$), and using the theorem of the parallelogram. The resultant passes through the intersection I of the lines of action of $\mathbf{F_1}$ and $\mathbf{F_2}$ in the layout plan (Figure 6.9). The sum $\mathbf{R_{1,2}}=\mathbf{a_0a_2}$ of the two forces is determined in the force plan and its direction can thus be used to construct the resultant in the layout plan by drawing a line parallel to $\mathbf{a_0a_2}$ through I. We continue the process of reduction by reducing both $\mathbf{R_{1,2}}$ and $\mathbf{F_3}$ by applying the theorem of the parallelogram (provided that these two forces are concurrent). Point J, the intersection of their lines of action through which their resultant $\mathbf{R_{1,3}}$ will pass, is thus determined. The latter is determined in force plan by constructing the sum of $\mathbf{R_{1,2}}$ and $\mathbf{F_3}$. To do this, it is advised to use vector $\mathbf{R_{1,2}}$ which is already built and to add the force vector $\mathbf{F_3}$ to it. This gives $\mathbf{R_{1,3}}=\mathbf{a_0a_3}$, for which the direction allows us to plot its line of action through J in the layout plan. By continuing the process with successive resultants and subsequent forces until the last, we obtain the resultant force vector **Fr** in the force plan, as well as the line of action of the resultant force in the layout plan. In the example in Figure 6.9, the last resultant passes through point L. The above steps can only be performed if the resultant and the force it consists of are not parallel. In this case (Figure 6.9), the points of intersection of the lines of action of intermediate resultants and subsequent forces are well defined (I, J, K and L).

The magnitude and direction of the resultant force are obtained simply by the vector sum of forces constructed by the circuit of forces in the force plan (which corresponds to an analytical approach). The position of the resultant force in the layout plan depends on the position of the lines of action and therefore of the *pressure polygon*, which we will define below.

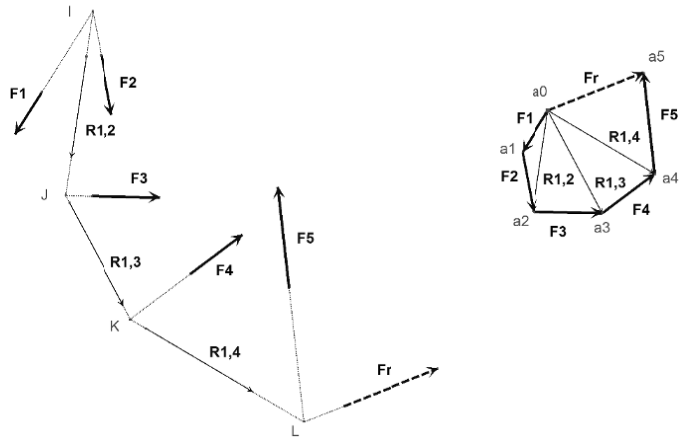


**Figure 6.9.** *Reduction of a system of arbitrary forces by successive applications of the theorem of the parallelogram of forces*

DEFINITION OF THE PRESSURE POLYGON.– *The lines of action of the first force and subsequent resultants form a polygonal contour called the pressure polygon. The points of intersection of the lines of action of the resultant of k first forces with the k+1st are the vertices of this pressure polygon (IJKL in the example of Figure 6.9).*

The order of forces affects the pressure polygon, but not the final resultant, which remains identical whatever the order (as shown in Figure 6.10, where the pressure polygon comprising of vertices I′J ′K ′L ′ is constructed in the order 1, 3, 5, 4, 2). This result is obvious, because its line of action is unique for a given system. Thus, regardless of the order, the last point of the pressure polygon will be on the line of action of the resultant (L and L′ in Figure 6.10 define the same line of action of **Fr** well).

COMMENT 6.3.– We have just seen that the reduction of an arbitrary system of *n* forces can be determined and reduced to a resultant force by successive applications of the parallelogram theorem. A limitation of the application of this theorem is that there must be at least two concurrent forces. It thus excludes the case of the reduction of *n* parallel forces. However it can be used if at least one force is not parallel to the others in order to determine a point of intersection of the two lines of action.

COMMENT 6.4.– Another limitation of this method, due to the use of the parallelogram theorem, lies in the fact that a resultant with a certain step may be parallel to the subsequent force. In this case, we can try a different order for which there would be no parallelism.

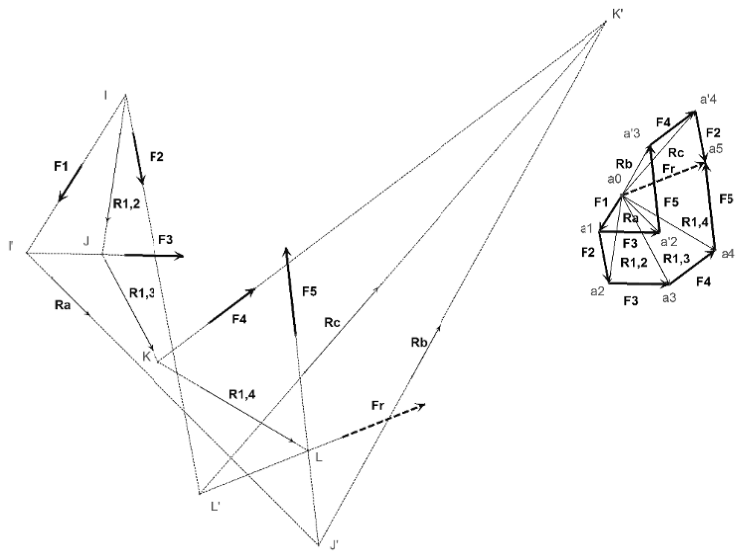


**Figure 6.10.** *Two pressure polygons within a system of n forces*

### 6.3.2. *Resultant couple*

A special case of reduction of a system of *n* forces appears when the vector sum of forces is zero, that is to say, when **Fr=0** and therefore $a_0 = a_n$ (this is the first equilibrium condition relative to the overall translational movement of a solid). In this case, we are interested in the resultant $\mathbf{R_{1,n-1}}$ of *n*-1 first forces of the same intensity but opposite to $\mathbf{F_n}$. The line of action of $\mathbf{R_{1,n-1}}$ is known (by application of the method seen previously) as well as that of $\mathbf{F_n}$, which is a fact of the problem. If the lines of action of these two forces are distinct, we say that the *pressure polygon is open*, and we get the resultant couple formed by $\mathbf{R_{1,n-1}}$ and $\mathbf{F_n}$. The resultant moment is that of this couple. Such a configuration is illustrated in Figure 6.11, where the resultant couple is ($\mathbf{R_{1,4}}$, $\mathbf{F_5}$). Such a system is not in equilibrium because the sum of moments is not zero. If the lines of action of $\mathbf{R_{1,n-1}}$ and $\mathbf{F_n}$ are combined, we say that

the *pressure polygon is closed*, and the resultant moment is zero, as is the sum of forces, and the system is in equilibrium.

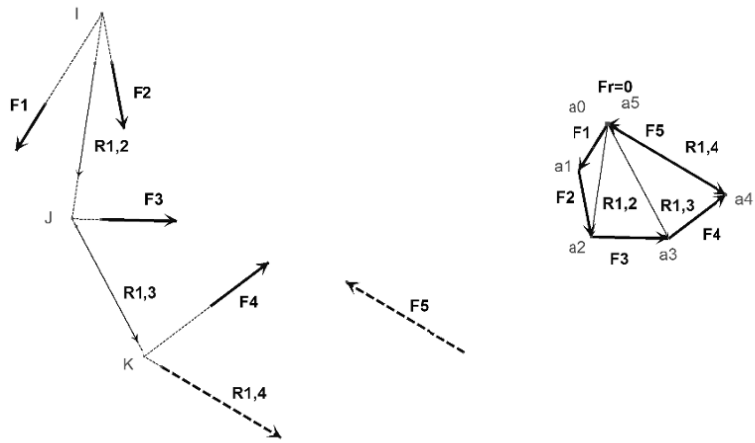


**Figure 6.11.** *Resultant couple from a system of n forces*

### 6.3.3. *Equilibrium condition of n arbitrary forces*

From previous results, we can deduce different cases of possible reduction based on polygons of forces and pressures and the conditions of equilibrium of a system of *n* arbitrary forces. Several cases are possible:

1) *the force polygon is open*: the sum of forces is not zero. The system is not in equilibrium. All forces are reduced to a single equivalent force positioned in the layout plan;

2) *the force polygon is closed*: the sum of the forces is zero. Two cases are possible:

i) *the pressure polygon is open*: we get a resultant couple, the sum of moments is not zero. The system is not in equilibrium. The system of forces is reduced to a single couple in the layout plan;

ii) *the pressure polygon is closed*: the sum of moments is zero, and as the sum of the forces is zero, the system is in equilibrium.

Hence, we see that a required condition for the system of $n$ forces to be in equilibrium is that the force polygon is closed and the pressure polygon is also closed.

## 6.4. Bibliography

[FRE 98] FREY F., *Analyse des structures et milieux continus, Statique appliquée,* 2e édition, Presses polytechniques et universitaires romandes, Lausanne, vol. 1, 1998.

# 7

# Funicular Polygons

## 7.1. Reduction of a system of parallel forces

Systems of parallel forces are frequently encountered in all structures, since forces due to gravity are vertical. In masonry, the weight of materials is a particularly important set of parallel external forces. The reduction of a system of parallel forces is fundamental to the study of equilibrium in masonry. In the previous chapter, we saw that the reduction of a system of arbitrary forces can be performed with the successive use of the parallelogram theorem (associated to the theorem of sliding forces). A limitation of this method is that it can be applied to a system of parallel forces, because none of the lines of action of forces intersect. Therefore, the process cannot be initiated. We note that it may be a similar situation in the case of forces for which the lines of action intersect outside the plot area. To overcome this limitation, a first approach is to add two forces in equilibrium (so directly opposing) to the system and to reduce the new system. A second method, which seems to be less immediate but is particularly useful, is based on the decomposition of each of the forces into two concurrent forces: this is the method of constructing *funicular polygons*. These are the two methods that we discuss below.

### 7.1.1. *Reduction by adding two directly opposing forces*

The limitation of the method of successive composition of forces through the parallelogram theorem can be easily avoided by using an equivalent system of forces made by adding two directly opposing and non-parallel forces to those of the original system. As these two forces are in equilibrium, the equilibrium principle can be applied and therefore the new system is

*Sustainable Masonry: Stability and Behavior of Structures,*
First Edition. Thierry Ciblac and Jean-Claude Morel.

statically equivalent to the first. Otherwise known as a system of $n$ parallel forces $\mathbf{F_1}$, $\mathbf{F_2}$, ... , $\mathbf{F_n}$ (Figure 7.1 in the case of three parallel forces $\mathbf{F_1}$, $\mathbf{F_2}$ and $\mathbf{F_3}$). Two directly opposing forces of magnitude $\mathbf{F_0}$ are added to this system. The problem then boils down to reducing the system of $n$ + 2 forces consisting of forces $\mathbf{F_0}$, $\mathbf{F_1}$, $\mathbf{F_2}$, ..., $\mathbf{F_n}$ and $-\mathbf{F_0}$. Both forces $\mathbf{F_0}$ and $-\mathbf{F_0}$ can be placed anywhere in the layout plan on the same line of action, and they may have any (non-zero) magnitude and take any direction that is not parallel to the initial system of forces. In a first instance, the force polygon with vertices O, $a_0$, $a_1$, $a_2$,…, $a_n$ and O′ is constructed (Figure 7.1, where $n$ = 3). The resultant force **Fr** is given by the vector $\mathbf{OO'}$, which is equal to $\mathbf{a_0a_n}$. The polygon of pressures is built step by step by positioning successive resultants $\mathbf{Oa_1}$, $\mathbf{Oa_2}$, ..., $\mathbf{Oa_n}$ and $\mathbf{OO'}$ in the layout plan on the lines of action, respectively passing through points $S_1$, $S_2$, ..., $S_n$, S (points of intersection of previous resultants with subsequent forces). The resultant force **Fr** of the entire system passes through the last point S of the pressure polygon.

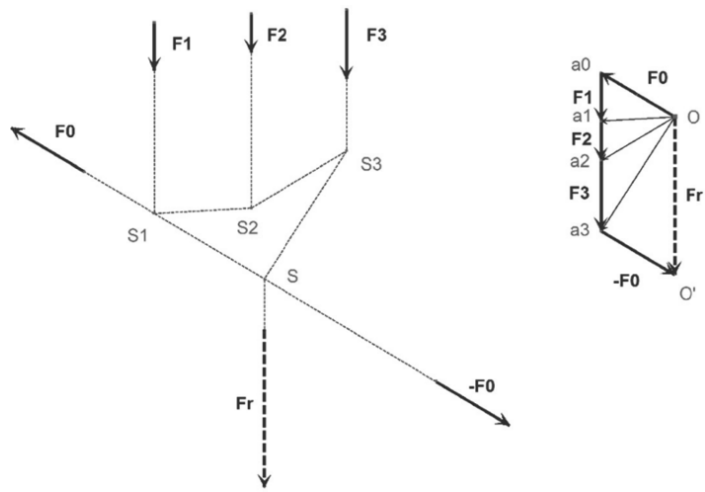


**Figure 7.1.** *Reduction of a system of three parallel forces by addition of two directly opposing forces*

We notice that although force $\mathbf{F_0}$ is chosen arbitrarily (not parallel to the initial forces), the position of the *line of action of the resultant* **Fr** *passing through S only depends on the initial forces* ($\mathbf{F_1}$, $\mathbf{F_2}$,…, $\mathbf{F_n}$). In this regard, it is interesting to check this property if dynamic geometry software is used to make constructions, because it would then be seen that by varying $\mathbf{F_0}$, the line of action of **Fr** remains unchanged.

### 7.1.2. *Reduction by decomposition of forces using a pole and construction of the funicular polygon*

Another way to reduce a system of *n* parallel forces is to decompose each of the forces $\mathbf{F_1}$, $\mathbf{F_2}$,…, $\mathbf{F_n}$ into two concurrent forces. This gives a system of *2n* forces equivalent to the first system which, if suitably selected, enable reduction of the system. We proceed with the decomposition in ascending order of the indices of forces. This procedure comprises the following steps:

– decomposition of $\mathbf{F_1}$: earlier (in section 6.2.3.1), we have seen that the decomposition of a force into two concurrent forces is easily done if the lines of action are known, since we just need to construct the triangle of forces in the force plan in order to determine their directions and magnitudes. Here, no assumption is made on the lines of action of forces decomposing $\mathbf{F_1}$, we can choose them freely, both as regards their directions (but not parallel forces of the initial system) and their positions in the layout plan, taking care, however, to intersect them on the line of action of $\mathbf{F_1}$. We can therefore choose a point A anywhere in the layout plan (Figure 7.2), and then draw a first line of action in any orientation intersecting the line of action of $\mathbf{F_1}$ in $S_1$. From point $S_1$, we then draw the line of action in any orientation of the second force decomposing $\mathbf{F_1}$. This way, we define the decomposition of force $\mathbf{F_1}$ by the lines of action of the two concurrent forces in $S_1$. We can then build these forces in the force plan by drawing the parallel forces decomposing $\mathbf{F_1}$ from points $a_0$ and $a_1$. This determines a point O, apex of the triangle $a_0Oa_1$ for which the sides $a_0O$ and $Oa_1$ define the forces decomposing $\mathbf{F_1}$;

– decomposition of $\mathbf{F_2}$: we will now seek to decompose $\mathbf{F_2}$ into two concurrent forces, such that the forces decomposing $\mathbf{F_1}(\mathbf{Oa_1})$ can balance one of those that will decompose $\mathbf{F_2}$. One of the forces decomposing $\mathbf{F_2}$ must be directly opposite to $\mathbf{Oa_1}$; this will be the force $\mathbf{a_1O}$, for which the line of action passes through $S_1$. This line of action intersects the line of action of $\mathbf{F_2}$ in $S_2$. The second force that decomposes $\mathbf{F_2}$ is then easily deduced in the triangle of force $sa_1$ O $a_2$ (in the force plan): this is $\mathbf{Oa_2}$. Force $\mathbf{F_2}$ is split into two concurrent forces $\mathbf{a_1O}$ and $\mathbf{Oa_2}$ in $S_2$;

– decomposition of other forces $\mathbf{F_k}$: we repeatedly use the same process as for $\mathbf{F_2}$. Thus, the decomposition of any force $\mathbf{F_k}$ is determined (*k* ranging from 2 to *n*) in order to balance the force $\mathbf{Oa_{k-1}}$ resulting from the decomposition of force $\mathbf{F_{k-1}}$. Thus, $\mathbf{F_k}$ is decomposed into $\mathbf{a_{k-1}O}$ and $\mathbf{Oa_k}$ and the point of intersection of the forces decomposing $\mathbf{F_k}$ are at the intersection of the lines of action of forces $\mathbf{Oa_{k-1}}$ and $\mathbf{F_k}$;

– end of the process: the process stops at force $\mathbf{F_n}$. Out of $2n$ forces decomposing $n$ initial forces, only two are not balanced by other forces: these are the first $\mathbf{a_0O}$ and last $\mathbf{Oa_n}$ ($\mathbf{Oa_3}$ where $n = 3$, illustrated in Figure 7.2). Thus, the set of $n$ forces is statically equivalent to two forces $\mathbf{a_0O}$ and $\mathbf{Oa_n}$, for which the lines of action are determined and intersect at point S through which the resultant **Fr** of the system passes.

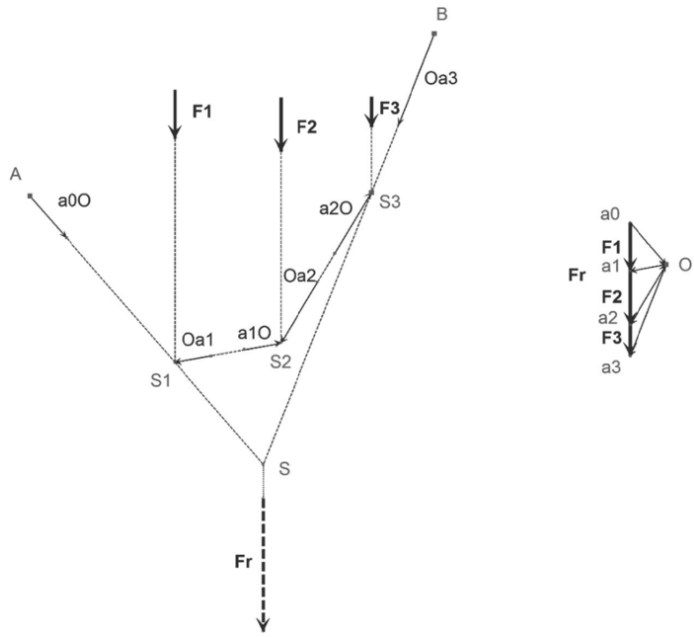


**Figure 7.2.** *Reduction of a system of three parallel forces by the funicular polygon method*

POLE.– The method that we just discussed shows the importance of the point O of the force plan. This point enables the decomposition of each of the forces of the system while ensuring the existence of pairs of directly opposing forces and therefore equilibrium. Point O is called the *pole*.

In the present method, pole O is deducted from an arbitrary choice of lines of action of forces that decompose the first force $\mathbf{F_1}$ into two concurrent forces. Thus, another way to define decomposition of the first force (wherefrom all other decompositions) is to choose a pole O that is positioned anywhere in the force plan (but outside of the line $(a_0a_1)$ in order to decompose F1 into two forces in different directions).

FUNICULAR POLYGON.– The method of reduction of $n$ forces by decomposition using pole O leads to the construction of $n$+1 lines of action, supporting decomposition forces $\mathbf{a_0O}$, $\mathbf{a_1O}$,…, $\mathbf{a_nO}$. These lines of action intersect at points $S_1$, $S_2$,…, $S_n$ and the extremity lines support forces $\mathbf{a_0O}$ and $\mathbf{Oa_n}$, which pass through points A and B. The polygon A, $S_1$, $S_2$,…, $S_n$, B builds on these lines of action and is called the *funicular polygon*. This name is given with reference to the shape taken by a thread in equilibrium under the load of point forces (funicular comes from the Latin *funiculus* meaning small rope). Indeed, the funicular polygon A, $S_1$, $S_2$,…, $S_n$, B gives the geometry of a massless and infinitely flexible thread hanging from A and B and subjected to forces $\mathbf{F_1}$, $\mathbf{F_2}$,…, $\mathbf{F_n}$ applied at $S_1$, $S_2$,…, $S_n$. Reactions $\mathbf{R_A}$ and $\mathbf{R_B}$ of the thread in A and B balancing the system of forces are respectively equal to $\mathbf{-a_0O}$ and $\mathbf{-Oa_n}$ ($\mathbf{-a_0O}$ and $\mathbf{-Oa_3}$ in the case of the 3 forces illustrated in Figure 7.3) and the tension in each segment of the thread is given by the lengths of segments $a_0O$, $a_1O$,…, $a_nO$. Several shapes can be taken by the thread depending on the position of the pole, and we must ensure that the wire is properly stretched.

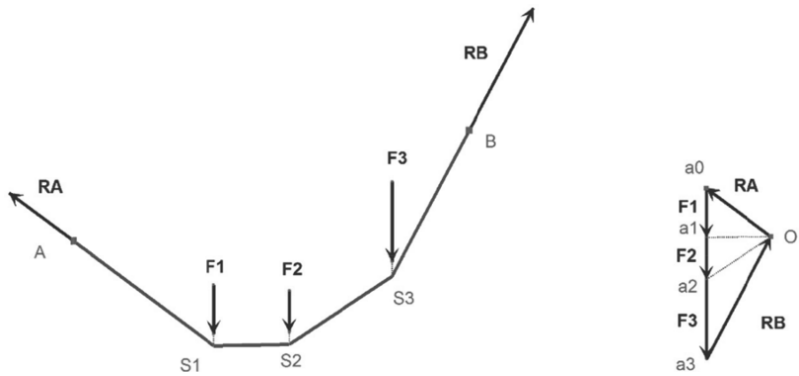


**Figure 7.3.** *Funicular polygon – shape taken by a thread under a given load*

COMMENT 7.1.– *The line of action of the resultant from the system of forces is independent of the position of the pole.* Indeed, as in the case of reduction by addition of two directly opposing forces, the method of reduction by construction of a funicular polygon gives a resultant force that depends on the initial forces only. It does not depend on the choice of the position of pole O.

COMMENT 7.2.– The method of addition of two directly opposing forces and the funicular polygon method are equivalent and lead to identical constructions.

Indeed, by observing the method of addition of two directly opposing forces, we can see that force $\mathbf{F_1}$ can be decomposed into two forces: $\mathbf{-F_0}$ ($\mathbf{a_0O}$) and $\mathbf{a_0a_1}$ (Figure 7.1). These two forces are concurrent at $S_1$. Force $\mathbf{F_2}$ can be decomposed into two concurrent forces $\mathbf{-a_0a_1}$ and $\mathbf{-a_1a_2}$ at $S_2$ in the layout plan. At this stage, we note that the forces $\mathbf{a_0a_1}$ and $\mathbf{-a_0a_1}$ share the same line of action and are therefore in equilibrium. They can therefore be removed from the system of forces, keeping only $\mathbf{-F_0}$ and $\mathbf{a_1a_2}$ plus remaining forces $\mathbf{F_3}$,…, $\mathbf{F_n}$. By continuing the process, the directly opposing intermediate forces (in equilibrium) are removed, to keep only the first $\mathbf{a_0O}$=$\mathbf{-F_0}$ and last $\mathbf{Oa_n}$ forces from the system of *2n* forces, placed in the layout plan on the lines of action. Both methods lead to identical constructions, thus giving point O an important role (as shown in Figure 7.4 compared to Figure 7.1). The construction of pole O is done directly from knowledge of $\mathbf{F_0}$ from the relationship $\mathbf{a_0O} = \mathbf{-F_0}$.

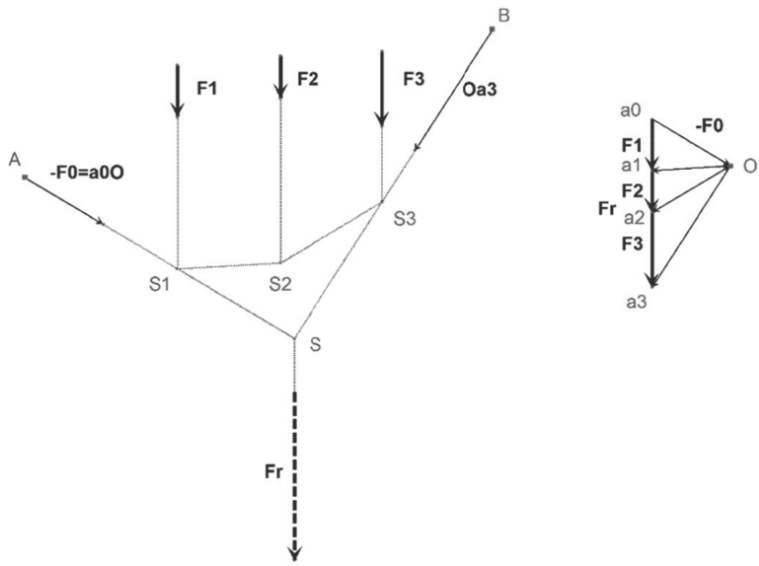


**Figure 7.4.** *Reduction of a system of three parallel forces by construction of a funicular polygon from the force* $\boldsymbol{F_0}$ *of the method by addition of two directly opposing forces*

## 7.2. Funicular polygon of a system of *n* arbitrary forces

The method of reduction of a system of *n* arbitrary forces through the construction of a funicular polygon is strictly the same as that established in the particular case of a system of parallel forces (Figure 3.5, where $n = 3$). It is based on the following steps:

1) definition of *pole* O in the force plan enabling the decomposition of each of the forces $\mathbf{F_k}$ ($k$ varying from 1 to $n$) in two concurrent forces $\mathbf{a_{k-1}O}$ and **Oa**. Pole O can be chosen freely in the force plan, but not from the lines containing the forces to be decomposed. The definition of pole O can be done directly by positioning it in the force plan, or indirectly by giving, for example, conditions on the directions of the lines of action of the forces that decompose $\mathbf{F_1}$ (as in section 7.1.2);

2) construction of points of intersection of systems of two forces that decompose each of the forces of the initial system (by choosing, step by step, directly opposing forces): these points ($S_1$, $S_2$,…, $S_n$) are the vertices of the *funicular polygon* for which the extremities (A and B) are on the lines of action of the two extreme forces $\mathbf{a_0O}$ and $\mathbf{Oa_n}$;

3) reduction of a system with two forces $\mathbf{a_0O}$ and $\mathbf{Oa_n}$ (corresponding to the first decomposing force $\mathbf{F_1}$ and the second decomposing force $\mathbf{F_n}$). These two forces are concurrent at point S and reduce themselves to the resultant **Fr** of the system. The line of action of **Fr** therefore passes through S.

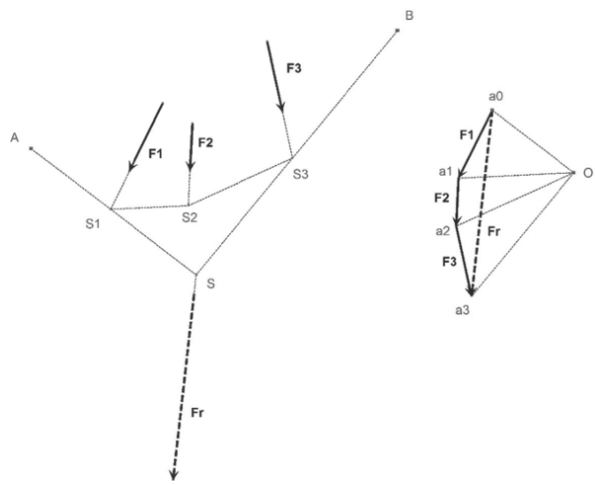


**Figure 7.5.** *Reduction of a system of three arbitrary forces by construction of a funicular polygon*

FEATURES OF THE REDUCTION OF A SYSTEM OF FORCES DEPENDING ON THE OPENING OR CLOSING OF FORCE AND FUNICULAR POLYGONS.– In the *general case where the force polygon is open*, the system of forces is reduced to a resultant force **Fr**, which can be placed in the layout plan. In the case where the *force polygon is closed, the system is then reduced to a couple or is in equilibrium.*

Indeed, if the force polygon is closed, then the vector sum of forces is zero (**Fr = 0**) and points $a_0$ and $a_n$ are combined. All forces are then reduced, by the construction of the funicular polygon, to two zero-sum forces $\mathbf{a_0O}$ and $\mathbf{Oa_0}$ (as $a_n$=$a_0$). Two situations are possible:

1) these two resultant forces form a *couple* if the lines of action of parallel forces through $S_1$ and $S_n$ ($AS_1$ and $BS_n$) are not combined. The funicular polygon is then *open*. The initial system is thus reduced to a couple and is therefore not in equilibrium. Such a configuration is shown in Figure 3.6 for three forces, and Figure 7.8 for four forces;

2) the two resultant forces are in *equilibrium* if their lines of action are combined, because $\mathbf{a_0O}$ and $\mathbf{Oa_0}$ are then directly opposed. The funicular polygon is then *closed*. The initial system is in equilibrium. Such a configuration is shown in Figure 7.7 for three forces in equilibrium and Figure 3.9 for four forces in equilibrium.

COMMENT ON THE EQUILIBRIUM OF THREE FORCES.– The equilibrium condition on a system of three forces, namely that the force polygon and the funicular polygon are closed, must be consistent with other previously established results: that the three forces in equilibrium are concurrent. Geometrically, this property is verified (Figure 7.7) by checking that the lines of action of forces $\mathbf{F_1}$, $\mathbf{F_2}$ and $\mathbf{F_3}$ converge at a point I. This property was obviously not satisfied in the case of forces reduced to a couple (Figure 7.6). For four forces in equilibrium, the forces are not necessarily concurrent (as shown in Figure 7.9), but some properties can be established as we will see later.

NECESSARY AND SUFFICIENT CONDITIONS FOR THE REDUCTION OF A SYSTEM OF FORCES.– The construction of a funicular polygon for an arbitrary system of forces can give the necessary and sufficient graphics conditions for reduction to:

– a force: the force polygon is open (non-zero sum of forces);

– a couple: the force polygon is closed and the funicular polygon is open (sum of moments is non-zero);

– equilibrium: the force polygon is closed (zero-sum of forces) and the funicular polygon is closed (zero-sum of moments).

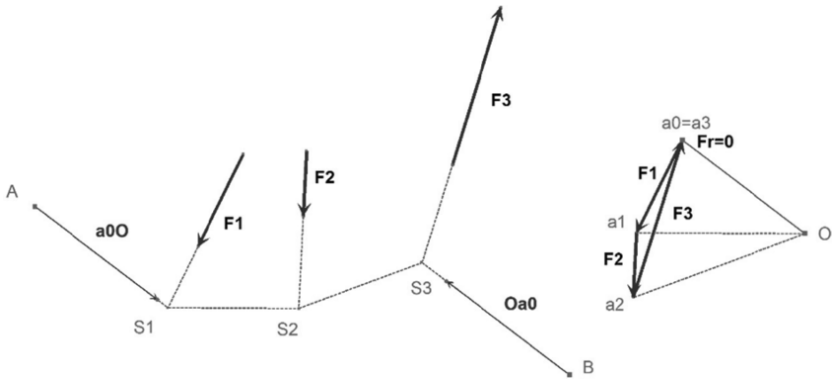


**Figure 7.6.** *System of three forces reduced to a couple (force polygon closed and funicular polygon open)*

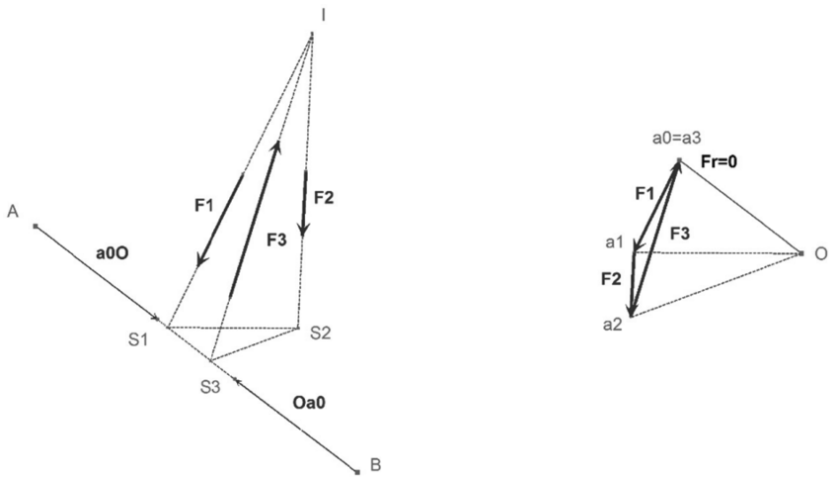


**Figure 7.7.** *System of three forces in equilibrium (force polygon closed and funicular polygon closed)*

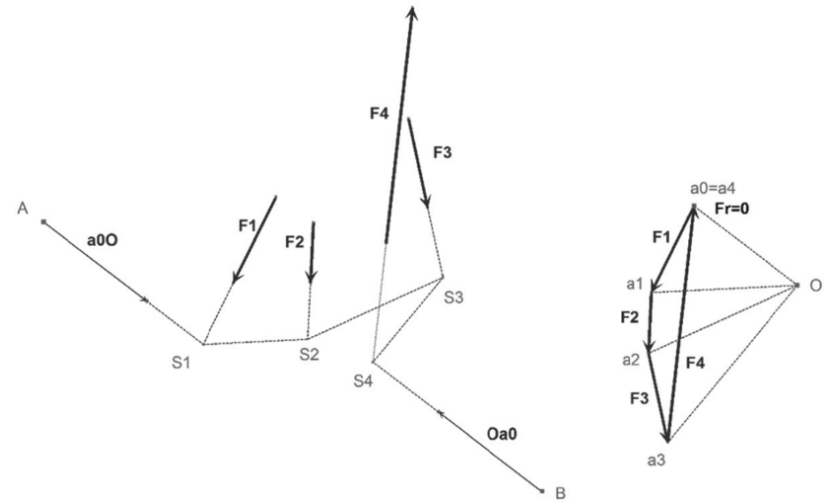


**Figure 7.8.** *System of four forces reduced to a couple (force polygon closed and funicular polygon open)*

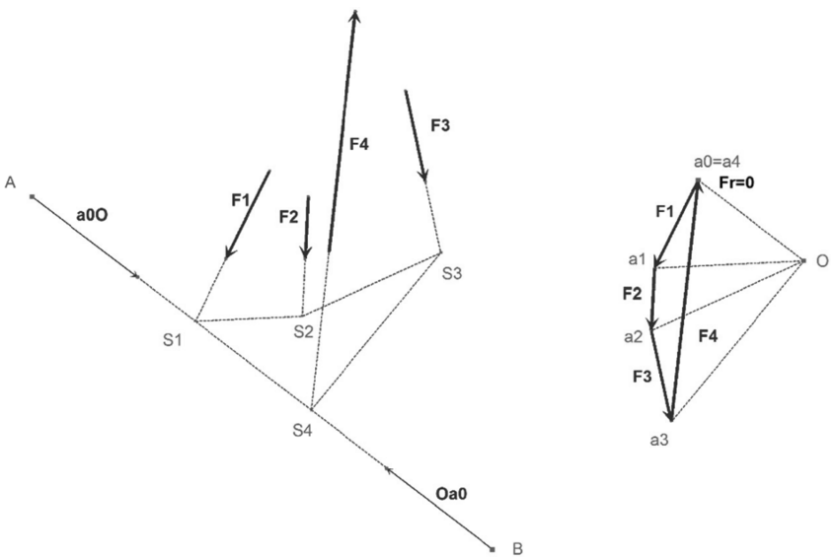


**Figure 7.9.** *System of four forces in equilibrium (force polygon closed and funicular polygon closed)*

## 7.3. Properties of funicular polygons

The method of reduction of a system of *n* forces by building a funicular polygon is based on the introduction of pole O that is *chosen freely* in the force plan. This pole allows the decomposition of each of the forces into two concurrent forces but it also allows the decomposition of the resultant force into two concurrent forces for which the lines of action are the first and last of the funicular polygon. The position of the first line of action is given by an *arbitrary point A of the layout plan* and the line of action of the second force is derived from the construction of the funicular polygon (these two lines of action are thus the beginning and the end of the funicular polygon). The point of application of the second force is an arbitrary point B of this line of action. Thus, we see that for a given system of forces, it is possible to construct an infinite number of funicular polygons that can reduce this system. These funicular polygons depend on the position of pole O and point A. In practice, a particular polygon can be sought depending on additional conditions which may result in a particular position of the pole and point A. These conditions may involve the intersection points of forces that are balancing the system of forces, the direction of the forces and their magnitude. For example, determination of reactions depending on connecting elements or searches for geometries that are compatible with yield design criteria is based on the properties of funicular polygons. Therefore, it is necessary to understand these in order to respond to these multiple constraints.

### 7.3.1. *Funicular polygons of subsystems of forces*

Let us consider a system of *n* forces and an associated funicular polygon; we can easily notice that a subsystem of these forces (taken in the defined order for the construction of the funicular polygon) has its own funicular polygon included in the overall funicular polygon. The resultant of this subsystem is derived from the associated force sub-polygon and its line of action passes through the intersection of the extreme sides of the funicular polygon. With the notation used above, this property is expressed as follows.

Let us consider a system of *n* forces $\mathbf{F_1}$, $\mathbf{F_2}$,…, $\mathbf{F_n}$. Let us also consider a subsystem of *p* forces (with $p < n$) for which the first force is $\mathbf{F_k}$: $\mathbf{F_k}$, $\mathbf{F_{k+1}}$,…, $\mathbf{F_{k+p-1}}$ (with $k+p-1 \leq n$). The resultant of this subsystem is given by force $\mathbf{a_k a_{k+p-1}}$, and an associated funicular polygon is the polygon $S_{k-1}$,…, $S_{k+p}$, which is included in the overall funicular polygon. The points $S_{k-1}$ and $S_{k+p}$ can be taken as the points of application of two extreme forces $\mathbf{a_k O}$ and

$\mathbf{Oa_{k+p-1}}$ to which the subsystem of forces reduces. Thus, the point of intersection Sr and the lines of action ($S_{k-1}$ $S_k$) and ($S_{k+p-1}S_{k+p}$) give a point on the line of action of the resultant $\mathbf{F_{Sr}}$ of the subsystem of forces.

Figure 7.10 shows this property in the case of a subsystem of three forces $\mathbf{F_2}$, $\mathbf{F_3}$, $\mathbf{F_4}$ that are included in a system of five forces from which the funicular polygon was constructed. The polygon ($S_2$, $S_3$, $S_4$) is a funicular polygon of this subsystem and its resultant $\mathbf{F_{Sr}} = \mathbf{a_1a_4}$ passes through the point of intersection Sr on its extreme sides $S_1S_2$ and $S_4S_5$.

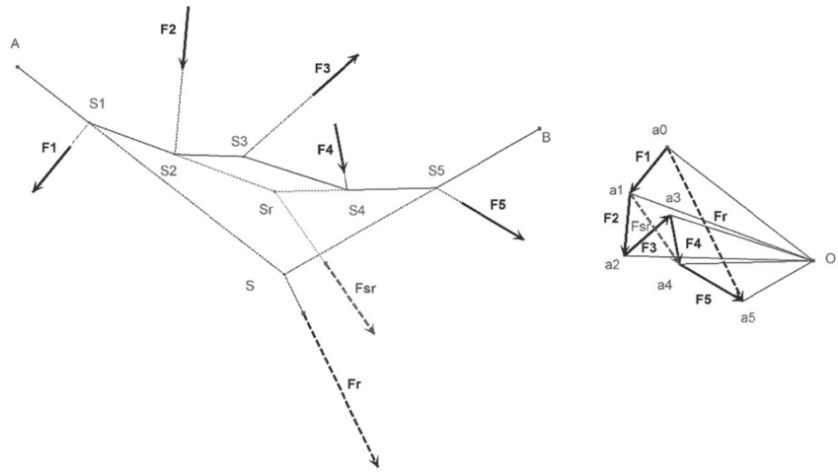


**Figure 7.10.** *Funicular polygon and resultant of a subsystem of forces*

### 7.3.2. *Funicular polygon through two a priori fixed points*

If we consider the construction of the funicular polygon (seen in section 7.2), we notice that its extreme sides pass through points A and B (points of application of two forces $\mathbf{a_0O}$ and $\mathbf{Oa_n}$ reducing the system of forces). In this construction, only point A is chosen freely in the layout plan. Point B must be positioned on the line of action of $\mathbf{Oa_n}$. However, in some cases it may be useful to construct a funicular polygon that passes through two *a priori* fixed points C and D. For example, in the case of a thread hung from two points C and D and subjected to *n* forces for which the positions and magnitudes are known. The problem then is to define the geometry(ies) through this thread in equilibrium under the load of *n* forces.

This problem can be solved easily if an initial funicular polygon associated to pole O has been constructed (polygon A, $S_1$, $S_2$,…, $S_n$, B). Indeed, the resultant Fr of the system is known and passes through S. We therefore seek a new funicular polygon associated to the same system of forces and passing through C and D. The new funicular must lead to the same resultant. Thus, the extremity lines of the new funicular must intersect the line of action of **Fr** (line parallel to $\mathbf{a_0a_n}$ passing through S) at a point S′. S′ can be selected from anywhere on the line of action of **Fr**. The new decomposition of **Fr** is thus defined and pole O′ of the new funicular and can be determined by drawing lines parallel to the lines of action CS′ and S′D, respectively passing through $a_0$ and $a_n$. We can then build the new funicular polygon from $S_1'$ (intersection of CS′ and the line of action of $\mathbf{F_1}$) and polar radius O′$a_1$. By repeating this process, points $S_2'$,…, $S_n'$ are obtained. We must then verify that the point $S_n'$ obtained like this coincides with that obtained knowing the last side of the funicular polygon. $S_n'$ must also be at the intersection of the line S′D and line of action of $\mathbf{F_n}$. Figure 7.11 illustrates this method for three arbitrary forces.

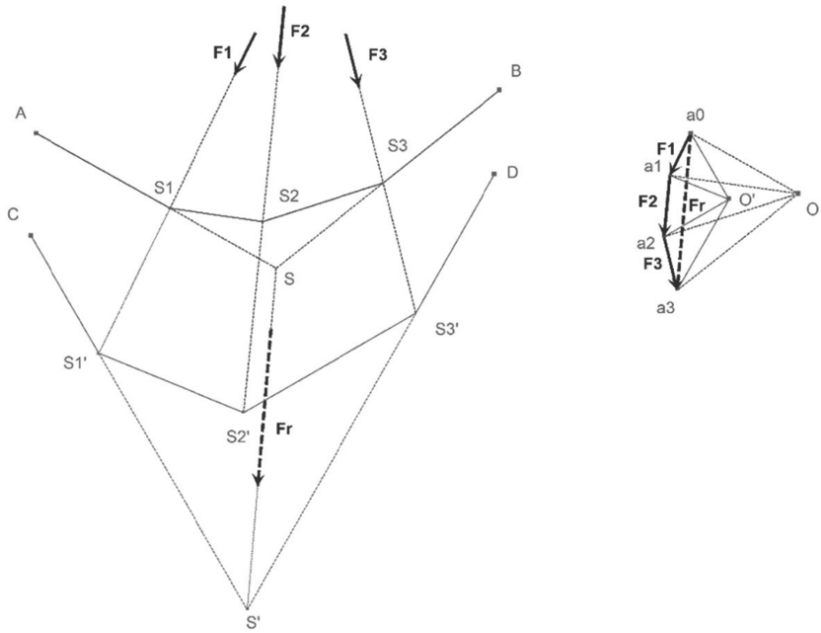


**Figure 7.11.** *Construction of a funicular polygon passing through two a priori fixed extreme points C and D*

COMMENTS ON THE ARBITRARY CHOICE OF POINTS.– Arbitrarily choosing point S′ on the line of action of **Fr** influences the direction of extreme forces that decompose **Fr** and thus the shape of the funicular polygon. There are infinite funicular polygons that pass through C and D. We also note that as point A was chosen arbitrarily, A and C could have been identified at the start.

Thus we see that to particularize a funicular polygon, it is useful to construct an arbitrary initial funicular polygon to determine the resultant of the system of forces. Knowing the resultant, we can reconstruct another funicular based on the constraints that we wish to apply to it. In general, two funicular polygons must therefore be constructed to particularize a problem. It is also useful to consider the geometric properties that link two funicular polygons in order to explore the potential of this approach.

### 7.3.3. *Relationship between funicular polygons constructed from two distinct poles*

The geometric properties that link funicular polygons constructed from two distinct poles are deduced from the fact that their resultant **Fr** is the same. At first, in section 7.3.3.1, we will focus on the equilibrium system formed by the initial system and two forces balancing **Fr**. Then, from the results thus established, in section 7.3.3.2 we will deduce a relationship between funicular polygons built from two distinct poles.

#### 7.3.3.1. *Feature of a funicular polygon of a system in equilibrium resulting from the reduction of an initial system reduced to a force*

Let us consider a system of $n$ forces $\mathbf{F_1}$, $\mathbf{F_2}$,…, $\mathbf{F_n}$ from the resultant **Fr**. The funicular polygon of this system of forces has the geometry of the polygon A, $S_1$, $S_2$,…, $S_n$, B, where A and B are the points of application of the two reactions $\mathbf{R_A}$ and $\mathbf{R_B}$ balancing the system of forces. Thus, due to the construction of the funicular polygon of $n$ resultant forces **Fr**, we can consider a system of $n$+2 forces in equilibrium consisting of $n$ forces and the two reactions $\mathbf{R_A}$ and $\mathbf{R_B}$. The forces of this new system in equilibrium are taken in the following order: $\mathbf{R_A}$, $\mathbf{F_1}$, $\mathbf{F_2}$,…, $\mathbf{F_n}$ and $\mathbf{R_B}$. Points associated with these forces in the force plan are respectively O, $a_1$,…, $a_n$, O. Thus, if we construct the force polygon and the associated funicular polygons, the two polygons must be closed. The closure of the force polygon (O, $a_0$, $a_1$,…, $a_n$, O) is obvious, since $\mathbf{R_A}$ and $\mathbf{R_B}$ balance the forces $\mathbf{F_1}$, $\mathbf{F_2}$,…, $\mathbf{F_n}$. Closing the funicular polygon must verify itself by producing its construction.

We therefore propose to build a funicular polygon of the system, $\mathbf{R_A}$, $\mathbf{F_1}$, $\mathbf{F_2}$,…, $\mathbf{F_n}$ and $\mathbf{R_B}$ (Figure 7.12 where $n = 3$). We first give an arbitrary pole O′ in the layout plan and an arbitrary point M through which the line of action of the first force $\mathbf{O'O}$ decomposing $\mathbf{R_A}$ (the first force of the new system) will pass. Thus, the line parallel to $\mathbf{OO'}$ that passes through M intersects the line of action of $\mathbf{R_A}$ at A′. We then draw the line of action of $\mathbf{O'a_0}$ (the second force decomposing $\mathbf{R_A}$) passing through A′. This line intersects the line of action of $\mathbf{F_1}$ at $S_1'$. The point $S_2'$ is then constructed at the intersection of the line of action of $\mathbf{O'a_1}$ passing through $S_1'$ with that of $\mathbf{F_2}$. This is done until $S_n'$ is constructed (intersection of the line of action of $\mathbf{O'a_{n-1}}$ passing through $S'_{n-1}$ with the line of action of $\mathbf{F_n}$). Point B is then constructed at the intersection of the line of action of $\mathbf{O'a_n}$ passing through $S_n'$ with the line of action of $\mathbf{R_B}$. Finally, the line of action of force OO′ passing through B′ is constructed (N is chosen arbitrarily on the line parallel to (OO′) passing through B′). As $\mathbf{OO'}$ must balance the first force $\mathbf{O'O}$ passing through M, their lines of action (MA′) and (NB′) must be combined (closure of the funicular polygon of the new system of forces in equilibrium). This closure property of the funicular polygon of the system of forces ($\mathbf{R_A}$, $\mathbf{F_1}$, $\mathbf{F_2}$,…, $\mathbf{F_n}$ and $\mathbf{R_B}$) results in the following two geometric properties:

1) the points M, A′, B′ and N are aligned;

2) the line A′B ′ is parallel to the line (OO′).

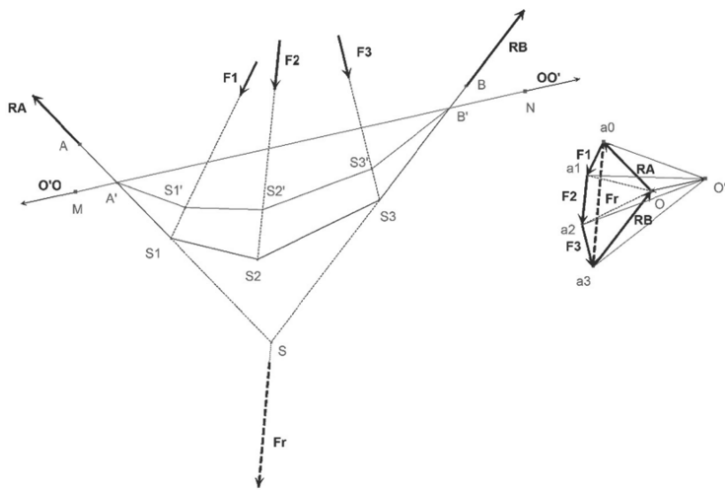


**Figure 7.12.** *Construction of a funicular polygon of forces in equilibrium* $\boldsymbol{R_A}$, $\boldsymbol{F_1}$, $\boldsymbol{F_2}$, $\boldsymbol{F_3}$ *and* $\boldsymbol{R_B}$ *built from pole O′*

Figure 7.12 illustrates these properties for three forces $\mathbf{F_1}$, $\mathbf{F_2}$ and $\mathbf{F_3}$. The accuracy of plots is essential to verify the alignment of M, A′ and B′. The use of a computer plotting tool is invaluable in this case. In particular, dynamic geometry software can give an indication of the membership of a point to a line. But in this case, it is only a computational result linked to the precision of numerical calculations.

7.3.3.2. *Application of the previous properties to the relationship between funicular polygons constructed from two distinct poles*

The funicular polygon pole O′ of the system of forces in equilibrium $\mathbf{R_A}$, $\mathbf{F_1}$, $\mathbf{F_2}$,…, $\mathbf{F_n}$ and $\mathbf{R_B}$ is the closed polygon M, A′, $S_1'$, $S_2'$,…, $S_n'$, B′, N. The initial system of forces $\mathbf{F_1}$, $\mathbf{F_2}$,…, $\mathbf{F_n}$ is a subsystem of this system of forces, so it includes the polygon A′, $S_1'$, $S_2'$,…, $S_n'$, B′ (property seen in section 3.3.1) as the funicular polygon pole O′. Thus, this system can be reduced to two forces $\mathbf{a_0O'}$ and $\mathbf{O'a_n}$ with point of application A′ and B′. Therefore, the system can be balanced by two reactions $\mathbf{R_{A'}} = -\mathbf{a_0O'}$ and $\mathbf{R_{B'}} = -\mathbf{O'a_n}$ applied in A′ and B′. The intersection S′ of the lines of action of these two forces passes through the resultant **Fr** of the system of forces $\mathbf{F_1}$, $\mathbf{F_2}$,…, $\mathbf{F_n}$, as the resultant also passes through point S (intersection of the lines of action of reactions $\mathbf{R_A}$ and $\mathbf{R_B}$ from the first funicular polygon). We then deduce the following geometric property: (*SS*′) *is parallel to* $\mathbf{Fr} = \mathbf{a_0a_n}$ (shown in Figure 7.13 for three forces).

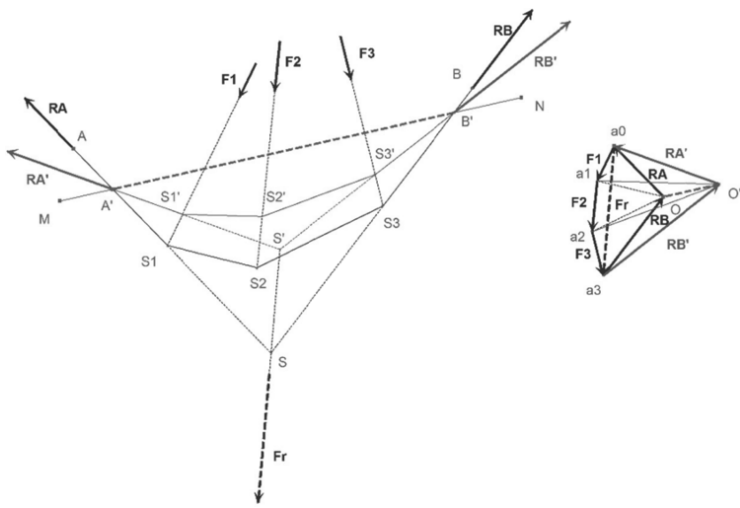


**Figure 7.13.** *Relationship between funicular polygons of forces* $\boldsymbol{F_1}$, $\boldsymbol{F_2}$ *and* $\boldsymbol{F_3}$ *constructed from poles O and O′*

We will now focus on the points of intersection $I_j$ of the sides of the same rank j of funicular polygons constructed from poles O and O′. The point $I_j$ ($1 \leq j \leq n+1$) is therefore the point of intersection of the sides of the funiculars passing through $S_j$ and $S_j'$ that are respectively parallel to $Oa_{j-1}$ and $O'a_{j-1}$. Thus, by definition $A'=I_1$ and $B'=I_{n+1}$ (see Figure 7.14 where $n = 3$). In section 7.3.3.1, we have seen that we get the property:

– $I_1I_{n+1}$ is parallel to the line OO′ (because $A'B' = I_1I_{n+1}$).

This property holds for all funiculars built from pole O and O′ and therefore for all funiculars of subsystems of forces of the initial system. By considering all the subsystems beginning with $\mathbf{F_k}$ and ending with $\mathbf{F_n}$, for all $k$ from 2 to $n$, we deduce that all lines $I_kI_{n+1}$ are parallel to (OO′). We conclude that the points $I_j$ ($1 \leq j \leq n+1$) are aligned on a line parallel to (OO′).

Properties that link funicular polygons are summarized below and illustrated in Figure 7.14 in the case of three arbitrary forces.

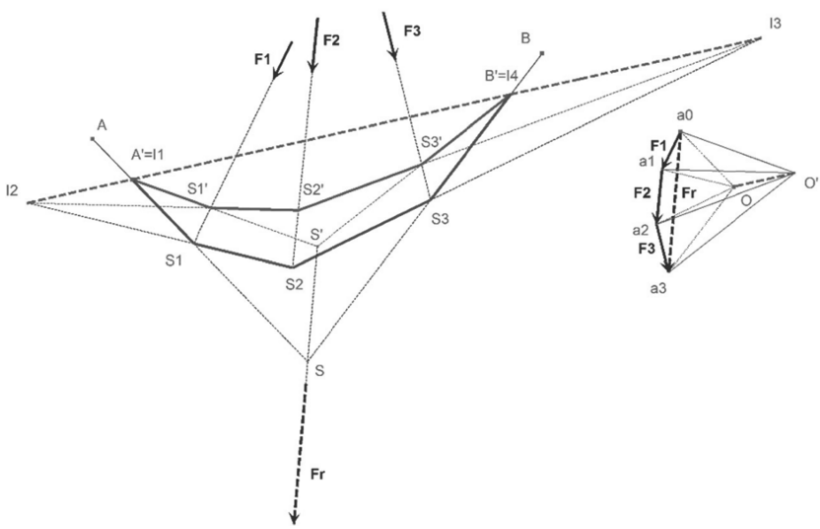


**Figure 7.14.** *Relationship between funicular polygons of forces* $\boldsymbol{F_1}$, $\boldsymbol{F_2}$ *and* $\boldsymbol{F_3}$ *constructed from poles O and O′*

PROPERTIES LINKING FUNICULAR POLYGONS CONSTRUCTED FROM TWO DISTINCT POLES.– For a system of $n$ forces, funicular polygons constructed from two distinct poles O and O′ satisfy the following properties:

1) vertices of rank i of funicular polygons are located on the line of action of the force of the same rank (that is to say, $S_i$ and $S_i'$ are on the line of action of $\mathbf{F_i}$ with $1 \leq i \leq n$);

2) the extreme sides of funicular polygons intersect on the line of action of the resultant;

3) the points of intersection of sides of the same rank of funicular polygons are aligned on a line parallel to the line of the poles (OO′) (points $I_j$ ($1 \leq j \leq n+1$) are aligned on a line parallel to OO′).

The coherence of a figure can be checked using these properties. For example, in the case of a funicular polygon passing through two *a priori* fixed points (section 7.3.2), two polygons were constructed based on two distinct poles (Figure 7.11). The resulting figure may be completed by the construction of points $I_k$ and verification of their alignment on a line parallel to OO′. Conversely, knowledge of these properties can be a way to build funicular polygons in another way. They may also allow particular constructions based on constraints, as we will see in the next section.

## 7.4. Applying the properties of funicular polygons

### 7.4.1. *Relationships between a tensed cable and compressed arc*

A particular application of the properties seen in section 7.3.3.2 considers relationships that can be deduced for systems of parallel forces. These systems are frequently encountered due to the existence of gravity. Examples are cables supporting masses or simply stretched under their own weight. Similarly, compressed masonry arches are systems of masses in equilibrium.

PROPERTIES LINKING A STRETCHED THREAD AND AN ARC COMPRESSED BY THE SAME SYSTEM OF FORCES WITH THE SAME ORIENTATION.– Consider a system of *n* parallel forces, with the same orientation. We consider the following gravitational forces, i.e. vertical downward forces. We get the following properties:

1) funicular polygons (A $S_1$ $S_2$... $S_n$ B) and (A $S_1'$ $S_2'$...$S_n'$ B) passing through two points A and B respectively constructed from two distinct poles O and O′ by considering that the forces in the same order (left to right, for example, as in Figure 7.15) are deduced from each other by an affinity axis (AB) and the direction parallel to forces. This property is a direct application of the general properties linking two funiculars (seen in section 7.3.3.2) to the

particular case of a system of parallel forces. Indeed, all funicular polygons have their identical invariant points (A = $I_1$, $I_2$,…, $I_n$, B = $I_{n+1}$) on the line (AB) and the corresponding vertices of different polygons are located on parallel lines. These lines respectively intersect each axis (AB) at A, $H_1$, $H_2$,…, $H_n$, B. The ratio of affinity *k* transforms the funicular of pole O into that of pole O′ to satisfy equality:

$$k = \frac{\overline{H_i S_i}'}{\overline{H_i S_i}} \text{ , } 1 \leq i \leq n \qquad [7.1]$$

2) if the poles are located on either side of the polygon of forces, then the funicular polygons correspond, one to a stretched thread and the other to a compressed arc. The stretched thread corresponds to a pole located to the right of the polygon of forces if the forces are taken from left to right (in the case of O and O′ in Figure 7.15), and the compressed arc corresponds to a pole located to the left of the polygon of forces if forces are taken from left to right (in the case of O''in Figure 7.15);

3) if line (AB) is horizontal, then the affinity linking the two funicular polygons is orthogonal. The particular orthogonal affinity of ratio -1 is the symmetrical relative to the horizontal line.

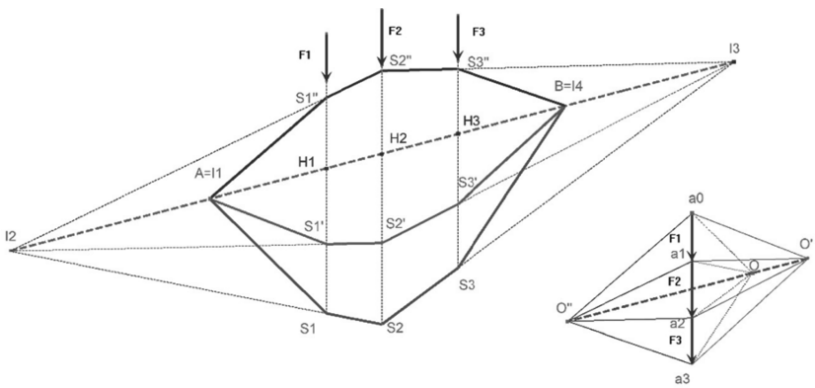


**Figure 7.15.** *Relationships between a stretched thread and compressed arc by the same system of vertical forces*

Property 3) can be applied, with a large number *n* of forces, to compare the shape taken by a rope or heavy chain (the chain problem) and the symmetrical arc relative to the horizontal line. This was stated, but not

proven, by Robert Hooke (1635–1703) in 1675 in his work [HOO 75] in the form of an anagram of the Latin phrase "*Ut pendet continuum flexile, sic stabit contiguum rigidum inversum*", translated into English as "as hangs the flexible line, so but inverted will stand the rigid arch'' [HEY 98]. The term "*inverted*" means the symmetry relative to the horizontal line. This interpretation is found in the works of Giovani Poleni (1683–1761) in 1748 on the dome of St. Peter's Basilica in Rome [POL 48] where an illustration of this property can be found in the form of a hanging chain and a symmetrical line associated with an arch (Figure 7.16) and a theoretical study of the application of cracks in the dome [BEN 91, HEY 95]. This same property is the origin of the use of physical models of hanging chains or weights. The famous models by Antoni Gaudí (1856–1926) used in the design of these masonry buildings are emblematic examples. We will see in the third part of the book, in Chapter 10, how the analogy expressed by Hooke can be interpreted in the context of the study of the stability of curvilinear masonry with the help of yield design.

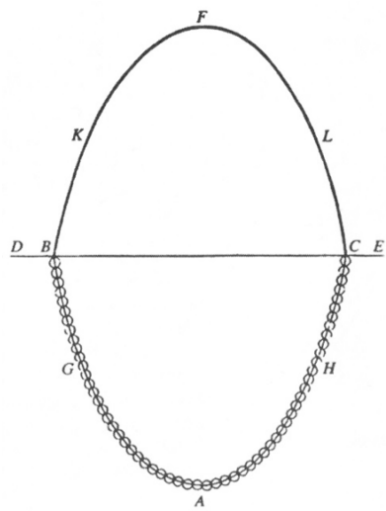


**Figure 7.16.** *Hooke's hanging chain and symmetrical arc, according to Poleni*

### 7.4.2. *Condition on the magnitude of forces*

Let us consider the problem of a thread hanging at two points A and B and subjected to point forces. We assume that a funicular polygon passing through A and B (from the method seen in section 7.3.2 for example) and its

associated pole O are known. We seek to determine the shape of the thread when the maximum tension $T_{lim}$ value is reached at a point. To solve this problem, we construct a circle of radius $T_{lim}$. Like how polar rays from O ($Oa_0$, …, $Oa_n$) have tensions in the thread as length, we can draw the circle of radius $T_{lim}$ from O, to see if the tensions are below this limit. We may also note that the largest polar radius $Oa_k$ will have a length that is smaller than $T_{lim}$. Thus, the circle center $a_k$ and radius $T_{lim}$ will correspond to the positions of a pole O′ for which tension is maximum at $O'a_k$. However, we know the thread is attached to A and B, which means that the line (OO′) must be parallel to (AB) (property 3 in section 7.3.3.2). Thus, we conclude that the point O′ is at the intersection of the circle and the line parallel to (AB) passing through O. Two points are possible. The one at which the thread is actually stretched will be retained.

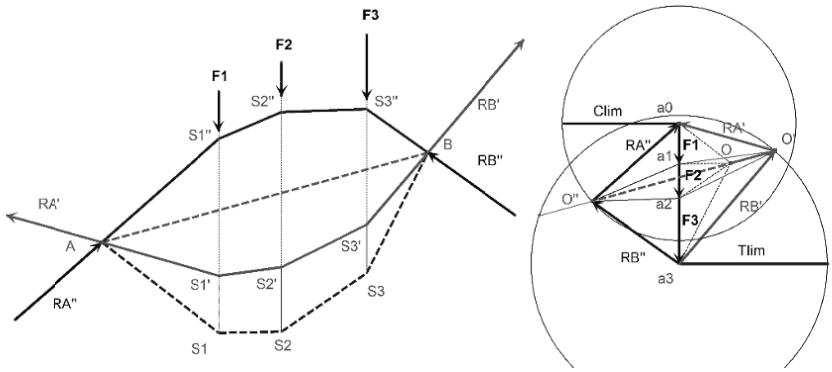


**Figure 7.17.** *Determination of the shape of a wire depending on a tension limit and an arc shape based on a compression force limit*

Figure 7.17 shows the case of a thread hung at A and B and subjected to three vertical forces. An initial funicular, A $S_1$ $S_2$ $S_3$ B, associated with pole O is assumed to be constructed. We check that the thread is stretched over its entire length. The forces acting on the vertices of polygons are aligned in the direction corresponding to a thread under tension; for example in $S_1$, the forces due to the action of the thread are $\mathbf{a_0O}$ and $\mathbf{Oa_1}$. The maximum tension is observed on the last side of the polygon. It balances the reaction $\mathbf{R_B}=\mathbf{a_3O}$. The tension limit $T_{lim}$ is defined by a segment of length $T_{lim}$ that is used to draw a circle centered at $a_3$. Pole O′ is on this circle and the line parallel to (AB) passing through O. The other point of intersection corresponds to a compressed structure, which is not permissible for a thread, but is desired for

materials that are only resistant to compression, such as masonry. Thus, we construct a thread A $S_1'$ $S_2'$ $S_3'$ B for which the last strand $S_3'$B is stretched with a tension equal to $T_{lim}$. The initial geometry, for which the sag was bigger, subjected the thread to lower tensions than $T_{lim}$, as its maximum tension $Oa_3$ is within the circle. The geometries which would lower the sags correspond to tensions above $T_{lim}$, for which the poles would be outside of the circle, to the right of O′ on the line (OO′). The shape of an arc subjected to the same forces and passing through A and B is determined in a similar manner. We then seek to determine the shape of the arc when the maximum compressive force of value $C_{lim}$ is reached at a point. Pole O″ of this arc is on the line parallel to (AB) passing through O and therefore (OO′), but as forces $\mathbf{F_1}$, $\mathbf{F_2}$ and $\mathbf{F_3}$ are parallel, O″ will be located on the other side the half-plane defined by their resultant of forces **Fr**. In Figure 7.17, pole O″ is located on the left whereas O′ was on the right. The $C_{lim}$ value is reached in the $AS_1''$ part of the arc. The position of O″ is thus determined at the intersection of a circle of radius $C_{lim}$ passing through $a_0$ and the line OO′. The arc A $S_1''$ $S_2''$ $S_3''$ B is constructed using polar rays from O″. The arcs which would lower sags correspond to compression forces greater than $C_{lim}$ for which the poles are outside of the circle of radius $C_{lim}$, to the left of O″ on the line (OO′).

### 7.4.3. *Passage of a funicular through three points*

In some cases, it may be useful to control the shape of a funicular polygon associated with a system of forces. For example, in an architectural project, to impose a height or a gap to a structure of support points. Thus, we are led to construct a funicular that passes through specific points. To do this, it is useful to use the geometric properties linking two funiculars. For example, we may seek to make a funicular polygon with three given points. By repeating the arc problem from two points A and B and subjected to point forces, we will seek to make it pass through a third given point C. This point C can be defined, by example, so that the arc passes close to a specific area without crossing it.

In the case shown in Figure 7.18, point C is a point of the contour of an area (shaded) that the arc must not cross. In this case, knowledge of the first funicular polygon passing through A and B and vertices $S_1$ $S_2$ $S_3$ suggests that passing through C is a borderline case for which the arc does not intersect the area. The problem is to construct a funicular polygon with vertices $S_1'$ $S_2'$ $S_3'$ passing through A, B and C. We know that points $S_2'$ and $S_3'$ pass through the lines of action of forces $\mathbf{F_2}$ and $\mathbf{F_3}$ (property 1 in section 7.3.3.2). However, C

is between these two lines of action, so we will first look for a way to find the points $S_2'$ and $S_3'$ such that they are aligned with C. We also know that the lines $(S_2S_3)$ and $(S_2'S_3')$ intersect on a line AB at point $I_3$ (property 3 in section 7.3.3.2). We can therefore deduce the construction of points $S_2'$ and $S_3'$ by first constructing $I_3$ (intersection of $S_2S_3$ and AB) then building $(I_3C)$. This last line intersects the lines of action of $\mathbf{F_2}$ and $\mathbf{F_3}$, respectively in $S_2'$ and $S_3'$. By similarly building $I_2$ and the line $(S_1S_2)$, we can deduce $S_1'$ at the intersection of $I_2S_2'$ and the line of action of $\mathbf{F_1}$. In the case of a system with more forces, the reasoning is the same and the set of points of the funicular polygon is determined step by step by using properties 1 and 3. We note that it was not necessary to use the polygon of forces, or to build the new pole O to construct the new funicular polygon. These last constructions are useful for determining the compressive forces in the rods of the arc and the reactions.

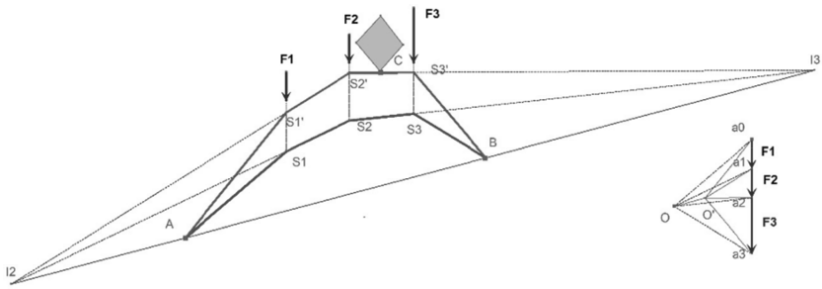


**Figure 7.18.** *Construction of a funicular polygon through three points*

## 7.5. Bibliography

[BEN 91] BENVENUTO E., *An Introduction to the History of Structural Mechanics*, Spinger Verlag, New York, 1991.

[HEY 95] HEYMAN J., *The stone skeleton: Structural Engineering of Masonry Architecture*, Cambridge University Press, Cambridge, 1995.

[HEY 98] HEYMAN J., *Structural Analysis: A Historical Approach*, Cambridge University Press, Cambridge, 1998.

[HOO 75] HOOKE R., A Description of Helioscopes, and Some Other Instruments, London, 1675.

[POL 48] POLENI G., Memorie istoriche della gran cupola del tempio Vaticano e de' danni di essa, e de' ristoramenti loro, Nella Stamperia del Seminario, Padua, 1748.

# 8

# Projective Properties and Duality

## 8.1. Projective properties and graphic statics

This chapter discusses the geometric properties of constructions using graphic statics. Its first goal is to understand the coherence between results derived through static reasoning and results obtained through purely geometrical arguments. Its second objective is to show how the use of these projective properties and reciprocal figures (figures linked by reciprocity relationships) have enabled the development of graphic statics and practical calculation methods such as that of trusses, commonly known as the *Cremona method*. Beyond these theoretical and historical aspects, these approaches and especially *duality*, as reciprocal relationships that associate one figure to another, have a practical interest that is always valid with the use of computers, whether for planar or spatial problems. In this first section, we present links between projective properties and graphic statics. The subsequent sections will look at the use of reciprocal figures and applications of this duality.

So far, we have implicitly placed ourselves in the context of Euclidean geometry. We have been faced with limitations particularly due to the fact that two distinct parallel lines do not intersect by the axiom of parallels from Euclid's fifth postulate. In a first instance, we had to exclude the case of parallel forces because the intersection of their lines of action was not defined. The introduction of funicular polygons allowed us to no longer make this distinction, because the method is applicable to any system of forces through the introduction of non-parallel forces. Thus, it may seem logical to

*Sustainable Masonry: Stability and Behavior of Structures,*
First Edition. Thierry Ciblac and Jean-Claude Morel.

think that since funicular polygons can be used to remove distinctions due to parallelism, it can use the results of a particular geometry which does not use Euclid's fifth postulate: *projective geometry*. Without going into the mathematical development of projective geometry, we can say that it involves properties of figures conserved by central plane projections. We note that the *perspective*, defined as the central projection of a three-dimensional scene on a plane, expresses its geometric properties in projective geometry [FLO 63]. In projective geometry, all lines in the plane are considered to be intersecting, even parallel lines for which the intersection is unique and called the *point at infinity*. Thus, an affine line (Euclidean plane line) becomes a projective line if a point at infinity is added. Girard Desargues (1591–1661) is credited with the first "normalization" of the point at infinity and laying the foundations of projective geometry [DES 39]. By treating the points at infinity the same as other points in the plane, projective geometry allows us to establish general results without distinguishing parallel lines. In Euclidean geometry, it is always possible to particularize the result of projective geometry by stating, for example, that two straight lines intersecting at a point at infinity are parallel. The projective plane is an extension of the affine plane containing the *line at infinity* formed by the set of points at infinity of all lines in the plane. One way to implement the concepts of the point at infinity of a line and the line at infinity of a plane is to note that their perspectives (their central projections in a plane) generally respectively correspond to the *vanishing point* of the line and the *vanishing line* of this plan. In projective geometry, lengths and angles are not conserved. Projective geometry therefore focuses primarily on incidence, so intersections of lines and planes, and thus in particular to alignments of points and membership of points to lines. The works of Girard Desargues were pursued by Blaise Pascal (1623–1662) particularly with his theorem of the mystic hexagram, but it was not until developments by Jean-Victor Poncelet (1788–1867) [PON 22] that projective geometry was widely disseminated. Although Jean-Victor Poncelet was also interested in funicular polygons [CHA 04], it was his work on geometry that was used by Karl Culmann (1821-1881), considered to be the founder of graphic statics, in his treatise on graphic statics [CUL 64]. In its approach, Karl Culmann relied on projective geometry to determine the properties that link figures in the layout plan and the force plan. In particular, he used the fact that the line of action of a force in the layout plan and its representation in the force plan are parallel and therefore the corresponding lines intersect the line at infinity.

In previous chapters, we discussed graphic statics based on the principles of statics expressed in graphical form but we did not use projective geometry

to develop the results. Coherence of geometric figures built in the layout plan and force plan is justified by statics reasoning. Thus, closure of a funicular polygon reflects the nullity of the sum of moments of forces of the system in equilibrium and closure of the force polygon reflects the nullity of the sum of these forces. Similarly, other funicular polygon properties are deduced from reasoning based on the principles of statics. Figures formed in the two plans must satisfy the properties of statics that can result in geometric properties. It is interesting to note that two application properties of funicular polygons correspond to projective geometry theorems: the Desargues theorem and the Jakob Steiner theorem. We will develop these two cases below.

### 8.1.1. *The Desargues theorem and equilibrium of three forces*

Here, we consider the relationships between projective geometry and properties of three forces in equilibrium. Desargues' theorem is a fundamental result of projective geometry stated by the mathematician from Lyon in 1648. It is formulated here in its projective version, incorporating terms from the work of Y. Ladegaillerie [LAD 02].

DESARGUES' THEOREM 8.1.– (PROJECTIVE).– Let ABC and A′B′C′ be two non-flat triangles of a *projective plane* such that A, A′, B, B′ and C, C′ are distinct. Lines (AA′), (BB′) and (CC′), assumed to be distinct, are concurrent *if and only if* the points of intersection R of (AB) and (A′B′), P of (BC) and (B′C′) and Q of (AC) and (C′A′) are aligned.

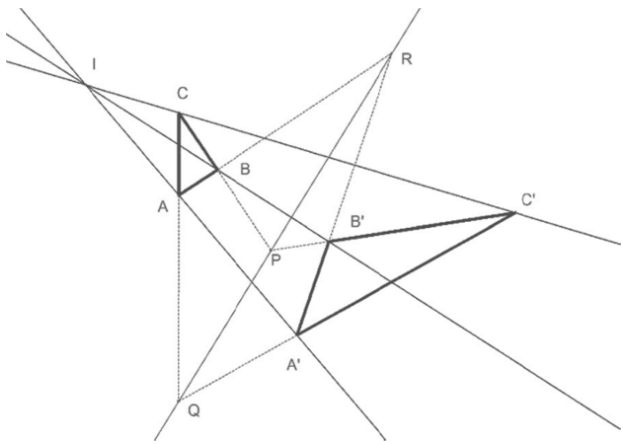


**Figure 8.1.** *Desargues' theorem*

It is said that the two triangles ABC and A′B′C′ are *perspective* relative to the point of intersection I of lines (AA′) (BB′) and (CC′).

Expressing Desargues' theorem in its projective version implies that the points P, Q, R and I can or cannot be at infinity, so that Desargues' theorem formulation in the Euclidean plane is expressed depending on its corresponding parallelism. Figure 8.1 shows the case where none of the points P, Q, R and I are at infinity. Figure 8.2 shows the case where two homothetic triangles correspond to the case where the points P, Q, R are positioned on the line at infinity, since the lines (AB) and (A′B′) are parallel, as well as lines (BC) and (B′C′) and lines (C) and (C′A′).

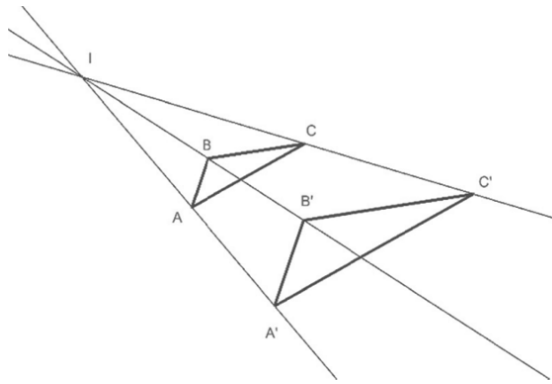


**Figure 8.2.** *Two homothetic triangles (P, Q and R are at infinity)*

Proof of Desargues' theorem is difficult if we stay in the Euclidean plane. Thus, assuming that the two triangles ABC and A′B′C′ have their sides intersecting two by two at a point I, it is not easy to prove the alignment of points P, Q and R. However, passing into three-dimensional space makes its proof simpler (see [FLO 63]). Without going into the details of this proof, we can see that Desargues' theorem figure can be considered as the planar projection (central or parallel) of a three-dimensional figure where the two triangles ABC and A′B′C′ are in two separate planes of Euclidean space and not in the same plane. Thus, the point of intersection I of lines (AA′), (BB′) and (CC′) becomes the vertex of a pyramid with base ABC or A′B′C′. The trihedron formed by three planes IAB, IBC and IAC is intersected by both planes ABC and A′B′C′. Let D be the line of intersection of the planes ABC and A′B′C′. The lines (AB) and (A′B′) are included in the plane IAB, their point of intersection R therefore exists and belongs to planes ABC and

A′B′C′ and therefore to D. Similarly, we show that Q and R belong to line D. The line of intersection D of planes ABC and A′B′C′ contains the points P, Q and R. We can then interpret Desargues' theorem figure (Figure 8.1) as being the planar projection of a truncated triangular pyramid.

We now consider the case of three forces in equilibrium from a geometrical point of view. We have seen that the construction of a funicular polygon determines the force balancing any two arbitrary forces that do not form a couple. This construction must be compatible with the fact that three non-parallel forces in a plane can only be in equilibrium if they are concurrent (comment in section 7.2). If they are parallel, the construction of the funicular polygon also shows the position of forces in the force plan. Constructing a second funicular polygon gives a construction with additional properties (see section 7.3.3.2) that is the same as if the forces were concurrent (Figure 8.3) or parallel (Figure 8.4). In particular, "the points of intersection of the sides of the same rank of funicular polygons are aligned on a line parallel to the line of poles (OO′)". Thus, in Figures 8.3 and 8.4 we get the following property: $I_1$, $I_2$ and $I_3$ are, respectively, the intersection point of lines ($S_1S_3$) and ($S_1'S_3'$), ($S_2S_3$) and ($S_2'S_3'$), ($S_1S_2$) and ($S_1'S_2'$), however the points $I_1$, $I_2$ and $I_3$ are aligned and parallel to the line (OO′). The equilibrium property of three forces indicates that the lines ($S_1S_1'$), ($S_2S_2'$) and ($S_3S_3'$) are concurrent (or parallel in the case of parallel forces). $S_1$ and $S_1'$ belong to the line of action of $\mathbf{F_1}$, which will be called $D_1$, and $S_2$ and $S_2'$ belong to $D_2$ (line of action of $\mathbf{F_2}$) and $S_3$ and $S_3'$ belong to $D_3$ (line of action of $\mathbf{F_3}$). We may notice that these properties are true for all positions of O and O′ in the force plan and consequently for all points $S_1$ and $S_1'$, anywhere on $D_1$, all points $S_2$ and $S_2'$ anywhere on $D_2$ and all points $S_3$ and $S_3'$ anywhere on $D_3$. If we express all these properties in a purely geometric manner, we notice that the alignment of points $I_1$, $I_2$ and $I_3$ is equivalent to the fact that lines $D_1$, $D_2$ and $D_3$ are concurrent or parallel. This equivalence is due to the fact that both methods of construction reflect the equilibrium of three forces. Thus, we get the result of Desargues' theorem with, in the case of concurrent forces, point I to a finite distance (Figure 4.3) and in the case of parallel forces, point I at infinity (Figure 4.4). In the latter case, we can see the figure as being an orthogonal projection of a prism intersected by two intersecting planes. It is remarkable to note that based on statics principles, we can get a powerful result of projective geometry like Desargues' theorem. We also note that the figures linking funicular polygons in the case of three forces in equilibrium can be seen as planar projections of pyramids or prisms (of base $S_1S_2S_3$ in Figures 8.3 and 8.4). We will see later that we can generalize this approach to the projection of polyhedra for equilibrium of *n* forces.

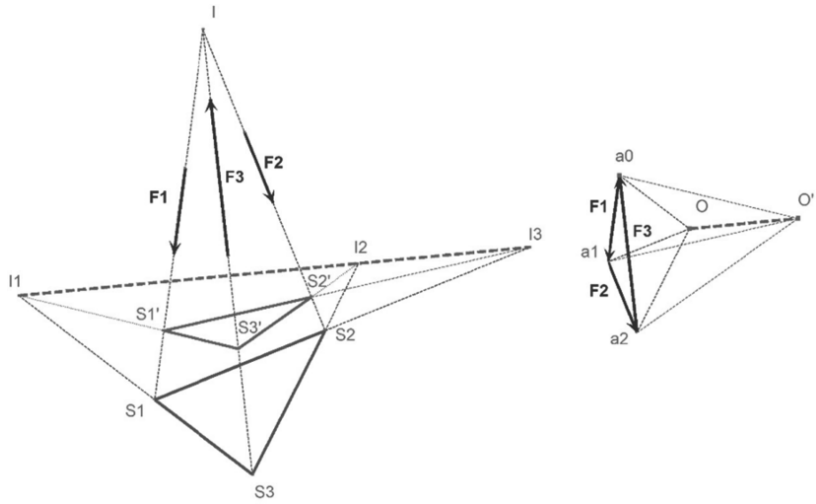


**Figure 8.3.** *Relationship between two funicular polygons of three non-parallel forces in equilibrium*

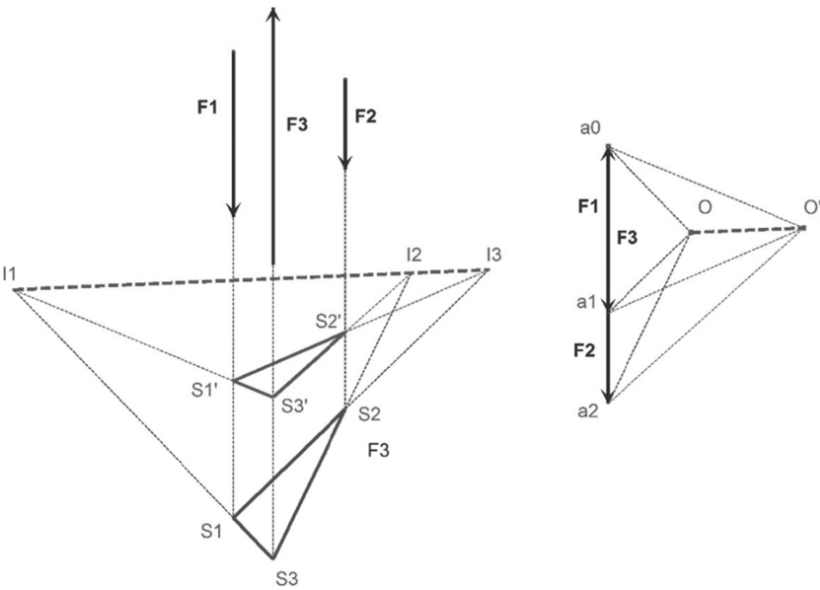


**Figure 8.4.** *Relationship between two funicular polygons of three parallel forces in equilibrium*

### 8.1.2. *Steiner's theorem and equilibrium of n forces*

Here, we will focus on projective geometric properties linking *n* forces in equilibrium in the plane expressed by Jacob Steiner's theorem (1796–1863). Initially, we will focus on properties of *n*-laterals. An *n*-lateral is a polygon defined by a set of *n* lines considered in a plane in a *given order* such that three successive lines (taken in the given order) are not concurrent. The intersections of these lines taken in successive pairs define *n* vertices. These *n* vertices, connected in order, form an *n*-sided polygon, also called *n*-gon. We note that *n*-lateral is defined by lines (side supports) while a polygon is defined by points (vertices). Steiner's theorem on *n*-laterals is formulated as part of *geometry of position*, which considers the *evolution* of patterns formed by lines and points when these change position. Here, we give an equivalent wording to that given by Pirard [PIR 67][1].

STEINER'S THEOREM 8.2.– Take an *n*-lateral from the plane ($d_1$, $d_2$, $d_3$,..., $d_n$ with vertices A, B, C, ....), and *n-1* lines from all vertices except one ($d_a$, $d_c$,... if B is omitted, as in Figure 8.5). u is a line. *n* sides of the *n*-lateral intersect line u at *n* points ($M_1$, $M_2$,... $M_n$). Any other *n*-lateral for which lines ($d_1$, $d_2$, $d_3$,..., $d_n$) successively pass through ($M_1$, $M_2$,... $M_n$), and for which *n-1* vertices (A′, C′, ...) are respectively on *n-1* lines ($d_a$, $d_c$,...) from the vertices of the initial *n*-lateral, has its nth vertex located on a fixed line ($d_b$, passing through point B as shown in Figure 8.5).

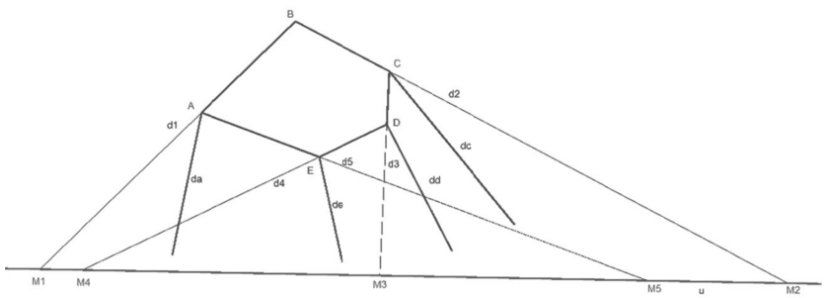


**Figure 8.5.** *Initial elements of Steiner's theorem*

1 Steiner's theorem is formulated in terms of geometry of positions: "If *n* sides of an *n*-lateral from a plane change by each pivoting around fixed points, all located on the same line u, while *n-1* of its vertices move on fixed lines, the nth vertex will also travel on a fixed line". [PIR 67].

Figure 8.5 shows the initial elements of Steiner's theorem, namely the *n*-lateral, where $n = 5$, defined by lines $d_1$ to $d_5$. The corresponding polygon is ABCDE. The $n\text{-}1 = 4$ vertices (ACDE) move on 4 fixed lines, arbitrary directions $d_a$, $d_c$, $d_d$ and $d_e$. The nth vertex (5th peak) is point B in the example. The arbitrary line u allows construction of fixed points $M_1$ to $M_5$ on it, around which lines $d_1$ to $d_5$ will rotate. Steiner's theorem states that point B moves on a fixed line that can be determined.

The movement of vertices on lines $d_a$ to $d_e$ can be done step by step by choosing, to begin with, a point A′ on $d_a$. To do this, we must build line $M_1A' = d_1'$ and line $M_5A' = d_5'$, which allow us to define the point E′ on $d_e$ (Figure 8.6). We then construct the line $M_4E' = d_4'$, and point D′ on $d_d$. Similarly, we construct line $M_3D' = d_3'$ and point C'. And finally, we construct line $M_2C' = d2'$. Thus, all lines $d_1'$ to $d_5'$ are defined. Steiner's theorem then states that point B′, the intersection of lines $d_1'$ and $d_2'$, is located on a fixed line $d_b$.

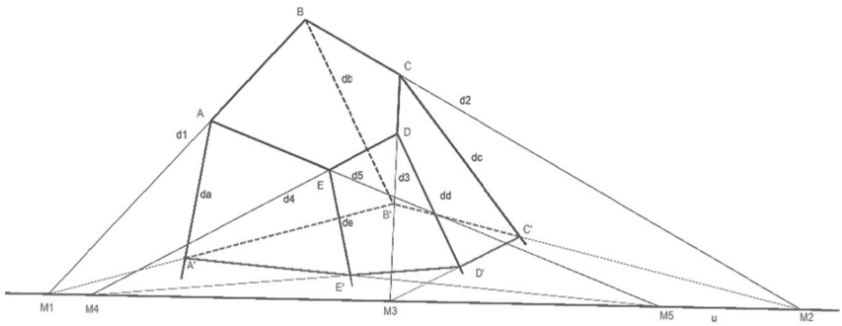


**Figure 8.6.** *Steiner's theorem*

According to the theorem, line u is arbitrary. This means that the nth line is fixed regardless of the position of line u.

We also note that if the *n*-lateral is a triangle, we get the figure constructed in the case of Desargues' theorem, the points $M_1$, $M_2$ and $M_3$ having to identify with P, Q and R. We should see that the three lines $d_a$, $d_b$ and $d_c$ are concurrent at I as a consequence of this same theorem.

As for Desargues' theorem, we can seek to interpret the Steiner theorem figure, constructed in the plane, as the planar projection of a three-dimensional construction. Suppose that the initial elements of Steiner's

theorem (Figure 8.5) represent the partial projection view of a polyhedron, so a volume formed of planar faces. The planar faces ABCDE and edges $d_a$, $d_c$, $d_d$ and $d_d$ from A, C, D and E are plotted, but it lacks edge $d_b$ from B. Now imagine that line u is the line of intersection of plane P containing the face ABCDE and an arbitrary plane Q. We can then try to construct the intersection of edges $d_a$, $d_b$, $d_c$, $d_d$ and $d_e$ with plane Q. From point A′, assumed to be known, intersection of $d_a$ and $d_e$ Q, we construct the lines of intersection of each of the planes containing the faces based on the polygon ABCDE and for which the edges $d_a$, $d_c$, $d_d$ and $d_e$ are known. We notice that the points $M_1$, $M_2$, $M_3$, $M_4$ and $M_5$ belong to planes P and Q, thus we verify that the Steiner's theorem conditions stating that lines $d_1$' to $d_5$' and $d_1$ to $d_5$ respectively pass through points $M_1$ to $M_5$ are verified (*n* sides of *n*-laterals intersect line u at *n* points ($M_1$, $M_2$,... $M_n$)). Point B′ is obtained from the intersection of $d_1$′ and $d_2$′ and line $d_b$ is then determined. With this approach, $d_b$ is the edge from B of the faces defined by *n-1* known edges from the face ABCDE. This edge is thus perfectly defined and thus fixed relative to the others. It is in projection and Steiner's theorem reflects this projective property.

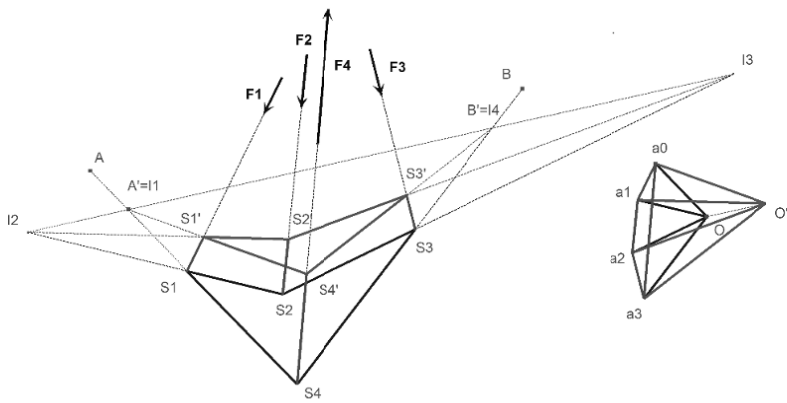


**Figure 8.7.** *Steiner's theorem in the funicular polygons of four forces in equilibrium*

Now let us come back to graphic statics and the equilibrium of *n* forces. The constructed figures consider the relationships between lines and points. By analyzing these relationships, we will find the conditions of Steiner's theorem. If we consider a set of *n* forces in equilibrium and we consider the relationships between two funicular polygons associated with these forces,

we can apply the results of section 7.3.2.2 to a system of *n-1* forces plus a force balancing **Fr**. To illustrate this, Figure 8.7 uses Figure 7.13 from section 7.3.3.2, considering that force $\mathbf{F_4}$ balances the resultant **Fr** of forces $\mathbf{F_1}$, $\mathbf{F_2}$ and $\mathbf{F_3}$. Thus, the forces $\mathbf{F_1}$, $\mathbf{F_2}$, $\mathbf{F_3}$ and $\mathbf{F_4}$ are in equilibrium and the funicular polygons corresponding to poles O and O′ are respectively $S_1$ $S_2$ $S_3$ $S_4$ and $S_1'$ $S_2'$ $S_3'$ $S_4'$. We notice that the assumptions of Steiner's theorem can be found in the properties linking funicular polygons. The figure from Steiner's theorem and that linking funicular polygons can be identified by noting that the *n*-laterals correspond to funicular polygons, fixed lines passing through the vertices ($d_a$, $d_b$...) correspond to the lines of action of forces, line u corresponds to the line parallel to (OO′), and the fixed points ($M_1$, $M_2$...) correspond to the points of intersection of the sides that are of the same rank as funicular polygons ($I_1$, $I_2$...)[2].

### 8.1.3. *Scope of geometric properties in constructions using graphic statics*

We can study graphic statics figures just as we can geometric constructions, linked to each other by rules of parallelism, through lines crossing at points, etc. With such an approach, a statics problem becomes an application of a geometric problem with a more general scope. Choosing this second path leads to the same result as regards statics and may seem superfluous. Yet it presents theoretical and practical advantages. From a theoretical point of view, it allows the study of geometric problems independent of statics problems and can make a link between purely geometric properties and properties of statics. In addition, the geometric approach, through its theoretical and mathematical side, allows us to tackle problems by analyzing the logic of constructions of figures and their properties. Thus, from a practical point of view, constructions can be led in a systematic manner only based on constructions and geometric properties shared with statics. It is only then that reasoning through statics can enlighten geometric constructions. A significant benefit of this double look on structures is also to ensure their coherence through multiple criteria. These criteria are geometrics and statics, but are also, as we have seen, from the properties of planar projections of polyhedra. Another advantage is the possibility of using systematic construction methods allowing simultaneous monitoring of results. Reciprocal figures and their dual relationships are an expression of these methods. They enlighten, in a geometrical manner, the

2 Note that Cremona, in his book on reciprocal figures in graphic statics [CRE 85]) refers to this subject of Pappus porisme made by Poncelet in his *treatise on projective properties* [PON 22].

links between figures constructed in the layout plan and the force plan in graphic statics.

## 8.2. Reciprocal figures and projections of polyhedra

In 1864, James Clerk Maxwell (1831–1879) published an article [MAX 64] describing the properties of reciprocal figures and their application to force diagrams. He begins with a purely geometric definition of reciprocal figures and studies their properties, including those related to conditions of existence. He proposes a general approach, first considering the geometric properties of figures before moving to applications of statics. In what follows, we use the foundations of Maxwell's approach.

### 8.2.1. *Reciprocal plane figures*

Reciprocal figures are such that properties of the first relative to the second are the same as those of the second relative to the first. The reciprocity in question involves figures made of line segments that join a system of points and form closed polygons (Maxwell uses the term *line* in the meaning of *segment*). Reciprocity concerns the existing constant relationship between the directions of all segments of a figure with those of segments corresponding to it in the other figure. In the plane figures, the corresponding segments may be either parallel, perpendicular, or forming a constant angle between them. The segments meet at a point in the figure and form a closed polygon that is also in the other. Maxwell also adds that in the case of a figure in space, the segments of one figure are perpendicular to a plane in the other, and the planes corresponding to the segments that meet at a point form a polyhedron in the other. We will limit ourselves here to plane figures. Maxwell defines reciprocity of two plane figures formed of line segments that join a system of points by forming closed contours. He gives the following definition:

DEFINITION 8.1.– *Two plane figures are reciprocal if*:

1) *they have the same number of segments*;

2) *the corresponding segments of both figures are parallel*;

3) *the converging segments in a figure form a closed polygon in the other figure*.

APPROACH 8.1.– Condition 2) can be extended to cases where the corresponding segments of both figures make a constant angle between each other, because then it suffices to perform the appropriate rotation of a figure to get parallelism.

APPROACH 8.2.– From condition 3), we can deduce that each point of a figure corresponds to a closed polygon in its reciprocal figure, and that through its reciprocity property, each closed polygon of a figure is a point in its reciprocal figure.

PROPERTY 8.1.– As each segment of a figure only has two ends where other segments can converge, each segment of the reciprocal figure can only belong to two closed polygons.

We can try to determine the simplest reciprocal figures. To do this, we notice that a closed polygon has at least three sides and therefore, at every point in the reciprocal figure, at least three segments must converge (Figure 8.8). The simplest plane figure fulfilling these conditions consists of six segments connecting four points in pairs (Figure 8.10). The reciprocal figure comprises six parallel segments respective to those of the initial figure, and the points of one correspond to the triangles of the other.

Let us detail the above reasoning. Figure 8.8 shows a triangle with vertices $S_1$, $S_2$ and $S_3$ with sides called $A_1$, $A_2$ and $A_3$. Segments constructed by the reciprocity procedure are named $a_1$, $a_2$ and $a_3$. They are respectively parallel to segments $A_1$, $A_2$ and $A_3$ and converge at point $z_1$. Thus, the triangle $S_1S_2S_3$ is associated with point $z_1$ of the reciprocal figure. The ends $z_2$, $z_3$ and $z_4$ are chosen freely on the lines parallel to $A_1$, $A_2$ and $A_3$ since no other conditions are imposed on their position. By the principle of reciprocity, the triangle formed by points $z_2$, $z_3$ and $z_4$ must be associated with a point in the reciprocal figure (Figure 8.9). Point $S_4$ is the reciprocal point of this triangle and is at the point of convergence of segments $A_4$, $A_5$ and $A_6$ constructed in parallel to segments $a_4$, $a_5$ and $a_6$ forming the triangle $z_2$ $z_3$ $z_4$. It is remarkable to see that the three lines $(A_4)$, $(A_5)$ and $(A_6)$ converge, reflecting a demonstrable geometrical property. Associating the two configurations gives the simplest reciprocal figures, each consisting of four points, four triangles and six segments. The reciprocal relationships, also termed *dual*, between the triangles of one and the points of the other, associate the points $S_1$, $S_2$, $S_3$ and $S_4$ respectively to $z_1z_2z_4$ $(=a_1a_3a_4)$, $z_1z_2z_3$ $(=a_1a_2a_5)$, $z_1z_3z_4$ $(=a_2a_3a_6)$, $z_2z_3z_4$ $(=a_4a_5a_6)$ in Figure 8.10. This example illustrates that the reciprocity relationships of figures involve relationships that link the number of points, segments and polygons. These relationships

have general implications on the conditions of existence of reciprocal figures, which have been completely developed by Maxwell.

It is interesting to note that reciprocity relationships of figures are invariant under rescaling.

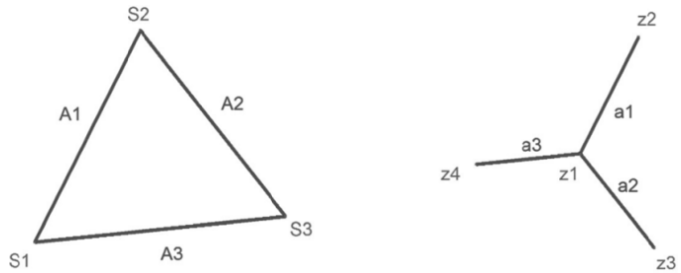


**Figure 8.8.** *Construction of three converging segments from a triangle*

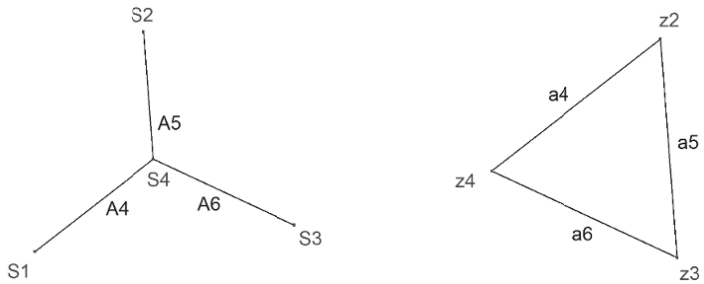


**Figure 8.9.** *Construction of a triangle from three converging segments*

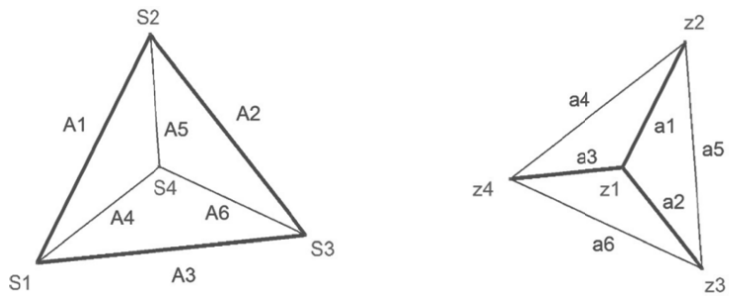


**Figure 8.10.** *Construction of the simplest scenario of reciprocal figures*

To illustrate the procedure for determining reciprocal figures for another simple case, let us consider a polygon with four sides, the tetragon $S_1\ S_2\ S_3\ S_4$ equal to the quadrilateral $A_1\ A_2\ A_3\ A_4$ (Figure 8.11). The reciprocal (dual) point of the tetragon is point $z_1$, from which four segments parallel to $A_1$, $A_2$, $A_3$ and $A_4$ start, respectively ending at points $z_2$, $z_3$, $z_4$ and $z_5$. The dual point of the quadrilateral $a_5\ a_6\ a_7\ a_8$ is the point $S_5$. This point is then the vertex of 4 triangles for which the reciprocal (dual) points are $z_2$, $z_3$, $z_4$ and $z_5$. In Figure 8.11, the sides of the triangles denoted ($A_1$...) are associated with converging segments denoted ($a_1$...) with the same number. Thus, the segments $a_1\ a_5\ a_6$ converge at $z_2$, and $z_2$ is the dual of triangle $A_1\ A_5\ A_6$.

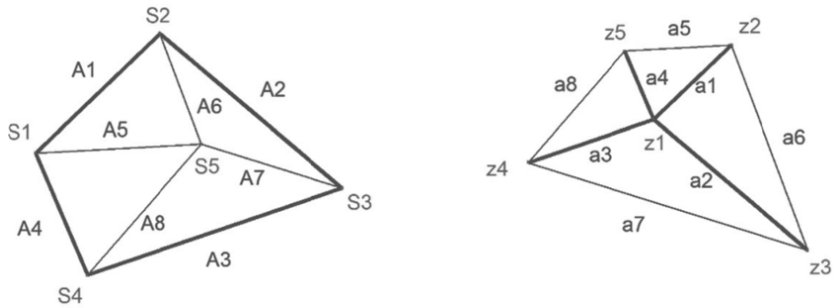


**Figure 8.11.** *Construction of simple reciprocal figures from a quadrilateral*

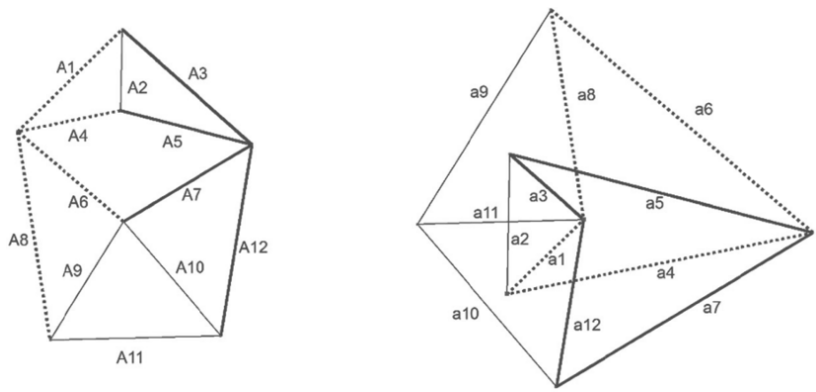


**Figure 8.12.** *Example of reciprocal figures containing twelve segments*

Maxwell gives a slightly more complex example (Figure 8.12) of reciprocal figures each with 12 segments and 7 points corresponding to 7 polygons in the other figure. We denote $A_1$ to $A_{12}$ the segments of the first figure and $a_1$ to $a_{12}$ the segments corresponding to the reciprocal figure. By assumption, segments $A_1$ to $A_{12}$ are respectively parallel to segments $a_1$ to $a_{12}$. Among the 7 polygons of the first figure is a pentagon ($A_1$ $A_3$ $A_{12}$ $A_{11}$ $A_8$) to which a point in the reciprocal figure corresponds, where the 5 segments $a_1$, $a_3$, $a_{12}$, $a_{11}$ and $a_8$ converge. The other polygons are a quadrilateral ($A_4$ $A_5$ $A_7$ $A_6$) and five triangles. The seven polygons of the reciprocal figure are easily determined by identifying convergent segments from the initial figure: ($a_1$ $a_2$ $a_3$), ($a_2$ $a_4$ $a_5$), ($a_3$ $a_5$ $a_7$ $a_{12}$), ($a_1$ $a_4$ $a_6$ $a_8$), ($a_6$ $a_7$ $a_9$ $a_{10}$), ($a_{10}$ $a_{11}$ $a_{12}$) and ($a_8$ $a_9$ $a_{11}$). In Figure 8.12, the polygon ($a_3$ $a_5$ $a_7$ $a_{12}$) and its reciprocal segments have been drawn in bold and the polygon ($a_1$ $a_4$ $a_6$ $a_8$) and its reciprocal segments have been drawn in dashed bold.

### 8.2.2. *Reciprocal figures seen as projections of polyhedra*

Polyhedra are three-dimensional objects consisting of planar faces, edges and vertices. The faces of a polyhedron define a closed volume. The edges have the following properties: (1) an edge joins two points only and (2) an edge joins two faces only. A polyhedron projected onto a plane will become a plane figure for which each segment has two ends only, onto which other segments can converge and where each segment of the figure can only belong to two closed polygons corresponding to the projections of two connected polyhedron faces. Here, we find a consequence of property 1 of reciprocal figures. Thus, there is an analogy between the properties of reciprocal figures and those of the projection of a polyhedron. Furthermore, each of the reciprocal figures verifies the properties of a projected polyhedron. Thus, a polyhedron may be associated with each of the projected figures. For example, the first two cases of reciprocal figures presented above (Figures 8.10 and 8.11) show figures that can each be seen as *projections of pyramids* for which the base is a triangle or a quadrilateral. Maxwell generalized this result to projections of polyhedra for all figures satisfying the conditions of reciprocity.

PROPERTY 8.2.– A figure and its reciprocal figure can be considered as projections of polyhedra.

From this property, we can deduce that reciprocal figures verify the projective properties of polyhedra projections. We also note that polyhedra,

for which projections correspond to reciprocal figures, must be dual, so are connected by a duality relationship. A relationship of this type exists for example in regular polyhedrals, said to be platonic. The duality relationship in this case is defined by connecting the center of faces to the vertex of the dual polyhedron. A cube is thus the dual of the octahedron and vice versa. Similarly, the dodecahedron and the icosahedron are duals. Finally, the simplest of them, the tetrahedron is its own dual. We note that the simplest reciprocal figures (Figure 4.10) correspond exactly to tetrahedrons, but are not necessarily regular.

8.2.2.1. *Relationship linking a polyhedron to its projection and its reciprocal figure*

In this regard, it may be interesting to consider the relationship linking a polyhedron to its projection and the corresponding reciprocal figure. One answer is to consider a particular projection of a polyhedron as an *orthogonal projection*. An orthogonal projection is a parallel projection for which the projection direction is orthogonal to the plane of projection. In this projection, the projected polyhedron dual figure is constructed by combining a point on the projection plane T to each face of the polyhedron. The construction of dual points is done as described in the following. Consider a fixed point Ω that does not belong to a projection plane. For each face, the point of intersection with the projection plane of the line perpendicular to the face passing through a fixed point Ω is constructed. Dual points obtained are then only connected if the corresponding faces of the polyhedron have a common edge. We note that parallel faces have the same dual point because their perpendicular lines have the same direction. With this method, we will show that the obtained dual figure must be rotated 90° so that the segments of reciprocal figures are parallel. This approach can be used to ensure coherence of projections of polyhedra when these are only defined by a projection. It is mainly used in computer applications of 3D reconstruction from projections, for example by Sugihara in 1982 [SUG 82] (see also [CIB 08, GUE 08]).

To demonstrate and understand the relationships between the orthogonally projected polyhedron and dual points associated with faces, we will look at the intersection of two planes A and B that are parallel to two connected faces Fa and Fb of the polyhedron. We choose to make the planes A and B pass through a fixed point Ω (Figure 8.13). The intersection of A and B with the projection plane T are lines TrA and TrB. These lines intersect at point j. Thus, planes A and B intersect along line (Ωj). By denoting O the orthogonal projection of Ω on T, we deduce that the orthogonal projection of

(Ωj) is line (Oj). Let "a" be the point of intersection of the line perpendicular to A passing through Ω with T, and let "b" be the point of intersection of the line perpendicular to B passing through Ω with T. Points a and b are, by definition, the dual points of Fa and Fb. We can then easily show that line (ab) is perpendicular to line (Oj) which, we recall, is the orthogonal projection of the intersection of planes A and B. Thus, after a 90° rotation of dual points (relative to any point on T) giving dual points a′ and b′, we deduce the following property: *the intersection of planes A and B and consequently, the common edge of faces Fa and Fb are projected orthogonally on T along a segment parallel to (a′b′)*. Figure 8.14 shows this duality relationship, which is characteristic of reciprocal figures. In this figure, line Δ is the projection of the intersection of planes A and B. The dual points a and b are on a line perpendicular to Δ. The points a′ and b′ obtained by a 90° rotation are on a line parallel to Δ. We may notice that if we move Ω away from T, the dual figure transforms homothetically, which corresponds to a simple change of scale.

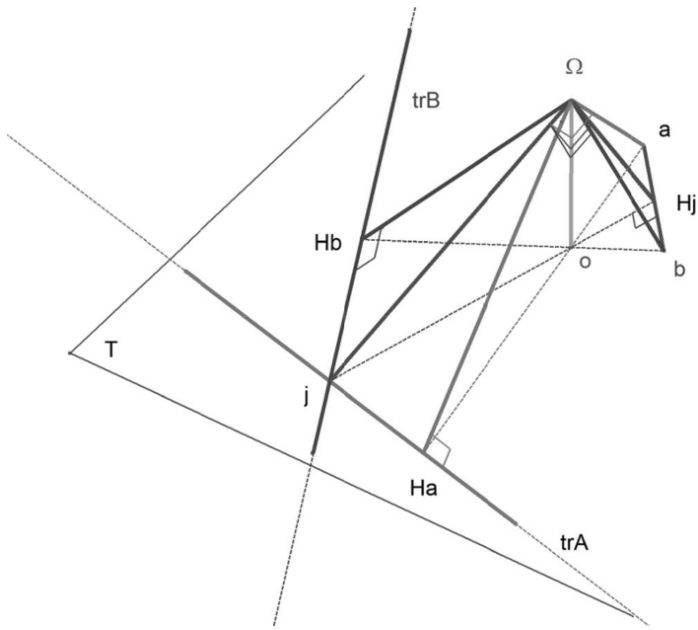


**Figure 8.13.** *Intersections on plane T of perpendicular lines and parallel planes to those passing through a fixed point Ω.*

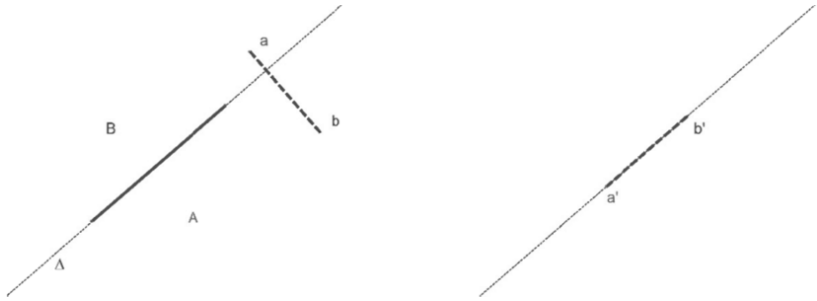


**Figure 8.14.** *Duality relationship between the orthogonal projection of the intersection of planes A and B and their dual points a and b, and after a 90° rotation of points a´and b´*

It is interesting to note that the relationships established between a polyhedron, its orthogonal projection and the associated reciprocal (dual) figure allow:

1) the construction of the reciprocal figure of a figure from a coherent initial figure, through the construction of dual points. This procedure is detailed in section 8.2.2.2. We note that the reciprocal figure can also be interpreted as the projection of a polyhedron;

2) the definition of a coherent initial figure seen as the projection of a polyhedron. The use of duality allows us to impose a flatness condition to the faces of the polyhedron and thus ensures coherence of its projection. This coherence, reflecting projective properties, is also valid if we consider the figure as being the central projection of a polyhedron. In section 8.2.2.3, we will see how duality allows us to find Steiner's theorem;

3) the interpretation of a dual point as a feature of the direction of a polyhedron plane if it is orthogonally projected. This gives a powerful interpretation of the link between an orthogonally projected face and a point on the associated reciprocal figure;

4) determination of the projection of the intersection of two planes, knowing their dual points. A segment connecting two dual points gives the direction of the projection of the intersection of two corresponding planes. This property is coherent with an orthogonal projection, because parallelism is conserved. It also allows construction of an orthogonal projection, due to duality, of the intersection of a polyhedron with a plane, knowing its dual point.

8.2.2.2. *Construction of the reciprocal of figure of a polyhedron projection*

We have just seen that one way to address two reciprocal figures is to interpret them as polyhedra projections. We also saw that the dual point of the direction of the plane of the latter can be associated with the first face of a polyhedron. The direction of a common edge with two faces, in projection, is parallel to the segment linking the associated dual points. Thus, due to this property, it is advisable to name the faces of the polyhedron and its projection and give these names corresponding dual points. By proceeding in this manner in the example of Figure 8.12, Figure 8.15 is obtained where polygons associated with faces of the polyhedron are labeled A, B, C, D, E, F and G, and the reciprocal points associated with dual points are named a, b, c, d, e, f and g. The letters A, B, C, D, E and F are positioned in the center of the polygons. The letter G is positioned outside the pentagonal contour of the figure but specifically names it. Pentagon G must be seen as the projection of a pentagonal planar face for which the dual point is g. We note, for example, that segment gf of the dual figure corresponds to the common edge of G and F. With this convention, we see that it is very easy to build a reciprocal figure from a coherent initial figure. Coherence of the initial figure must be the same as the projection of a closed polyhedron. We can then easily name the faces on the initial figure. We start by giving a point on the reciprocal figure associated with a face, for example, point a for face A. We draw a parallel line passing through a to the common edge with another face, for example G. Thus, a point g on this line defines a second reciprocal point. Reciprocal points are then obtained, step by step, by intersection of lines parallel to the common segments with two faces, for which at least one of the reciprocal points is known. Thus, point b is defined by plotting the point of intersection of lines parallel to the common segments of (A and B) and (G and B) respectively passing through a and g. Point c can then be built at the intersection of lines parallel to the common segments of (A and C) and (B and C) respectively passing through a and b. Similarly, we can construct f, d and e.

If we wish to interpret the left figure as the projection of a polyhedron, we will notice that face C of the polyhedron must intersect the face of G, as they have two vertices in common. We should verify that the segment connecting these vertices in the left figure is parallel to segment gc in the right figure. We can also deduce that the common vertex of faces ABC and common vertex of faces CDEF are located on either side of face G. If, in the same manner, we wish to interpret the figure on the right as the projection of a polyhedron, we will see that face (bcdg) of the polyhedron must intersect face

(acfg) because their vertices c and g are in common. We should therefore check the parallelism of segment gc with the segment connecting the corresponding dual points in the other figure.

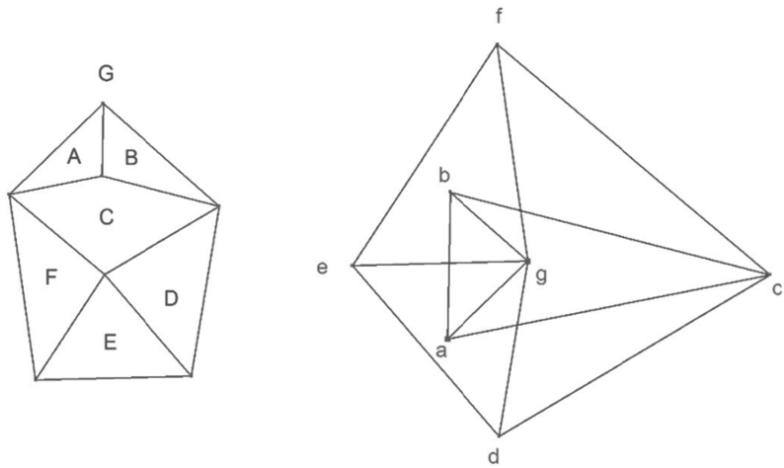


**Figure 8.15.** *Reciprocal figures identical to that of Figure 8.12 where polygons of the first figure (initial projected polygon faces) and the points of the reciprocal figure (dual points of faces) are named*

8.2.2.3. *Steiner's theorem considered through duality*

In section 8.1.2, we saw that Steiner's theorem can be interpreted as characterizing the coherence property of the planar projection (central or parallel) of a polyhedron. In particular, knowing the projection of a polygonal planar face with *n* sides and *n-1* edges from these adjacent faces, the projection of the *nth* edge may only be on a single line. Here, we will determine its position through a reasoning using duality. Figure 8.16 shows, on the left, the initial data from Steiner's theorem in the case of a five-sided polygon (from example section 8.1.2). The faces are named P on the pentagonal face, and $A_1$, $A_2$ $A_3$, $A_4$ and $A_5$ for the faces with a common edge with P. The five edges of the pentagon are known but only four of the five edges from the vertices of the pentagon in projection are known. Let us construct the dual figure of the left projection. Point p is the dual of point P. Let us also construct a point $a_1$ that is the dual of $A_1$. To do this, we just have

to take point $a_1$ on the line parallel to the common edge of P and $A_1$ passing through p. From here onwards, we will denote common edges of two faces by square brackets, for example [P $A_1$] for the common edge of P and $A_1$. $a_5$ is then easily deduced at the intersection of lines passing through p and $a_1$, respectively parallel to edges [P $A_5$] and [$A_1$ $A_5$]. Similarly, $a_4$ is the intersection of lines passing through p and $a_5$, respectively parallel to edges [P $A_4$] and [$A_5$ $A_4$]. Then $a_2$ is the intersection of lines passing through p and $a_1$, respectively parallel to edges [P $A_2$] and [$A_1$ $A_2$]. Finally, $a_3$ is the intersection of lines passing through p and $a_4$, respectively parallel to edges [P $A_3$] and [$A_4$ $A_3$]. Thus, the dual points of all faces are determined. The direction of the missing edge [$A_2$ $A_3$] is therefore known since it is parallel to ($a_2a_3$), shown in dotted lines on the figure.

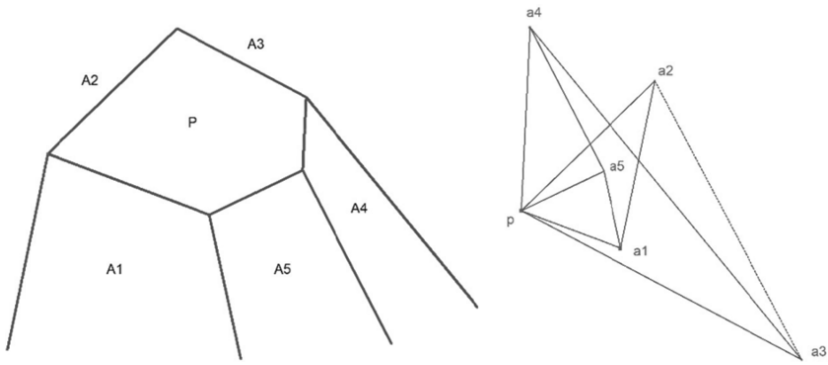


**Figure 8.16.** *Determination by duality of the direction of the missing edge of Steiner's theorem*

We note that the line u mentioned in the assumptions of Steiner's theorem is not necessary to determine the direction of the missing edge. Figure 8.17 shows the missing edge on the left figure and the closure of a polyhedron by a face Q for which the dual is q. Line u may thus be interpreted as the projection of the intersection of planes containing P and Q. Thus, we verify that points $M_1$, $M_2$, $M_3$, $M_4$ and $M_5$ are aligned on a line parallel to line (pq). The figures representing the projection of the polyhedron formed by faces (P, $A_1$, $A_2$, $A_3$, $A_4$, $A_5$ and Q) and its dual for which the vertices are (p, $a_1$, $a_2$ $a_3$, $a_4$, $a_5$ and q) are reciprocal figures. They are represented by continuous lines in Figure 8.17.

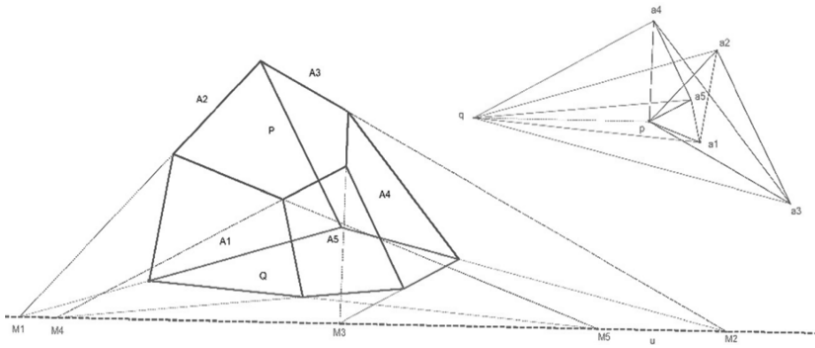


**Figure 8.17.** *Complete configuration of Steiner's theorem figure and its associated dual figure*

The use of reciprocal figures and their interpretation as dual figures of polyhedra projections may seem distant from statics calculations. However, if we note, as did Maxwell, that the coherence properties of projections are the same as those of a system of forces in equilibrium in a reticulated structure with nodes that are only in equilibrium under the effect of compression or tension in the rods, it may be easier to "see" reciprocal figures as projections of polyhedra rather than as more abstract constructions considering forces. Later, we will see how duality can be interpreted and usefully implemented in graphic statics calculations, including such applications as the calculation of Cremona truss structures. We will also see that Bow's notation, usually associated with these methods, shows how to name the faces and dual points that we used in polyhedra projections. These methods of truss calculation are useful for the study of equilibrium of masonry if we consider the weight of the blocks as being a system of external forces, and if we match resultant stresses at the interfaces to forces in the rods.

## 8.3. Duality in graphic statics

### 8.3.1. *Interpretation of reciprocal figures in the case of reticulated structures*

Static interpretation of reciprocal figures is partially contained in the known results of funicular polygons including works by Culmann. It was generalized by Maxwell and developed by Cremona in graphic statics. Thus,

reciprocal figures may be considered from not only a purely geometrical point of view but also as systems of points on which forces act along the connecting segments. We could imagine a structure in equilibrium consisting of rods connected together by joints and thus only subjected to compression or traction effects. If all segments of the figure correspond to rods, it is assumed that the structure is not subjected to any external force. The structure thus conceived is free, so not connected to the external environment, which is considered to be a fixed solid. Equilibrium of the structure is reflected by the equilibrium of each rod and of each of its nodes. The equilibrium of a node results in nullity of the sum of the forces at the node and thus closure of the associated force polygon. For each rod, the equilibrium condition results in the fact that the force polygons connected to both ends must have a common side.

It is thus remarkable to note that the reciprocal figure of the structure may also be considered a reticulated structure in which the equilibrium of a node results in closure of the polygon corresponding to the initial figure. For example, we could interpret Figure 8.15 on the left as being a planar reticulated structure. Equilibrium of the node at the intersection of faces (or polygons) A, B and G results in closure of the force polygon abg. The forces in equilibrium in this node are the vectors **ag**, **gb** and **ba** (they could also have been in the opposite direction, **ba**, **gb** and **ag**). To ensure equilibrium of the rod [A G], force **ga** must balance **ag** of the other node. The other node is also common to G, A, C and F. The forces in equilibrium are thus the vectors **ga** (to balance **ag**), **ac**, **cf** and **fg**. Conversely, the right figure can be seen as a reticulated structure and the left figure as force polygons. Thus, equilibrium of the node is reflected by closure of the force polygon for which the vectors coincide with the sides of polygon A. This is the same as for equilibrium of nodes b, c, d, e, f and g, respectively associated with polygons B, C, D, E, F and G. Figure 8.18 shows these two interpretations with, on top, the reticulated structure on the left and equilibrium of nodes in rod [A G] expressed by force polygons on the right. Forces are returned to the same scale as the nodes on the left-hand side figure. At the bottom of Figure 8.18, the right-hand side figure shows the reticulated structure, and the left shows that equilibrium of point g results in closure of the force polygon where the vectors are drawn. Forces are returned to the same scale as node g in the right-hand side figure. We note that the structures corresponding to reciprocal figures are not necessarily isostatic. Reciprocal figures from Steiner's theorem in section 8.17 show, on the left, a hypostatic structure (mechanism) in equilibrium under the forces defined by polygons of forces of the

reciprocal figure on the right. In the case of indeterminate hyperstatic structures, non-uniqueness of the reciprocal figure may be observed.

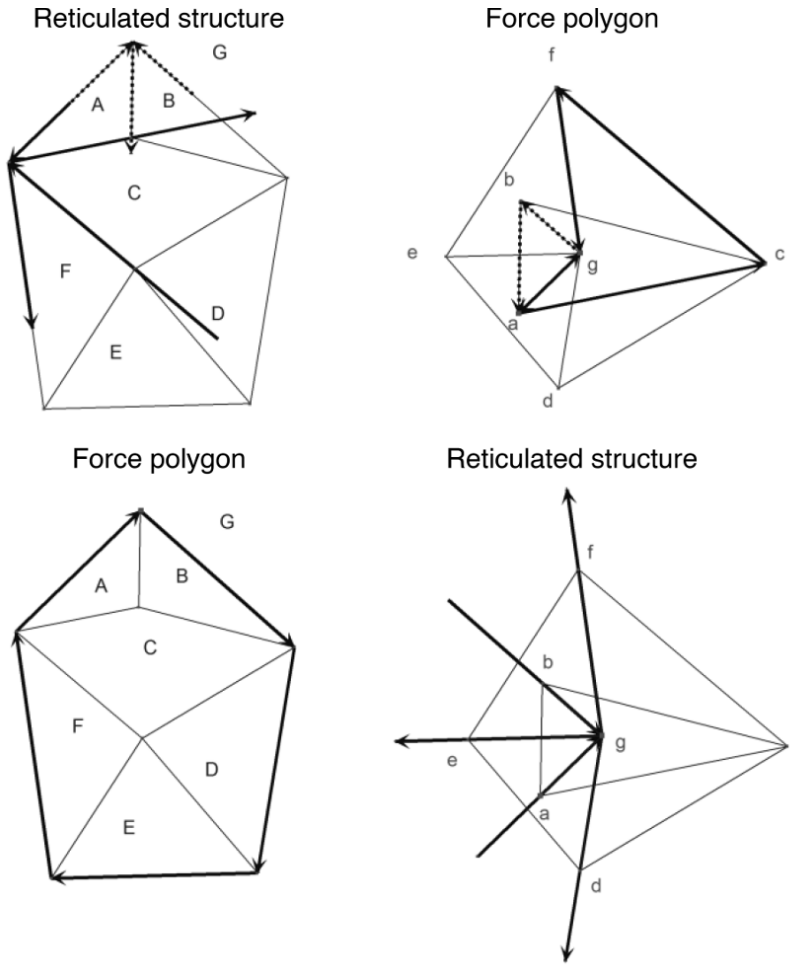


**Figure 8.18.** *Two interpretations of reciprocal figures*

### 8.3.2. *Reciprocal figures and funicular polygons*

Previously, we introduced the concept of a funicular polygon independent of the concept of reciprocal figures. However, associating a system of forces

from a layout plan to that of a force plan through the construction of funicular polygons suggests a close link must unite these concepts. As a first step toward understanding the relationship between reciprocal figures as defined by Maxwell and graphic statics figures, we first note that the criterion of parallelism of segments is satisfied between figures of the layout plan and those of the force plan (criterion 2 of the definition of reciprocal figures by Maxwell). Moreover, we recall that criterion 3 defining reciprocal plane figures states that converging segments in a figure form a closed polygon in the other figure. If we mainly consider systems of forces in equilibrium in graphic statics, we note that:

– concurrent forces in equilibrium in the layout plan correspond to a closed force polygon in the force plan;

– a funicular polygon forming a closed circuit in the layout plan is associated with rays converging toward the associated pole in the force plan. (We recall that the funicular polygon reflects the equilibrium of moments of a system of forces in equilibrium). These properties are consistent with the third criterion but the figure must also be complete, so that each segment belongs to two closed polygons.

If we consider *n* forces in equilibrium $\mathbf{F_1}$, $\mathbf{F_2}$,…, $\mathbf{F_n}$ (for example, by balancing *n-1* arbitrary forces with their opposing resultant **Fr**), it is then possible to draw an associated funicular polygon with pole O (Figure 8.19). We can thus begin a figure consisting of a polygon and *n* edges for which we know that the directions and an end belonging to the polygon. The associated dual figure consists of edges from O and is connected to points $a_0$, $a_1$...$a_{n-1}$. To complete the reciprocal figures, if the forces $\mathbf{F_1}$, $\mathbf{F_2}$,…, $\mathbf{F_n}$ are not concurrent (generally the case for $n > 3$), it is necessary to build a second associated funicular polygon with a second pole O′. Thus, the number of segments will be exactly the same in the dual figures and they satisfy the reciprocity criteria. We note that it is then a case of Steiner's theorem and the associated polyhedron is formed of two polygonal faces with *n* sides and *n* quadrilateral faces. We note that generally, *n* edges linking two polygonal faces with *n* sides have no reason to converge, as the forces in equilibrium are not generally convergent. In the particular case of a system of concurrent forces in equilibrium, the polyhedron may be limited to a pyramid with a polygonal base with *n* sides, with the vertex of the pyramid projecting the point of intersection of forces. Thus, in the simplest case – three forces in equilibrium, so concurrent – a tetrahedron is obtained (Figure 8.20). We can then truncate the pyramid by a second plane

and construct a second funicular polygon to form more complicated reciprocal figures (Figure 8.21).

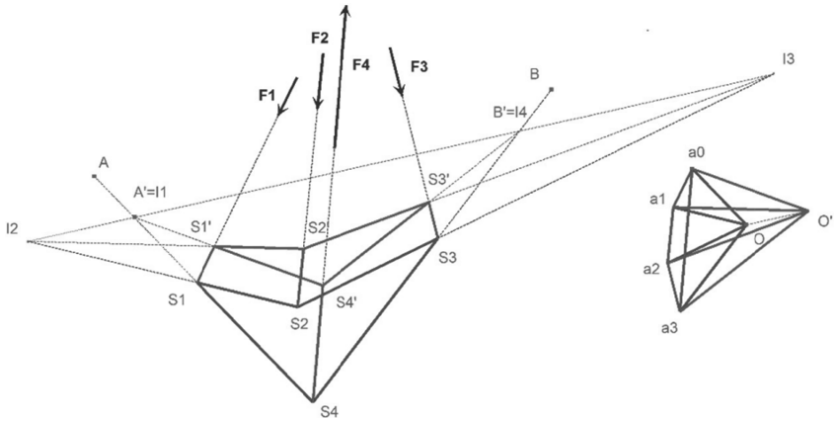


**Figure 8.19.** *Reciprocal figures linking four forces in equilibrium from associated funicular polygons*

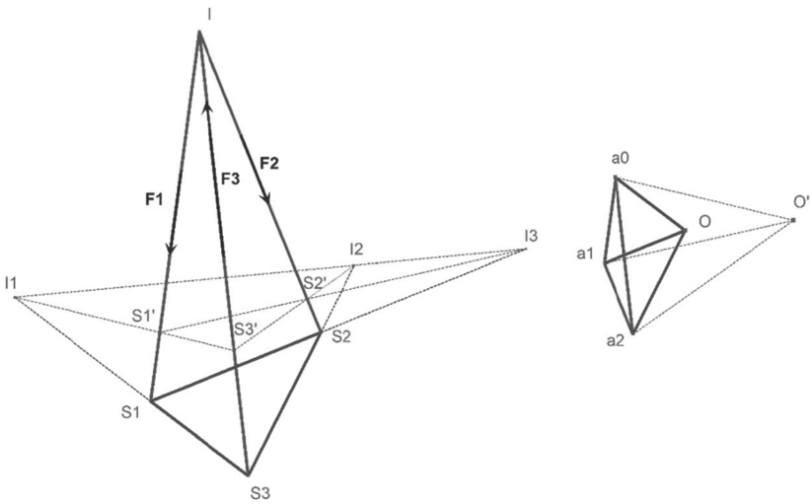


**Figure 8.20.** *The simplest reciprocal figure linking three forces in equilibrium*

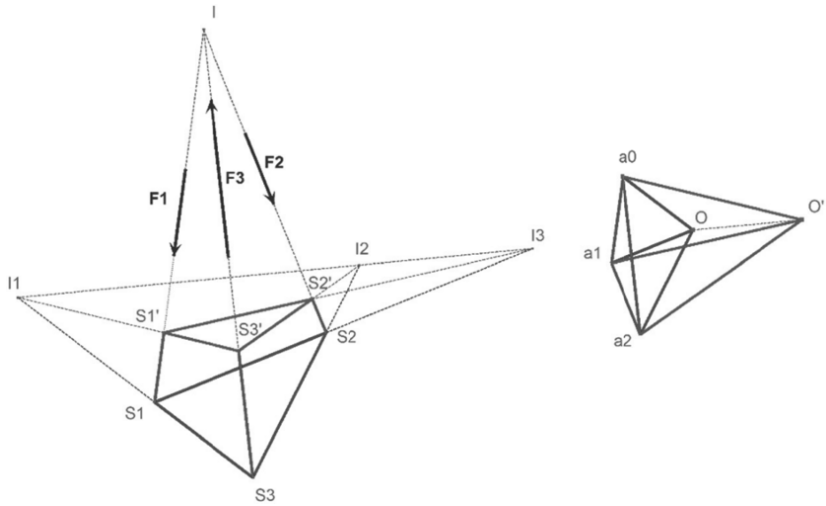


**Figure 8.21.** *Other reciprocal figures linking three forces in equilibrium*

### 8.3.3. *Application in the search for tensile planar structure shapes*

As we have seen, reciprocal figures are not connected to the outside, however physical structures are usually in interaction with the external environment that is generally assumed to be statically fixed. If the interaction is done through a connecting element such as a joint or single support in the plane, we can consider linking certain rods from reticulated structures to the external environment; the link then becomes a *support*. The connecting elements are implicitly connected together via the external environment that is considered to be a rigid solid. The way in which these supports are interconnected in the external environment does not matter since study of the structure only considers what happens within it. Only reactions at the supports matter as they must balance the action of the structure on the external environment. Thus, we can easily see the reticulated structure of Figure 8.19 on the left decomposed into two parts:

– a reticulated structure formed of 4 connecting rods connecting $S_1'$, $S_2'$, $S_3'$ and $S_4'$, and 4 rods connecting these points respectively to support points $S_1$, $S_2$, $S_3$ and $S_4$;

– an external environment composed of 4 rods connecting the support points $S_1$, $S_2$, $S_3$ and $S_4$.

We can then assume, for example, that forces $\mathbf{F_1}$ to $\mathbf{F_4}$ are the reactions at the support points. In this case, with reference to the direction of the forces shown in Figure 8.19, the rods [$S_1$ $S_1'$], [$S_2$ $S_2'$] and [$S_3$ $S_3'$] work in traction and the rod [$S_4$ $S_4'$] is in compression.

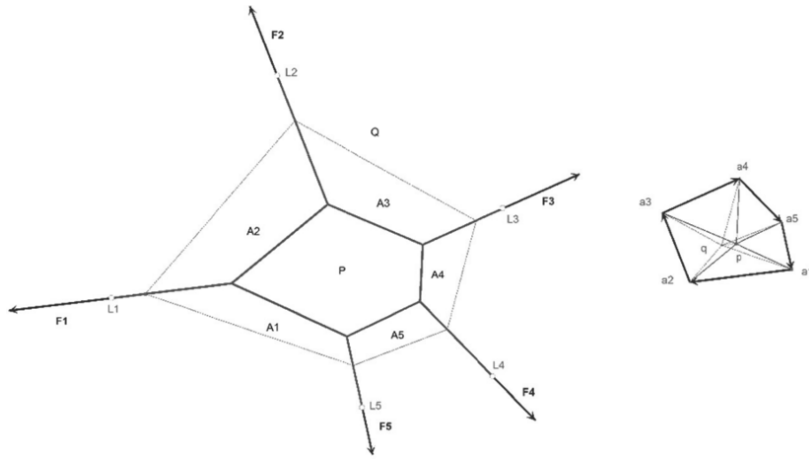


**Figure 8.22.** *Tensile planar structure determined using a funicular polygon*

Following the same logic, we can try to build a similar structure for which all rods would work in traction. Figure 8.22 gives an example of such a structure for which we give 5 supports $L_1$,..., $L_5$ and 4 directions of the rods with 4 associated forces. The 5th force must balance the other 4. We have seen that Steiner's theorem implies that the direction of the fifth rod depends on the 4 others. The construction of a funicular polygon with pole p allows us to determine the direction of the rod linked at $L_5$ as well as the reaction force at this support. Moreover, the corresponding funicular polygon can construct rods of polygon P connecting the first five constructed rods. We note that it is not necessary for points $L_1$,..., $L_5$ to form a funicular polygon (for example, the dotted line) because the tension in a rod from a support remains unchanged irrespective of the position of the support on the corresponding line of action. In this case, it simply means that the external environment cannot be reduced to rods connecting supports. We note that in the case where supports are arranged along the vertices of a funicular polygon associated to q for example (dotted line in the figure), the external environment may be limited to *compressed* rods forming this polygon. To complete it, we must ensure that the structure is actually tensile. To do this, the equilibrium of each node must be verified, which allows us to determine

the direction of the action exerted by the rod on the node. For example, the common node with $A_2$, $A_3$ and P is subjected to the action $\mathbf{a_2a_3}$ of rod [$A_2$ $A_3$], $\mathbf{a_3p}$ of rod [$A_3$ P] and $\mathbf{pa_3}$ of rod [P $A_2$]. The direction of forces applied to this node is therefore that of path $a_2$, $a_3$, p in the dual figure. It corresponds to a pulling action.

We note that the tensile structure we designed according to the 4 forces $\mathbf{F_1}$, $\mathbf{F_2}$, $\mathbf{F_3}$ and $\mathbf{F_4}$, balanced by $\mathbf{F_5}$, may be in equilibrium under the action of directly opposing forces; in this case, the structure is entirely compressed. More generally, we also note that once the shape of the structure is fixed, we can seek other equilibrium states corresponding to forces $\mathbf{F_1'}$, $\mathbf{F_2'}$, $\mathbf{F_3'}$ and $\mathbf{F_4'}$, balanced by $\mathbf{F_5'}$. We can easily find that dual points $a_1'$,..., $a_5'$ associated with faces $A_1'$,..., $A_5'$ must be homothetic to points $a_1$,..., $a_5$ with respect to point p, noting that the directions of forces are fixed. A homothetic negative ratio then corresponds to compressed structures.

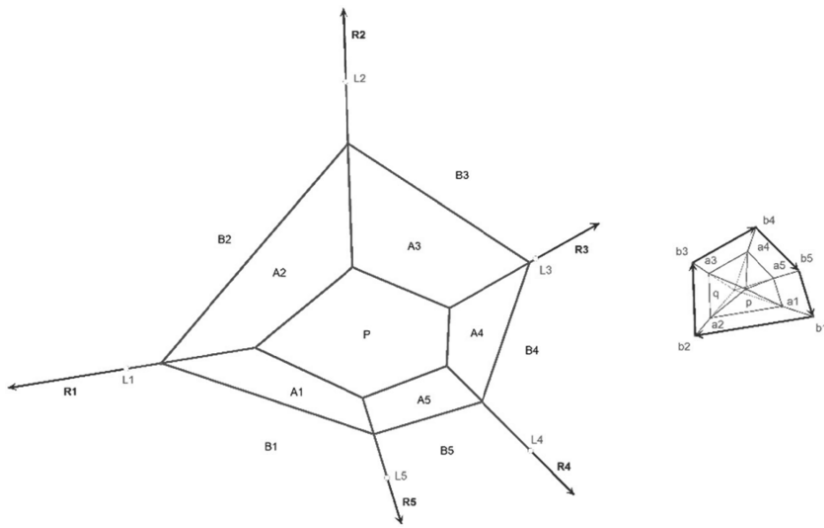


**Figure 8.23.** *Tensile planar structure determined using duality*

We can use duality to define a more complex tensile reticulated structure and determine tensions in the rods. We can, for example, begin with the 5 anchors (as before) and the 4 reactions $\mathbf{R_1}$ to $\mathbf{R_4}$. The 5th reaction is then defined by a funicular polygon by considering for example, pole q, so the associated dual points are $b_1$, $b_2$,..., $b_5$ (Figure 8.23). We can use the funicular thus defined to build 5 rods delineating areas $B_1$ to $B_5$. If rods are built in line

with the directions of reactions, we define 5 nodes where 5 rods converge, for which equilibrium must result in closed quadrilaterals in the dual figure of the force plan. Such a quadrilateral is ($a_1$ $b_1$ $b_2$ $a_2$) for the common point of the faces $A_1$, $B_1$, $B_2$ and $A_2$. If the constructed rods are then connected, on the lines of action of reactions, by rods forming polygon P, we ensure equilibrium of the nodes and their position is defined based on the dual point p. We note that the points ($a_1$, $a_2$, $a_3$, $a_4$) and ($b_1$, $b_2$, $b_3$, $b_4$) form homothetic figures with respect to point q and could be combined with a ratio of 1. This would simply mean that tensions in the rods [$A_1$ $B_1$] to [$A_4$ $B_4$] are zero. We can see that for the same geometry, stress distribution in the rods may be multiple. To finalize this, we must ensure that the structure is tensile. To do this, we can check the equilibrium of each node and determine the direction of the action exerted by the rod on the node.

The structures that we have just studied are only subjected to the action of reactions applied to supports. However, it is very easy to consider these structures as only being subjected to external forces at certain nodes, for example at forces $\mathbf{R_1}$ to $\mathbf{R_5}$ for the structure in Figure 8.23. It is thus possible to generally address reticulated structures loaded with nodes.

### 8.3.4. *Search for support reactions of a solid*

A first condition of stability of a structure is to ensure that it is in equilibrium under a load consisting of a set of external forces and reactions to connections with the external environment. External forces are assumed to be known and reactions are to be determined such that they balance them. Thus, to determine reactions, we first search for the resultant of all external forces applied to the structure. Reaction forces must balance this resultant. We use the construction of the force polygon and the funicular polygon of all forces applied to the structure such that both are closed. To determine the reactions, we use knowledge of the resultant that is to be balanced and the directions and known crossing points of lines of action of reactions. The line of action of the reaction is known in the case of a simple support since it passes through the defined point and is perpendicular to the support surface. In the case of a joint, we only know that the line of action passes through the point indicating its position. In all cases, we can define or at least name the zones (Figure 8.24) between the forces (external and reaction) and construct the dual points at the same time as the funicular polygon. We illustrate the method for the case of a solid connected to the outside by a joint and a simple support and subjected to three external forces $\mathbf{F_1}$, $\mathbf{F_2}$ and $\mathbf{F_3}$ (Figure 8.24). The system is isostatic, because the supports block the 3 degrees of freedom

of the solid. We name A, B, C, D and E the 5 zones successively defined between the forces $\mathbf{F_1}$, $\mathbf{F_2}$, $\mathbf{F_3}$, $\mathbf{R_2}$ and $\mathbf{R_1}$. The line of action of the reaction $\mathbf{R_2}$ at the simple support is known since by definition it is perpendicular to the surface (shown as a dotted line in Figure 8.24). However, only the crossing point $M_1$ of the line of action of the reaction $\mathbf{R_1}$ is known at the joint. We simply know that this line through $M_1$ separates zones E and A.

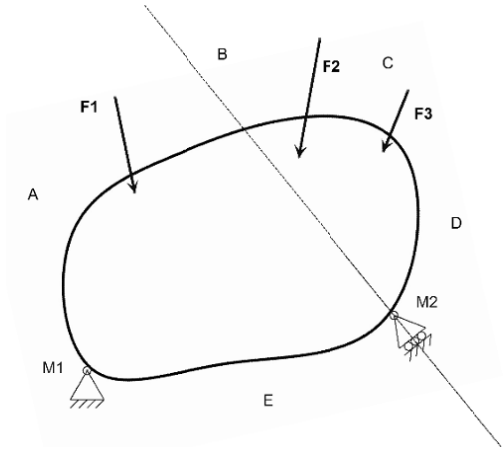


**Figure 8.24.** *Initial data for a problem of determination of support reactions*

Determining the resultant **Fr** of forces $\mathbf{F_1}$, $\mathbf{F_2}$ and $\mathbf{F_3}$ is done through a funicular polygon with an arbitrary pole o. To do this, we construct the dual points a, b, c and d by drawing the vector sum of the force polygon of $\mathbf{F_1}$, $\mathbf{F_2}$ and $\mathbf{F_3}$ (Figure 8.25). The resultant **Fr** is the vector **ad**. The funicular polygon $S_1$, $S_2$, $S_3$, $S_4$, associated with the forces in equilibrium $\mathbf{F_1}$, $\mathbf{F_2}$, $\mathbf{F_3}$ and **-Fr**, is constructed from any point $S_1$ taken on the line of action of $\mathbf{F_1}$. It closes at point $S_4$ on the sides parallel to (oa) and (od) on the line of action of **Fr**. Thus, the line of action of **Fr** is determined by point $S_4$ and its direction (ad). This line of action will allow us to determine the reactions $\mathbf{R_1}$ and $\mathbf{R_2}$. Reactions $\mathbf{R_1}$ and $\mathbf{R_2}$ must balance the force **Fr**. The three forces are therefore concurrent. The point of intersection of $\mathbf{R_2}$ and **Fr** is point $T_0$. And $\mathbf{R_1}$ passes through $T_0$. The line of action of $\mathbf{R_1}$ is to the right of line ($M_1T_0$). Point e can thus be constructed at the intersection of the parallel lines of action of $\mathbf{R_1}$ and $\mathbf{R_2}$ respectively passing through a and d. By identifying $\mathbf{R_1}$ to **ea** and $\mathbf{R_2}$ to **de**, the reactions are perfectly determined. If construction is performed correctly, we may check closure of the funicular polygon associated to forces in

equilibrium $\mathbf{F_1}$, $\mathbf{F_2}$, $\mathbf{F_3}$, $\mathbf{R_1}$ and $\mathbf{R_2}$. Thus, the end points $T_1$ and $T_2$, constructed using the first funicular polygon, need to be on a line parallel to **oe**.

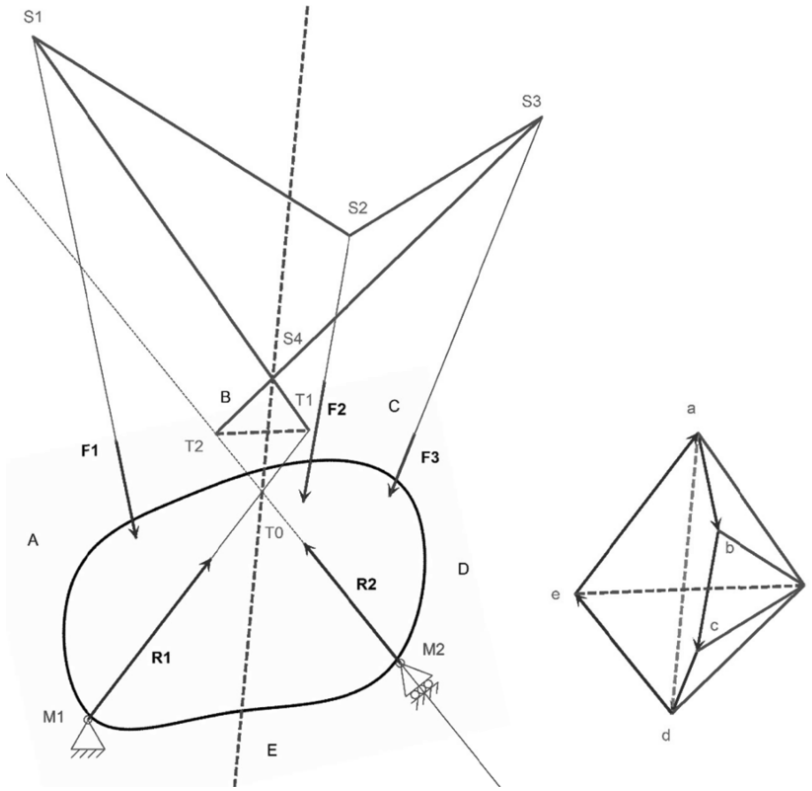


**Figure 8.25.** *Determination of support reactions*

We note that the construction gives a unique solution, since the structure is isostatic. If the solid had been linked by two joints to the external environment, 4 degrees would be blocked while just 3 are sufficient to immobilize the solid. In this case, the system would be hyperstatic and its hyperstatic degree would be 1. This would result in giving the system an infinite number of reactions that are compatible with the load. As in this case, the line of action of the reaction of the support at $M_2$ would be indeterminate, so the solutions would be those obtained for all possible directions of this line of action.

If we consider the particular case of external forces parallel to the direction of reaction $\mathbf{R_2}$, we are considering the case of Figure 8.26. By proceeding in the same manner as above, we see that points a, b, c, d are aligned and point e must be on the same line. The reaction $\mathbf{R_1}$ is therefore also parallel to other forces. The line of action of **Fr** is deducted from the funicular polygon $S_1$ $S_2$ $S_3$ $S_4$, but point $T_0$ cannot be constructed given the parallelism of lines of action. However, the direction of $\mathbf{R_1}$ and $\mathbf{R_2}$ is known. We can therefore construct the funicular polygon of $\mathbf{R_1}$, $\mathbf{R_2}$ and **Fr** and deduce its vertices $T_2$ and $T_1$ that complete the triangle with vertex $S_4$. The direction of line ($T_1T_2$) is then used to construct point e at the intersection of the line parallel to ($T_1T_2$) passing through o and the line (ab). The reactions are then determined.

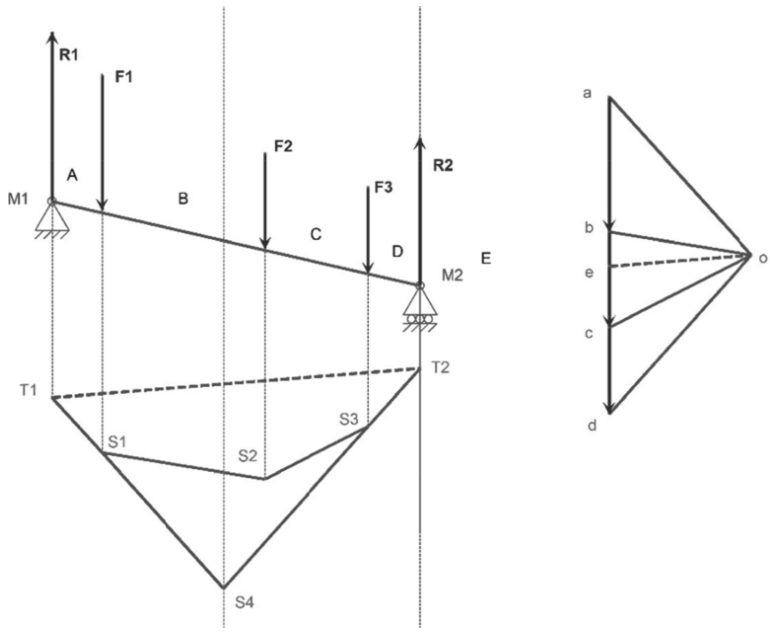


**Figure 8.26.** *Determination of support reactions in the case of forces and parallel reactions*

### 8.3.5. *Application to the calculation of reticulated structures loaded at the nodes*

The principle of calculating a structure through graphic statics is to establish equilibrium relationships of the whole structure and each of its

elements using the dual figure made from all polygons of forces. In the case of a reticulated structure that is loaded at the nodes (all or only some of them) and linked to the outside, the equilibrium reactions at the supports are defined first. To do this, a previously developed procedure (in section 8.3.4) is used by considering the reticulated structure as a solid in equilibrium under the considered load. The complete determination of forces in the rods then uses the dual figure constructed by considering the zones bounded by contiguous closed polygons defining the reticulated structure.

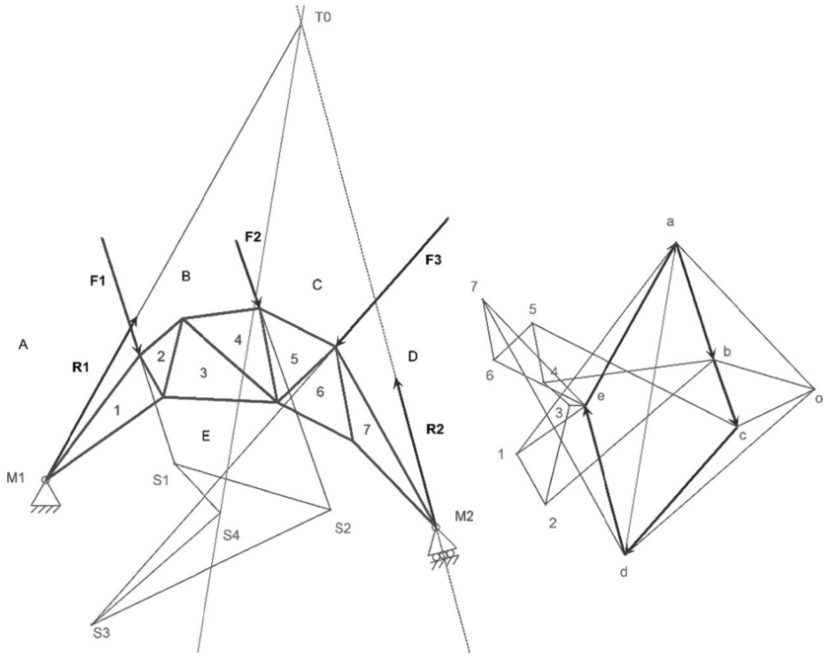


**Figure 8.27.** *Determination of forces in a triangulated structure*

To illustrate this method, we consider the reticulated structure in Figure 8.27, which has the distinction of being triangulated and consists of 7 contiguous triangles. The structure thus formed is isostatic and is linked to the outside by a simple support and joint. The system is therefore isostatic. Forces $\mathbf{F_1}$, $\mathbf{F_2}$ and $\mathbf{F_3}$ are applied to the nodes of the structure. The areas between the external forces and reactions are named from A to E. Each triangle is numbered from 1 to 7. In a first instance, we determine the reaction with the procedure developed earlier (in section 8.3.4). Thus, the dual points a, b, c, d, and e are determined. Dual points of triangles 1 to 7 are

constructed step by step from known points. Thus, dual point 1 is constructed from points a and e at the intersection of lines parallel to [1 A] and [1 E]. Dual point 2 is constructed from points b and 1 at the intersection of lines parallel to [2 B] and [2 1]. We proceed in a similar manner until point 7. Finally, we verify coherence of the figure if line (7d) is parallel to rod [7 D].

Determination of forces in rods is then done step by step from the nodes for which we at least know the direction of forces acting upon it. For example, the common node of zones A, B, 2 and 1 is subjected to force $\mathbf{F_1}$ represented by **ab** in the force polygon. By passing from one zone to another in the same rotation direction, clockwise for example, equilibrium of the node is reflected as the forces polygon in direction a, b, 2, 1. Thus, the node is subjected to, in addition to force **ab**, force **b2** through the action of rod [B 2], **21** through the action of rod [2 1], **1a** through the action of rod [1 A]. The direction of corresponding forces indicates that rods [B 2], [2 1] and [1 A] are compressed. Thus, we can deduce that the common node of B, 4, 3 and 2 is subjected to force **2 b** from rod [B 2]. The force polygon in this node must follow the order 2, b, 4, 3, that is to say, follow the same direction of rotation as above for the corresponding zones. The direction of forces in this node indicates that rods [4 3] and [3 2] are tensile and that rod [B 4] is compressed. After reviewing all rods, we can conclude that for the given load of the structure, the top rods ([A 1] [B 2] [B 4] [C 5] [D 7]) are all compressed; the bottom rods are tensile ([E 1] [E 3] [E 6] [E 7]) and intermediate rods [1 2] and [5 6] are compressed, the remaining rods remaining tensile.

The ability to uniquely determine the forces in a rod is in agreement with the fact that the structure is isostatic. If the structure was hyperstatic, there would be an infinite number of solutions, and if the structure was hypostatic, there would generally be no solution. The only possible solutions require that the shape of the structure is adapted to the loads it is subjected to, as a flexible wire does, for example. In the case of the present structure, we could remove a rod, for example rod [4 3]. For the structure to be in equilibrium under the same load, the tension in the rod should be zero. However, this tension is given by the length of vector **34** in the dual figure. This shows that the structure cannot be in equilibrium if rod [4 3] is removed. It would be possible to find a structure shape such that under the same tension, the load in rod [4 3] is zero. To do this, dual points 3 and 4 would need to be combined. This could be done by changing the position of the common node of B, 4, 3 and 2 such that dual points 3 and 4 are combined. Such an approach is not generally used in designing reticulated structures, but we can try to optimize the shape of a structure based on the main loads it will be subjected to.

## 8.4. Bibliography

[CHA 04] CHATZIS K., "La réception de la statique en France durant le dernier tiers du XIX^e siècle", *Revue d'histoire des mathématiques*, vol. 10, pp. 7–43, 2004.

[CIB 04] CIBLAC T., MACE P., UNTERSTELLER L.-P., "Recherche de l'intersection de polyèdres dans un seul dessin en perspective", *Actes des Journées AFIG et Chapitre Français d'Eurographics*, Poitiers, Futuroscope, November 2004.

[CIB 08] CIBLAC T., UNTERSTELLER L.-P., "Géométrie dynamique et modélisation géométrique: de la pédagogie à la pratique architecturale", *Actes de la conférence: La Geometria fra Didattica e Ricerca*, Florence, April 2008.

[CRE 72] CREMONA L., *Le figure reciproche nella statica grafica*, 1872.

[CRE 85] CREMONA L., *Les figures réciproques en statique graphique*, Gauthier-Villars, Paris, 1885.

[CUL 64] CULMANN K., *Die graphische Statik*, Verlag von Meyer & Zeller J.C., Zürich, 1864.

[CUL 80] CULMANN K., *Traité de statique graphique*, Translation of the German 2nd edition, Dunod, Paris, 1880.

[DES 39] DESARGUES G., Brouillon project d'une atteinte aux événements des rencontres du cône avec un plan, Par L, S, G, D, L., Paris, 1639.

[FLO 63] FLOCON A., TATON R., *La perspective*, Presses Universitaires de France, Paris, 1963.

[GUE 08] GUENA F., UNTERSTELLER L.-P., "Computing different projections of a polyhedral scene from a single 2D sketch", *Proceedings of the 26th Conference on Education in Computer Aided Architectural Design in Europe*, Anvers, September 2008.

[LAD 02] LADEGAILLERIE Y., *Géométrie affine, projective, euclidienne et anallagmatique*, Ellipses, Paris, 2002.

[MAX 64] MAXWELL J.C., "On reciprocal figures and diagrams of forces", *Philosophical Magazine and Journal of Science*, vol. 27, 4th series, pp. 250–261, 1864. Reprint: *The scientific papers of James Clerk Maxwell*, vol. 1, pp. 514–525, Cambridge, 1890.

[MAX 90] MAXWELL J.C., "On reciprocal figures, frames and diagrams of forces", *Transactions of the Royal Society of Edinburgh*, vol. 6, pp. 1–47, 1890.

[PIR 67] PIRARD A., *La statique graphique*, 3rd edition, Dunod, Paris, 1967.

[PON 22] PONCELET J.-V., *Traité des propriétés projectives des figures*, Bachelier, 1822.

[SUG 82] SUGIHARA K., "Mathematical structures of line drawings of polyhedrons-toward man machine communication by means of line drawings", *IEEE transactions on pattern analysis and machine intelligence*, vol. 1, no. 5, September 1982.

PART 3

# Yield Design Applied to Masonry

# 9

# Principles of Yield Design

## 9.1. Objective and position of the yield design problem

Yield design focuses on the ability of a structure or civil engineering works to support loads applied in a near-static manner (such that inertia can be ignored in dynamics equations). This approach only requires knowledge of geometry, loads and strength of the constituent materials. Yield design is based on the required condition for stability[1] expressed by the compatibility between near-static equilibrium equations and conditions imposed by the strength of provided materials. The reasoning used in yield design has been implemented since the 17th Century to answer the question of resistance of a structure to the conditions imposed upon it. In this regard, we mention approaches by Galileo [GAL 38], Coulomb [COU 73] and Méry [MER 40]. Theories based on elastic behavior and plasticity only emerged later. This chapter aims to introduce the principles of yield design in the formal setting of works by J. Salençon [SAL 83, SAL 90, SAL 02, SAL 13].

To consider the problem of yield design, it is assumed that three types of data relative to the structure are known:

1) the geometry of the civil engineering work or the structure;

2) the applied loading mode;

3) the strength of constituent materials.

1 The term *stability* is defined relative to compatibility with yield criterion, and not relative to the stability theory used in buckling studies for example (elastic instability).

*Sustainable Masonry: Stability and Behavior of Structures,*
First Edition. Thierry Ciblac and Jean-Claude Morel.

The geometry of the structure is given by its volume V and perimeter surface S. We assume a loading mode that is dependent on a finite number $n$ of real parameters. The load is a vector $\mathbf{Q}$ with $n$ real components $Q_i$, with i varying from 1 to $n$.

It is located in the formalism of continuum mechanics (three dimensional). However, this formalism can be transposed to two-dimensional environments (plate-like structure) and lattice structures made of beams under traction-compression (example in section 9.2) and curvilinear structures (Chapter 10).

Strength of a constituent material is defined by strength domain $G(\mathbf{x})$ of the material at any point $\mathbf{x}$ of $V$. $G$ is defined in the $\mathbf{R}^6$ space of Cauchy stress tensors $\boldsymbol{\sigma}(\mathbf{x})$:

$$\begin{cases} \boldsymbol{\sigma}(\mathbf{x}) \notin G(\mathbf{x}) \text{ is impossible} \\ \boldsymbol{\sigma}(\mathbf{x}) \in G(\mathbf{x}) \text{ is allowed} \end{cases} \quad [9.1]$$

It is assumed that the strength domain satisfies the following (experimentally verifiable) properties:

– $G(\mathbf{x})$ contains the zero stress tensor:

$$\boldsymbol{\sigma}(\mathbf{x}) = \mathbf{0} \in G(\mathbf{x}) \quad [9.2]$$

– $G(\mathbf{x})$ is convex:

$$\begin{cases} \forall (\boldsymbol{\sigma}^{(1)}(\mathbf{x}), \boldsymbol{\sigma}^{(2)}(\mathbf{x})) = \mathbf{0} \in G^2(\mathbf{x}),\ \forall \alpha \in [0, 1], \\ \alpha \boldsymbol{\sigma}^{(1)}(\mathbf{x}) + (\alpha - 1)\boldsymbol{\sigma}^{(2)}(\mathbf{x}) \in G(\mathbf{x}) \end{cases} \quad [9.3]$$

Yield design aims to determine, for a given geometry, if it is possible for a given load $\mathbf{Q}$ to predict hold or yield of the system, knowing the strength of the constituent material.

## 9.2. Potential stability and potentially bearable loads

### 9.2.1. *Notion of potential stability, domain of potentially bearable loads and extreme loads*

The approach used to understand the question of stability of the system defined above is based on the following necessary condition:

$$\text{Stability of the structure under Q} \Rightarrow \exists \boldsymbol{\sigma} \text{ such that } \begin{cases} 1)\ \boldsymbol{\sigma} \text{ is statically possible with Q,} \\ \text{(near-static equilibrium with Q)} \\ 2)\ \boldsymbol{\sigma}(\mathbf{x}) \in G(\mathbf{x}),\ \forall \mathbf{x} \in V \\ \text{(satisfies strength capacity of the material)} \end{cases} \quad [9.4]$$

Relationship [9.4] indicates a necessary condition and not an equivalence. Thus, it is not enough to just satisfy both conditions of equilibrium and strength of the material to ensure stability of the structure. Hence, we introduce the notion of *potential stability* of a structure under **Q** through equivalence [9.5]. Thus, under load **Q**, satisfying both conditions of equilibrium and strength of the material reflects a stability that is said to be potential:

$$\textbf{Potential stability} \text{ of the structure under Q} \Leftrightarrow \exists \boldsymbol{\sigma} \text{ such that } \begin{cases} 1)\ \boldsymbol{\sigma} \text{ is statically admissible with Q} \\ 2)\ \boldsymbol{\sigma}(\mathbf{x}) \in G(\mathbf{x}),\ \forall \mathbf{x} \in V \end{cases} \quad [9.5]$$

This notion allows the definition of domain $K$ of *potentially bearable loads* as being all loads **Q** for which the structure is potentially stable. Properties [9.2] and [9.3] of $G(\mathbf{x})$ allow us to deduce that $K$ contains the zero load and is convex [9.6]:

$$\begin{cases} \mathbf{Q} = \mathbf{0} \in K \\ K \text{ is convex} \end{cases} \quad [9.6]$$

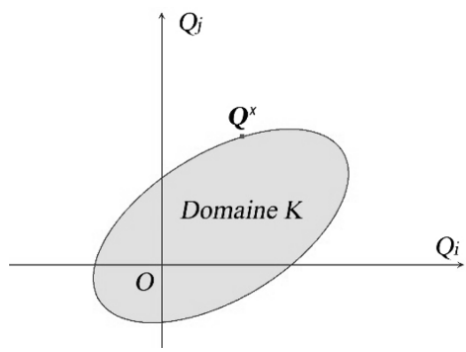


**Figure 9.1.** *Domain K of potentially bearable loads*

Loads located on the border of *K* are called *extreme loads*. Figure 9.1 represents domain *K* of potentially bearable loads and extreme loads $\mathbf{Q}^x$ located on the border of *K*. All loads located in *K* are potentially bearable while any load outside *K* causes instability.

### 9.2.2. *Potentially bearable loads in a reticulated structure*

To illustrate the necessary condition [9.4] and the notion of a "potentially bearable" load from [9.5] and the search for K, J. Salençon [SAL 83] provides the example of a reticulated structure shown in Figure 9.2. This is a square frame hinged at its vertices ABCD comprising two diagonal beams that are also hinged. The structure is subjected to two directly opposing forces of intensity Q applied in A and C. The loading mode therefore depends on a single parameter Q (i=1). The transposition formalism from continuum mechanics to lattice structure is done by considering $N_i$ forces in the rods. Strength is assumed to be identical for all beams of the system and is such that perpendicular forces $N_i$ must remain between +L (traction) and –L (compression). Therefore, we get:

$$|N_i| \leq L, \forall i = 1,...,6 \qquad [9.7]$$

From the equilibrium equations of nodes A, B, C and D, the following relationships are obtained:

$$\begin{cases} N_1 = N_2 = N_3 = N_4 \\ N_5 + N_1\sqrt{2} = Q \\ N_6 + N_1\sqrt{2} = 0 \end{cases} \qquad [9.8]$$

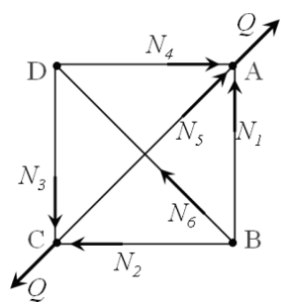


**Figure 9.2.** *Lattice made of six beams connect by 4 hinges (figure from [OIK 09])*

Relationship [9.5] expressing potential stability can be transcribed in the case of a reticulated structure according to perpendicular stresses in the beams. Equilibrium and strength conditions are respectively given by equations [9.8] and [9.7]. By considering $N_1=T$, $N_5=U$ and $N_6=V$, we then get:

$$\textbf{Potential stability} \text{ of the frame under Q} \Leftrightarrow \text{compatibility between} \begin{cases} U + \mathrm{T}\sqrt{2} = \mathrm{Q} \\ V + \mathrm{T}\sqrt{2} = 0 \\ |T| \le \mathrm{L},\ |U| \le \mathrm{L},\ |V| \le \mathrm{L} \end{cases} \quad [9.9]$$

We note that the system of equations [9.9] has an infinite number of solutions that can be expressed in terms of a single parameter, $T$ for example. The structure is hyperstatic by 1 degree. We can express relationship [9.9] according to the load parameter Q and parameter $T$, chosen as the hyperstatic parameter. Thus, we get:

$$\textbf{Potential stability} \text{ of the frame under } \textbf{Q} \Leftrightarrow \text{compatibility between} \begin{cases} |T| \le \dfrac{\mathrm{L}}{\sqrt{2}} \\ \left|Q - T\sqrt{2}\right| \le L \end{cases} \quad [9.10]$$

Figure 9.3 shows the points satisfying inequalities expressed in relationship [9.10] in the plane (Q, T). These are in the parallelogram ABCD. The set $K$ of potentially bearable loads consists of all values Q for which a point exists in the parallelogram ABCD. Thus, $K$ is the projection of parallelogram ABCD on the Q axis. Therefore, we get:

$$\mathrm{K}=[-2\mathrm{L}, +2\mathrm{L}] \quad [9.11]$$

K contains the zero load and is convex (in accordance with the properties stated in section 9.2.1). The structure is potentially stable if $\mathrm{Q} \in \mathrm{K}$. Thus, we can conclude that instability of the structure is certain for all loads $\mathrm{Q} \notin \mathrm{K}$, so if Q>2L or Q<-2L. In this case, it is impossible to ensure equilibrium of the structure under the strength conditions. It is however not possible to assert that all loads Q belonging to $K$ will not damage the structure. To affirm that the structure is safe, we need to determine the value of hyperstatic parameter

*T*, which is not possible with knowledge of geometry, load and strength of the material alone.

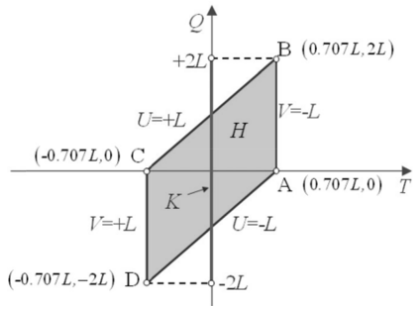


**Figure 9.3.** *"Potentially bearable" loads for the structure in Figure 9.2 (Figure from [OIK 09])*

To conclude on the stability of a structure, additional data are needed: the behavior of materials, knowledge of initial self-stress of the structure, the loading history of the structure.

## 9.3. Search for domain K of potentially bearable loads

### 9.3.1. *Static approach from the inside*

Relationship [9.5] allows the direct construction of *K* through the search for potentially bearable loads. Thus, from a practical point of view, we look for a load **Q**, a stress field $\boldsymbol{\sigma}$ that is statically admissible and that satisfies the conditions of strength. If it is found, this load belongs to *K*. This results in relationship [9.12]:

$$\exists \boldsymbol{\sigma} \text{ statically admissible with Q and } \forall \mathbf{x} \in \text{V}, \boldsymbol{\sigma}(\mathbf{x}) \in G(\mathbf{x}) \quad \Rightarrow \mathbf{Q} \in \text{K} \qquad [9.12]$$

$G(\mathbf{x})$ is usually associated with the *yield criterion* $g$, function of $\boldsymbol{\sigma}(\mathbf{x})$, defined as:

$$\boldsymbol{\sigma}(\mathbf{x}) \in G(\mathbf{x}) \quad \Leftrightarrow \quad g(\boldsymbol{\sigma}(\mathbf{x})) \leq 0 \qquad [9.13]$$

Construction of domain *K* involves determining a finite number *p* of potentially bearable loads $\mathbf{Q}_1$, $\mathbf{Q}_2$, ..., $\mathbf{Q}_p$ (points represented in Figure 9.4).

According to equation [9.12] and as $K$ is convex, the convex envelope Ks of all corresponding loads is included in $K$ (Figure 9.4). This corresponds to the construction of $K$ from the inside. The example given in section 9.2.2 was done this way. This approach from the inside, transposed to beam formalism, will be used in Chapter 10.

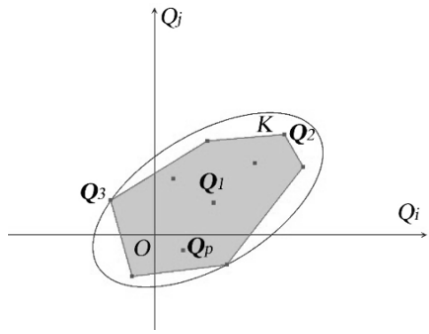


**Figure 9.4.** *Approximation through the inside of boundary K*

### 9.3.2. *Static approach from the outside*

This approach involves finding loads for which instability is ensured based on the contraposition proposal of equation [9.4]. To increase the effectiveness of this method, we define a necessary condition for stability that is lower than that in equation [9.4] and is easily manipulated. Thus, it is possible to limit verification of equilibrium to that of overall equilibrium of a subsystem. If the necessary weakened condition is not satisfied for load **Q**, then **Q** will be outside $K$. Construction of domain $K$ is approached by determining a finite number $p$ of loads $\mathbf{Q}_1$, $\mathbf{Q}_2$, ..., $\mathbf{Q}_p$ outside $K$ (points represented in Figure 9.5). We cannot use the convexity property in this set, which makes the method not very effective, even if it sometimes provides the boundary points of $K$.

This approach is rarely used in practice. However, it has some theoretical relevance. Thus, in the current formal framework of yield design, J. Salençon [SAL 02] analyzes Galileo's reasoning on the console beam supporting a load P at its end. He shows that Galileo's result, which is generally regarded as tainted with error because only the equilibrium of moments is verified, can be interpreted coherently if it is considered to be a static approach from the

outside. Load *P* calculated by Galileo is thus located outside *K* and therefore overestimates the extreme value sought.

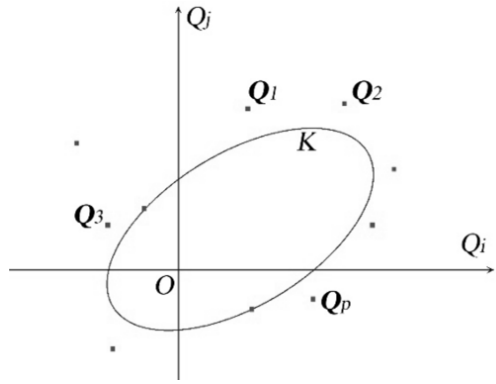


**Figure 9.5.** *Approximation through the outside of the boundary of K*

### 9.3.3. *Kinematic approach from the outside*

The kinematic approach from the outside is the most commonly used approach from the outside for building domain *K*. This approach is based on the principle of virtual work. Kinematically admissible virtual velocity **v** fields are introduced, meaning velocity fields that are continuously differentiable piecewise and that respect velocity boundary conditions. The principle of virtual work is then expressed as follows:

$$\begin{aligned} &\forall \boldsymbol{\sigma} \text{ statically admissible with Q and} \\ &\forall \mathbf{v} \text{ kinematically admissible with q,} \\ &\int_V \boldsymbol{\sigma}(\mathbf{x}) : \mathbf{d}(\mathbf{x}) \mathrm{d}V + \int_S (\boldsymbol{\sigma}(\mathbf{x}).\mathbf{n}(\mathbf{x}))[\mathbf{v}(\mathbf{x})] \mathrm{d}S = \mathbf{Q}(\boldsymbol{\sigma}).\dot{\mathbf{q}}(\mathbf{v}) \end{aligned} \qquad [9.14]$$

where:

$\boldsymbol{\sigma}(\mathbf{x})$ is the Cauchy stress tensor at point $\mathbf{x}$;

$\mathbf{d}$ is the strain rate tensor at point $\mathbf{x}$;

$\mathbf{n}(\mathbf{x})$ is the line perpendicular to S at $\mathbf{x}$;

$[\mathbf{v}(\mathbf{x})]$ is the jump of velocity at $\mathbf{x}$.

This method consists of measuring the *maximum resisting work* for a given virtual velocity field based on equation [9.14] and the yield strength domain of the material. If the work of a load **Q** in a virtual velocity field is greater than the maximum resisting work, **Q** cannot be supported by the structure. This approach provides an estimation of excesses of extreme loads. Developments of this approach are detailed in [SAL 83, SAL 02, SAL 13].

The kinematic approach from the outside has the advantage of relying on the definition of yield mechanisms expressed in velocity fields. A velocity field (vector) is generally easier to define than a stress field (tensor), which makes this method effective. This advantage is particularly significant for three-dimensional problems. A second advantage is that we can rely on assumptions of potential yield of the structure with a "physical sense" in the search for virtual velocity fields that define kinematic calculation. But beware, in no case can these (virtual) kinematics justify a real mode of yield. In fact, completely unrealistic virtual kinematics can give satisfactory results with respect to the search for domain *K*.

The kinematical approach from the outside will be used in Chapter 11.

## 9.4. Bibliography

[COU 73] COULOMB C.A., Essai sur une application des règles de maximis et minimis à quelques problèmes de statique, relatifs à l'architecture, Mémoires de Mathématique et de Physique présentés à l'Académie Royale des Science par Divers Savans et lus dans ses Assemblées, vol. 7, pp. 343–382, Paris, 1773.

[GAL 38] GALILEI G., *Discorsi e Dimonstrazioni matematiche intorno a due scienze attenanti alla mecanica ed i movimenti locali*, Leiden, Elsevier, 1638.

[MER 40] MERY E., "Sur l'équilibre des voûtes en berceau", *Annales des Ponts et Chaussées*, vol. 1, pp. 50–70, 1840.

[OIK 09] OIKONOMOPOULOU A., Approches numériques pour l'étude du comportement des structures maçonnées anciennes: un outil basé sur le calcul à la rupture et la visualisation graphique, PhD thesis, Université Paris Est et de l'Ecole nationale supérieure d'architecture de Paris la Villette, Paris, 2009.

[SAL 83] SALENÇON J., *Calcul à la rupture et analyse limite*, Presses de l'ENPC, Paris, 1983.

[SAL 90] SALENÇON J., "An introduction to the yield design theory and its applications in soil mechanics", *European Journal of Mechanics. A/Solids*, vol. 9, no. 5, pp. 477–500, 1990.

[SAL 02] SALENÇON J., *De l'élastoplasticité au calcul à la rupture,* Presses de l'Ecole Polytechnique, Palaiseau, 2002.

[SAL 13] SALENÇON J., *Yield Design*, ISTE, London and John Wiley & Sons, New York, 2013.

# 10

# Stability of Curvilinear Masonry

## 10.1. Yield design applied to planar curvilinear masonry

In this chapter, we consider a macro-mechanical approach, a scale at which the structure can be considered homogeneous and continuous. We consider structures consisting of a single homogeneous and isotropic material with specific gravity $\gamma$. Curvilinear masonry is a structure for which one dimension (1D) is much higher than the other two (piers, arches, flying buttresses, etc.). Statics in curvilinear environments are mainly known by contemporary construction professionals (architects, engineers, technicians) for the calculation of beams in assumptions of beam theory. This approach forms the basis of calculations of structures made of metal, wood or concrete. The elastic behavior of these materials under both tension and compression (concrete is reinforced to withstand traction) is used to determine the stresses and strains of beams. Hyperstatic systems can be determined under these assumptions. For a given geometry and load, a single solution is obtained through knowledge of the elasticity modulus of materials. For curvilinear masonry, we may be tempted to use this approach. Indeed, the elastic behavior of stone, for example, can be measured (see Chapter 2). However, if the tensile strength is zero, as we assume it is for masonry, the behavior cannot be elastic under tension. However, a bending beam contains tension and compression areas. Thus, under the assumption of zero resistance to

*Sustainable Masonry: Stability and Behavior of Structures,*
First Edition. Thierry Ciblac and Jean-Claude Morel.

traction, when bending appears, beam theory cannot account for the behavior of masonry[1].

Yield design (see Chapter 9) can address the question of strength of a structure by considering the strength criteria of materials, but making no assumption on the behavioral law of the material, unlike limit analysis, which considers a perfectly plastic elastic material. Assumptions for yield design allow us to consider structures for which there is little information on the mechanical properties of the materials. However, yield design does not provide the actual static state of a structure (which beam theory does), but a set of potentially safe states. The implementation of yield design involves evaluating strength criteria at all points of the structure. The curvilinear geometry of studied structures leads us to evaluate the criteria of sections that may coincide with joints. These criteria can then be expressed in a comprehensive manner for a section based on generalized stresses (normal force $N$, bending moment $M$, shear force $T$).

The purpose of this section is to implement yield design in curvilinear masonry structures. The geometric definition of the studied structures is given in section 10.1.1. We place ourselves under the assumptions made by J. Heyman [HEY 66]: 1) no tensile strength, 2) infinite compressive strength and 3) no yield through slipping. The choice of assumptions will be discussed in relation to other strength criteria (section 10.1.2) and their expressions in terms of generalized stresses on the sections (section 10.1.3). Within the context of limit analysis, the assumptions made by Heyman allow the use of plasticity theorems. In particular, the *safe theorem* forms the basis for many masonry analyses and will be presented in section 10.1.4.

### 10.1.1. *Geometric definition of planar curvilinear masonry*

Curvilinear masonry is a structure where one dimension is much greater than the other two. We are particularly interested in two-dimensional (2D) planar curvilinear structures that correspond to constant depth volumes $h$ in the third dimension in three-dimensional (3D) space. Arches, flying buttresses, jack arches and rectangular section piers fall under this category.

1 Note that if we step away from the beam theory assumptions, finite element calculation models can be used to integrate complex laws of behavior and criteria for non-resistance to traction. It is also possible to consider non-symmetrical elasticity under tension and compression (unilateral effect of damage models with constant damage).

Curvilinear masonry can be seen in buildings as well as in works of engineering. They may be connected to another structure at their ends, such as flying buttresses, or be part of a masonry assembly, such as the arch of a bridge. These structures support their own weight, the reactions of their supports are at their ends (like a flying buttress or pier), but sometimes can also include additional loads along their length (such as a loaded arch at extrados, in the case of an arch bridge or a discharging arch in a wall). We consider the case of unreinforced structures in order to consider only materials without tensile strength.

Evaluation of strength criteria is done on planar sections S of curvilinear masonry. These sections can correspond to joints of masonry blocks if their geometry is known. In general, these joints are not necessarily known and strength criteria may apply to continuously defined sections. We will focus on two types of geometric descriptions of a curvilinear masonry structure: a discrete description considering an assembly of blocks and a continuous description, defined by a guiding curve and a thickness that can be variable. Given the 2D nature of structures, sections S of constant depth $h$ will be defined by a segment in the representation plan.

10.1.1.1. *Curvilinear assembly blocks*

A curvilinear masonry structure can be seen as a set of blocks assembled through contact at the interfaces (joints) and each block is connected to the rest or to the outside through two contact surfaces (dry joint or mortar). The blocks are assumed to be non-deformable and strength criteria will only be evaluated at the interfaces (Figure 10.1).

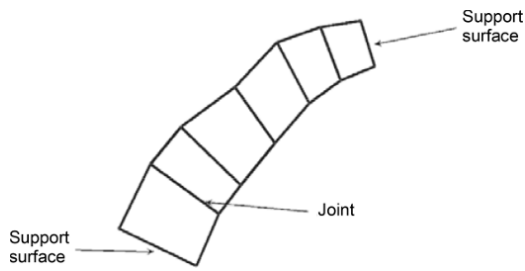


**Figure 10.1.** *Curvilinear assembly of blocks*

The orientation of joints in a curvilinear masonry structure has multiple rules for which the origin can be assumed to be constructive or geometric and

related to stereotomy[2]. Indeed, cutting stones consists of precisely determining the shape of the various blocks needing adjustment to form a predetermined assembly. We cite, for example, cutting planes that radiate according to circular curves at intrados, a method found in flying buttresses and jack arches.

From a computational point of view, this description by blocks can easily lead to graphical approaches because gravitational forces are easily deduced from the geometry of blocks and the number of forces at play is finite. Graphic statics may be considered for the study of equilibrium conditions. We will discuss this aspect in section 10.3.

10.1.1.2. *Continuous description along a guiding curve*

The continuous geometric description of a masonry structure is adapted to the case of a homogeneous material for which the strength criteria are assessed on any section defined from a guiding curve. This section may be perpendicular to the guiding curve, but this is not a necessity. This approach allows us to define the orientation of sections that may correspond to joints, but it is also useful if the position of joints is not precisely known. Continuous description can be seen as a generalization of the discrete description for which strength criteria are measured more accurately in the structure. This implies that results obtained using the continuous approach go in the direction of safety if static interior approach calculations are carried out, as we will do next. From a computational point of view, this description may be amenable to analytical approaches for simple geometries (rectangles, circle arches, for example). It can also be readily reduced to a description through blocks of simple discretization of geometry, so by regular cutting. We will use these considerations in our study of a semi-circular arch (section 10.2.3).

In this section, we identify a guiding curve with all centers of inertia $G_S$ of section S. Thickness of the masonry at the section is denoted by $t$. This thickness may be variable as in Figure 10.2. Given the 2D character of masonry, its depth $h$ is constant. Section S is therefore rectangular with an area equal to $ht$. We graphically represent the masonry in parallel projection to the plane, and the sections are represented by a segment (dotted

2 *Stereotomy*, for which the etymology has Greek origins meaning *solid* and *cut*, corresponds to the art of stone cutting, that is to say, drawings of stone cuts. The three-dimensional definition of volumes is thus based on the construction of their correlated planar projections. The formalization of this approach led to the development of *descriptive geometry* by Gaspard Monge (1746-1818) [SAK 98].

line in Figure 10.2). We note that $y$ is the algebraic distance to the center of inertia $G_S$ of section $S$, and varies between $-\frac{t}{2}$ and $\frac{t}{2}$.

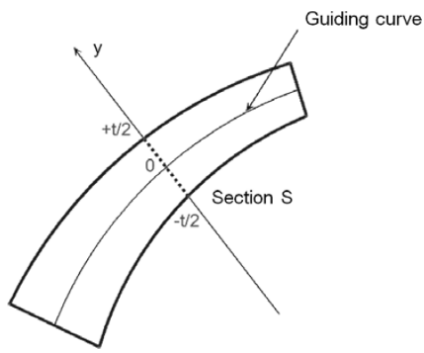


**Figure 10.2.** *Two-dimensional curvilinear structure along a guiding curve*

### 10.1.2. *Strength criteria*

Mechanical tests that were developed in the first part of this book allow us to determine the strength criteria for materials used in masonry at different scales. We consider the macroscopic scale of a structure largely exceeding that of its constituents. At this scale, "masonry" material can be likened to a homogeneous material. The strength criteria usually used for masonry on the macroscopic scale are the following:

– *tensile strength is zero*. Masonry constituent blocks may have non-negligible resistance to traction, but the presence of joints between blocks makes the resistance to overall traction extremely low for mortar joints, and zero in the case of butt joints. The assumption of zero tensile strength goes more in the direction of safety;

– *resistance to simple compression is "great" or even infinite*. Resistance to simple compression is denoted by $\sigma_0$ and can be finite, especially in the case of structures subjected to large loads such as road or railway bridges [DEL 82]. In some cases, it may be considered infinite, so far greater than the compressive stresses actually present in the masonry. This resistance assumption of infinite compression is used by Heyman [HEY 95] for most architectural masonry buildings, especially those made of stone. In some cases, it may nevertheless be useful to test this assumption *a posteriori*;

– *the shear criterion of joints is ignored*. This assumption reflects the fact that we assume that there is *no sliding* of joints. Thus, considering Coulomb's shear criterion of dry friction, it is assumed that the following relationship is always satisfied:

$$|\tau| \leq C + \sigma \tan \varphi \qquad [10.1]$$

where $C$ is cohesion, $\sigma$ and $\tau$ are the normal and tangential stresses and $\varphi$ is the angle of friction.

Assuming zero cohesion $C$ under the assumption of non-sliding, mobilized friction at the interfaces is therefore assumed to be sufficient to oppose sliding. We note that from a historical point of view, this assumption was not immediately accepted. The first scientific approaches to stability of masonry arches, including that of Philippe de la Hire (1640–1718) [HIR 95] (see [CIB 12]) which is considered to be the first, assumed that there was no friction at the joints. This amounts to considering that the interfaces behave as perfectly smooth surfaces with no shear (which is the same as taking $C = 0$ and $\varphi = 0$). It was not until the work of Charles Augustus Coulomb (1736–1806) [COU 73] that full measure of the importance of friction was taken, and it was quantified. Thus, ignoring the shear criterion allows us to assume that friction is always sufficiently mobilized to prevent yield through sliding. This assumption is generally valid for configurations that are usually encountered in curvilinear masonry. However, it remains that in some special cases, sliding can occur.

In this chapter, we mainly consider Heyman's assumptions, namely 1) no tensile strength, 2) infinite compressive strength and 3) no yield through sliding. The associated strength criterion for masonry encountered in architecture only involves perpendicular stress $\sigma$. With the sign convention associating a positive sign with compression[3], the strength criterion of masonry is written under these assumptions at any point:

$$\sigma \geq 0 \qquad [10.2]$$

3 This sign convention, commonly used in soil mechanics apparently for reasons of convenience given the preponderance of compression, also seems appropriate in the context of masonry structures. We note however that this sign convention is opposite to that usually adopted in continuum mechanics and in particular by Jean Salençon.

### 10.1.3. *Strength criteria expressed in terms of generalized stresses*

A condition necessary for the stability of a given load is that the strength criteria are satisfied at every point of the structure. If we consider a section S of the structure, the criteria should be satisfied at all points of the section. This means that there is a distribution of normal and tangential stresses $\sigma$ and $\tau$ satisfying the strength criteria. Generalized stresses allow us to express these criteria for a section S.

#### 10.1.3.1. *Generalized stresses*

Generalized stresses for section S correspond to the normal force, the shear force and the bending moment. These concepts are familiar to structural engineers as they include the classical definitions of moments and forces in beam theory. However, here we do not place ourselves under the beam theory assumptions since we take the strength criteria into account and we do not introduce elastic behavior law.

Generalized stresses are defined as:

– normal force $N$:

$$N = \iint_S \sigma dS \qquad [10.3]$$

– shear force $T$:

$$T = \iint_S \tau dS \qquad [10.4]$$

– bending moment $M$:

$$M = \iint_S \sigma y dS \qquad [10.5]$$

where $y$ is the algebraic distance to the center of inertia $G_S$ of section $S$. $\tau$ is the component of tangential shear stress. We use the notations defined in section 10.1.1.2.

#### 10.1.3.2. *Relationship between generalized stresses with Heyman's assumptions*

Considering that the strength criterion is $\sigma \geq 0$, we see that only $N$ and $M$ will be affected by this condition.

Let us express the force and moment $N$ and $M$. We can write equation [10.3] in the following way:

$$N = h\int_{-t/2}^{+t/2} \sigma dy \qquad [10.6]$$

As $\sigma \geq 0$, we get $|\sigma| = \sigma$, where from:

$$N = h\int_{-t/2}^{+t/2} |\sigma| dy \qquad [10.7]$$

Let us express equation [10.5] in the following form:

$$M = h\int_{-t/2}^{+t/2} \sigma y dy \qquad [10.8]$$

Taking the absolute values of the terms, we get:

$$|M| = h\left|\int_{-t/2}^{+t/2} \sigma y dy\right| \qquad [10.9]$$

We deduce the following inequality:

$$|M| \leq h\int_{-t/2}^{+t/2} |\sigma y| dy \qquad [10.10]$$

But $|y| \leq \frac{t}{2}$, where from:

$$|M| \leq h\frac{t}{2}\int_{-t/2}^{+t/2} |\sigma| dy \qquad [10.11]$$

Hence, according to equation [10.7], we deduce the following relationship between $M$ and $N$:

$$|M| \leq \frac{t}{2}N \qquad [10.12]$$

Geometric interpretation: generalized stresses make up a torsor formed from the force $F$ of components $N$ and $T$ applied at the center of inertia $G_S$ of the section and moment M. It is therefore possible to search for the application point $J$ of a force equivalent to this torsor in the plane of the section. Distance $G_SJ$ = e, called eccentricity, is the lever arm of the moment of $N$ relative to $J$. The shear force $T$ has its line of action through $J$, the moment of $T$ with respect to $J$ is therefore zero. So, moving F from $G_S$ to $J$ introduces a moment of absolute value equal to Ne. To balance the moment $M$, we must have the relationship:

$$|M| = Ne \qquad [10.13]$$

Equation [10.13] then allows us to write inequality [10.12] in the form:

$$e \leq \frac{t}{2} \qquad [10.14]$$

This last relationship [10.14] allows us to establish the following geometric property.

GEOMETRIC PROPERTY 10.1.– The strength criterion defined by inequality [10.2], which characterizes non-resistance under traction and infinite resistance under compression, geometrically results in the fact that, in the plane containing section S, the point of application of the force that is equivalent to the torsor of generalized stresses is located within the section.

To illustrate this, we consider a parallelepiped block placed on a planar surface. The block is assumed to be monolithic and we are only interested in the resistance of support AB (Figures 10.3 and 10.4). The block is subjected to its own weight $P$ applied in $G$. Equilibrium of the block on this support requires that the reaction of the supporting surface has a resultant that is directly opposite to $P$. Thus, it is an isostatic problem. The action exerted by the block on surface AB is limited to force $P$. $P$ is therefore the force that is equivalent to the torsor of generalized constraints. By applying the geometric property that we just established, the strength criterion is satisfied if the line of action of $P$ intersects the segment AB. For a horizontal support, the point of intersection J of the line of action of $P$ with AB is at the center $I$ of the bearing surface (Figures 10.3(a) and 10.4(a)). $I$ therefore corresponds to $G_S$. We note that moment $M$ of the torsor is zero. For an inclined support (Figures 10.3(b) and 10.4(b)), the point of intersection $J$ of the line of action of P with AB is no longer combined with $I$. Moment $M$ of the torsor is

non-zero since the lever arm $e = IJ$ of the component is non-zero. If the block is lying flat (Figure 10.3(b)), $J$ is within section AB. The strength criterion is satisfied. In contrast, if a block is placed on an inclined support (Figure 10.4(b)), $J$ is outside section AB. The strength criterion is not satisfied, and the block is not stable. We understand that it will swing around B.

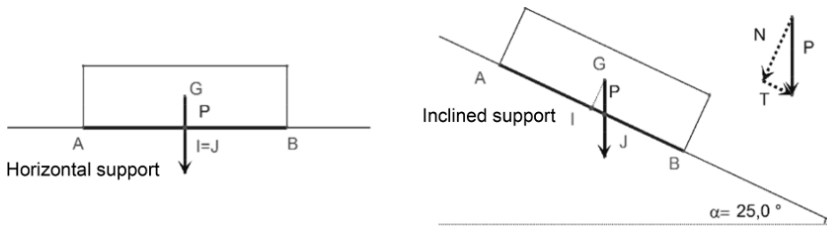


a) b)

**Figure 10.3.** *Parallelepiped block placed flat on a horizontal a) or inclined b) support*

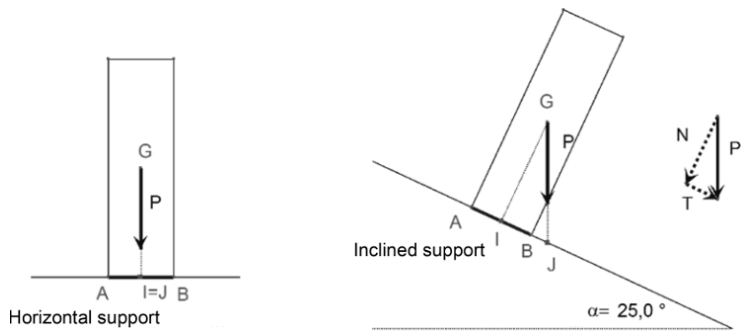


a) b)

**Figure 10.4.** *Parallelepiped block placed upright on a horizontal a) or inclined b) support*

The geometric property stated above, by its very simple geometric character, reveals the role played by the point of application J of the force that is equivalent to the torsor of stresses on the plane of section S. All these points relating to all the sections form a curve called “the line of thrust”. In section 10.2, we will present the concept of a line of thrust and consider its

relationship with the equilibrium conditions of a curvilinear structure in more detail.

Although in this chapter we limit ourselves to the consideration of Heyman's assumptions, in sections 10.1.3.3 and 10.1.3.4, we focus on the consequences of taking the Coulomb criterion (shear strength) and a finite resistance to compression $\sigma_0$ into account. The reader will thus have the elements to verify or justify their non-inclusion in the case of curvilinear masonry.

10.1.3.3. *Relationship between generalized stresses for the Coulomb criterion*

The shear strength condition according to the Coulomb criterion [10.1] with zero cohesion implies the relationship:

$$|T| \leq N \tan \varphi \qquad [10.15]$$

If we place ourselves in the context of Heyman's assumptions, we can verify, *a posteriori*, if this relationship is satisfied. We may, for example, assess this criterion for a block on an inclined plane with angle $\alpha$ (Figures 10.4 and 10.5). As the weight $P$ of the block is vertical, we get the following relationship:

$$|T| = N \tan \alpha \qquad [10.16]$$

We immediately deduce that the criterion is satisfied for $\alpha$ smaller than or equal to $\varphi$ and sliding occurs if $\alpha$ is greater than $\varphi$. This result is the same whether the block is flat or upright. We recall that in this example, the strength criterion on $\sigma$ [10.2] is not satisfied if the block is upright.

More generally, it can reflect relationship [10.15] through the following geometrical condition.

GEOMETRIC PROPERTY 10.2.– The Coulomb criterion [10.1] with zero cohesion geometrically results in the fact that the angle relative to the line perpendicular to section S of the force that is equivalent to the torsor of generalized stresses must be less than $\varphi$.

10.1.3.4. *Relationship between generalized stresses for a finite resistance to compression*

In the case of a finite resistance to compression σo, the relationship linking *M* and *N* is:

$$|M| \leq N\frac{t}{2}\left(1-\frac{N}{\sigma oS}\right) \qquad [10.17]$$

where $S = ht$ is the area of the section being considered.

If we consider the limiting case of an infinite compressive strength $\sigma_0$, we get relationship [10.12].

Rigorous demonstration of relationship [10.17] can be found in [DEL 82]. We note, however, that we can imagine distributions of the normal stresses on the section that allow us to find the upper bound of the absolute value of *M*. We may first note that if $\sigma=\sigma_0$ over the entire section, then $M=0$ and $N=\sigma_0 S$. For a given value of *N*, the value of *M* will be increasingly greater with normal stresses located on the same side as the inertia center of the section and near an edge. Let us suppose that the normal stresses are constant piecewise and such that for a value of $y_0$ between *-t/2* and *t/2*, we have:

$$\begin{cases} \sigma = 0 & \text{if} \quad y \in \left[-\frac{t}{2}; y_0\right] \\ \sigma = \sigma_0 & \text{if} \quad y \in \left[y_0; \frac{t}{2}\right] \end{cases} \qquad [10.18]$$

The graphical representation of this distribution is given in Figure 10.5.

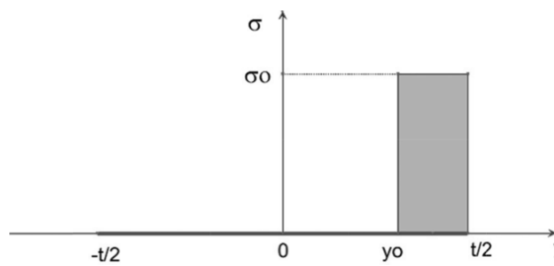


**Figure 10.5.** *Distribution of maximum normal stresses near an edge*

We can then easily calculate $N$ corresponding to the normal stress distribution [10.18] according to equation [10.7]:

$$N = \sigma_0 h\left(\frac{t}{2} - y_0\right) \qquad [10.19]$$

Similarly, we can calculate $M$ corresponding to the normal stress distribution [10.18] according to equation [10.8]:

$$M = N\left(\frac{t}{2} - \frac{1}{2}\left(\frac{t}{2} - y_0\right)\right) \qquad [10.20]$$

Using equation [10.19], equation [10.20] can be written:

$$M = N\left(\frac{t}{2} - \frac{1}{2}\frac{N}{\sigma_0 h}\right) \qquad [10.21]$$

This equation can then be written as:

$$M = N\frac{t}{2}\left(1 - \frac{N}{\sigma_0 S}\right) \qquad [10.22]$$

Equation [10.22] therefore gives a good expression of $M$ corresponding to the upper bound of inequality [10.16].

Graphical representation of inequality [10.16]. Let us consider the dimensionless parameters $n$ and $m$, defined below:

$$n = \frac{N}{\sigma o S} \qquad [10.23]$$

$$m = \frac{2M}{\sigma o S t} \qquad [10.24]$$

Inequality [10.16] can be written in terms of $n$ and $m$:

$$|m| \le n(1-n) \qquad [10.25]$$

Similarly, inequality [10.12] is written in terms of $n$ and $m$:

$$|m| \leq n \qquad [10.26]$$

Thus, we can represent inequalities [10.25] and [10.26] in the reference ($O$, $n$, $m$) relative to the criteria for, respectively, finite and infinite resistance to simple compression (Figure 10.6).

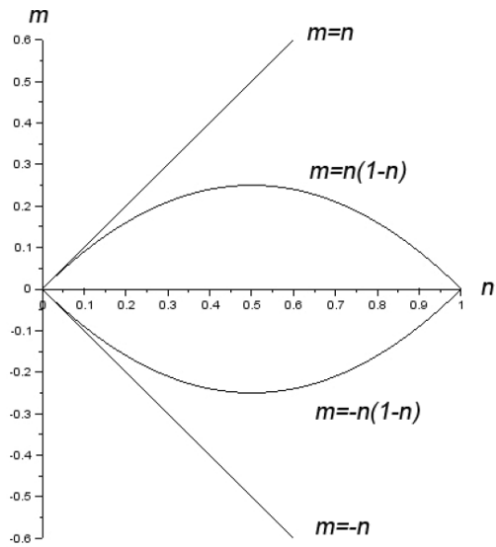


**Figure 10.6.** *Graphical representation of inequalities [10.25] and [10.26]*

Inequality [10.25] holds for all points located between the portions of parabolas of equations $m=n(1-n)$ and $m=-n(1-n)$. Inequality [10.26], in turn, holds for all points located between the lines of equations $m=n$ and $m=-n$.

To assist in the interpretation of the parabola of equation $m=n(1-n)$, we note that $n$ decreases from 1 to 0 as $y_0$ increases from $-t/2$ to $t/2$. We can then easily deduce that $m$ increases with $n$ from 0 to $n$=0 (so for $y_0=t/2$) to a maximum of $m_{max}$ at $n$=0.5 ($y_0$=0, so for maximum normal stresses on one side of $G_S$). $m$ decreases to 0 at $n$=1 (for $y_0=-t/2$, so the maximum normal stresses across the section thus balance either side of $G_S$).

The points satisfying inequality [10.25] are included in the set of points satisfying inequality [10.26]. This reflects the fact that the assumption of

infinite resistance to compression implies more cases of potential stability than finite resistance. We further note that the closer $n$ is to its maximum equal to 1, the bigger the gap is between the limiting curves of inequalities [10.25] and [10.26]. Conversely, the closer $n$ is to 0, the closer the curves are. However, values of $n$ close to 0 correspond to much lower normal stress levels than $\sigma_0$, at around $0.1\sigma_0$. The two criteria thus provide areas of potential stability that are nearly identical for normal stresses well below $\sigma_0$, which is usually the case in masonry architecture (see [HEY 95]).

We note however that the small gap between the two domains for values of $n$ close to 0 correspond to the case where normal stresses can be very high locally and exceed $\sigma_0$. In particular, when the point of application of $N$ is near an edge, the associated normal stresses are then concentrated and can be very high. A local crushing may then appear, increasing the contact surface until the yield point is reached. This point then behaves like a hinge.

### 10.1.4. *Yield design and limit analysis*

The yield design approach is based on the *necessary condition for stability* of a structure that can be expressed as follows: "If the structure is stable, then for the applied load, the structure is in equilibrium and strength criteria are satisfied". This prerequisite is not sufficient in that it is not enough that equilibrium conditions and strength criteria of materials are satisfied for the structure to be stable under a given load (in this regard, see the example of a hyperstatic system composed of hinged rods by Salençon [SAL 83]). This limitation has the effect of introducing the concept of *potential stability* of a structure under a given load. We say that a structure is *potentially stable* if it simultaneously satisfies the equilibrium conditions and strength criteria of materials. Thus, an equivalent way to express the necessary condition for stability (contrapositive proposal) is: "If a structure is not potentially stable, then it is not stable". The search in domain K for potentially bearable loads can rely on a static interior approach or a kinematic exterior approach (see Chapter 9). The concept of a line of thrust (characterizing a permissible field of stresses) associated with geometric property 1 (characterizing the strength criterion under Heyman's assumptions 1 and 2) allows the search for domain K with the interior approach. We will use this approach hereon.

Limit analysis considers materials for which the behavior law is elastic and standard perfectly plastic and studies the load limits of structures. In the

1950s, development of the theory of plasticity resulted in applications on masonry including the case formerly studied by Coulomb, revisited by Kooharian [KOO 52]. Yield design, meanwhile, takes strength criteria into account, but not behavior law. Theoretical developments and links between the two approaches can be found in [SAL 83]. The assumptions used in the context of this chapter, with a computational approach to yield design, are those issued by J. Heyman in his work on masonry [HEY 66], namely 1) no tensile strength, 2) infinite compressive strength and 3) no yield through sliding. However, his approach is based on a limit analysis that considers the masonry as a material for which the behavior law is perfectly plastic. Assumptions made by Heyman allow us to use plasticity theorems. The fundamental theorem on which the analysis of masonry is mainly based on supports the lower bound theorem or static theorem or *safe theorem*[4]. His statement can be formulated based on the concept of a line of thrust (concept introduced in section 10.1.3.2, which we develop in section 10.2).

SAFE THEOREM.– For a given load, if it is possible to find a line of thrust inside the masonry, so its stability is ensured.

This theorem neither asserts that the line of thrust found inside the masonry is actually present in the structure, nor does it give yield load to the masonry, but it gives vital information on its stability. The two other plasticity theorems (the uniqueness theorem and the theorem of the upper bound or kinematic theorem) allow us to determine the load limit. The search for a load limit is not yet a priority for studying existing masonry, according to Heyman [HEY 95], since ensuring stability for the actual load is the primary information on its behavior. Limit loads can however be used to calculate safety factors, but Heyman proposes a geometric safety factor instead.

The limit analysis of a masonry structure made of blocks combines voussoir kinematics to joints. The assumption of no yield through sliding allows the possibility of rotating blocks about the edges. Infinite compressive strength allows the existence of an ad hoc joint. In fact, compressive strength is not infinite and local crushing can occur at the joint (see section 10.1.3.4).

4 This approach has been discussed and used for masonry by J. Heyman and gave rise to many publications of which we only cite [HEY 66, HEY 95, HEY 99]. A more complete bibliography can be found in French in [ACA 01] and [SMA 01] and in Spanish in [HUE 04], as well as a summary of the theoretical aspects of this approach.

Thus, when a force that is equivalent to the torsor of generalized stresses passes through the edge of a joint, a hinge is formed (Figure 10.6). In other words, there is formation of joints at the contact points of the line of thrust with the edges of masonry joints.

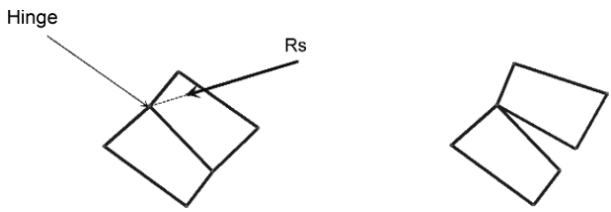


**Figure 10.7.** *Formation of a hinge between two voussoirs a) and its kinematics b)*

The central role of a line of thrust in yield design is seen in Heyman's assumptions[5], and in limit analysis under the same assumptions through the static theorem. In both cases, the position of the line of thrust within the masonry provides information on the stability of the masonry under a given load. In the first case, stability is potential and in the second case, it is ensured. This important distinction is due to the fact that in the first case, the behavior law is not known, and in the second, it is assumed to be perfectly plastic. The line of thrust is the common "instrument" in both approaches. In what follows, we will consider a practical determination of the line of thrust through various methods.

## 10.2. Line of thrust

The line of thrust is a curve only constructed from the equilibrium conditions of a curvilinear structure. Its construction is therefore independent of the strength criterion of the material. Geometric translation of the strength criterion enables use of the line of thrust in yield design or limit analysis. Initially, we introduce the concept of a line of thrust with respect to its

5 Within the context of studies on masonry bridges, [DEL 82] developed yield design calculations from the outside with a finite compressive strength criterion and Coulomb's friction criterion. Expression of these generalized stresses criteria were given in section 10.1.3. Lines of thrust are also used in this approach.

relevance to the strength criterion of a material that is not resistant to traction and with infinite resistance to compression. We then discuss the construction of lines of thrust of isostatic or hyperstatic curvilinear systems through stacks of cantilever blocks and a semi-circular arch. Finally, we discuss the interpretation of extreme line of thrust that can be constructed within the material.

### 10.2.1. *Definition of a line of thrust*

In section 10.1.3, we have seen that strength criteria could be expressed in terms of generalized stresses that are the normal force $N$, shear force $T$ and bending moment $M$. Thus, it is not necessary to know the stress distribution on a section to assess satisfaction of the strength criterion, we just need to know the resulting torsor at the inertia center of the section. We saw in Part 2 of the book that a torsor can be reduced to a single force. It is precisely by seeking the point $J$ of the plane of section $S$ through which the line of action of the force equivalent to the torsor of generalized stresses passes that we could geometrically translate the strength criterion under Heyman's assumptions (geometric property in section 10.1.3.2). Thus, the strength criterion is not satisfied if $J$ is outside section $S$. These considerations define the concept of a line of thrust as being the set of points $J$ defined for each section $S$.

DEFINITION OF A LINE OF THRUST.– *If in each section S of curvilinear masonry, the normal force N is non-zero, then the generalized stresses (N, T and M) can be reduced to a single force for which the line of action intersects the plane of section S at point J. All points J form a curve called the "line of thrust". For a continuous set of sections, the line of thrust is a continuous curve. In the case of a finite set of sections, the line of thrust is visualized by the polygonal curve for which the vertices are the points J, but only the latter may be used to assess satisfaction of the strength criterion.*

If $N = 0$ for a section, the equivalent force of generalized stresses ($N$, $T$, $M$) is parallel to the section and therefore does not intersect it. The line of thrust can only be built if, for each section, the normal force is non-zero. In the case of zero normal force, the strength criterion (following Heyman's assumptions) is not satisfied. Physically, this shows that a single bending

moment associated with shear must imply the presence of tensile and compression stresses within the section[6].

The definition of a line of thrust as given here is intended to be as general as possible since it is aimed at curvilinear masonry such as we have defined them, that is, it can be applied to a curvilinear assembly of blocks or a continuous curvilinear structure for which a continuous set of sections is defined. We introduced this definition by relying on the notion of generalized stresses and the fact that it allows us to geometrically evaluate the criterion of tensile non-resistance and infinite compressive strength. The concept of a line of thrust is thus seen as intimately associated with masonry even if its definition does not refer to a strength criterion. From a historical perspective, we can see the beginnings of this concept in Hooke's analogy in 1675 between the behavior of a suspended chain and that of masonry (see section 7.4.1). Indeed, the shape taken by the inverse chain corresponds to a line of thrust since, given the flexibility of the chain at each point $M = 0$ and, consequently, at each point of the curve, the corresponding resultant passes through this point. The reader will find historical elements of the concept of lines of thrust in the work of E. Benvenuto [BEN 91] (in the section on arches, domes and vaults). In the 1830s, two lines were defined in relation to the study of arches from resultant forces, the first named "*line of resistance"* is none other than the "*line of thrust*" that we defined above and the second named "*line of pressure*" is the set of successive intersection points of the lines of action of resultant forces. The properties of these two lines were studied by Moseley in 1831 [MOS 31], but according to [TIM 53], the first studies of the "line of pressure" were by F.G. Gerstner [GES 31]. Figure 10.8 shows the difference between the two lines. The English term "*line of thrust"* (term used by [HEY 95] for example) refers to the thrust of an arch. In French, the term currently used is "ligne de pression" or "ligne de centres de

6 If we consider the beam theory assumptions, where we have a linear elastic behavior (which we do not in the present study on masonry), the nullity of $N$ corresponds to pure bending. There is then traction on one side of the median fiber (location of the centers of inertia of sections) and compression on the other side. Thus, under the beam theory assumptions, a steel or wooden horizontal beam placed on simple supports and subjected to a vertical load works in pure bending and mobilizes all sections of compression and tension. These materials are resistant to compression and tension up to a certain limit. Under the same assumptions, with a material that is not resistant to traction, the strength criterion will be violated at any section, which reflects the impossibility of constructing a line of thrust in this case. We note that we can build the line of thrust knowing diagrams $M$ and $N$ (if $N$ is non-zero, the absolute value of the $M/N$ ratio gives the distance of the line of thrust to the median fiber (line of centroids)).

pression" [DEL 82], in reference to the pressure (compression) exerted on the section by the resultant force. We note that Viollet-le-Duc mainly uses the term "courbe de pression", but also uses the expression "ligne de pression" in the chapter on "construction" in his dictionary [VIO 56].

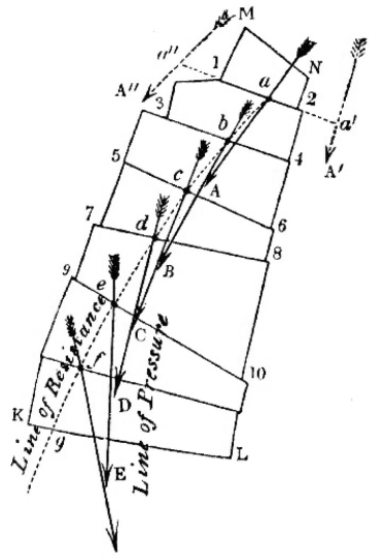


**Figure 10.8.** *Line of resistance corresponding to the line of thrust and line of pressure according to Moseley*

Determination of the torsor of generalized stresses on section *S* and deduction of the equivalent single force is done by consideration of equilibrium alone. This torsor expresses the action exerted by the part of the structure located beyond section *S*. Writing the overall equilibrium of the structure and equilibrium of the part located below (or beyond) section *S* allows us to determine the torsor. In the case of support systems, only one steady state is possible, as in the case of corbelled stacks under their own weight (see section 10.2.2). For multiple support systems, as in the case of arches under their own weight with two supports (see section 10.2.3), multiple states of equilibrium can be found because no behavior law is given and the system is hyperstatic. For each equilibrium state found, verification of strength criteria allows us to determine whether stability of the structure is possible or not.

Thus, the study of stability depending on lines of thrust is based on the following two properties:

1) construction of a line of thrust geometrically reflects the equilibrium conditions of the structure in each section S;

2) the position of the line of thrust within or outside of the material respectively reflects satisfaction or not of the strength criterion in each section (under Heyman's assumptions).

### 10.2.2. *Systems with one support: example of corbelled stacks under their own weight*

The concept of the line of thrust that we defined previously considers a set of sections of a continuous masonry structure or contiguous blocks on each section S. This definition can easily be extrapolated to a set of partially contiguous blocks provided that the contact surfaces are planar. We will then be able to search for the line of thrust in the case of a stack of parallelepiped blocks. To illustrate this, let us consider that the blocks are identical (for example, bricks) and we stack them on a level surface by shifting them by the same distance.

For the first block alone, we take the example given in section 10.1.3.2 and illustrated in Figure 10.3(a). The line of thrust is limited to a point at the centroid of the single contact surface. We consider the system formed by two blocks numbered 1 and 2 stacked by corbelling (Figure 10.9). Block 1 is supported by the ground on section $S_1$ (=$A_1B_1$) and undergoes the action of block 2 of section $S_2$ (=$A_2C_1$). The action of block 2 on block 1 at section $S_2$ is limited to weight $\mathbf{P_2}$ the weight of block 2. We can therefore easily deduce $J_2$ at the intersection of the plane of section $S_2$ and the line of action of $\mathbf{P_2}$. The action of the structure formed by the assembly of the two blocks is reduced to resultant $\mathbf{P_{12}}$ of weights $\mathbf{P_1}$ and $\mathbf{P_2}$ of the two blocks. We therefore deduce that $J_1$ is at the intersection of the plane of section $S_1$ and the line of action of $\mathbf{P_{12}}$. As $\mathbf{P_1}$ and $\mathbf{P_2}$ have the same magnitude, the line of action of $\mathbf{P_{12}}$ is equidistant from those $\mathbf{P_1}$ and $\mathbf{P_2}$. Thus, we determined the line of thrust formed by the two points $J_1$ and $J_2$. We note that in Figure 10.9, the two points are in the sections. This would not be the case for $J_2$ if the offset of block 2 were to exceed half the length L=$D_1C_1$ of the block (so if $C_1B_2$ > 0.5 L). In this case, block 2 would shift around $C_1$.

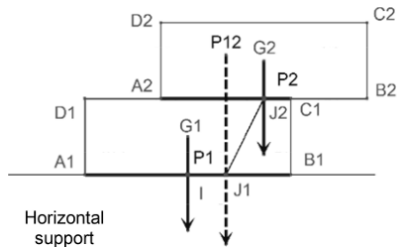


**Figure 10.9.** *Two stacked blocks*

Let us now consider a stack of three blocks. Compared to the previous case, a third block, numbered 3, is placed on block 2 with the same offset as before (Figure 10.10). A third contact surface $S_3$ is thus formed. The point $J_3$ can be easily determined first, since the action of block 3 at $S_3$ is limited to $\mathbf{P_3}$. $J_3$ is at the intersection of the plane of section $S_3$ and the line of action of $\mathbf{P_3}$. The action of blocks 2 and 3 in $S_2$ is reduced to resultant $\mathbf{P_{23}}$ of the weight of the two blocks. $J_2$ is the intersection of the plane of section $S_2$ and the line of action of $\mathbf{P_{12}}$. The action in $S_1$ of the entire structure formed of blocks 1 to 3 is reduced to resultant $\mathbf{P_{13}}$ of the weight of the three blocks. $J_1$ is at the intersection of the plane of section $S_1$ and the line of action of $\mathbf{P_{13}}$. As the offsets are constant and the blocks are identical, the line of action of $\mathbf{P_{13}}$ coincides with that of $\mathbf{P_2}$. We note that in Figure 10.10(a), point $J_2$ is outside of section $S_2$ (=$A_2C_1$), which means that the strength criterion is not satisfied, so the set of blocks 2 and 3 would therefore shift around $C_1$. In Figure 10.10(b), the offset of blocks is smaller than in Figure 10.10(a), which allows the three points of the line of thrust ($J_1$ to $J_3$) to be in the sections and therefore not contradict the strength criterion.

We proceed in the same way if we were to continue the stack. We note that by starting to determine points of the line of thrust from the last block, the procedure is iterative and easy to do. We can easily determine the resultants of weights located above the sections using graphic statics. Figure 10.11 shows, in the case of a corbelled stack of six blocks, the construction of a funicular polygon associated with six weights of blocks ($\mathbf{P_1}$ to $\mathbf{P_6}$). To determine the action of the weights *i* to *n* on the block i-1, we use the subsystem formed by weights $\mathbf{P_i}$ to $\mathbf{P_n}$ (n = 6 in Figure 10.11). The resultant of these forces is obtained by considering the funicular polygon $S_i$, $S_{i-1}$,..., $S_n$, *M*. Indeed, the line of action of the resultant passes through the point of intersection $Sr_i$ of lines ($S_i$ $S_{i-1}$) and ($S_n$, M). The points $J_i$ of the line of thrust ($J_1$ to $J_6$) in Figure 10.11 do not all belong to their section, which

means that the strength criterion is not satisfied. In contrast, in Figure 10.12, the points of the line of thrust all belong to their section, so the line of thrust is located within the outlines of the masonry at the interfaces.

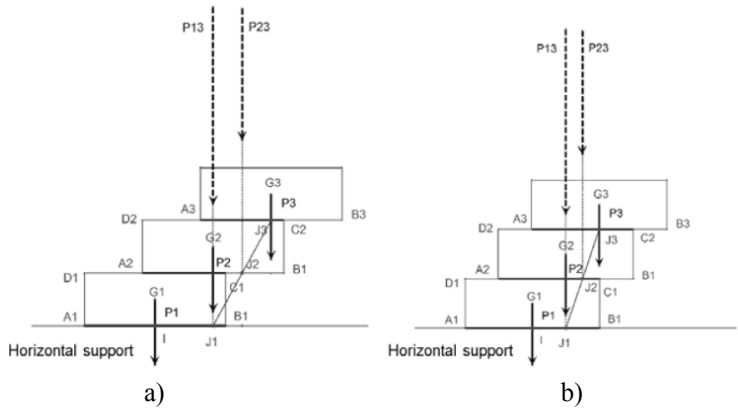


**Figure 10.10.** *Three blocks stacked by corbelling, a) unstable, b) potentially stable*

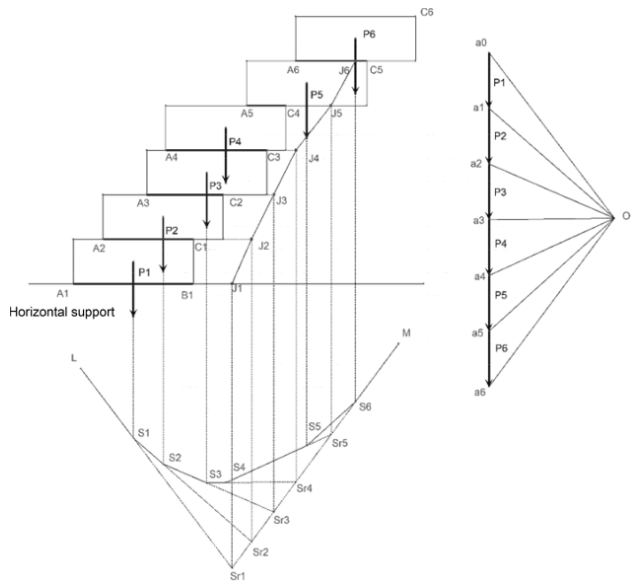


**Figure 10.11.** *Determination of the line of thrust of corbelled stacked blocks through the construction of funicular polygons*

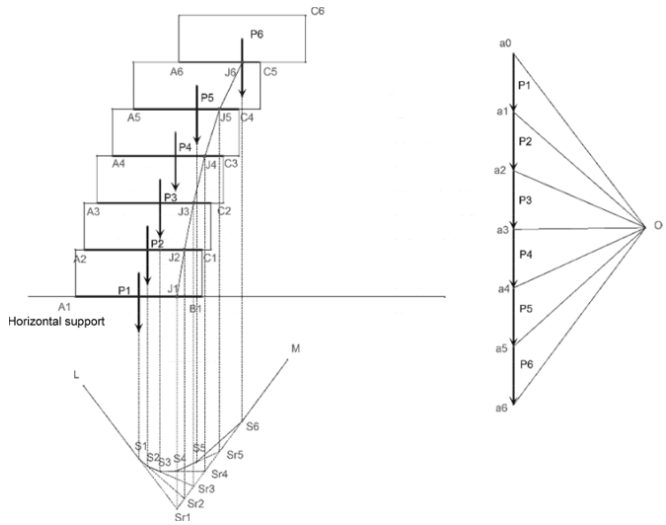


**Figure 10.12.** *Determination of the line of thrust of corbelled stacked blocks through the construction of funicular polygons. Case where the line of thrust is entirely in the joints*

Between the above two cases, there is a stack geometry for which the line of thrust is at the limit of the masonry. By searching for this geometry, we determine the extreme case of stability of the corbel under its own weight. We consider the positions of blocks i beyond the first (i>1) where point $J_i$ is the limit of the corresponding section $S_i$, so the points $C_{i-1}$. The resultants of weights of the upper blocks must then go through the extreme edge of the support block. Thus, we get in three blocks: $J_3=C_2$ and $J_2=C_1$, where the total weight of the three blocks has a resultant through $J_1$. The corresponding offsets are not constant and may be determined by barycentric calculation. Indeed, for block i in question, we just need to define the resultant of the weight of the block and the weight of all the overhanging blocks (including the line of action passing through $C_i$). Thus, for a length L of blocks, extreme offset of the last block (block n) is L/2. The following block (block n-1) will not be offset by more than L/4, the following (block n-2) by L/6, then L/8, etc. The offset of block i (i>1 because block 0 is not offset) is L/(2(n-i+1)). Figure 10.13 illustrates the case of a stack of six identical blocks corresponding to the extreme position of the line of thrust in any section. Points $J_2$ to $J_6$ are by definition from the extreme line, combined with the extreme points of sections (edge of blocks). Offsets are those deduced from previous calculations. The line of action of the total weight of the structure

passes through point $J_1$ at a distance of L/2n from the edge of the block. We note that if one load pile was formed by filling the stack with blocks to form a vertical wall on the left of the stack, the centroid of the assembly would shift to the left. Thus, horizontal blocks extending to the left vertical would result in passing the line of thrust to the inside the masonry. It would no longer be in a borderline position of stability: this is the stabilizing effect of a load pile.

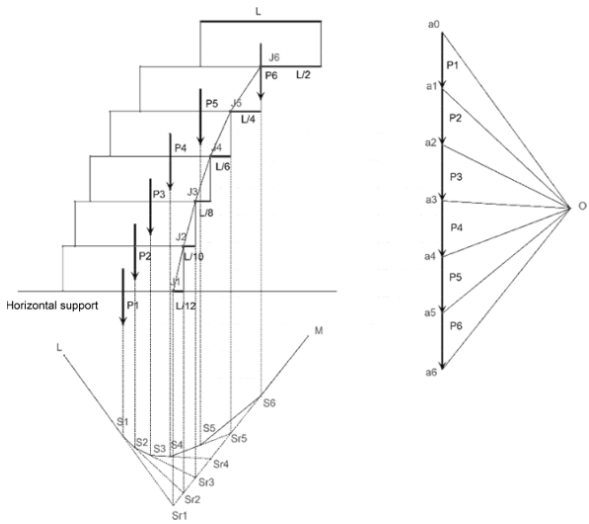


**Figure 10.13.** *Six blocks stacked by corbelling for the extreme position of the line of thrust*

A stack of blocks in corbel has the distinction of being a system based on a single external support. Since the reaction of the support must be in equilibrium with the weight of the complete structure, it is fully determined. The isostatic nature of the system implies that a single line of thrust is associated with a stack. We can generalize by saying that, for a given load, a system based on one external support only has one line of thrust.

### 10.2.3. *Systems with two supports: example of the semi-circular arch under its own weight*

Here, we will focus on a curvilinear masonry system linked to the outside by more than one support. The most representative system of a masonry

resting on two supports is the arch. The two supports upon which the arch rests each exercise a reaction. The only relationship between these two support reactions reflects the fact that they must balance the total weight of the system. This results in undetermined reactions. If we were to make an assumption on the behavior law of the material and its links with the outside, we would get a unique solution. Given the few assumptions that we make, all possible reactions may be considered. We assume, however, that the strength criterion of supports should not be violated. We therefore limit the study to reactions for which the line of action passes through the support sections. The latter assumption implies that the lines of action of reactions pass through the support sections. The semi-circular arch (so in the shape of semi-circles) of constant thickness has the advantage of being both present in many structures and also very simply defined mathematically. The sections of the arch will be radial, in accordance with the continuous description following a guiding curve (section 10.1.2.2) with the guiding curve of a semi-circle of radius $r$, where $r$ is the mean radius of the arch. The configuration discussed here is shown in Figure 10.14. It involves a semi-circular arch centered at $\Omega$, with inner radius $R_{\text{int}}$ and outer radius $R_{\text{ext}}$. The thickness of the arch is denoted by $t$. We get the following relationships:

$$t = R_{ext} - R_{\text{int}} \qquad [10.27]$$

$$r = \frac{R_{ext} + R_{\text{int}}}{2} \qquad [10.28]$$

The arch supports are located at AB and CD. The reactions of these supports are respectively denoted $\mathbf{R}_g$ and $\mathbf{R}_d$ and their points of application at the supports are noted $M_g$ and $M_d$. These points are taken on any segment [AB] and [CD] to meet the strength criteria of supports. We consider any radial section EF of the arch. The arch is thus divided into two parts: part 1 or block 1 between AB and EF, and part 2 or block 2, located between EF and CD. We therefore seek the point of application $J$ of the action of part 2 of the arch on part 1. To do this, we just need to know the weights $\mathbf{P}_1$ and $\mathbf{P}_2$ of each part of the arch, and their lines of action. The centroids $G_1$ and $G_2$ of the two blocks are on the bisectors of the corresponding arches and are located at distances $\rho_1$ and $\rho_2$ from center $\Omega$. The values of magnitudes $\mathbf{P}_1$, $\mathbf{P}_2$ and the values of $\rho_1$ and $\rho_2$ are calculated analytically. To get these, we rely on the general formulas for a circular crown with opening angle $\alpha$ for radii inside and outside of $R_{\text{int}}$ and $R_{\text{ext}}$. The magnitude of weight $\mathbf{P}_\alpha$ is deduced from the surface $S_\alpha$ of the portion of crown of angle $\alpha$. The surface $S_\alpha$ and

distance $\rho_\alpha$ from the centroid in the center of the crown are given by equations [10.29] and [10.30] where $\alpha$ is expressed in radians:

$$S_\alpha = \frac{\alpha}{2}\left(R_{ext}{}^2 - R_{\text{int}}{}^2\right) \qquad [10.29]$$

$$\rho_\alpha = \frac{4\sin(\alpha/2)}{3\alpha}\left(\frac{R_{ext}{}^3 - R_{\text{int}}{}^3}{R_{ext}{}^2 - R_{\text{int}}{}^2}\right) \qquad [10.30]$$

Thus, by denoting the angle between ($\Omega$E) and ($\Omega$C) as $\theta$, equations [10.29] and [10.30] applied for $\alpha = \theta$ can be deduced, so the values of surface $S_2$ of the crown portion 2, and $\rho_2$.

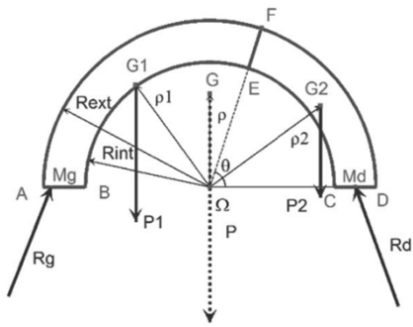


**Figure 10.14.** *Semi-circular arch cut in two by a radial section S*

As weights $\mathbf{P}_1$ and $\mathbf{P}_2$ are known, it only remains to determine the reactions at the supports and deduce the resultant of the action of part 2 on part 1.

Let us consider a graphic statics context (Figure 10.15). Reactions $\mathbf{R}_g$ and $\mathbf{R}_d$ must balance the total weight **P** of the arch. Therefore in the particular case of this problem, given the symmetry of the semi-circular arch, we know the line of action **P**: this is the axis of symmetry of the arch. If the case in question were not symmetrical, it would have been necessary to determine the resultant with a funicular polygon. As the three forces $\mathbf{R}_g$, $\mathbf{R}_d$ and **P** must be in equilibrium, we deduce from the theorem of three forces (see section 6.2.4) that their lines of action are concurrent. Taking a point S anywhere on the line of action of **P**, we determine the lines of action ($M_g$ S) and ($M_d$, S) of reactions $\mathbf{R}_g$ and $\mathbf{R}_d$. In the force plan, the sum **P** of $\mathbf{P}_1$ and $\mathbf{P}_2$

is constructed as are the lines parallel to the lines of action of reactions through $a_0$ and $a_2$. Thus, we determine pole O and the magnitudes of reactions $\mathbf{R}_g$ and $\mathbf{R}_d$. The reactions are now fully known and the action of block 2 on block 1 can therefore be determined. Block 2 undergoes forces $\mathbf{R}_d$ and $\mathbf{P}_2$ of the resultant $\mathbf{R}_s$. The line of action of $\mathbf{R}_s$ passes through the point of intersection $S_2$ of lines of action of forces $\mathbf{R}_d$ and $\mathbf{P}_2$. The direction of $\mathbf{R}_s$ is given in force plan by $\mathbf{a_1O}$ as $\mathbf{R}_s=\mathbf{a_1O}$. The line of action of $\mathbf{R}_s$ is parallel to $(a_1O)$ and passes through $S_2$. This line is none other than line $(S_1S_2)$ of the funicular polygon $(M_g, S_1, S_2, M_d)$ of a system of forces $\mathbf{P}_1$ and $\mathbf{P}_2$ constructed using center O. The sought point J is the point of intersection of the lines $(S_1S_2)$ and (EF).

The complete line of thrust is constructed by searching for all points J for all radial sections of the arch. If graphic statics and dynamic geometry software are used, it is possible to construct a section *EF* from a "dynamic" point *E* (for example) on the arc BC. The "dynamic" nature of point E means it can be moved on the arc. Thus, the construction of a single funicular polygon giving the position *J* allows us to construct all points *J* defined by the path of point E on the arc BC. Dynamic geometry software has a command that allows us to construct the location of a point based on another point. Figure 10.15 was constructed using dynamic geometry software (*Cabri geometry*), which made construction of the line of thrust (curve through $M_g$, *J* and $M_d$) possible using the construction of a single funicular polygon. An analytical approach can also be conducted in view of the detailed knowledge of the geometry and centroids. We need to simply write the equations of equilibrium of forces and moments of a system of forces $\mathbf{P}_1$, $\mathbf{P}_2$, $\mathbf{R}_g$ and $\mathbf{R}_d$ (with $\mathbf{R}_g$ and $\mathbf{R}_d$ unknowns) based on points $M_g$ and $M_d$ to determine reactions and deduce the position of J. By developing these calculations, we note that if we place a condition on $\mathbf{R}_g$, for example the angle of the vector relative to the horizontal or if we are given the horizontal component, which is also called "thrust" if it is in the direction of compression, solving the equilibrium equations of the system gives a single solution. This imposed condition is equivalent to the arbitrary choice of point S (intersection of the lines of action of three forces in equilibrium $\mathbf{P}$, $\mathbf{R}_g$ and $\mathbf{R}_d$) made using the graphic statics approach. We note that the horizontal component of the reaction $\mathbf{R}_g$ is directly opposite to that of $\mathbf{R}_d$. This is because these two reactions balance the total weight of the arch $\mathbf{P}$, which is a vertical force by definition. The magnitude of the horizontal component is given in the force polygon by the segment $[Oh_O]$ (Figure 10.15), where $h_O$ is the intersection of the horizontal line passing through the pole O with the vertical line

containing the sum of weight vectors (meaning the line containing points $a_0$, $a_1$ and $a_2$).

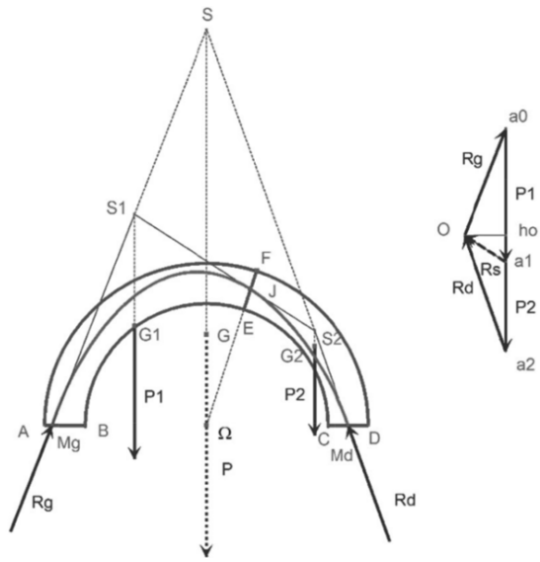


**Figure 10.15.** *Construction of a point of the line of thrust of a semi-circular arch with graphic statics and representation of the complete line of thrust*

From the construction of lines of thrust of a semi-circular arch under its own weight, we deduce that:

– for given intersection points of support reactions, several lines of thrust may be constructed based on magnitude H of their horizontal component. If this component involves a compression (as shown in Figure 10.15), H is the magnitude of the *thrust of the arch* on its supports;

– we can easily notice that if we assume that H = 0, we place ourselves under the assumption that the arch does not exercise horizontal thrust. The reactions are then vertical and point S is not defined (in Euclidean geometry). The action of block 2 on block 1 is the sum of two vertical forces. For the vertical section located on the axis of symmetry of the arch, we would thus get a resultant parallel to a section. A consequence of this is making point J at infinity. The line of thrust could be constructed and strength criterion is not satisfied. This implies that at least one non-zero thrust is needed to build a line of thrust;

– if we place ourselves in the context of yield design, we consider H to be a parameter of the load of the structure that is mobilized through supports. Thus, it is possible to search for the potential stability domain of the structure according to H and the considered strength criterion;

– if we consider that the material is not resistant to traction and has infinite compressive strength, the lines of thrust must be located within the masonry in order to not violate the strength criterion. The example of the line of thrust shown in Figure 10.15 satisfies this condition. The value of H is within the domain of potential stability. To find the domain of potential stability, it will be necessary to explore all the lines of thrust located inside the masonry. Figure 10.16 shows, for fixed positions of $M_g$ and $M_d$, various lines of thrust for varying thrusts. Figure 10.16(a) shows lines of thrust located within or through the material. Figure 10.16(b) only shows the lines of thrust located within the material. If we vary the positions of points $M_g$ and $M_d$, we can determine the lines of thrust for which thrust values are extreme. Thus, it is possible to determine the maximum thrust $H_{max}$ that corresponds to a pressure line located inside the material. A pressure line is obtained for the points of application of reactions located on the upper surface (in A and D) and tangent to the lower surface of the arch (Figure 10.17). Similarly, one can determine the position of the thrust line for which thrust is minimal and denoted $H_{min}$. The corresponding thrust line is tangent to the lower surface (intrados) at two points and tangent to the upper surface (extrados) at a point on the axis of symmetry of the arch (Figure 10.18).

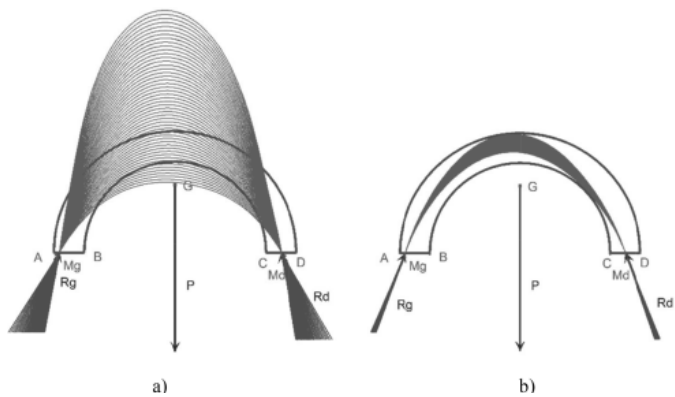


**Figure 10.16.** *Lines of thrust of a semi-circular arch under its own weight for fixed points of application of the reactions. In a) the lines of thrust cross or do not cross the masonry, in b) only the internal lines of thrust of the arch are shown*

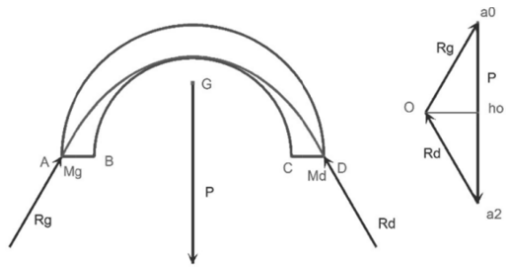


**Figure 10.17.** *Inner line of thrust arch corresponding to the maximum thrust*

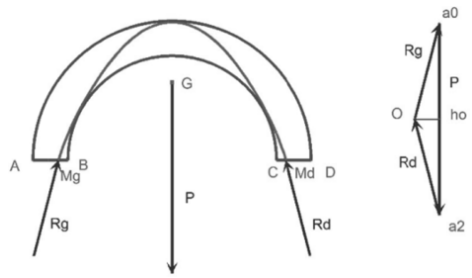


**Figure 10.18.** *Inner line of thrust arch corresponding to the minimum thrust*

In the case of the arch studied in Figures 10.15 to 10.18, the thickness of the arch corresponds to a value of $t/r = 0.29$. In this case, we note that the line of thrust corresponding to $H_{max}$ has only a lower surface point of tangency on the axis of symmetry of the arch. For a thinner arch, we can observe two lower surface tangency points that are symmetrical about the axis of symmetry of the arch, which would give four contact points of the line of thrust with masonry limits. One such example is given in Figure 10.19(a) for a smaller thickness of the arch ($t/r = 0.16$);

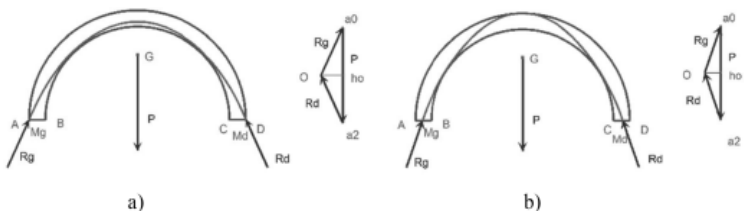


**Figure 10.19.** *Extreme lines of thrust for t/r=0.16*

– if we consider limit analysis with the same strength criterion and perfect plastic behavior, we deduce from the safe theorem [HEY 66, HEY 95] that the arch is stable under its own weight. However, this same theorem does not ensure that the line of thrust that was constructed corresponds to the actual state of forces in the structure. In particular, it does not mean that the mobilized thrust has the value of H corresponding to the line of thrust.

### 10.2.4. *Extreme lines of thrust, joints and associated mechanisms*

In the previous section, we saw that in the case of an arch, it is possible to determine extreme lines of thrust that correspond to the extreme values $H_{min}$ and $H_{max}$ of the thrust of the arch. If we consider yield design, we deduce from these values that the domain of potential stability of the arch is given for the values of H between $H_{min}$ and $H_{max}$. In other words, if we consider a load H between these limits, we know that there is a line of thrust contained within the masonry and so the strength criteria are satisfied for all sections. This is a static approach from the inside since the values sought satisfy the criteria.

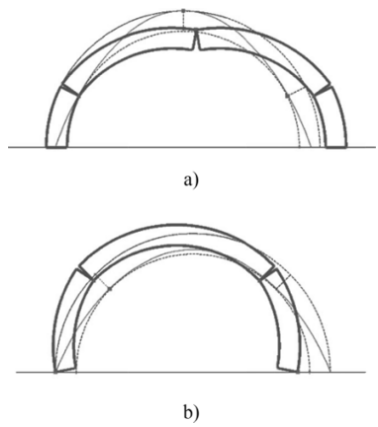


**Figure 10.20.** *Lines of thrust and kinematics associated with horizontal displacements of the right support of a semi-circular arch by a) distancing of supports associated with minimum thrust, and b) supports moving closer associated with maximum thrust*

In section 10.1.4, we saw that the contact points of a line of thrust with the edges of the masonry determine the positions of joints. These joints can be interpreted in terms of the kinematics of yield mechanisms that can be

associated with them. For a semi-circular arch, Heyman emphasizes that when the arch is removed after construction, the arch begins to exert thrust on its supports. Small displacements of the supports result and the arch undergoes a kinematic allowing it to adapt geometrically. Limit analysis can take these small quasi-static displacements (no inertia effect) into account. Assuming a slight horizontal spacing of supports, we find that the three joints determined by the line of thrust correspond to the minimum thrust $H_{min}$ (Figures 10.18 and 10.19(b)) and allow us to determine the admissible kinematic with the imposed displacement. Figure 10.20(a) shows the kinematics which correspond to a distancing of supports by horizontal displacement of the right support. This figure is done for a large support displacement in order to make the rotations about the three joints and the opening of cracks opposite to the joints visible. The actual displacement of the support is supposed to be much lower so as not to affect the overall geometry, but it is undetermined. Thus, a spacing of the (undetermined) supports involves a mechanism corresponding to the line of minimum thrust and will evaluate the corresponding thrust $H_{min}$. We can describe this state of the arch as *passive* (referring to the passive state of a flying buttress exerting minimum thrust as described by Heyman [HEY 95]) in that it accompanies a support displacement. This concept of *active* and *passive* states is particularly present in soil mechanics in the design of retaining structures. In yield design, these statements have an impact on the direction of the inequality of bounds[7]. These two types of load are distinguished in the context of kinematics, depending on the sign of the associated virtual power [SAL 13].

Let us now suppose the supports move slightly closer. The four joints (Figure 10.19(a)) given by the line of thrust corresponding to the maximum thrust $H_{max}$ allow us to determine an acceptable kinematic with the imposed displacement. Figure 10.20(b) shows the kinematics corresponding to an approximation of the supports through a horizontal displacement of the right

7 Usually, the *active* state of earth corresponds to the case where the retaining structure is displaced by moving away from earth. The resulting force is called *active thrust* and it corresponds to a lower bound in yield design. The *passive* state of earth is where the retaining wall is displaced by moving closer to earth. The resultant force is called *passive thrust* and it corresponds to the upper bound in yield design. J. Heyman emphasizes that the optimal structural behavior of a flying buttress is associated with maximum thrust, which is the abutment of the flying buttress, for which its supports move closer. This is called the *active* state, while this state would be *passive* depending on soil mechanics. Thus, the *active* and *passive* states relative to the thrust of earth are inverted with respect to the states defined by J. Heyman relative to the flying buttress. This inversion, of a purely conventional nature, seems related to the interpretation of the role of this structural element.

support. This figure is made for a large support displacement for the same reasons as before. The actual displacement of the support is supposed to be much lower so as not to affect the overall geometry, but it is undetermined. Thus, an approximation of supports (even unknown ones) involves a mechanism corresponding to the line of maximum thrust and will allow us to evaluate the corresponding thrust $H_{max}$. We can describe this state of the arch as *active* (referring to the active state of a flying buttress exerting maximum thrust as described by Heyman [HEY 95]) in that it resists a displacement imposed by the support.

We note that with the kinematic exterior approach for yield design, potential yield mechanisms associated with fields of virtual velocity are used. Their kinematics also consider the movement of rigid blocks around the edges of masonry joints. Despite their virtual nature, mechanisms may correspond to experimentally observed yield mechanisms.

### 10.2.5. *Minimum thickness and geometric factor of safety*

The existence of extreme values $H_{min}$ and $H_{max}$ of thrust for a semi-circular arch loaded under its own weight, of relative thickness *t/r*, implies that it involves a minimum relative thickness $t/r_{min}$ of the arch for which $H_{min}$ and $H_{max}$ are equal. In the case of a semi-circular arch, the value obtained by static approach from the inside (section 10.2.3) is 0.1075. A kinematic approach from the outside developed by [OCH 02] gives the same value. A comparative study of different static and kinematic approaches is given by [OIK 09] and shows the sensitivity of the results depending on assumptions and numerical methods. An arch of minimum relative thickness $t/r_{min}$ is shown in Figure 10.21(a). For an arch of radius *r*, the minimum thickness $t_{min}$ is denoted as *d*. The corresponding line of thrust shows 5 contact points with the limit of the masonry (2 on the lower surface and 3 on the upper surface of the supports and vertices), forming just as many potential joints. An arch of thickness *t* greater than *d* is shown in Figure 10.21(b), superimposed with the minimum arch and its associated line of thrust.

The existence of a minimum thickness of the arch below which stability is impossible is used by Heyman [HEY 66] to define the geometric factor of safety *Fs* of an arch of thickness *t* as a function of *d* (equation [10.31]):

$$Fs = \frac{t}{d} \qquad [10.31]$$

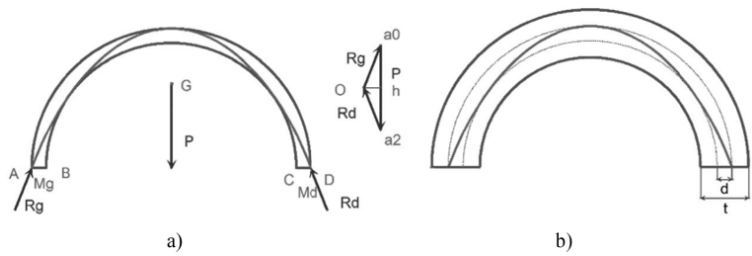


**Figure 10.21.** *Semi-circular arch of minimum thickness d a) and semi-circular arch of thickness t greater than d b)*

The *Fs* factor equals 3 for an arch of thickness $t = 3d$ and the line of thrust of the minimum arch is therefore located in the central third of thickness *t* of arch. This particular case refers to the rule known as the "middle third rule" by Méry [MER 40] requiring passage of the line of thrust of an arch of thickness *t* to be within the central third of the masonry. But it differs slightly as lines of thrust of the minimum arch and that of an arch of thickness *t* are not exactly the same. It should be noted that Méry's rule assumes affine distribution of normal stresses linked to the linear elastic behavior assumption of stone (see [DEL 82]). The Méry graphic construction is a funicular polygon inscribed in the central third of masonry with a variable thickness. It was the basis for the design of a lot of masonry in the 19th and 20th Centuries. The safety factor *Fs* associated with this design is close to 3 for a semi-circular arch and translates the safety feature of Méry's graphic construction.

### 10.2.6. *Dimensional similitude*

A very remarkable property of lines of thrust constructed for loads under their own weight is that if we change the scale of the structure, lines of thrust undergo the same scaling as the structure itself. In particular, this implies that the relative position of a line of thrust to the boundaries of the masonry will be retained. If we consider Heyman's three assumptions, the strength criterion results in a geometric property (geometric property 1) that is preserved by scaling. We deduce that in this case, if a change of scale of the masonry structure is carried out, the properties concerning stability are similar. In particular, the relative position of boundary lines of thrust will be the same. The position of joints can be deduced by simple scaling. If we consider limit analysis and the safe theorem, finding a line of thrust within

the initial masonry implies certainty of the stability of the structure, and thus this certainty remains through scaling (if Heyman's assumptions are satisfied). This allows us to study structures loaded under their own weight only according to their proportions. For example, a semi-circular arch of thickness given by ratio *t/r* can be studied independently of a specific value of *t* or *r*. This is actually what was done implicitly in sections 10.2.3 and 10.2.4. These properties explain the central position occupied by the geometry in the study of the stability of curvilinear masonry under Heyman's assumptions. This property can easily be tested by observing actual cases. This may also shed light on the use of purely geometric models by masonry builders through the ages.

Changing the scale of a structure by keeping the same material is generally accompanied by a change in behavior. We can then question this "anomaly" in the case of masonry. The purpose of the remainder of this section is to consider the interpretation, the theoretical justification and the limits of this property. To do this, we briefly introduce the concepts of dimensional similitude for which the purpose is to study the conditions for modeling on a smaller (or larger) scale for a physical study.

The influence of scaling a structure on its mechanical behavior was highlighted in 1638 by Galileo [GAL 38]. Galileo's fundamental observation was to show that physical quantities do not all evolve the same way by changing the scale and this has consequences on the resistance of structures. It is readily apparent that if all lengths of an object are doubled through scaling (scale length = 2), all surfaces are multiplied by $2^2 = 4$ and volumes will be multiplied by $2^3 = 8$. We generalize by saying that the surface of an object changes with the square of the length scale, and its volume relative to the cube of the length scale. If the same material is used for the two objects, mass also varies relative to the cube of the length scale. If both models remain under gravity, weight follows the same cubic law. If we are interested in, for example, the stress, assumed to be uniform, exerted by a parallelepiped block of stone placed horizontally on one side, the latter will vary as the ratio of its own weight to the contact surface, or as the ratio of the cube on the square of the length scale factor. Compressive stress will vary as the length scale. If we consider a finite limiting compressive strength $\sigma_0$ for stone, not reached by the initial object, it will be achieved by a sufficiently large scale factor. In this case, we find that a change in scale with the same material affects the stability of the structure. The two objects are not equivalent in terms of stability.

Generalization of these properties related to scale changes is based on the study of dimensions of physical quantities subjected to *dimensional analysis*. The dimensions of a physical quantity are characterized by their unit in a coherent system, the international system of units (SI), for example. A length dimension denoted as L is expressed in m (in SI units). Surface area is expressed in m² and has a squared dimension of length denoted as L². A time dimension is denoted as T and a mass dimension is denoted as M. The relationship between physical quantities of a problem depends on their dimensions. Thus, any surface has dimension L² and any volume has dimension L³. A density expressed in kg/m³ (in SI units) has the dimension $ML^{-3}$. A ratio of two of the same dimensions is dimensionless (a proportion, length ratio for example). Homogeneity of a physical equation based on units characterizes the coherence of physical dimensions of the quantities involved. Dimensional analysis examines exactly what only dimensional relationships can bring to the study of a physical problem. *Dimensional similitude* laws rely on dimensional analysis to define the necessary scaling factors for establishing reduced (or enlarged) models of a prototype. The theoretical foundations of dimensional similitude and their applications to the use of reduced models for the study of physical problems are developed in [SAI 71, SED 77, MAN 62].

We denote by the star symbol * (as in [MAN 62]) the scale factor corresponding to a physical quantity. Thus, the scale factor on a quantity $G$ will be denoted as G*. The scale factor of length $l$ is denoted as $l^*$ and corresponds to what is usually called the model scale. Comparing an object, called *prototype*, to its reduced or enlarged model of the same material across the scale $l^*$ (=1/10 for example for a reduced model), the scale factor for the surfaces $s^*$ is equal to $l^{*2}$, and the scale factor for volumes $v^*$ will be equal to $l^{*3}$. Maintaining gravity for both models, gravitational acceleration g will be conserved and therefore $g^* = 1$ (this is no longer the case if we artificially increase gravity using a centrifuge). If density $\rho$ is conserved, we get $\rho^* = 1$. For a mechanical problem not involving consideration of thermodynamics, the dimensions of considered quantities can be expressed as the products of the powers of $L$, $M$ and $T$. Knowledge of $l^*$, $g^*$ and $\rho^*$ can be used to determine the scale factors and $m^*$ and $t^*$ as a function of $l^*$. Homogeneity of equations or units of quantities can be used to deduce scale factors of other quantities. Table 10.1 gives the scale factors corresponding to similitude conditions under gravity and with conserved density. The dimensional similitude between a prototype and a reduced model is complete if all the physical quantities of the same dimension describing the physical problem have the same scale factor. For example, pressure, stress, a ratio of force to a

surface, Young's modulus (elasticity modulus) have the same scale factor $l^*$ since they are expressed in the same unit and are therefore the same size (see Table 10.1). In this case, the behavior of the model is representative of the behavior of the prototype and vice versa. We note, for example, that if we look at the elastic behavior of a structure, Young's modulus of the reduced model will be in proportion to $l^*$. We will therefore have to change materials. It is not always possible to get a reduced model satisfying all the conditions imposed by the conditions of similitude, this is called limited similitude.

| Symbol | Quantities (G) | Dimension | G* |
|---|---|---|---|
| l | Length | L | $l^*$ |
| ε | Strain | Dimensionless | 1 |
| g | Gravitational acceleration | $LT^{-2}$ | 1 |
| t | Dynamic time | T | $l^{*1/2}$ |
| ρ | Density | $ML^{-3}$ | 1 |
| σ | Stress | $ML^{-1}T^{-2}$ | $l^*$ |
| E | Young's modulus | $ML^{-1}T^{-2}$ | $l^*$ |
| ν | Poisson's coefficient | Dimensionless | 1 |
| F | Force | $MLT^{-2}$ | $l^{*3}$ |
| s | Surface | $L^2$ | $l^{*2}$ |
| v | Volume | $L^3$ | $l^{*3}$ |
| m | Mass | M | $l^{*3}$ |

**Table 10.1.** *Similitude conditions under gravity and conserved density*

Let us suppose that we want a reduced model of a masonry arch and we are only interested in stability. The theoretical model assumes yield design and involves the parameters of geometry, density, gravitational acceleration and strength criteria. For models meeting the conditions of similitude, all parameters of the problem must have scale factors equal to those in Table 10.1. The stresses have a scale factor equal to $l^*$. They are present in the strength criterion [10.2]. This criterion remains unchanged by scaling since under traction, $0 \times l^* = 0$. The infinite compressive strength criterion also remains unchanged by scaling since infinity remains infinity after multiplication by $l^*$. However, if we consider a finite resistance $\sigma_0$, we require a material of resistance equal to $\sigma_0.l^*$ to satisfy the similitude conditions. The non-sliding assumption is also conserved when considering criterion [10.2] with C=0. Heyman's strength criteria are conserved by scaling. However, we should still ensure that the assumption of infinite compressive strength is always in accordance with the considered scale.

## 10.3. Construction of lines of thrust in graphic statics

The aim of this section is to show how graphic statics can be used to construct lines of thrust of curvilinear masonry defined by blocks. We used graphic static reasoning in the stacking examples in section 10.2.2, but it was a special case because, given the uniqueness of the support, only a single line of thrust could be constructed. The example of the arch that we studied in section 10.2.3 helped to construct the line of thrust in graphic statics, but used the case of equilibrium of two blocks limited by a variable section. Drawing the line of thrust in the case of masonry defined by blocks will mobilize the properties of funicular polygons. This method, also usable on paper, is greatly facilitated through the use of dynamic geometry.

### 10.3.1. *Construction of lines of thrust using funicular polygons*

10.3.1.1. *Method and stages of construction for masonry defined by blocks*

The initial data for the construction of a line of thrust are the geometry of blocks, their interfaces and their considered support surfaces. The assumption of a homogeneous material of constant density implies that the weight of blocks is proportional to the area of each element depicting the block in the representation plan. Similarly, the centroid of each block corresponds to the centroid of the surface representing the block. Here, we consider an irregular arch structure formed of quadrilateral section blocks in the representation plan (Figure 10.22).

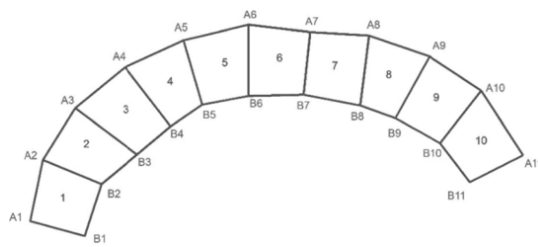


**Figure 10.22.** *Arch formed of blocks*

The steps in the construction of a line of thrust are:

1) determining the area and centroid of each quadrilateral in order to construct the weight vectors of each block;

2) determining the resultant of all the weights of blocks by construction of an arbitrary funicular polygon;

3) constructing a funicular polygon passing through two points, $M_g$ and $M_d$, belonging to the supports of the arch;

4) determining the line of thrust using the funicular polygon constructed in the previous step.

These steps are discussed in sections 10.3.1.2 to 10.3.1.4.

10.3.1.2. *Determination of the centroid of a quadrilateral*

10.3.1.2.1. Wittenbauer's Method

A direct method for determining the centroid of a homogeneous quadrilateral flat plane was demonstrated by F. Wittenbauer (1857–1922). We divide each side into three equal parts. Let us draw lines adjacent to vertices passing through the points of division. These lines form a parallelogram for which the centroid G is also that of the quadrilateral ABCD (Figure 10.23).

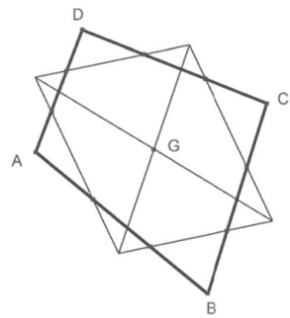


**Figure 10.23.** *Determination of the centroid of a quadrilateral by Wittenbauer's method*

10.3.1.2.2. Graphic statics method

This method, which is longer than the previous, is based on the property of the centroid being the crossing point of the weight regardless of its position relative to gravitational acceleration. In a first instance, we divide the quadrilateral into two triangles, and their centroid and weight are determined. The equivalent force is then determined (by a funicular polygon). We apply this method again by changing the direction of the gravitational field. The

intersection of the lines of action of two equivalent forces is the centroid (Figure 10.24).

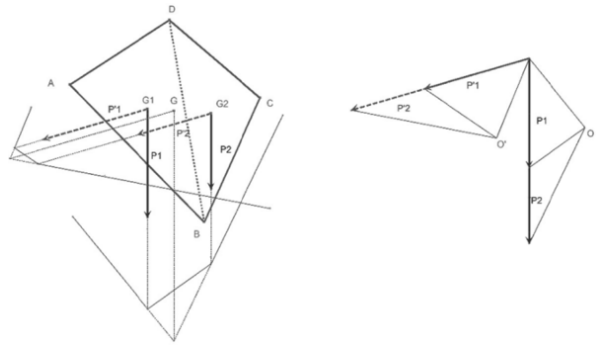


**Figure 10.24.** *Determination of the centroid of a quadrilateral by graphic statics*

10.3.1.2.3. Third method

A third method allows direct construction without the use of parallelism or a trisection method as in Wittenbauer's method. We begin by constructing the middle of each side of the quadrilateral. This involves considering the quadrilateral as two triangles joined together for which we know how to construct the centroids by intersection of medians. The centroid of the quadrilateral can only be on the line passing through the two centroids of triangles (Figure 10.25(a)). The operation is repeated by cutting the quadrilateral into two triangles along the other diagonal, and there is a second line that contains the centroid of the quadrilateral (Figure 10.25(b)). The latter can only be located at the intersection of these two lines (Figure 10.25(c)).

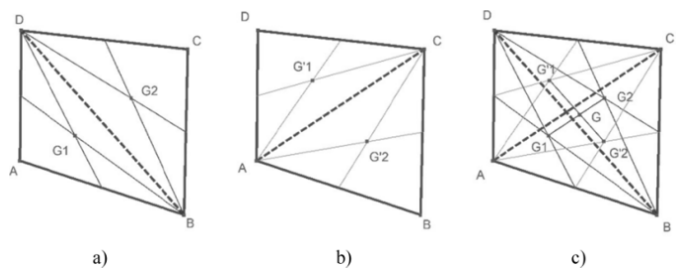


**Figure 10.25.** *Steps in the construction of the third method for determining the centroid of a quadrilateral*

10.3.1.3. *Search for the resultant of the weight of the complete structure*

In the general case of a non-symmetrical arch relative to the vertical, it is necessary to determine the resultant of all weights of blocks in order to construct the line of action of the total weight of the masonry and the corresponding vector. Construction of an arbitrary funicular polygon (A $S_1$ $S_2$... $S_n$ B) gives the resultant immediately (see Chapter 7 and Figure 10.26). We took the forces in the successive order of blocks for clarity of the figure. The second funicular polygon that we construct in section 10.3.1.4 to determine the line of thrust will follow the same order, but for a physical reason this time.

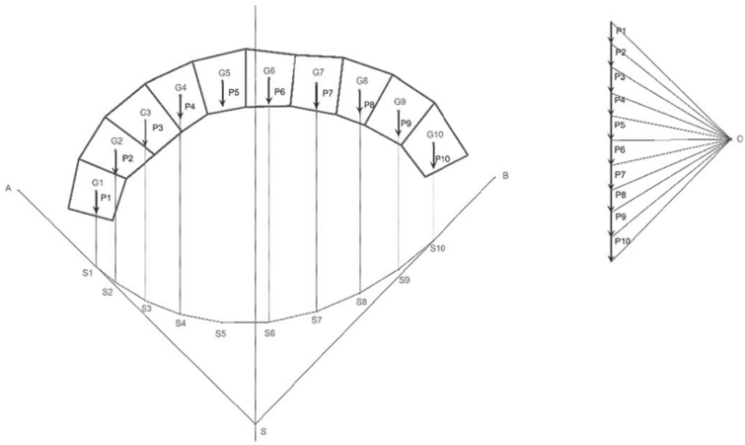


**Figure 10.26.** *Construction of the resultant giving the total weight of the masonry through the construction of a funicular polygon*

10.3.1.4. *Construction of a line of thrust*

The construction of a funicular polygon through two points, $M_g$ and $M_d$, belonging to support sections of the arch is the first step to construct a line of thrust passing through the masonry supports. Reactions $\mathbf{R_g}$ and $\mathbf{R_d}$ at the supports respectively pass through $M_g$ and $M_d$ and must balance the total weight **P** of the masonry determined in section 10.3.1.3. The three forces $\mathbf{R_g}$, $\mathbf{R_d}$ and **P** must intersect at a single point (three forces theorem) on the line of action of **P**, which is known. By taking an arbitrary point S′ on the line of action of **P**, we determine lines of action ($M_gS'$) and ($M_dS'$) of $\mathbf{R_g}$ and $\mathbf{R_d}$ respectively (Figure 10.27).

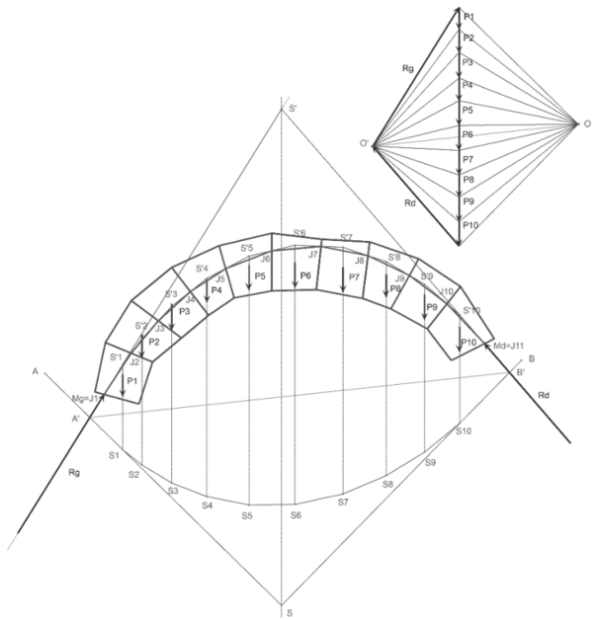


**Figure 10.27.** *Construction of a line of thrust*

We can then deduce pole O′ of the corresponding funicular polygon in the force plan. The corresponding force polygon and ($M_g$ $S_1'$ $S_2'$...$S_n'$ $M_d$) can thus be constructed. The relationships between funicular polygons constructed from two distinct poles explained in section 7.3.3 can be seen in Figure 10.27. Construction of the line of thrust associated with reactions $\mathbf{R_g}$ and $\mathbf{R_d}$ defined above, is based on the determination of the resultant of forces applied by half the structure on the other half at each joint. We must consider the forces in the order of the blocks so that the resultants are defined joint-by-joint using a unique funicular polygon. Let us consider a section given in Figure 10.27, for example the joint between blocks 4 and 5 denoted as [$A_5B_5$] (see Figure 10.22). The sub-structure formed by blocks 5 to 10 exerts a force equal to the resultant of weights $\mathbf{P_5}$ to $\mathbf{P_{10}}$ and the reaction $\mathbf{R_d}$ on the section. The resultant has the line of action of line ($S'_4S'_5$) of the funicular polygon. The intersection point of line ($A_5B_5$) passing through joint [$A_5B_5$], and the line of action ($S'_4S'_5$) of the resultant is the point $J_6$ of the desired line of thrust. By generalizing all the joints, the line of thrust is constructed by the intersection of the lines of the funicular polygon with lines of corresponding joints. Thus, for i varying from 1 to n-1, the points $J_{i+1}$ are the intersection points of lines ($S'_iS'_{i+1}$) and lines ($A_{i+1}B_{i+1}$). The line of thrust thus

constructed can be fully contained within the masonry, as shown in Figure 10.27, but by varying the position of S′ on the line of action of P, this line may leave the limits of the masonry, as in the case of a semi-circular arch (see Figure 10.6).

10.3.1.5. *Special case of symmetrical arches relative to a vertical axis*

The case of symmetrical arches relative to a vertical axis, loaded under their own weight only, has the distinction of having the line of action of their total weight combined with their axis of symmetry. This simplifies the search process since the weight of the resultant of the whole structure no longer requires construction of an initial funicular polygon (described in section 10.3.1.3).

10.3.1.6. *Additional loads*

The method presented above considers the load of an arch under its own weight. If we want to construct the lines of thrust for the case where the arch undergoes an additional load, the method is the same, except that the load on each block is considered, for example, a force $\mathbf{F_i}$ applied to the block i. The resultant force $\mathbf{R_i}$ of weight $\mathbf{P_i}$ of the block and its overload $\mathbf{F_i}$ will have the same role as force $\mathbf{P_i}$ without overload. The total resultant of loads applied to the arch will of course be changed. Figure 10.28 shows structures relating to the determination of the line of thrust in the case of an additional load $\mathbf{F_8}$ applied to block 8.

10.3.1.7. *Additional structure: three supports*

Additional charges that were discussed in section 10.3.1.7 may have various origins. This may be vertical loads due to a filler material above the arch, for which there would be no additional support. But it can also be the action of another curvilinear element supported on a block of the arch and on another external support. Thus, in the example shown in Figure 10.28, the force $\mathbf{F_8}$ could be the action of an arch supported by block 8. Thus, we constructed a second arch comprising of six blocks, supported by the first on block 8 (Figure 10.29) and on an external support at its other end. In the same way as for a single arch, it is possible to construct a line of thrust based on the application points $M'_g$ and $M'_d$ of reactions $\mathbf{R'_g}$ and $\mathbf{R'_d}$. The lines of thrust also depend on the direction of the reaction $\mathbf{R'_g}$. Funicular polygons and corresponding force polygons are represented separately from those of the first arch so as not to overload the figure. So that the equilibrium conditions are met, we must identify $\mathbf{F_8}$ to $\mathbf{R'_g}$. This is reflected in the force plan by the fact that the points $a_8$ and $b_0$ are combined and that the origin of

vector $\mathbf{P_9}$ coincides with $O'_1$. It is therefore possible to construct lines of thrust for structures on three supports by taking care to ensure the equilibrium of the connecting block (block 8 of the first arch).

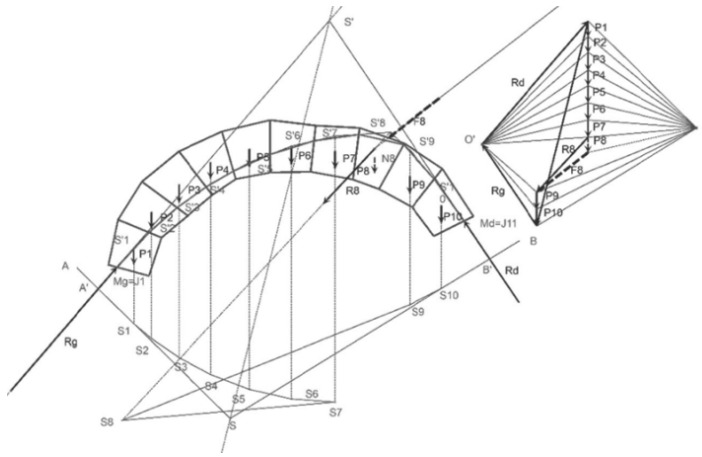


**Figure 10.28.** *Construction of a line of thrust with an additional load on a block*

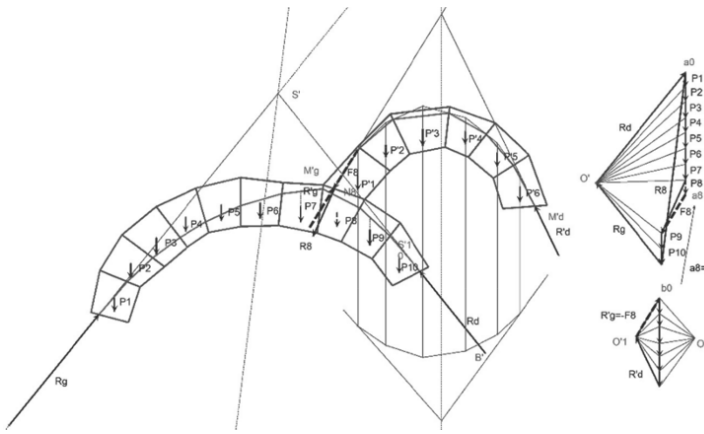


**Figure 10.29.** *Construction of a line of thrust in the case of an additional arch bearing on a block of an existing arch and an external support*

We note that the addition of an arch and an additional support doubles the number of parameters varying the position of lines of thrust in the entire

structure. Thus, we added the three parameters of the second arch (positions of $M'_g$ and $M'_d$ and the angle of $\mathbf{R'_g}$) to the three parameters of the first arch with positions $M_g$ and $M_d$ and the angle of $\mathbf{R_g}$. Manipulation of these parameters in dynamic geometry makes it easy to determine a line of thrust within the masonry in the present case. This allows us to apply the static theorem of limit analysis and conclude on the stability of the assembly. For thinner layers, it may be more difficult to find a line of thrust inside the masonry. If the geometry of the structure is not imposed, but if an architect wants to define a stable and optimized shape with respect to the thickness of the masonry, the dynamism of the figure is used to affine the structure depending on the line of thrust. An example is given in Figure 10.30 as masonry deduced from visualization of the line of thrust after some trial and error manipulation of the geometry and the parameters.

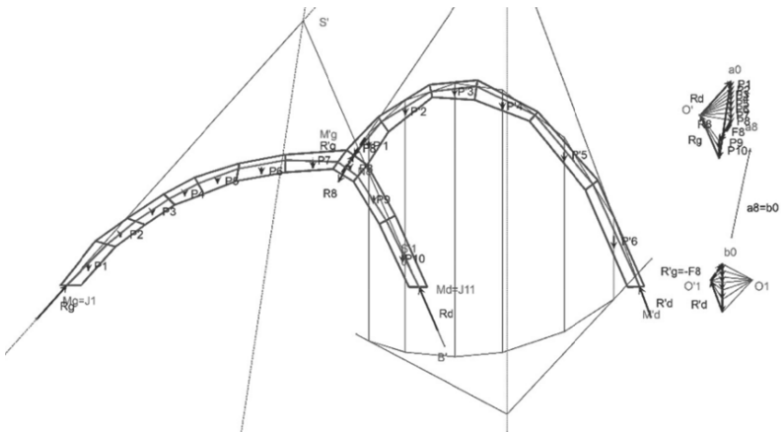


**Figure 10.30.** *Geometry of an optimized masonry from a line of thrust*

The complexity of geometric configurations of masonry involves a complexity in the search for extreme lines of thrust, especially if we manipulate a dynamic figure. Numerical methods are used to overcome these difficulties. We will discuss some methods in section 10.4.

### 10.3.2. *Parametric study of the semi-circular arch and pointed arches under their own weight*

Here, we present the case of a figure constructed with dynamic geometry software (Cabri geometry) allowing us to vary the geometry of an arch to

study the lines of thrust of a semi-circular arch in the pointed arch. This application was developed in an academic setting and is presented in [CIB 10]. The dynamic figure[8] allows us to go from a semi-circular arch to a pointed arch formed by two symmetrical circles for which the centers are on the line horizontal to the base of the arch (Figure 10.31). The semi-circular arch is defined by its center and two points at the base of the arch defining the inner and outer radii. The transition to a pointed arch is done while maintaining the width and thickness of the initial semi-circular arch by giving an RO parameter that characterized the aspect ratio of the arch, which we call its pointed ratio. We denote the inner half-width $R_{int}$, the outer half-width $R_{ext}$, and the internal height of the arch (or arrow) $H_{int}$. RO is defined by relationship [10.32]:

$$RO = \frac{H_{int}}{R_{int}} \qquad [10.32]$$

For a semi-circular arch, we get RO = 100% ($H_{int} = R_{int}$) and the values of $R_{int}$ and $R_{ext}$ correspond to those defined in section 10.2.3. For a drop arch (vertices of an equilateral triangle), RO = 173% ($H_{int} = \sqrt{3}\, R_{int}$). The geometry of an arch may be defined by the two dimensionless parameters: *t/r* and *RO*. In the dynamic geometry example presented here, the arch is composed of 18 blocks. Geometry is controlled by the position of two points at the base of the arch (the left part of the arch), which sets the inner half-width $R_{int}$ and outer half-width $R_{ext}$ of the arch. The RO pointed ratio (variable with a cursor on the dynamic figure) completely defines the geometry of the arch.

The variation parameters of the line of thrust are:

– $\theta$: the angle of the reaction $\mathbf{R_g}$ relative to the horizontal line;

– $\lambda_1$ and $\lambda_2$, position parameters of $\mathbf{R_g}$ and $\mathbf{R_d}$, equal to the distance of the point of application of reactions at the base of the arch measured from the inside, divided by the thickness *t* of the arch.

By varying these parameters in the dynamic figure (manipulating the application points of reactions and the slope of the left reaction), the user can determine the funicular polygons that are entirely contained within the arch

8 The dynamic figure is available on this link: http://www.paris-lavillette.archi.fr/MTC.

and, through trial and error, deduct the minimum (Figure 10.32(b)) and maximum thrust (Figure 10.32(a)) and the positions of the associated ball joints.

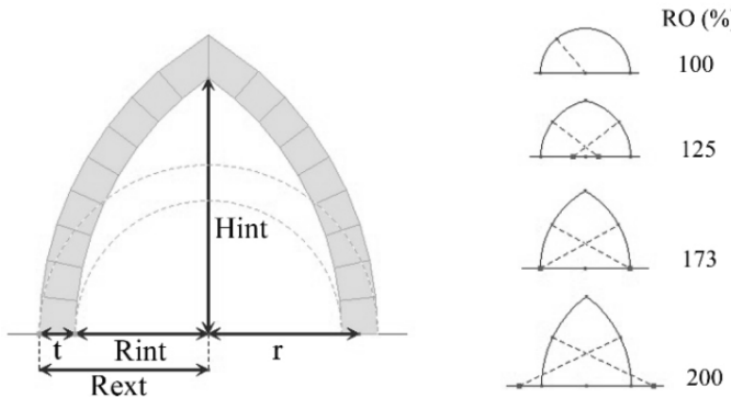


**Figure 10.31.** *Geometrical parameters of the studied arches*

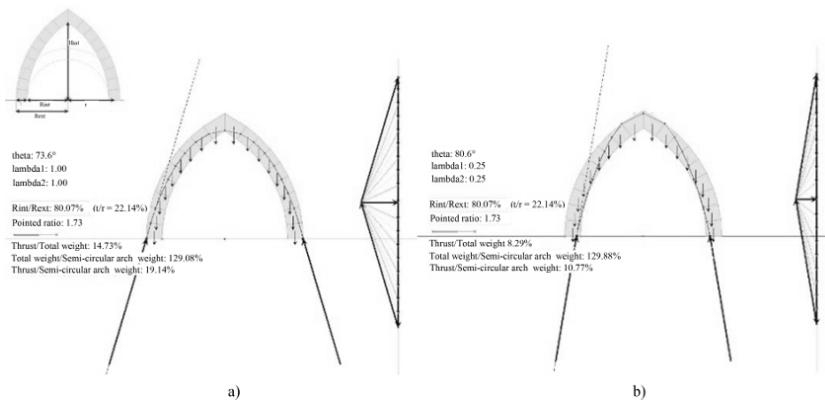


**Figure 10.32.** *Search on a single dynamic figure for funicular polygons and lines of thrust corresponding to the maximum thrust a) and minimum thrust b), in a drop arch*

This type of tool has the advantage of being perfectly adapted to geometric parameterization of a range of structures from a single construction. In addition, an interactive real-time approach allows the structure behavior to be tested, even by students.

Limitations of the tool are due to the nature of dynamic geometry software: dedicated to teaching, it is not designed to be programmed (or very little with macros). Thus, feasible configurations are predetermined and are limited to simple structures. Furthermore, iterative calculations may not be implemented, which makes it impossible to automatically determine extreme lines of thrust. The proposed tool that was used to study the structure of defined geometry can also be used for parametric studies involving various kinds of parameters (geometry, loads, safety factors). For example, we conducted a parametric study on the arches presented in dynamic geometry.

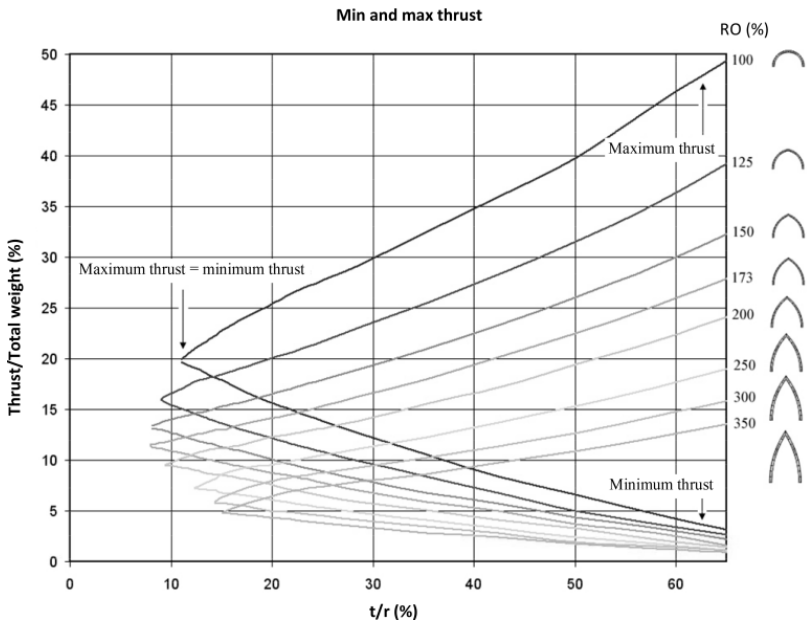


**Figure 10.33.** *Minimum and maximum thrust based on the weight of the arch depending on t/r (thickness of the arch relative to the average spacing of the arch) for arches ranging from semi-circular (RO = 100%) to a pointed arch of ratio (RO = 350%)*

This study aims to investigate the influence of the geometry of an arch on the minimum and maximum thrust, and determine its minimum thickness (where minimum thrust is equal to maximum thrust). To use the results obtained in the most general manner possible, we have presented them in the form of graphics based on dimensionless parameters (Figure 10.33). This is possible under the similitude conditions set in section 10.2.6. For a dimensional case, we only need to know some dimensional values (spacing, height, etc.) and deduct the dimensional parameters sought from dimensionless parameters. The limiting curves for minimum and maximum thrust based on the total weight of the arch are given in terms of $t/r$ for variable values of RO. For a given aspect ratio of the arch (constant RO), the area between the extreme thrust curves defines a possible equilibrium zone. The contact point of the curves gives the minimum relative thickness $t/r_{min}$ of the arch such that equilibrium is possible. We note that for RO ranging from 100% to 173%, $t/r_{min}$ decreases and goes from 10.9% to 7.9%, while for RO ranging from 173% to 350%, $t/r_{min}$ increases and goes from 7.9% to 15%. These results are consistent with the optimal character of the drop arch (RO = 173%).

This example shows how a parametric study of structure can shed light on limit values of arch thickness. We could choose to study the minimum thicknesses of other elements such as buttresses, flying buttresses, arches, etc. Such approaches also allow us to assess the safety factors of structures and could be used by construction historians to study typologies of buildings.

### 10.3.3. *Case of an earthquake: quasi-static approach*

Taking into account, the effect of an earthquake on a masonry can be done by considering horizontal acceleration in the structure plan. This acceleration, in a quasi-static approach, corresponds to the addition of a horizontal component $\mathbf{g}_h$ to gravitational acceleration $\mathbf{g}$. In this case, the same approach as above may be used, except that the direction of the resultant acceleration is no longer vertical. Figure 10.34 shows adaptation to the structure studied in section 10.3.1.

### 10.3.4. *Pseudo 3D study of arches or domes*

With a few modifications, calculation methods for curvilinear structures can be used for approaches involving revolution or cylindrical 3D geometries that we can reduce to a planar problem. Passing from a curvilinear structure to a 3D structure can be done through geometrical translation operations to

form arches or rotation to form revolution domes. Associated stability calculation models consider slices for which the planes of symmetry contain the involved forces. For a cylindrical arch, use of the 2D case assumes that the arch acts as a succession of contiguous arches without friction. In the case of a dome, a pseudo 3D model considers slices intersected by planes passing through the axis of revolution (such as orange slices). Two opposing slices (symmetrical relative to the axis) can be divided into blocks such that their weights will all be contained in the same plane. This approach is used by Poleni (see section 7.4.1). It is then possible to construct a line of thrust for the assembly formed by the two slices. This method produces a first approach to the behavior of a dome, but does not take the possible presence of compressed rings into account. The relative simplicity of these approaches do not demean the approach, since observations of radial cracks of domes are consistent with this assumption. In this regard, J. Heyman's analyses [HEY 95] are particularly recommended to the reader.

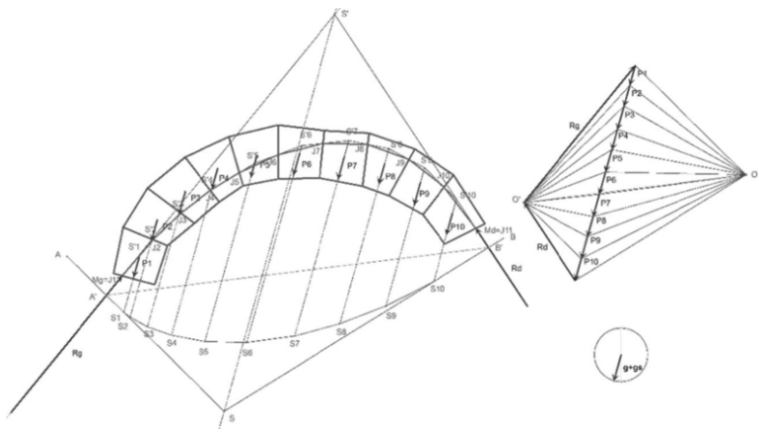


**Figure 10.34.** *Case of an earthquake: quasi-static loading*

## 10.4. Numerical methods for the construction of lines of thrust

### 10.4.1. *Force network method*

Masonry loaded with vertical forces (own weight and additional vertical loads) are widely encountered in masonry structures. The special character of the load allows the implementation of numerical procedures involving only linear systems of equations. In this context, D. O'Dwyer [ODW 99] developed the force network method, which is an approach for generalizing

the 2D concept of a line of thrust to the 3D concept of thrust surface. This approach was the basis of developments by P. Block [BLO 09] that is compatible with complex 3D geometry based on duality (concept discussed in Chapter 8). Indeed, the projection of a force network on the horizontal plane is reduced to a compressed planar structure, with unloaded nodes, that becomes a tensed planar structure (discussed in section 8.3.3) if the direction of reactions is reversed. These developments do not fall within the scope of this chapter, but the method of force networks can easily be applied to a 2D case.

Applied to the 2D case, the force network method amounts to algebraically determining a funicular polygon. Let us consider a force network consisting of $n$ forces $\mathbf{P_i}$ (i varying from 1 to $n$). In the coordinate system ($O$, $x$, $z$), we place $\mathbf{P_i} = (0,-P_i)$; the lines of action of these forces are vertical and respectively have abscissa values $x_i$ (i varying from 1 to $n$). We search for the coordinates of points $S'_i$ of the funicular polygon such as the one built in section 10.3.1.4 (see Figure 10.35). The points $S'_i$ have coordinates ($x_i$, $z_i$) in the system ($O$, $x$, $z$) where $z_i$ are unknown and where $x_i$ are defined by the lines of action of forces $\mathbf{P_i}$. We place $S'_0=M_g$ and $S'_{n+1}=M_d$. Thus, the values ($x_0$, $z_0$) and ($x_{n+1}$, $z_{n+1}$) are defined. Reactions $\mathbf{R_g}$ and $\mathbf{R_d}$ have their horizontal components respectively equal to H and -H (by directing $x$ toward the line), with H being the thrust of the arch. The forces $\mathbf{F_i}$ are defined as those of polar rays $\mathbf{O'a_i}$ for all i ranging from 0 to $n$. We can then write the equilibrium equations of each force $\mathbf{P}_i$ with the forces $\mathbf{F_{i-1}=O'a_{i-1}}$ (on the left) and $\mathbf{-F_i=a_iO'}$ (on the right). We then get:

$$\mathbf{P}_i+\mathbf{F_{i-1}}-\mathbf{F_i} = \mathbf{0} \text{ for i ranging from 1 to } n \qquad [10.33]$$

The coordinates of forces $\mathbf{F_i} = \mathbf{O'a_i}$ are ($F_{x,i}$, $F_{z,i}$). The $F_{x,i}$ coordinates are equal to H = O′h. Thus, we get:

$$F_{x,i} = H \text{ for i ranging from 0 to } n \qquad [10.34]$$

Furthermore, considering equation [10.34] and the coordinates of points $S'_i$, we get the following relationship expressing the equality of coefficients governing lines ($S'_iS'_{i+1}$) and ($O'a_i$):

$$F_{z,i} = \frac{z_{i+1} - z_i}{x_{i+1} - x_i} H \text{ , for i ranging from 0 to } n \qquad [10.35]$$

The Z-coordinates of equation [10.33] give:

$$-P_i + F_{z,i-1} - F_{z,i} = 0 \text{, for i ranging from 1 to } n \qquad [10.36]$$

Equations [10.35] and [10.36] give:

$$-P_i + \frac{z_i - z_{i-1}}{x_i - x_{i-1}} H - \frac{z_{i+1} - z_i}{x_{i+1} - x_i} H = 0 \text{, for i ranging from 1 to } n \qquad [10.37]$$

We then deduce:

$$\left( \frac{H}{x_{i+1} - x_i} + \frac{H}{x_i - x_{i-1}} \right) z_i - \left( \frac{H}{x_i - x_{i-1}} \right) z_{i-1} - \left( \frac{H}{x_{i+1} - x_i} \right) z_{i+1} = P_i \qquad [10.38]$$

for i ranging from 1 to $n$.

These equations form a system of $n$ equations with $n$ unknowns $z_i$ (i varying from 1 to n); z0 and zn+1 are defined by Mg and Md. This system can be written in matrix form and solved by matrix inversion.

Once the funicular polygon is obtained, and the line of thrust is not constructed, [ODW 99] forces the funicular polygon to stay inside the masonry, which is in the interest of safety. However, it is perfectly possible to deduce the line of thrust from the funicular polygon by simple intersections of lines, so systems of two equations with two unknowns.

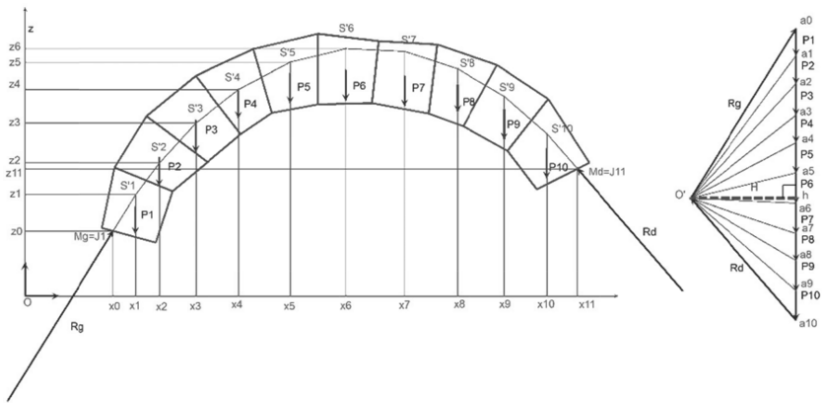


**Figure 10.35.** *Funicular polygon and notations of the force network method*

### 10.4.2. *Complex systems*

The use of the force network method in the plane allows the development of numerical calculations similar to those developed for graphic statics, but for configurations that can be complex and making the establishment of graphics or implementation in other systems possible. A. Oikonomopoulou [OIK 09] used this approach to develop a method and a tool for the study of complex systems to study the behavior of ancient masonry. Here, we present an example of a structure derived from [OIK 09]. Figure 10.36 shows a section inspired by a Romanesque church defined by geometrical parameters. Given the symmetry of the structure, only the right half is shown. Symmetrical points relative to Oz of points M on the right side are denoted M′. The structure is composed of an arch ABB′A′ supported by two piers ABFU and A′B′F′U′, and two flying buttresses BCJG and B′C′J′G′ supported by abutments JGQT and J′G′Q′T′. The objective is the determination of the extreme lines of thrust and associated joints. The construction of lines of thrust is done by considering the equilibrium of the connecting block ABCD which supports the arch ABB′A′ and the flying buttress BCJG. Thus, the pier is considered as an element DCFU that supports the connecting element ABCD. Given the symmetry of the geometry and the load (its own weight), extreme lines of thrust are symmetrical relative to (Oz). This defines the two horizontal forces $H_{arc}$ and $H_{ab}$. The first applies to supports PR and AB of the half-arch and the second to the flying buttress supports (BC and JG). An iterative procedure is proposed to determine combinations of extreme values of forces $H_{arc}$ and $H_{ab}$ for which the line of thrust is everywhere inside the structure. Figure 10.37 shows the lines of thrust constructed by this approach for extreme cases.

The $H_{arc}$ and $H_{ab}$ parameters can be considered as the parameters defining the equilibrium domain of the structure. This choice reconsiders that proposed by [SMA 00] and taken by [BLO 06], but with a comprehensive approach to the structure. The domain of all eligible combinations of thrusts $H_{arc}$ and $H_{ab}$ for the system can thus be defined as the convex envelope of combinations of $H_{arc}$ and $H_{ab}$ that define the potential stability of all elements of the system (Figure 10.38); this is a direct consequence of the static theorem of yield design (see Chapter 9). Extreme thrusts of the arch (abscissa) and the flying buttress (ordinate) are given as a percentage of each element's own weight.

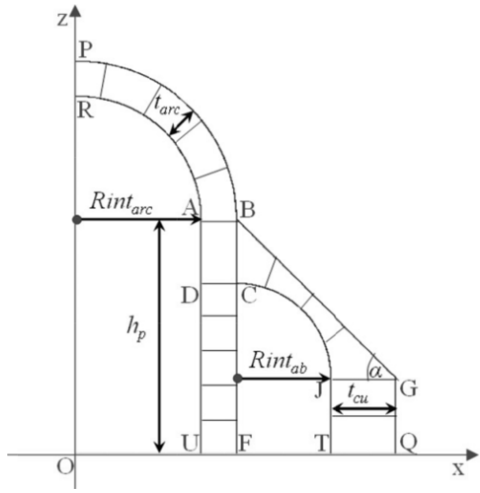


**Figure 10.36.** *Geometry of the considered system: arch – flying buttresses – pier [OIK 09]*

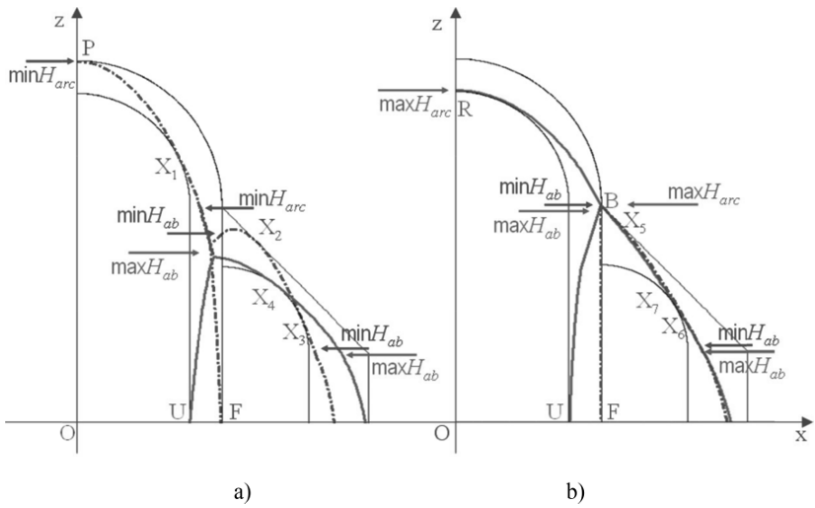


**Figure 10.37.** *Lines of thrust of the system for a) minHarc, minHab < Hab < maxHab and b) maxHarc, minHab <Hab < maxHab [OIK 09]*

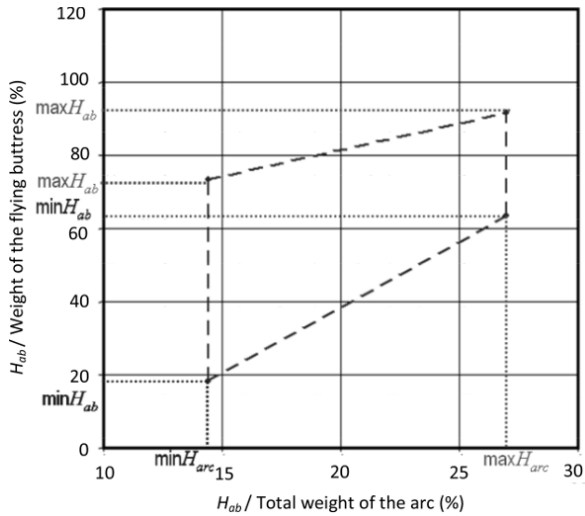


**Figure 10.38.** *Domain of equilibrium of the system [OIK 09]*

Here, we present the principle of the tool developed by [OIK 09], which also addresses more complex systems and seismic events through the quasi-static approach (discussed in section 10.3.3).

## 10.5. Bibliography

[ACA 01] ACARY V., Contribution à la modélisation mécanique et numérique des édifices, PhD thesis, Ecole supérieure de mécanique de Marseille, 2001.

[BEN 91] BENVENUTO E., *An Introduction to the History of Structural Mechanics*, Springer Verlag, New York, pp. 432–435, 1991.

[BLO 06] BLOCK P., CIBLAC T., OCHSENDORF J., "Real-time limit analysis of vaulted masonry buildings", *Computers and Structures*, vol. 84, pp.1841–1852, 2006.

[BLO 09] BLOCK P., Thrust network analysis, exploring three-dimensional equilibrium, PhD thesis, Massachusetts Institute of Technology, 2009.

[CIB 10] CIBLAC T., OIKONOMOPOULOU A., GUÉNA F., "Approches numériques pour l'étude du comportement des structures maçonnées anciennes", *Edifices et artifices, Histoires constructives*, pp. 273–282, Picard, 2010.

[CIB 12] CIBLAC T., "Analysis of Philippe de la Hire's arc theory using graphic statics", *Nuts and Bolts of Construction History*, vol. 1, pp. 367–374, Picard, 2012.

[COU 73] COULOMB C.A., Essai sur une application des règles de maximis et minimis à quelques problèmes de statique, relatifs à l'architecture, Mémoires de Mathématique et de Physique présentés à l'Académie Royale des Science par Divers Savans et lus dans ses Assemblées, vol. 7, pp. 343–382, Paris, 1773.

[DEL 82] DELBECQ J.-M., Les ponts en maçonnerie, Ministère des Transports, Direction des routes, SETRA, 1982.

[GAL 38] GALILEI. G., *Discorsi e Dimonstrazioni matematiche intorno a due scienze attenanti alla mecanica ed i movimenti locali*, Elsevier, Leiden, 1638.

[GER 31] GERSTNER F.J., *Handbuch der Mechanik*, Prague, vol. 1, p. 405, 1831.

[HUE 04] HUERTA S., *Arcos, bóvedas y cúpolas, Geometría y equilibrio en el cálculo tradicional de estructuras de fábrica,* Instituto Juan Herrera, Escuela Técnica Superior de Arquitectura de Madrid, 2004.

[HEY 66] HEYMAN J., "The stone skeleton", *International Journal of Solids and Structures*, vol. 2, pp. 249–279, 1966.

[HEY 95] HEYMAN J., *The Stone Skeleton: Structural Engineering of Masonry Arcitecture*, Cambridge University Press, Cambridge, 1995.

[HEY 99] HEYMAN J., *The Science of Structural Engineering*, Imperial College Press, London, 1999.

[HIR 95] DE LA HIRE P., *Traité de mécanique*, Paris, 1695.

[KOO 52] KOOHARIAN A., "Limit analysis of voussoir (segmental) and concrete arces", *Journal of the American Concrete Institute*, vol. 24/4, pp. 317–328, 1952

[MAN 62] MANDEL, J., "Essais sur modèles réduits en mécanique des terrains – Etude des conditions de similitude", *Revue de l'Industrie Minière*, no. 9, pp. 611–620, 1962.

[MER 40] MÉRY E., "Sur l'équilibre des voûtes en berceau", *Annales des Ponts et Chaussées*, 1840.

[MOS 33] MOSELEY H., "On a new principle in statics, called the principle of least pressure", *Philosophical Magazine*, vol. 3, pp. 285–288, 1833.

[OCH 02] OCHSENDORF J.A., Collapse of masonry structures, PhD thesis, University of Cambridge, 2002.

[ODW 99] O'DWYER D., "Funicular analysis of masonry vaults", *Computers and Structures*, vol. 73, pp. 187–197, 1999.

[OIK 09] OIKONOMOPOULOU A., Approches numériques pour l'étude du comportement des structures maçonnées anciennes: un outil basé sur le calcul à la rupture et la visualisation graphique, PhD thesis, Université Paris Est et de l'Ecole nationale supérieure d'arcitecture de Paris la Villette, Paris, 2009.

[SAI 71] SAINT-GUILHEM R., *Les principes généraux de la similitude physique*, Editions Eyrolles, Paris, 1971.

[SAK 98] SAKAROVITCH J., *Epures d'architecture. De la coupe des pierres à la géométrie descriptive, XVI^e^-XIX^e^ siècles*, Birkhäuser, 1998.

[SAL 83] SALENÇON J., *Calcul à la rupture et analyse limite*, Presses de l'ENPC, Paris, 1983.

[SED 77] SEDOV L., *Similitude et dimensions en mécanique*, Mir, Moscow, 1977.

[SMA 00] SMARS P., Etudes sur la stabilité des arcs et voûtes, PhD thesis, Centre Raymond Lemaire pour la Conservation, Leuven, 2000.

[TIM 53] TIMOSHENKO S.P., *History of the Strength of Materials*, McGraw-Hill Book Company, New York, 1953.

[VIO 56] VIOLLET-LE-DUC E., *Dictionnaire raisonné de l'arcitecture française du XI^e^ au XVI^e^ siècle*, Paris, 1856.

# 11

# Homogenization and Yield Design of Masonry

In this chapter, we consider a micro-mechanical approach, i.e. on a scale of heterogeneities. By heterogeneity, we mean blocks and joints that are very different in nature. Taking heterogeneities into account through a homogenization process is then used to consider the structure as homogenous and continuous.

In this chapter, we present the principles of modeling through yield design coupled with homogenization of periodic regular masonry blocks, as established by De Buhan and De Felice [DEB 97]. This model was developed for plane stress problems. We give some examples for using this method in order to show its potential and use. In Chapter 10, a static approach within yield design was used. In this chapter, the kinematic approach from the outside is used.

Here, we consider the same assumptions of the behavior of masonry blocks as in Chapter 10. Given the strength of stones compared to that of joints, blocks are considered as having infinite compressive strength. In Chapter 3, we saw that this assumption can only be applied to stone masonry, and within the limit of a stress state that does not exceed that admissible by blocks. This excludes earth masonry and some vaulted stone structures. It is entirely possible to complete the model by taking the strength of blocks into account, but this work is not yet known. In this chapter, yield will take place exclusively at the joints. Here, we are interested in structures such as walls.

*Sustainable Masonry: Stability and Behavior of Structures,*
First Edition. Thierry Ciblac and Jean-Claude Morel.

## 11.1. 2D understanding of masonry walls

Many practical cases can be reduced to plane problems. There are two types of plane problems, those under plane strain and those under plane stress.

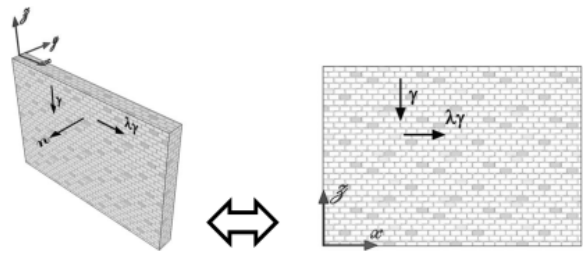


**Figure 11.1.** *Walls similar to structures under plane stress according to direction n "gamma" = unit weight of the masonry and "lamda gamma" = horizontal load (image by Rabia Charef-Morel)*

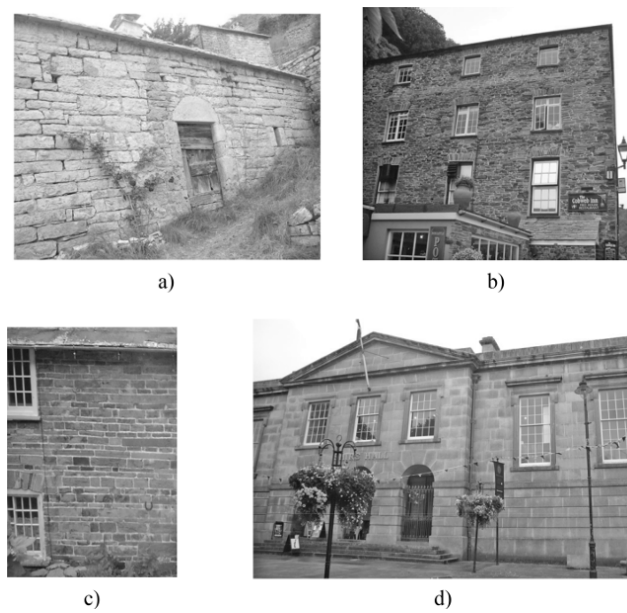


**Figure 11.2.** *Example of masonry walls that can be considered as under plane stress (loaded in plane); a) limestone blocks barn (Tarn, France), b) shale building (Cornwall, UK), c) sandstone blocks, d) monumental granite structure (Cornwall, UK).*

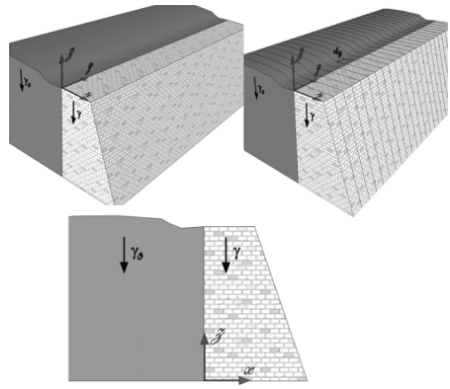

**Figure 11.3.** *Structures similar to structures in plane strain along y: example of a retaining wall (image by Rabia Charef-Morel)*

Structures with one very small dimension compared to the other two are modeled under plane stress (Figure 11.1); these are mainly responsible for building vertically loaded walls by weight of materials and service loads (Figure 11.2).

Structures with a very long dimension compared to the other two (Figure 11.3) are modeled under plane strain, for example, dikes, retaining walls, dams, etc. Examples of drystone retaining walls can be seen in Figures 11.4 and 11.5. Please note, the photographs only show one face of the wall, the plane strain geometry to consider is that of the plane thickness of the wall (Figure 11.3).

**Figure 11.4.** *Roadside retaining wall with typical claved masonry walls in contact with water. The wear of the stone (shale) by the tide in the lower part of the wall is very visible. About 4 meters high (Cornwall, UK)*

Felletin, France. New granite wall (2012), about 2.5 meters high. Instrumented wall: numbers in yellow determine the position of sensors.

**Figure 11.5.** *Drystone retaining wall masonry can be considered under plane strain, built by companies included in the ABPS[1]. Instrumentation is part of the PEDRA[2] project, photograph by Joachim Blanc-Gonnet*

## 11.2. 2D model developed by De Buhan and De Felice [DEB 97]

If the geometry of masonry is imagined as a set of regular blocks assembled in a staggered manner (Figure 11.6), we can then use the homogenization technique of periodic media within the framework of yield design theory as developed by [DEB 86] and [DEB 97]. In the photographs in Figure 11.2 (both dimensions being visible) and in Figures 11.4 and 11.5 (one dimension being visible), we see that this assumption is more or less realistic, depending on the masonry.

If we consider a heterogeneous structure for which geometric and mechanical characteristics are periodic, we can replace the heterogeneous masonry (Figure 11.6(a)) with an equivalent homogeneous medium (Figure 11.6(c)) for which the overall mechanical properties are representative of the initial heterogeneous medium. The homogenization process allows us to move from a microscopic scale that takes blocks and joints into account to a macroscopic scale, with a homogeneous view of the structure. The *representative elementary volume* (REV) of masonry is then defined as the smallest possible element for reconstructing the geometry of the entire structure.

Application of homogenization is only possible if there is sufficient REV in both directions of the plane axes. In Figure 11.6, for example, in the horizontal direction, REV is only reproduced 3 or 4 times, which is the lower

1 National association of builders using dry stone (*Association nationale des Artisans Bâtisseurs en Pierre Sèche*), http://www.pierreseche.fr.
2 PEDRA projet No. 10 MGC S 017.

limit of the applicability of the method. This is the basis for this method and more detailed explanations can be found in [DEB 86]. In Figure 11.5, the base thickness is 1.2 m, which allows us to have at least three REVs through the thickness.

We begin by identifying the characteristics of the microstructure, which consists of stone blocks of height *a* and width *b* and joints (Figure 11.7). The blocks are regular and joint dimensions can be ignored.

A Mohr–Coulomb law of pure friction is applied to the joints, which is expressed in terms of perpendicular and tangential stresses at the interface as:

$$g(\sigma, \tau) = |\tau| + \sigma \tan \varphi \leq 0 \qquad [11.1]$$

where φ is the angle of friction of stone against stone.

The REV proposed by De Felice and De Buhan is a diamond shape of volume M with its vertices located at the center of four adjacent blocks (Figure 11.7). We must ensure that the entire masonry assemblage can be reconstructed through translation of this REV. The REV thus formed consists of four pieces of blocks separated by three lines of joints, which will be denoted as J.

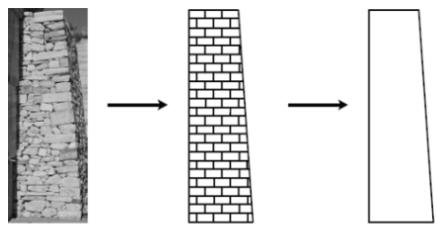


**Figure 11.6.** *a) Idealization of drystone masonry, b) regular periodic masonry, and c) periodic homogenization of regular masonry (picture by Anne-Sophie Colas [COL 09])*

The homogenization theory in the framework of yield design [DEB 86] allows us to deduce the characteristics of the equivalent homogenized medium from the REV characteristics, i.e. the macroscopic strength domain of masonry $G_{hom}$.

Given the assumptions, we give a first static definition of $G_{hom}$ based on macroscopic stress fields $\underline{\underline{\Sigma}}$:

$$G_{hom} = \left\{ \underline{\underline{\Sigma}} \,/\, \underline{\underline{\Sigma}} = \frac{1}{M} \int_M \sigma(x) dV \right\} \quad [11.2]$$

with ∀ x ∈M, M being defined in figure 11.7

$$\underline{\underline{\sigma}}(x) \epsilon \mathbb{R}^2 \text{and} \forall \text{ x} \in \text{J} \quad [11.3]$$

$$\underline{\underline{\sigma}}(x).\text{n(x)} \leq 0 \quad [11.4]$$

$$\text{div } \underline{\underline{\sigma}}(x) = 0 \quad [11.5]$$

$$\underline{\underline{\sigma}}(x).\text{n(x) anti-periodic} \quad [11.6]$$

We can also use a kinematic approach to define $G_{hom}$. To do this, we apply to the REV mechanism of virtual yield through rigid body motion (Figure 11.7). This allows us to calculate the maximum work dissipated through the macroscopic strain $\underline{\underline{D}}$. For dry joints, the homogenized maximum work is zero; this is explained by the lack of cohesion of joints for drystone masonry equation [11.7].

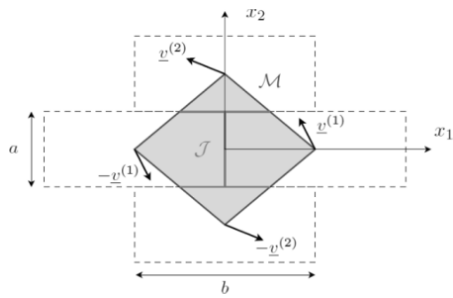


**Figure 11.7.** *Yield mechanism of REV blocks according to [DEB 97] to which four virtual velocity vectors are applied (picture by Anne-Sophie Colas [COL 09])*

$$\pi_{hom}(\underline{\underline{D}}) = 0 \quad [11.7]$$

with the conditions of existence of the support π-function (as defined by [DEB 97]), which must be verified. These conditions are inequalities that

relate to the macroscopic strain tensor $\underline{\underline{D}}$, defined on the basis of virtual velocities. These conditions are explained by the inequality system below, equation [11.8] [DEB 97]:

$$-D_{11} \leq 0$$

$$tan\varphi |D_{11}| \leq 2mD_{22}$$

$$|D_{12} + D_{21}| \leq tan\varphi D_{11} + \frac{1}{tan\varphi} D_{22} \qquad [11.8]$$

These conditions are expressed differently according to the aspect ratio of blocks m = a/b, larger or smaller than $\frac{1}{2\tan\varphi}$. Figure 11.8 shows the two areas thus defined.

We note that in most cases, stone or earth walls are found in zone B of Figure 11.8 as regards the average values generally observed for m (less than 0.5) and φ (less than 45°). The aspect ratio of blocks m = a/b and the angle of friction φ of blocks then meet the condition:

$$2\mathrm{m} \leq \frac{1}{\tan\varphi} \qquad [11.9]$$

The masonry in Figure 11.2 falls into this zone B of Figure 11.8. However, there are still many structures in zones A and C. This, for example, is the case for masonry in Figure 11.4, zone A and Figure 11.5, zone C.

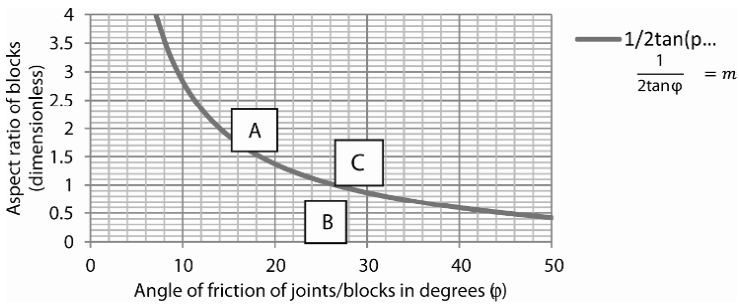


**Figure 11.8.** *2D model by [DEB 97]: two areas in which the conditions of existence of support functions are defined depending on the aspect ratio m and the angle of friction φ*

In the kinematic approach from the outside [DEB 86], we define the $G_{hom}$ domain as:

$$G_{hom} = \left\{ \underline{\underline{\Sigma}} \,/\, \underline{\underline{\Sigma}} : \underline{\underline{D}} \leq \pi_{hom} = 0 \right\} \qquad [11.10]$$

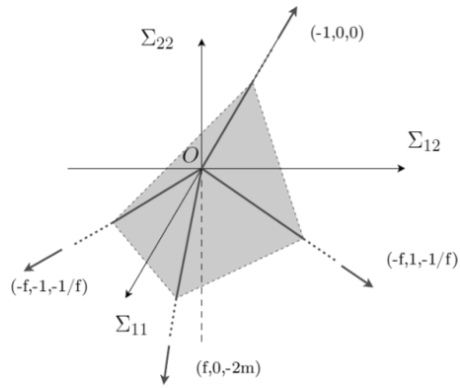


**Figure 11.9.** *$G_{hom}$ strength domain for homogenized masonry (image by Anne-Sophie Colas [COL 09])*

We represent the $G_{hom}$ strength domain (Figure 11.9) as a tetrahedral convex cone with vertex O, the origin of the stress space. This representation shows the anisotropy of the field strength of homogenized masonry, linked to low resistance of joints.

Figure 11.10 shows plane problems that represent various practical cases: walls of a building under plane stress under their own weight and with horizontal seismic load (proportional to its unit weight), a retaining wall, loaded by horizontal forces (hydrostatic pressure or land pressure without vertical friction with masonry), and a wall of a building subjected to the interaction of a perpendicular wall limited to a linear force distribution.

## 11.3. Application to structures under plane stress

In their work, De Felice and De Buhan [DEB 97] give an example of the application of their model for a rectangular wall, loaded by a horizontal volume force and its own weight (Figure 11.10(a)). In practice, this type of load corresponds to the static equivalence of a seismic load. Vector $\lambda\gamma$ is a volume force that can be generated by acceleration due to an earthquake.

Line OO′ in Figure 11.10(a) is the potential yield line. Virtual velocity is denoted v* and is given by:

$$\underline{v}^* = \underline{\chi} + \underline{y} \wedge \omega \underline{e_3} \qquad [11.11]$$

$$\underline{v}^* = \begin{vmatrix} \chi_1 + \omega\, y_2 \\ \chi_2 + \omega\, y_1 \\ 0 \end{vmatrix} \qquad [11.12]$$

The unknown λ is proportional to the maximum horizontal volume force allowable by the wall loaded under its own weight.

Calculation of the work of external forces $W_E$ given by [DEB 97] is:

$$W_E = \gamma \iint_{OO'AB} \lambda\, (\underline{e_1} - \underline{e_2})(\underline{\chi} + \underline{y} \wedge \omega \underline{e_3})\, dy_1 dy_2 \qquad [11.13]$$

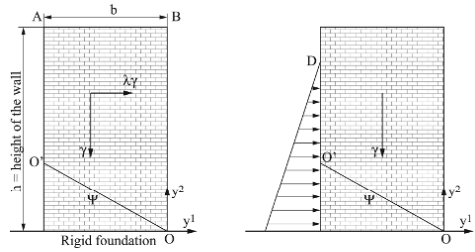


**Figure 11.10.** *Example of plane problems, boundary conditions and loads, γ unit weight of masonry; a) case studied by [DEB 97], b) linear load (for example, hydrostatic pressure)*

The calculation of maximum resisting work $W_{RM}$ (see [SAL 83, SAL 02]) is given by the following expression that reflects the π function of the Coulomb criterion:

$$W_{RM} = \gamma \frac{cL}{tan\varphi}\left(\chi_1 \sin\psi + \chi_2 \cos\psi + \omega \frac{L}{2}\right) with\ L = \frac{b}{cos\psi} \qquad [11.14]$$

Finally, the solution is given by minimizing the following inequality with respect to ψ, ω, χ, which are the parameters describing yield kinematics:

$$W_E < W_{RM} \qquad [11.15]$$

In the case of [DEB 97], there is only one unknown load parameter, which is λ, and by taking c=0, the calculations are simplified greatly. The parameters ψ, ω, χ are first subjected to the conditions obtained by the homogenization process, involving φ and m = a/b, aspect ratio of blocks (Figure 11.8). The next step is the minimization of λ relative to the parameters in this new domain from the homogenization process.

Figure 11.11 gives the results of the model which we compare to a calculation in which masonry is considered a rigid solid. The results corresponding to rigid bodies are represented by continued lines. Segment AB is obtained through the equilibrium of forces and line BC, through that of the moments. Lines ABC represent a certain yield criterion for a rigid solid and A′B ′C ′, for a homogenized solid. A′B ′ is obtained with a yield plane opening out on the vertex AB of the wall, Figure 11.10(a). Line B′C′ is obtained with a yield plane opening out on the face O′A of a wall, Figure 11.10(a). In both cases, the virtual velocity vector is a pure rotation χ=0. For a virtual velocity vector of pure translation ω=0, we get line AB, which is the same result as in the calculation of rigid bodies.

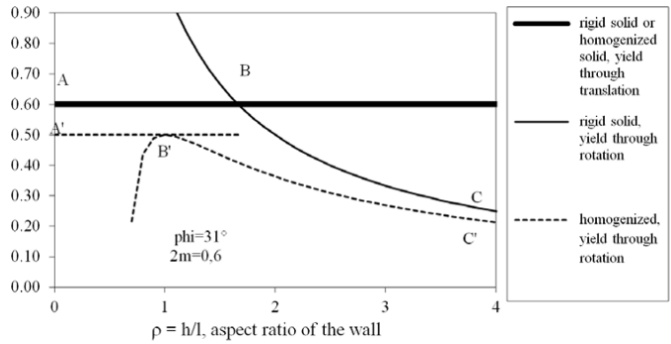


**Figure 11.11.** *Comparison of yield design with and without homogenization: case of horizontal loading volume λγ*

The allowable load values are substantially reduced (Figure 11.11) by taking into account a discrete medium through homogenization. There is a threshold for which equality of lines AB and A′B′ is between the two approaches (rigid or discrete medium). This case is achieved in Figure 11.12 for the values φ = 23 and 2m = 0.6. Beyond this, the translation limit becomes that of rigid bodies, and that of homogenized rotation continues to be separate from the rotation of rigid bodies.

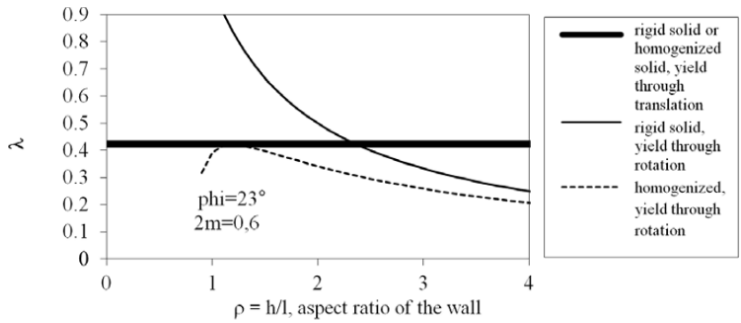


**Figure 11.12.** *Comparison of yield design with and without homogenization: border line case*

Taking the heterogeneity of the masonry of blocks into account modifies the yield threshold between the translation and rotation obtained for a rigid solid. Yield through rotation occurs for a smaller aspect ratio in the case of homogenized calculation.

## 11.4. Application to structures under plane strain

### 11.4.1. *Retaining walls*

In some structures, including drystone blocks, the assumptions for regular geometry blocks is very strong as most walls are built with irregular stones of all sizes. This has two consequences that will affect the mechanics. Jamming blocks against each other is done due to the skill of the mason who places each stone. It is less strong than perfectly parallelepiped blocks, as those blocks can then turn locally, as shown by [VIL 04]. Furthermore, the contact areas between each block are limited, so local yield through splitting or bending is possible. This would involve integrating a compression limit into yield design, corresponding to a splitting strength limit, which is about ten times less than the simple compressive strength of stone (see Chapter 3, section 3.1.2).

Furthermore, the number of blocks in the width of certain walls may be less than 3, which can be regarded as insufficient to homogenize.

Despite these reservations, [COL 09] showed the applicability of the model presented here to these problems.

The design of a retaining wall is dependent on pressure from the soil (Figure 11.3). In a first approach, it is possible to use the Caquot and Kerisel pressure coefficients that have been established for walls with rigid faces. In this case, the possibility of interaction between internal yield according to joints within the masonry and pressure forces is not taken into account.

Consideration of the interaction between soil and masonry was rigorously proposed by Denis Garnier and Anne-Sophie Colas [COL 08]. The two proposed kinematics are described in Figure 11.13. The relevance of these two kinematics has been validated in Anne-Sophie Colas' PhD thesis [COL 09] on scale 1 experiments.

Figure 11.14 shows the type of results obtained with these two virtual kinematics faced with smaller models (scale 1/10) of 2D anologic materials. The results are in accordance with this empiricism, such that when the batter increases, the wall becomes more resistant to overturning, and thus yield is preferably translational (Figure 11.14(a)). When the inclination of the beds increases, the effect is the same as an increase in friction at the joints, yield occurs through overturning.

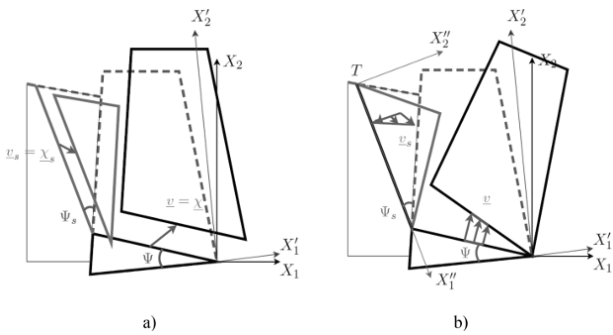


**Figure 11.13.** *a) Virtual kinematics of yield in translational motion of rigid bodies for the soil and masonry wall, and b) rotation of rigid bodies for the masonry wall and distortion in the soil (image by Anne-Sophie Colas)*

### 11.4.2. *Masonry dams*

This involves masonry dams with blocks and mortar, which are old dams in Europe or North America, and are always constructed in particular areas. In this case, previous developments are directly applicable, as the loads and geometry of structures belong to Figure 11.10(b).

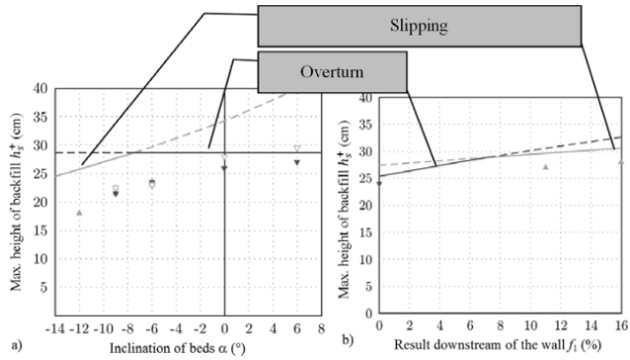


**Figure 11.14.** *Influence on kinematics of yield: a) from the inclination of beds (equivalent to friction between blocks), b) from the results [COL 09] the lines are given by the model, and each point (triangle) correspond to an experiment*

### 11.4.3. *Mixed rockfill and masonry dams*

This type of dam, made of rockfill with a drystone revetment on the downstream were built in the United States, Algeria, Europe (France, Italy, Portugal), amongst other places. In France, there are a dozen dams of this type that were built in the 1950s to produce hydroelectricity.

These dams are composed of a central part, the dam body, dumped and therefore permeable rockfill. The upstream slope, like the downstream one, is protected by drystone masonry, arranged by hand (thickness band $e$ in Figure 11.15). Waterproofness is ensured by a thin and highly waterproof face upstream that is often made of mortar placed over the drystone layer.

To implement the developed model in the previous sections, we should make the following assumptions:

– the size of a stone is 50 to 100 times smaller than the dam: 20 cm for 20 m, we can consider the embankment as a homogeneous granular material. It may therefore follow Coulomb's law with zero cohesion;

– the mortar layer ensures waterproofing and the drystone upstream revetment is not involved in the strength of the structure to its load;

– the downstream drystone revetment is sufficiently thick (more than three stones) so we can apply the homogenization method previously developed.

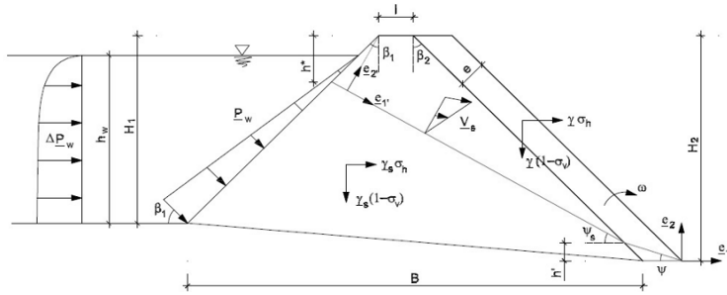


**Figure 11.15.** *Example of geometry of a rockfill and drystone revetment dam and virtual yield kinematics, $v_s$ velocity generated by shear and ω rotation of the rigid body of the revetment (image by Hong Hanh Le [LE 13])*

| Parameters | Units | Symbols |
|---|---|---|
| Upstream height of the dam | m | $H_1$ |
| Downstream height of the dam | m | $H_2$ |
| Width of the crest | m | l |
| Width of the base | m | B |
| Upstream batter of the dam | degrees | $\beta_1$ |
| Downstream batter of the dam | degrees | $\beta_2$ |
| Thickness of drystone revetment | m | e |
| Height of water | m | $h_w$ |
| Unit weight of water | kN/m$^3$ | $\gamma_w$ |
| Water pressure on the upstream face | kN/m$^2$ | $p_w$ |
| Additional water pressure due to earthquake | kN/m$^2$ | $\Delta p_w$ |
| Unit weight of rock | kN/m$^3$ | $\gamma_s$ |
| Angle of internal friction of the rock | degré | $\varphi_s$ |
| Unit weight of drystone revetment | kN/m$^3$ | γ |
| Angle of internal friction of the drystone revetment | degrees | φ |
| Angle determining the yield line in the drystone revetment | degrees | ψ |
| Angle determining the yield line in the rock | degrees | $\psi_s$ |

**Table 11.1.** *Definition of parameters of a dam as an example [LE 13]*

In section 11.4.1, dealing with the case of a retaining wall, we saw that we successively examine two different yield mechanisms in order to retain the most critical cases: yield through drystone revetment translation is associated with translation of the backfill soil and yield through overturning

in the drystone revetment is associated with shear of the backfill soil. Figure 11.15 shows the second kinematic with $v_s$ for the rockfill embankment and ω in the drystone revetment.

Based on these simplifying assumptions, the calculation model of the dam is constructed as shown in Figure 11.15. The symbols used are found in Table 11.1.

The loading parameters are:

– the volume forces applied to the drystone revetment:

$$\underline{\gamma} = \sigma_h \gamma \underline{e}_1 - (1 - \sigma_v)\, \gamma\, \underline{e}_2 \qquad [11.16]$$

where $\sigma_h$ and $\sigma_v$ are seismic coefficients. This is the combination of negative weight, so the acceleration component that reduces the weight. This is the most critical combination, since we are in the configuration of a structure stabilized by its own weight;

– the volume forces applied to the rockfill embankment:

$$\underline{\gamma_s} = \sigma_h \gamma_s \underline{e}_1 - (1 - \sigma_v)\, \gamma_s \underline{e}_2 \qquad [11.17]$$

– hydrostatic pressure (perpendicular to the upstream face) for which intensity is given by $p_w = \gamma_w.y$, where *y* denotes the depth of the point considered relative to the free surface of the water;

– the extra water pressure due to the seismic action may be taken as a force that is proportional to the seismic coefficient and of parabolic distribution along the upstream face [LED 03]. A simple model can be given through Zanghar's formula [LED 03] derived from that of Westergaard on dams with a vertical upstream face:

$$\Delta p_w = \frac{1}{2}\sigma_h \gamma_w h \left(0{,}735 \times \frac{2\beta_1}{\pi}\right) \times \left[\frac{y}{h}\left(2 - \frac{y}{h}\right) + \sqrt{\frac{y}{h}\left(2 - \frac{y}{h}\right)}\right] \qquad [11.18]$$

where *h* is the depth of the reservoir; *y* is the considered depth.

Calculations were made by [LE 13] for a structure with the dimensions given in Table 11.2.

| Parameters | Units | Data Values |
|---|---|---|
| Upstream height of the dam ($H_1$) | m | 15 |
| Downstream height of the dam ($H_2$) | m | 20 |
| Width of the crest (l) | m | 2 |
| Upstream batter of the dam ($\beta_1$) | degrees | 45 |
| Downstream batter of the dam ($\beta_2$) | degrees | 45 |
| Thickness of drystone revetment(e) | m | 1,2 |
| Unit weight of water ($\gamma_w$) | kN/m$^3$ | 10 |
| Unit weight of rock ($\gamma_s$) | kN/m$^3$ | 16 |
| Angle of internal friction of the rock ($\varphi_s$) | degrees | 37.7 |
| Unit weight of drystone revetment($\gamma$) | kN/m$^3$ | 21 |
| Angle of internal friction of the revetment ($\varphi$) | degrees | 29 |

**Table 11.2.** *Example of parameters describing a structure [LE 13]*

The dam example body is made of granite stones extracted on site and dumped. The thickness of the downstream drystone revetment is 1.2 m. It is also assumed that the dam is located in a seismic zone between level 3 (moderate) and 4 (average). According to the seismic zoning map of France that has been in force since 1st May 2011, $\sigma_h$ = 0.127 and $\sigma_v$ = 0.051. Calculations show that the minimum thickness of drystone revetment for the dam to be stable is 0.21 m (yield through overturning, kinematics described in Figure 11.15). A parametric study by [LE 13] on the structure presented in Figure 11.15 shows the crucial role of drystone revetment in the stability of the structure.

## 11.5. Conclusion

We have shown the potential of the model by [DEB 97] in the qualitative and quantitative analysis of the stability of masonry structures in 2D. This model is relatively new and it can be further developed and extended to more complex cases. We refer the reader to a work in progress supervised by Denis Garnier for extending the model to masonry in 3D [LE 13].

To use this model for earth masonry, we should consider the compressive strength of blocks and resistance, however small, of joints to tension. This last point is already proposed in [DEB 97] through the possible existence of a non-zero cohesion in the Coulomb criterion for joints. However, taking the

strength of blocks into account is more complex, because it requires rebuilding the whole homogenization process.

The methods developed in this chapter, and more generally throughout this book may be adapted to numerical analysis in order to extend the application to complex geometries that may describe all practical cases.

These methods will always maintain an undeniable advantage over more complex methods such as those for finite or discrete elements; because of their relative simplicity, they can be used for practical cases for which we only have limited information. This is the case for many vernacular architecture structures.

Measures or evaluations of additional parameters such as stiffness of joints, which is necessary for the implementation of conventional numerical methods (finite or discrete elements) are costly and delicate.

## 11.6. Bibliography

[DEB 86] DE BUHAN P., Approche fondamentale du calcul à la rupture des ouvrages en sols renforcés, Thesis, Université de Paris-VI, Paris, 1986.

[DEB 97] DE BUHAN P., DE FELICE G., "A homogenization approach to the ultimate strength of brick masonry", *Journal of the Mechanics and Physics of Solids,* vol. 47, no. 7, pp 1085–1104, 1997.

[COL 08] COLAS A.S., MOREL J.C., GARNIER D., "Yield design of dry-stone masonry retaining structures – Comparisons with analytical, numerical and experimental data", *International Journal for Numerical and Analytical Methods in Geomechanics*, vol. 32, pp. 1817–1832, 2008.

[COL 10] COLAS A.S., MOREL J.C., GARNIER D., "2D modelling of a dry joint masonry wall retaining a pulverulent backfill", *International Journal for Numerical and Analytical Methods in Geomechanics*, vol. 34, pp. 1237–1249, 2010.

[LE 13] LE H.H., Stabilité des murs de soutènement routiers en pierre sèche: modélisation 3D par le calcul à la rupture et expérimentation échelle 1, l'ENTPE PhD Thesis, 16 September 2013.

[LED 03] LE DELLIOU P., *Les barrages: conception et maintenance*, Presses Universitaires Lyon, Lyon, 2003.

# Conclusion

This book deals with the mechanical stability of masonry using earth materials. The earth materials described in this book are stone and earth. Earth as considered here is what makes up masonry structures of small elements (adobe or compressed earth blocks) or (rammed earth) layers. The stones are cut, squared, or even used uncut. Stones can be joined using weak earth mortar, sand and thin lime mortar (rubble stone masonry), or even without mortar. The latter case is dry stone masonry. The common point between these materials is that they show variability in their composition and shape. This variability is linked to the fact that the materials are removed from the local soil near the construction. It would be fruitless to hope to know the behavior of each of these materials. However it is possible, through a suitable approach, to manage, in a rigorous manner, to evaluate the mechanical stability of these structures.

This book consists of three complementary parts, the first part dealing with technologies and construction processes, the second with graphic statics and finally, the third dealing with the implementation of yield design applied to masonry structures.

After the introductory chapter, the subsequent three chapters (Part 1) detailed elements describing the phenomenology of these materials as masonry components, that is to say, the macroscopic behavior of stone and earth. This information can only be obtained through measurements from experiments on material samples large enough to accommodate the various heterogeneities in these materials. Here, we are particularly interested in describing the yield of materials and joints. This is the first step then, that

*Sustainable Masonry: Stability and Behavior of Structures,*
First Edition. Thierry Ciblac and Jean-Claude Morel.

allows us to be able to model, by the geometric or analytical approach, the stability of masonry structures using yield design.

Part 2 describes the formalism of the method of graphic statics, which provides a very suitable tool for understanding the stability of masonry structures. This approach was historically the first one used, mainly for its ability to provide the means for design, and is considered in a very practical manner in Part 3. This part introduces the application of the theory of yield design for masonry in the formal context of graphic statics and the mechanics of continuous periodic media.

Using graphic statics, we consider the stability of curvilinear structures or 2D structures as arches. In the context of mechanics of continuous periodic media, we describe the inclusion of joints in 2D media. The choices made in Part 3 have the advantage of considering a simple but representative resistance criterion for masonry. This approach is instructive and can perform diagnostics on existing heritage and in the design of structures.

The described approaches can be supplemented with digital methods, for example approaches with software using the discrete element method. The first comparative results are not surprising: both methods give the same result. However, regardless of improved speeds of computers in the future, digital methods will encounter the difficulty of knowing all the mechanical parameters required. The latter may only be used in practice for monumental structures, and not for the current masonry, which today represents an important socio-economic issue.

Research on sustainable masonry is currently experiencing increased growth in several directions. In particular, we refer to work on the inclusion of 3D geometry in yield design, which is considered in Chapter 11. Finally, aside from the mechanical aspect, research is developing in two fields: hydrothermal behavior of masonry with earth materials (as a porous media) and the first quantification of the sustainability of these constructions.

# Index




*Sustainable Masonry: Stability and Behavior of Structures,*
First Edition. Thierry Ciblac and Jean-Claude Morel.